STATISTICAL PHYSICS OF ISOTROPIC-GENESIS NEMATIC ELASTOMERS

BY

BING SUI LU

DISSERTATION

Submitted in partial fulfillment of the requirements
for the degree of Doctor of Philosophy in Physics
in the Graduate College of the
University of Illinois at Urbana-Champaign, 2012

Urbana, Illinois

Doctoral Committee:

Professor Shinsei Ryu, Chair
Professor Paul M. Goldbart, Director of Research
Professor Steve Granick
Professor John Stack

Abstract

Isotropic-genesis nematic elastomers (IGNEs) are materials that exhibit fascinating properties such as a remarkable softness in elasticity and do not undergo long-range nematic ordering, even at low temperatures. These materials are formed via the following process. Consider a melt or solution of nematogenic polymers, by which we mean long, flexible polymers carrying rod-like units. These units, which are also known as nematogens, and which give the system the possibility of exhibiting liquid crystallinity, may be integrated along the polymer chain backbones (the main-chain case) or in groups that dangle from the backbone (the side-chain or pendant case). An IGNE is formed when the polymers are permanently and randomly cross-linked to one another in the isotropic state of the nematogens; it is capable of "memorizing" both the positions of the chain segments and the orientations of the nematogen units at the instant of cross-linking. In this thesis, we derive a Landau-type theory of an IGNE, starting from from a microscopic model which consists of dimers that are randomly, permanently, and instantaneously cross-linked via springs. The Landau-type theory involves (a) a non-local, network-mediated, nematic-nematic interaction term, and (b) a random-field term that depends on the local, quenched environmental anisotropy, as well as the memorization of the random pattern of nematic fluctuations present at the instant of cross-linking. On the basis of this Landau-type theory, we address the following physical issues associated with the study of IGNEs:

(i) The origin, nature, and stability of a certain equilibrium state (known as the polydomain state) of an IGNE. This state is characterized by the presence of a short-ranged, "anti-correlated" pattern of nematic alignment. By taking the thermal fluctuations of the

elastomer medium into account, in addition to those of the nematogen orientations, we are able to predict, for sufficiently strongly cross-linked IGNEs, a novel type of nematic correlation behavior that is both oscillatory and decaying in space. Such oscillatory-decaying behavior is qualitatively consistent with the anti-correlation pattern observed in recent experiments by the Urayama group [28]. By means of a Gaussian variational analysis, we also find that the macroscopically isotropic state of IGNEs (of which the polydomain state is a particular instance) remains stable, at least locally, in the low-temperature regime. Chapters 2, 3, 4, 7 and 8 provide analyses pertaining to issue (i).

(ii) Next comes the issue of capturing aspects of the memorization capability of an IGNE theoretically. We show that the IGNE's memory of the random pattern of thermal nematic fluctuations present at the instant of cross-linking directly influences the pattern of nematic alignment that is subsequently "frozen in" to the IGNE via the cross-linking process. Moreover, we learn that the fidelity of this memorization of the initial fluctuation pattern depends on the strength (i.e., pervasiveness) of cross-linking as well as the temperature at which the cross-linking was performed. Chapter 2 contains a study of this memorization capability of an IGNE.

(iii) The third issue addressed in this thesis pertains to the much softer elastic response of IGNEs, compared to ordinary elastomers, observed experimentally. We propose a physical mechanism for elastic softening, in which the softening is driven by fluctuation correlations of the nematic alignment. Chapters 5 and 6 contain a detailed explanation of this mechanism.

For my family, especially my mother:

"Paradise lies at the feet of mothers."

— From a saying attributed to Prophet Muhammad

Acknowledgments

Riverrun, past Eve and Adam's, from swerve of shore to bend of bay, brings us by a commodius vicus of recirculation back to Howth Castle and Environs.

— James Joyce, *Finnegans Wake*

First and foremost I am grateful for having Paul Goldbart as my Ph.D. advisor. In addition to being a terrific advisor and an outstanding mentor, imparting to me a tremendous amount of physics insights, he has impressed on me the idea that physics is not always about solving problems; it is also about being able to listen to different perspectives; it is about "becoming unblind," intellectual blindness being often induced by self-conceit and prejudicial fondness for some particular interpretation, thereby causing one to miss other, more promising, avenues. Paul's approach to advisorship is not unlike the approach of a personal doctor, exuding care and compassion, frequently going to great lengths to ensure that his students have fully grasped some crucial concept before moving on to the next stage. He would feel sad if a student were to pretend to have understood some concept. Paul also encourages his students to keep what he calls a "rainy season" journal, a journal in which one jots down one's scientific musings and ideas as they occur. The journal could prove to be a vein to mine for ideas if ever one should experience "physicist's block." I can attest that keeping such a journal is indeed an extremely beneficial habit.

Paul has constantly encouraged me to aim to "be like Pierre-Gilles de Gennes"in the following sense: after having done a highly technical calculation, de Gennes would find the simplest possible explanation for it, so that his results would be accessible to the widest possible audience. Paul has also tried to inculcate in me a taste and empathy for the differ-

ent styles of physicists. For example, to some, collective fields have no deeper significance than that of a necessary algebraic crutch to arrive at certain physical results; but to others, collective fields are physically meaningful and autonomous characters. Many students of Paul's have remarked on his mathematical prowess and scientific acumen, which I can confirm. In addition to that, Paul is keen to stress the historical continuity of physics, i.e., no discovery in physics has ever occurred in isolation; he has quoted Newton, on more than one occasion, that we are "standing on the shoulders of giants," and it would be foolish for one to re-invent the wheel. As is evident from a glance through the contents of this thesis, the work described here owes its existence to the seminal work of many previous workers, in particular Landau, Onsager, Schwinger, Feynman, de Gennes and Sam Edwards, and also to the efforts of more recent workers, including Paul and his many collaborators, past and present, on vulcanization theory. Needless to say, I have reaped enormous benefit, both scientific and non-scientific, from day-to-day discussions with Paul.

Moreover, I am thankful for having had the opportunities to work with our collaborators Xiangjun Xing and Fangfu Ye. I have learnt a wholesome amount of physics from both of them. Xiangjun Xing, in particular, evinces by his behavior the ideal attitude of a theoretical physicist: uncompromisingly self-critical, open-minded, with a voracious appetite for scientific knowledge. I can hardly remember a minute spent in his presence without him reaching in quiet desperation for a piece of chalk and compulsively writing down an equation. At one banquet in Shanghai, there was no chalk, but I saw his finger trace out some mathematical symbols. Xiangjun inspiringly emphasizes the need for simplicity: if one really understands a problem then one should be able to offer a simple, intuitive, explanation. There should be no room for obscurity or ambiguity. In his book *The Character of Physical Law*, Feynman wrote that a good physicist is one who can give seven different explanations to the same problem; Xiangjun said he was not good because he could only come up with four. He is always measuring his scientific level according to standards set by physicists such as Landau and Feynman. As with Paul, I believe graduate students and post-docs can learn

a lot from Xiangjun's example.

I feel deeply privileged to have had the opportunities to discuss physics with many more experienced physicists, including Tom Lubensky, Leo Radzihovsky, Mark Warner, Kenji Urayama, Jonathan Selinger, Robin Selinger, Alfred Huan, Lock Yue Chew, Siew-Ann Cheong, Alex Levine, Turgay Uzer, Harold Kim, Jennifer Curtis, Dan Crow, Anton Souslov, Xiaoming Mao, Shizhang Zhang, Benjamin Fregoso, Dervis Can Vural, Sukrit Suksombat, Jitong Yu, Michael Brenner, and Shiladitya Banerjee. I have also gained enormously from the lectures of Nigel Goldenfeld on "Emergent States of Matter" and "Phase Transitions and the Renormalization Group."

Outside of physics, I am grateful for having friends such as Tau Wey, who regularly sends me videos of his musical performances in London, who has convinced me that the highest stage to which a musician can aspire to is to understand the *intention* of John Cage and hear his laugh of "musical Shunyata," and who has also promised to perform my thesis in his John Cage piano recitals; Dan Crow, for sharing many exquisite oysters and indelible impressions (from the salt breeze of Morlaix and the screaming squalls of Oost-Ende to the gusting gales of Boston), and enabling me to appreciate life in its happy sadness/hopeful pessimism/light gravity, whilst also enriching my mind with the fruits of psychoanalysis and Deleuzian philosophy; and Haroon Qureshi, who has constantly enriched my being with insights rooted in the Qur'an, the nazms of Allama Iqbal, the ghazals of Mirza Ghalib ("the Shakespeare of India"), and the compassionate philosophical vision of Maulana Azad (India's first Education Minister and founder of the Indian Institutes of Technology—IITs). Haroon taught me to behold everything in the world as "gems in the grand nazm of creation." In addition, I am happy to have found a wise and knowledgeable friend in Mohammad Khalil, with whom I shared many enjoyable hours of topical conversations on theology, jurisprudence, philosophy and history.

I am also grateful to Profs. Soo Ying Lee and Alfred Huan of Nanyang Technological University (Singapore), who made the decision six years ago to have my "bond" transferred

from the Singaporean Education Ministry to the School of Physical and Mathematical Sciences, thereby enabling me to embark on my Ph.D. studies in physics; and to Selina Toh, who facilitated the transfer.

Above all, I am grateful to my parents and my brother for having supported me throughout my years of physics education, from elementary school to graduate school. They fully understand the value of education, an understanding that I have at times struggled to possess.

The research work culminating in the present thesis was supported by the U.S. National Science Foundation via grant nos. DMR06-05860 and DMR09-06780, the Institute for Condensed Matter Theory and the Frederick Seitz Materials Research Laboratory at the University of Illinois at Urbana-Champaign, the Institute for Complex Adaptive Matter, and Shanghai Jiao Tong University.

Table of Contents

List of Tables

List of Figures

List of Abbreviations

IGNE	Isotropic-Genesis Nematic Elastomer
NGNE	Nematic-Genesis Nematic Elastomer
VT	Vulcanization Theory
HRS	Higher Replica Sector
LRS	Lower Replica Sector
1RS	One-Replica Sector
0RS	Zero-Replica Sector
RHS	Right Hand Side
LHS	Left Hand Side

List of Symbols

Ω	Order parameter for detecting random localization
Γ	Order parameter for detecting the random positional and orientational localization of dimers
$\mathbf{Q}$	Order parameter for detecting nematic order
$\mathbf{Q}^0$	Nematic order present at the instant of cross-linking
$\mathbf{Y}$	Memory-independent random field
$\mathrm{H}_\mathbf{0}$	Disorder strength
$\mathcal{L}$	Generalized stiffness in the Landau-de Gennes analog of the one-constant approximation
$\{\cdots\}$	Matrix trace
G	Gel fraction
a	Range of orientation interaction between dimers
b	r.m.s. spring length
ℓ	Length of an individual dimer
τ	Inverse square localization length
ξ_L	Typical localization length in an elastomer network
$\mathcal{C}^T$	Correlator of thermal nematic fluctuations
$\mathcal{C}^G$	Correlator of frozen-in nematic fluctuations
$\xi_{T,d}$	Decay length of $\mathcal{C}^T$
$\xi_{G,d}$	Decay length of $\mathcal{C}^G$
$\xi_{T,o}$	Oscillation lengthscale of $\mathcal{C}^T$

$\xi_{G,o}$	Oscillation lengthscale of $\mathcal{C}^G$
$\mathbf{P}^{\mathrm{T}}_{\Lambda}$	Transverse projection matrix in Fourier space

Chapter 1

Introduction: nematic liquid crystals and nematic elastomers

This thesis is about the physics of nematic elastomers. To understand what nematic elastomers are, one should first understand what *liquid crystals*, *nematic* liquid crystals, and *nematic elastomers* are. Accordingly, one purpose of the introduction is to explain these concepts as simply as possible, making contact with experimentally measurable observables where possible. In addition, we shall explain why nematic elastomers are objects worthy of theoretical study, by describing some of the observed physical properties of nematic elastomers. Finally, we shall describe the issues that the thesis aims to address. Being of an introductory nature, this chapter contains no original contributions by the author. Section 1.1 is based on material drawn from Refs. [1, 2], Sec. 1.2 follows Refs. [3, 4, 6, 7], and Sec. 1.3 is based on Refs. [5, 27].

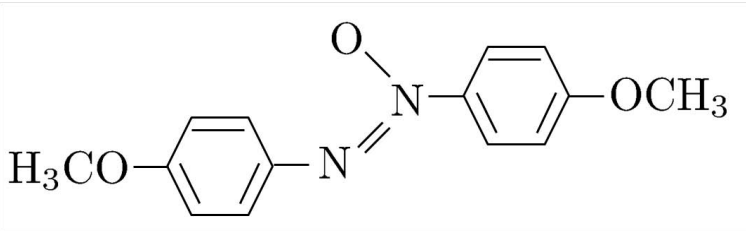

Figure 1.1: A standard nematogen: *p*-azoxyanisole (PAA). It can be regarded as a rigid rod of length $\sim 20\mathring{A}$ and width $\sim 5\mathring{A}$. The two benzene rings lie approximately in the same plane.

1.1 Nematic liquid crystals

First, we consider liquid crystals. These are systems in which (i) orientational anisotropy exists, and (ii) positional order, such as that present in a solid crystal, is absent in at least one direction in space. A liquid crystal that has orientational anisotropy but is devoid of positional order in any direction is called a *nematic* liquid crystal. Nematic liquid crystals typically consist of elongated objects. An example is the molecule *p*-azoxyanisole (PAA), which may be viewed as a rigid rod of length $\sim 20\mathring{A}$ and width $\sim 5\mathring{A}$ (see Fig. 1.1). A second example is the elongated molecule *N*-(*p*-methoxybenzylidene)-*p*-butylaniline (MBBA). These elongated entities are known as *nematogens*. They are materials that exhibit the nematic thermodynamic state, for which the rod-like entities tend to be parallel to some common axis in space over a certain range of temperatures; for example, MBBA is nematic from $\sim 293K$ to $\sim 320K$. At higher temperatures the rods are orientationally disordered and the liquid is said to be in the isotropic state.

How does one quantify the amount of orientational anisotropy in a nematic liquid crystal? For a start, one may think of using the parameter $\langle \cos\theta \rangle = \int f(\theta) \cos\theta d\Omega$, where θ is the angle with respect to a given macroscopic axis, which one can take to be the direction of macroscopic nematic alignment, and $f(\theta)$ is the distribution function that describes the probability of finding nematogens to be aligned within the infinitesimal solid angle $d\Omega \equiv \sin\theta d\theta d\phi$ around the direction (θ, ϕ) (where ϕ is the azimuthal angle around the alignment axis). However, this parameter is zero in both the isotropic state and the nematic state. It is zero in the isotropic state because $f(\theta)$ is then, by definition, constant, so that $\langle \cos\theta \rangle \propto \int_{-1}^{1} \cos\theta \, d\cos\theta = 0$. Note that the nematically aligned state whose direction of macroscopic alignment is specified by the unit vector $\boldsymbol{n}$ is not different from the state whose direction of macroscopic alignment is specified by $-\boldsymbol{n}$. This is equivalent to requiring that the distribution function obey $f(\theta) = f(\pi - \theta)$. The integral measure over the unit sphere, $\int d\Omega$, is invariant under the transformation $\theta \to \pi - \theta$, but $\cos\theta$ changes

sign. Thus, the parameter $\langle \cos\theta \rangle$ is also zero in the nematic state. Thus, an appropriate parameter for quantifying the amount of orientational anisotropy should take the form of a higher multipole moment of even order; the first nontrivial one is given by the quadrupole moment, viz.

$$S \equiv \frac{1}{2}\langle 3\cos^2\theta - 1 \rangle \equiv \frac{1}{2}\int (3\cos^2\theta - 1) f(\theta)\, d\Omega. \tag{1.1}$$

The parameter S has a value very close to unity when the rods are almost all parallel to one another [so that $f(\theta)$ is strongly peaked at $\theta = 0$ and π]. On the other hand, if the rods are orientationally disordered, $f(\theta)$ is independent of θ so that $S = 0$.

In experiments, a difference between the (high-temperature) isotropic state and the (low-temperature) nematic state of a liquid crystal has been observed in measurements of macroscopic tensor properties, such as the diamagnetic susceptibility and the dielectric constant. For example, the diamagnetic susceptibility tensor $\chi_{d_1 d_2}$ (where d_1, d_2 are Cartesian indices that take values from the set $\{1, 2, 3\}$) that relates the response in magnetic moment $\boldsymbol{M}$ (arising from molecular diamagnetism) to an applied external field $\boldsymbol{H}$, via $M_{d_1} = \chi_{d_1 d_2} H_{d_2}$, is an isotropic tensor (i.e., $\chi_{d_1 d_2} \propto \delta_{d_1 d_2}$) when the state is isotropic, but takes on the following, anisotropic form (choosing the z-axis to be parallel to the direction of nematic alignment) when the state is nematic:

$$\chi_{d_1 d_2} = \begin{pmatrix} \chi_\perp & 0 & 0 \\ 0 & \chi_\perp & 0 \\ 0 & 0 & \chi_\parallel \end{pmatrix}.$$

It is useful define a tensor $S_{d_1 d_2}$ that is proportional to the anisotropic part of the diamagnetic susceptibility tensor, viz.,

$$S_{d_1 d_2} \equiv Q(\chi_{d_1 d_2} - \frac{1}{3}\delta_{d_1 d_2} \sum_{d_3=1}^{3} \chi_{d_3 d_3}) = \frac{Q}{3} \begin{pmatrix} -\chi_a/3 & 0 & 0 \\ 0 & -\chi_a/3 & 0 \\ 0 & 0 & 2\chi_a/3 \end{pmatrix}, \tag{1.2}$$

where $\chi_a \equiv \chi_\parallel - \chi_\perp$.

How can one relate $\chi_{d_1 d_2}$, which is a *macroscopic* quantity (with axes $d_1, d_2 = x, y, z$ defined in the laboratory frame, with z parallel to the direction of macroscopic nematic alignment) to the magnetic polarizability tensor A_{ij} of a single nematogen (where $i, j = a, b, c$ are the axes of the nematogen's coordinate frame, so defined that the c-axis is parallel to the long axis of the nematogen), which is a *microscopic* quantity? The two quantities are related via the following way. By defining a transformation tensor $i_{d_1} j_{d_2}$, where i_{d_1}, j_{d_2} are direction cosines between the set of axes fixed in the nematogen's frame (i, j) and the set of axes fixed in the laboratory frame (d_1, d_2), one can construct the expression

$$\chi_{d_1 d_2} = \rho \sum_{ij} A_{ij} \langle i_{d_1} j_{d_2} \rangle, \tag{1.3}$$

where ρ is the number of nematogens per unit volume, and the angle brackets denote averaging over the orientation distribution function $f(\theta)$. As we shall see, this relation allows one to determine how the diamagnetic susceptibility is related to the direction of macroscopic nematic alignment, which we continue to denote by the unit vector $\boldsymbol{n}$ (which we shall take here to be parallel to the axis of macroscopic alignment z), and the intensity of nematic alignment, given by the scalar quantity S. For the anisotropic part of $\chi_{d_1 d_2}$, one finds that

$$\chi_{d_1 d_2} - \frac{1}{3}\delta_{d_1 d_2} \sum_{d_3} \chi_{d_3 d_3} = \rho A_{ij} \left\langle i_{d_1} j_{d_2} - \frac{1}{3}\delta_{ij}\delta_{d_1 d_2} \right\rangle. \tag{1.4}$$

To determine χ_a in terms of the parameters of the nematogen's magnetic polarizability tensor A_{ij}, we set $d_1 = d_2 = z$. This allows one to obtain, from Eq. (1.4), the result

$$\chi_a = \rho(A_\parallel - A_\perp)S, \tag{1.5}$$

where $A_\parallel$ and $A_\perp$ are, respectively, the nematogen's magnetic polarizability computed along the nematogen's axis and the directions perpendicular to that axis. The value of the constant

Q in (1.2) can be chosen as $(\rho(A_\parallel - A_\perp))^{-1}$. One then obtains the tensor component expression

$$\begin{aligned}
\mathbf{S} &= Q\rho(A_\parallel - A_\perp)S \begin{pmatrix} -1/3 & 0 & 0 \\ 0 & -1/3 & 0 \\ 0 & 0 & 2/3 \end{pmatrix} \\
&= S \begin{pmatrix} -1/3 & 0 & 0 \\ 0 & -1/3 & 0 \\ 0 & 0 & 2/3 \end{pmatrix} \\
&= S(\boldsymbol{n} \otimes \boldsymbol{n} - \frac{1}{3}\mathbf{I}),
\end{aligned} \tag{1.6}$$

where $\mathbf{S}$ denotes a 3×3 matrix having components $S_{d_1 d_2}$, and $\mathbf{I}$ is the 3×3 identity matrix. This equation shows that the anisotropic part of the experimentally measurable diamagnetic tensor $\chi_{d_1 d_2}$ is proportional to the intensity of nematic alignment S, and its tensor components reflect the direction of macroscopic nematic alignment $\boldsymbol{n}$.

One can now proceed to construct a quantity, known as the Landau-de Gennes order parameter, that (i) detects the transition from the isotropic to the nematic state, and (ii) quantifies the amount of orientational anisotropy, bearing in mind that this quantity should coincide with the tensor $S_{d_1 d_2}$ in (1.6) for a system that is nematically aligned. Generalizing to D spatial dimensions, such a quantity is defined microscopically by the following real, traceless, and symmetric tensor,

$$\langle Q_{dd'}(\mathbf{r}) \rangle = \frac{V}{N} \left\langle \sum_{i=1}^{N} \left(\nu_d^i \nu_{d'}^i - D^{-1} \delta_{dd'} \right) \delta^{(D)}\left(\mathbf{r} - \mathbf{c}^i \right) \right\rangle, \tag{1.7}$$

where N is the number of rod-like units, ν^i is the microscopic unit orientation vector of unit i and $\mathbf{c}^i$ is its microscopic position vector, $\mathbf{r}$ is an arbitrary position vector, and the angular brackets $\langle \cdots \rangle$ denote averaging over the distribution function for ν^i and $\mathbf{c}^i$. The expectation

value of $\langle Q_{dd'}(\mathbf{r})\rangle$ is zero in the isotropic state, but in the nematic state it acquires the value given in Eq. (1.6).

Why do nematic liquid crystals undergo a phase transition from the isotropic state to a nematic state? At high temperatures, entropy considerations dominate, which means that the state is isotropic. On going to low temperatures, the nematogens align owing to both energetic and entropic reasons. Energetically, the nematogens may have dipole interactions which are minimized when the nematogens are parallel to one another; entropically, the alignment of nematogens also minimizes their total excluded volume, so that the phase space available for the motion of their centers-of-mass is maximized. (In the limiting case of very dense packing of nematogens, they can still translate past one another if they are stacked parallel to one another; unlike the case if the packing is dense and the nematogens are oriented randomly, which results in jamming.)

We now present a brief overview of the basic ideas behind three major theoretical approaches to the isotropic-nematic transition in liquid crystal systems:

- (i) the theory of Onsager; see Ref. [8],
- (ii) the theory of Maier and Saupe; see Refs. [9, 10, 11], and
- (iii) Landau-de Gennes theory; see Refs. [12, 1].

These approaches can be divided into two broad categories. The first two approaches belong to the class of theories that are *molecular-statistical* in nature, and are based on appropriate, specific models of molecular interactions. The third approach belongs to the class of *phenomenological* theories, which rely on Landau's fundamental insight that the free energy of a system near the phase transition can be expanded in powers of a small-valued order parameter. Such theories depend on symmetry considerations, and it may be prima facie difficult to assign a physical meaning to the coefficients of such a "Landau expansion" (though it is possible, in principle, to connect the coefficients to a molecular-statistical-based

model via procedures such as that of Hubbard and Stratonovich; an example will be given in Chapter 3).

1.1.1 The theory of Onsager

We first describe the physical idea behind the Onsager theory of the isotropic-nematic phase transition in liquid crystals. One can regard the nematogens as long, thin, *hard* cylinders, and correspondingly, the excluded-volume effects of such cylinders will not only depend on their center-of-mass positions, but importantly, also on their relative orientations. The total excluded volume of parallel cylinders is smaller than that of perpendicular cylinders, and thus one expects that for a sufficiently large volume fraction of such cylinders it would be entropically favorable for the cylinders to be aligned parallel to one another. Indeed, Onsager found [8] that such systems undergo a transition from the isotropic state to the nematic state when the parameter $(\ell/a)\phi$ exceeds a certain value, where ϕ is the volume fraction occupied by the cylinders, ℓ is the length of a cylinder, and a is the diameter of the cylinder.

Onsager's theory applies to lyotropic systems, i.e., those for which the nematic-isotropic phase transition is driven not by temperature but by excluded-volume effects via concentration. However, many actual liquid crystal systems are thermotropic, i.e., the phase transition is driven by temperature. To describe the phase transition behavior of thermotropic systems, one can turn to the approach of Maier and Saupe and the Landau-type theory of de Gennes.

1.1.2 The theory of Maier and Saupe

The theory of Maier and Saupe is analogous to the Weiss molecular field theory for the ferromagnetic transition. It assumes that the nematogens interact via van der Waals interactions, and makes no use of the consideration of position- and orientation-dependent excluded-volume effects. The two-body potential for two nematogens located at $\boldsymbol{c}$ and $\boldsymbol{c}'$ is

assumed to have the dipolar form:

$$U(\boldsymbol{c},\boldsymbol{c}',\boldsymbol{\nu},\boldsymbol{\nu}') = -B\,P_2(\cos\gamma)/|\boldsymbol{c}-\boldsymbol{c}'|^6, \tag{1.8}$$

where $P_2(x) \equiv \frac{1}{2}(3x^2-1)$ is the second-order Legendre polynomial, and γ is the angle between the unit vectors $\boldsymbol{\nu},\boldsymbol{\nu}'$ describing the alignment of the two nematogens. For $B>0$, such a potential favors parallel alignment. The Maier-Saupe theory makes the mean-field assumption that a given nematogen of position $\boldsymbol{c}$ and orientation $\boldsymbol{\nu}$ is subject to the mean potential $\langle U(\boldsymbol{c},\boldsymbol{c}_i,\boldsymbol{\nu},\boldsymbol{\nu}_i)\rangle_i$, i.e., $U(\boldsymbol{c},\boldsymbol{c}_i,\boldsymbol{\nu},\boldsymbol{\nu}_i)$ averaged over the positions and orientations of all other nematogens (which we shall label by i). Position-averaging gives a constant

$$b = \sum_i \langle B/|\boldsymbol{c}-\boldsymbol{c}_i|^6\rangle_{\boldsymbol{c}_i}; \tag{1.9}$$

and orientation-averaging over a distribution function $f_i \equiv f(\theta_i)$ leads to

$$\begin{aligned}
\langle P_2(\cos\gamma)\rangle_f &= \langle P_2(\boldsymbol{\nu}\cdot\boldsymbol{\nu}_i)\rangle_{f_i} \\
&= \frac{4\pi}{5}\sum_{m=-2}^{2}\langle \mathrm{Y}^*_{2,m}(\boldsymbol{\nu}_i)\rangle_{f_i}\mathrm{Y}_{2,m}(\boldsymbol{\nu}) \\
&= \frac{4\pi}{5}\langle \mathrm{Y}^*_{2,0}(\boldsymbol{\nu}_i)\rangle_{f_i}\mathrm{Y}_{2,0}(\boldsymbol{\nu}) \\
&= \left\langle \frac{3}{2}\cos^2\theta_i - \frac{1}{2}\right\rangle_{f_i}\left(\frac{3}{2}\cos^2\theta - \frac{1}{2}\right) \\
&= S\,P_2(\cos\theta),
\end{aligned} \tag{1.10}$$

where in the second line we have used a spherical-harmonic decomposition of $P_2(\boldsymbol{\nu}\cdot\boldsymbol{\nu}_i)$ (i.e., the addition theorem), in the third line we have observed that only the $m=0$ component does not vanish under averaging over the azimuthal angle, and in the fourth line we have made use of the definition (1.1) and defined $\cos\theta_i$ to be the angle that the i-th nematogen makes with a given macroscopically defined axis. Equations (1.9) and (1.10) imply that the

mean-field potential acting on a given nematogen is given by

$$U(\cos\theta, S) = -bS\, P_2(\cos\theta), \tag{1.11}$$

so that the probability distribution is given by

$$f(\cos\theta) = C \exp(-U(\cos\theta, S)/T), \tag{1.12}$$

where C is a normalization factor. We can now look for the occurrence of an isotropic-nematic transition by studying the location of the minimum of the free energy of liquid crystallization per nematogen,

$$\Delta F \equiv F(S \neq 0) - F(S = 0) = \mathcal{E} - T\mathcal{S}, \tag{1.13}$$

as T is varied ($F(S = 0)$ is typically taken to be zero). Here, $\mathcal{E} \equiv \langle U \rangle/2 = -bS^2/2$ is the internal energy per nematogen (the factor of $1/2$ is to compensate for double-counting the interaction), and $\mathcal{S}$ is the orientational entropy per nematogen, given by

$$\mathcal{S} = -\int f(\cos\theta) \ln[4\pi\, f(\cos\theta)]\, d\Omega = -(bS^2/T) - \ln(4\pi\, C). \tag{1.14}$$

We then obtain for the free energy,

$$\Delta F \equiv F(S \neq 0) - F(S = 0) = (bS^2/2) + T \ln(4\pi\, C). \tag{1.15}$$

The local minima of the free energy are determined via the condition $\partial \Delta F/\partial S = 0$. This leads to a self-consistent equation for S:

$$S = 2\pi\, C \int_0^\pi P_2(\cos\theta) \exp[-U(\cos\theta, S)/T] \sin\theta\, d\theta. \tag{1.16}$$

One can numerically solve this equation for a range of values of T. The result is that the free energy has a stable minimum at $S = 0$ (corresponding to the isotropic state) for $T > b/4.55$, and the free energy has a stable minimum at $S \geq 0.44$ (corresponding to the nematic state) for $T < b/4.55$. The phase transition is thus *discontinuous*, as S jumps from zero to a non-zero, non-infinitesimal value at the transition temperature.

1.1.3 Landau-de Gennes theory

We now turn to the Landau-de Gennes theory of the isotropic-nematic phase transition. The construction of this theory involves three steps: (i) determining a suitable order parameter that reflects the symmetries of the system; (ii) carrying out an expansion of the free energy density g of the liquid crystal system in powers of the order parameter, and heeding the dictum: those terms that are not forbidden by symmetry are mandatory; and (iii) determining the local minima of the free energy, for given thermodynamic conditions (such as temperature). We have already introduced the order parameter $\mathbf{Q}$, which reflects the symmetries of the state of the nematogens. De Gennes then constructed the Landau expansion of the free energy density as a sum of rotationally invariant combinations of $\mathbf{Q}$:

$$g(T) \approx g_0 + \frac{1}{2}A(T)\,\{\mathbf{Q}\,\mathbf{Q}\} - \frac{1}{3}B(T)\,\{\mathbf{Q}\,\mathbf{Q}\,\mathbf{Q}\} + \frac{1}{4}C(T)\,\{\mathbf{Q}\,\mathbf{Q}\,\mathbf{Q}\,\mathbf{Q}\}. \tag{1.17}$$

Here, curly brackets—as in $\{\mathbf{S}\,\mathbf{S}'\}$—indicate the trace of the product of the tensors $\mathbf{S}$ and $\mathbf{S}'$, i.e., $\sum_{d,d'=1}^{D} S_{dd'}S'_{d'd}$. The terms in the Landau expansion are invariant under operations of symmetry of the nematic phase, as well as global rotations in space. The presence of a cubic-order term causes the isotropic-nematic phase transition to be discontinuous. To determine the *simplest possible* functional dependence of the coefficients A, B and C on temperature that would lead to the prediction of a phase transition, one argues "retrodictively" (i.e., "backwards") as follows: as the system is isotropic at high T and nematic at low T, we define A to be positive at high T and negative at low T, as this would result in the free

energy being minimized at $S = 0$ at high T and at $S \neq 0$ at low T. One aims for the simplest form of A that exhibits such behavior: it is given by writing A as a linear function of T: $A(T) = a(T - T^*)$. If the phase transition were continuous, T^* would have the meaning of the mean-field phase transition temperature; but for a discontinuous transition, T^* demarcates the phenomenological limit of metastability of the isotropic phase as the system is cooled, and this temperature is called the spinodal temperature. For simplicity, we assume that a, B and C are temperature-independent. To determine the temperature T_c at which the system undergoes a transition from the nematic to the isotropic state (as T is increased), we first insert (1.6) into (1.17); this gives

$$g = g_0 + \frac{1}{3}a(T - T^*)S^2 - \frac{2}{27}BS^3 + \frac{1}{9}CS^4. \tag{1.18}$$

The temperature T_c and the corresponding value S_c of S are then determined from the simultaneous conditions that the free energy densities of the two states be equal, and that g be minimized with respect to S. Thus, one finds that $T_c = T^* + (B^2/27aC)$ and $S_c = (B/3C)$. This completes our introduction to the basic physics of nematic liquid crystallinity.

1.2 Polymers and elastomers

What are elastomers and how are they formed? To answer this question, one should be acquainted with polymers, which are the basic building blocks of elastomers. Polymers are very long, flexible, chain molecules, made up of many small groups of atoms which have been essentially permanently combined in a given way. Each repeating small group is called a monomer. A typical polymer may consist of thousands of monomers. A polymer chain molecule can have a huge number of conformations. This is because of *stereoisomerism*. Consider the polyethylene molecule (see Fig. 1.2). This molecule is made out of repeating units of atoms, each unit consisting of one carbon atom and two hydrogen atoms. Each

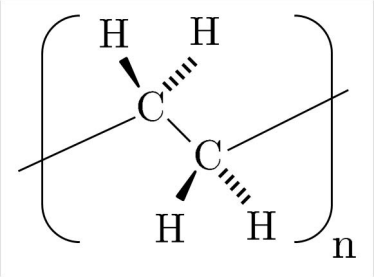

Figure 1.2: The repeating unit of polyethylene, showing its stereochemistry.

pair of carbon atoms (from adjacent repeating units) has an essentially constant separation $1.54\,\mathring{A}$, and the angle between neighboring carbon-carbon bonds is also essentially constant (at 68^o). However, the angle of a given carbon-carbon bond around the axis defined by its neighboring carbon-carbon bond (which we call the torsion angle) can vary. Thus, if the energy barrier between different choices of the torsion angle is comparable to or smaller than the thermal energy (set by the temperature T), the polymer can adopt a variety of torsional angles, and this makes accessible a huge number of polymer conformations at the given temperature.

To investigate the properties of polymers at length-scales much larger than the effective bond length ℓ_p (which is the length-scale of short-range relative orientational correlations of monomers along the polymer), and given that the arc-length L of a polymer chain molecule is much larger than ℓ_p, one can work with an idealized model in which polymers are regarded as the trajectories of a random walk. In three spatial dimensions, the distribution function of conformations of such a polymer is given by the Wiener distribution, viz.

$$\Phi(\boldsymbol{R}) \propto \exp\left(-\frac{3}{2\ell_p}\int_0^L d\sigma \left|\frac{d\boldsymbol{R}(\sigma)}{d\sigma}\right|^2\right), \tag{1.19}$$

where $\boldsymbol{R}(\sigma)$ denotes the position vector of a monomer situated an arc-length distance of σ from one end of the polymer. The Wiener distribution describes a Gaussian distribution of polymers, with a vanishing mean value for the end-to-end distance of a polymer, $\langle \boldsymbol{R}(L) - \boldsymbol{R}(0)\rangle = 0$, and a mean-square value $\langle |\boldsymbol{R}(L) - \boldsymbol{R}(0)|^2\rangle = L\,\ell_p$.

A more accurate model of the polymer has distinct monomers not occupying the same position in space, and thus the Wiener model should be augmented by an excluded-volume interaction term. The resulting model is known as the *Edwards model* [59], and it is described by the following distribution function,

$$\Phi(\boldsymbol{R}) \propto \exp\left(-\frac{3}{2\ell_p}\int_0^L d\sigma \left|\frac{d\boldsymbol{R}(\sigma)}{d\sigma}\right|^2 - \frac{u_0}{2\ell_p^2}\int_0^L d\sigma \int_0^L d\sigma'\, \delta(\boldsymbol{R}(\sigma) - \boldsymbol{R}(\sigma'))\right), \qquad (1.20)$$

where u_0 is a parameter proportional to the volume excluded as a result of the short-ranged monomer-monomer repulsion.

1.2.1 Gelation, vulcanization, and elasticity

When a sufficiently large fraction of polyfunctional units (i.e., molecules containing more than one group of atoms that can chemically react with certain reagents to form compounds) are *permanently* bonded together (meaning that the bonds do not break on experimentally accessible time-scales), the system can undergo what is known as permanent gelation, in which a single, giant macromolecule is formed that spans the entire volume of the space containing the monomers. *Vulcanization* is a special case of permanent gelation, in which the polyfunctional units are long, flexible polymers, and the bonding is made via cross-linkers (e.g., short chains of sulfur atoms in rubber) which are *permanent* and join *randomly chosen* pairs of monomers. An *elastomer* (commonly known as rubber) is a material formed by such a vulcanization process. *Vulcanized* rubber is an elastically rigid network medium characterized by having a non-zero static shear modulus, implying that under the application of a static shear stress, the network would respond by undergoing a static shear strain. This is to be distinguished from the case of *pure* rubber, essentially an uncross-linked polymer melt or an insufficiently cross-linked system, which is a visco-elastic liquid. This means that under the application of a shear stress, pure rubber would respond by flowing.

The property of elasticity, characteristic of sufficiently vulcanized rubber, can be under-

stood as an *entropic* effect, which is reflected in the fact that the shear modulus of vulcanized rubber depends on temperature. We can understand this entropic effect via the random walk picture of a polymer chain (with $N_m \equiv L/\ell_p$ monomers envisioned as "steps" each of length ℓ_p). In three spatial dimensions, the mean square of the end-to-end vector $\boldsymbol{R}$ for a random walk of N_m steps is given by

$$\langle R_d^2 \rangle = \langle |\boldsymbol{R}|^2 \rangle / 3 = \ell_p^2 N_m / 3, \tag{1.21}$$

where d $(= 1, 2, 3)$ are the Cartesian indices. The random-walk model of polymer chains leads to a Gaussian probability $P(\boldsymbol{R})$ for finding that a single chain conformation has an end-to-end vector $\boldsymbol{R}$:

$$P(\boldsymbol{R}) = \left(\frac{3}{2\pi R_0^2} \right)^{-3/2} \exp(-3R^2/2R_0^2), \tag{1.22}$$

where $R \equiv |\boldsymbol{R}|^2$ and $R_0 \equiv N_m \ell_p^2$. The free energy $F(\boldsymbol{R})$ for a chain having end-to-end vector $\boldsymbol{R}$ is then given by $F(\boldsymbol{R}) = -T \ln Z(\boldsymbol{R}) = 3TR^2/2R_0^2$ [up to an additive constant; we have used the fact that the partition function $Z(\boldsymbol{R})$ is proportional to $P(\boldsymbol{R})$].

To obtain the shear modulus of a system of vulcanized rubber (that consists of N polymer chains), and to see how it depends on temperature, one can consider, for simplicity, the classical theory of rubber elasticity, developed by Kuhn, Wall and Flory (see, e.g., Refs. [3]). The classical theory makes the following four assumptions. The first assumption is that polymer chains can be modeled as random walks. Secondly, the classical theory assumes there is no change in the volume of the system on deformation. Thirdly, the classical theory also assumes that the positions of the junctions of the polymer chains are fixed in a non-fluctuating elastic background medium, and the separation $\boldsymbol{R}$ between a given pair of junctions changes *affinely* to a new value $\boldsymbol{R}'$ when the medium is deformed:

$$R_d \to R'_{d'} \equiv \Lambda_{dd'} R_{d'} \tag{1.23}$$

where the deformation gradient $\Lambda_{dd'} \equiv \partial R'_d/\partial R_{d'}$, and volume conservation implies $\det \underline{\underline{\Lambda}} = 1$. The fourth assumption holds that the entropy of the network is equal to the sum of the entropies of constituent chains. Now, for the particular case of uniaxial strain, the deformation gradient is specified by

$$\underline{\underline{\Lambda}} = \begin{pmatrix} \lambda & 0 & 0 \\ 0 & 1/\sqrt{\lambda} & 0 \\ 0 & 0 & 1/\sqrt{\lambda} \end{pmatrix},$$

where the first diagonal entry means the rubber is being stretched (for $\lambda > 1$) by a factor λ in one (longitudinal) direction, whereas the second and third diagonal entries mean that it is simultaneously also being shrunk by a factor $1/\sqrt{\lambda}$ in the remaining two (transverse) directions. Under uniaxial deformation, the average free energy of a system of N chains under deformation is given by $F = 3NT\langle \boldsymbol{R}^{\mathrm{T}} \cdot \Lambda^{\mathrm{T}} \cdot \Lambda \cdot \boldsymbol{R} \rangle_{P(\boldsymbol{R})}/2R_0^2 = NT\,\mathrm{Tr}(\Lambda^{\mathrm{T}} \cdot \Lambda)/2$, where $\langle \cdots \rangle_P$ denotes an average over the Gaussian distribution P. (In deriving the free energy of the deformed collection of chains, this approach makes use of the elementary result $\langle R_d R_{d'} \rangle_P = \delta_{dd'} R_0^2/3$.) The shear modulus is then given by the coefficient of $\mathrm{Tr}(\Lambda^T \Lambda)/2$ in the free energy expression, viz., NT, which reveals an explicit linear dependence on temperature.

1.2.2 Theory of vulcanization

The classical theory of elasticity, just described, cannot be used to study the actual phenomenon of the gelation or vulcanization transition. To explain the occurrence of the gelation/vulcanization, various approaches based on the idea of percolation have been proposed by several workers. For example, the approach described by de Gennes [13] views the gelation transition essentially as a problem of percolation on a regular lattice. In it, a polymer chain is modeled as a set of "beads"occupying a number of lattice sites in a connected manner. Two chains are said to intersect if they have at least one site in common. One assumes that

two chains are cross-linked if they intersect one another. A set of intersecting chains is said to form a finite cluster if it does not span the entire lattice. Denoting the number of beads per site by c, the chains will start to overlap with one another and larger and larger clusters will form as c increases. Above a critical value of c, an infinite cluster forms, and percolation is said to have occurred. The strengths of the percolative model include its ability to explain certain experimental facts, such as the fact that at the vulcanization transition, a non-zero fraction of the monomers becomes bonded to form an infinite cluster. On the other hand, the percolative model does not explain the phenomenon of *elasticity*, which accompanies vulcanization (manifested in the system's acquisition of a non-zero shear modulus). As the classical theory of elasticity (described in the previous subsection) indicates, elasticity is intimately related to the entropy of conformations of polymer chains, which is missed out in the percolation picture. It thus appears unsatisfactory that one invokes the classical theory of elasticity when describing the *elastic* properties of rubber, and separately invokes percolation theory for understanding the *connectivity* or architecture of the vulcanization transition. A more complete theory of rubber should be able to account for both aspects, simultaneously.

Thus, we now turn to consider a more fundamental approach to the theory of the vulcanization transition, one that not only predicts the onset of percolation, but also predicts the acquisition by the system of elasticity at the vulcanization transition point. We shall call this approach "vulcanization theory" (see, e.g., [6]). This approach is rooted in the microscopic formulation of the statistical mechanics of rubber by Deam and Edwards [35] as well as the theory of spin glasses by Edwards and Anderson [36]. Based on the theoretical foundations and physical insights provided by these works, Goldbart and co-workers have investigated the critical behavior at the vulcanization transition as well as the structure and elastic behavior of the emergent random solid state, via polymer- and particle-based microscopic models (see, e.g., [6, 62]), symmetry-based Landau theory [7], and renormalization-group techniques [30].

We shall convey the main ideas of vulcanization theory by reviewing the Landau theory

of vulcanization described in [7]. In common with Landau theories of phase transitions, such as the isotropic-to-nematic phase transition reviewed in Sec. 1.1.3, the vulcanization transition, which is an equilibrium phase transition from a liquid state (in which the particles are spatially delocalized) to a random solid state (in which a macroscopic fraction of particles are spatially localized about certain *random* mean positions with *finite* but *random* r.m.s. displacements around their mean positions), is described by means of an order parameter. To construct the order parameter for the vulcanization transition, one may first think of using the particle density,[1] but this is not an appropriate order parameter as the system's density (after having averaged over the random realizations of the cross-linking constraints) is uniform in the random solid state, as it is in the liquid state. Instead, one considers the following Edwards-Anderson-like function of $1+n$ wave-vectors $\{\boldsymbol{k}^0, \ldots, \boldsymbol{k}^n\}$:

$$\left[\sum_{j=1}^{N} \langle e^{i\boldsymbol{k}^0\cdot\boldsymbol{c}_j}\rangle_\chi \ldots \langle e^{i\boldsymbol{k}^n\cdot\boldsymbol{c}_j}\rangle_\chi\right], \tag{1.24}$$

where $\hat{k}$ is the $(1+n)$-fold replicated wave-vector $(\boldsymbol{k}^0, \ldots, \boldsymbol{k}^n)$, N is the total number of particles, $\boldsymbol{c}_j$ is the position vector of particle j $(j = 1, \ldots, N)$, the angular brackets $\langle\cdots\rangle_\chi$ denotes the thermal expectation value for a given realization χ of the quenched disorder (i.e., the cross-linking constraints), and $[\cdots]$ denotes a suitable average over realizations of the quenched disorder. Equivalently, in real space, the function in (1.24) takes the form

$$\left[\sum_{j=1}^{N} \langle \delta(\boldsymbol{r}^0 - \boldsymbol{c}_j)\rangle_\chi \ldots \langle \delta(\boldsymbol{r}^n - \boldsymbol{c}_j)\rangle_\chi\right], \tag{1.25}$$

The order parameter for the vulcanization transition is given by $\langle\Omega\rangle$. In Fourier space, $\langle\Omega\rangle$ is defined by

$$\langle\Omega_{\hat{k}}\rangle \equiv \frac{1}{N}\left[\sum_{j=1}^{N} \langle e^{i\boldsymbol{k}^0\cdot\boldsymbol{c}_j}\rangle_\chi \ldots \langle e^{i\boldsymbol{k}^n\cdot\boldsymbol{c}_j}\rangle_\chi\right] - \prod_{\alpha=0}^{n} \delta_{\boldsymbol{k}^\alpha,\boldsymbol{0}}. \tag{1.26}$$

[1] Here, we are using the terms "particle" and "polymer" interchangeably, as the difference is one of microscopic detail. At large lengthscales, such being the case when the system is weakly cross-linked and thus near the vulcanization transition point, such microscopic differences become unimportant.

When all the particles are delocalized, every factor $\langle e^{i\boldsymbol{k}\cdot\boldsymbol{c}_j}\rangle_\chi$ has the value $\delta_{\boldsymbol{k},\boldsymbol{0}}$ (by the translational invariance of the state), and the order parameter $\Omega_{\hat{k}}$ takes the value zero, which characterizes the liquid state. On the other hand, in the random solid state, one expects that a non-zero fraction of particles are localized. We shall call the fraction of localized particles the gel fraction, and denote it by G. The gel fraction is found by carefully taking the $\boldsymbol{k}^\alpha \to \boldsymbol{0}$ limit of $\Omega_{\hat{k}}$. [2] For particles which are localized with mean position vectors $\langle \boldsymbol{c}_j \rangle \equiv \boldsymbol{b}_j$ and undergoing thermal excursions around their mean positions with localization lengths (or r.m.s. displacements) ξ_j, one may approximate

$$\langle \exp(i\boldsymbol{k}\cdot\boldsymbol{c}_j)\rangle_\chi \approx \exp(i\boldsymbol{k}\cdot\boldsymbol{b}_j - \frac{1}{2}k^2\xi_j^2). \tag{1.27}$$

This approximation is good if one is interested in studying properties of the system at lengthscales much larger than the typical localization lengthscale. The distribution of mean positions $\boldsymbol{z}$ and localization lengths ξ of the localized particles is given by

$$P(\boldsymbol{z},\xi) = \frac{1}{GN}\sum_{j\in\text{loc.}}[\delta(\boldsymbol{z}-\boldsymbol{b}_j)\delta(\xi-\xi_j)], \tag{1.28}$$

where $\sum_{j\in\text{loc.}}$ refers to a sum over the localized particles. We assume that the mean positions of the localized particles are distributed independently of how the localization lengths are distributed, i.e.,

$$P(\boldsymbol{z},\xi) = P(\boldsymbol{z})P(\xi). \tag{1.29}$$

Using Eqs. (1.27), (1.28) and (1.29), one can express Eq. (1.26) as

$$\langle\Omega_{\hat{k}}\rangle = G\int d\boldsymbol{z}\, d\xi\, P(\boldsymbol{z})P(\xi)\, e^{i\tilde{\boldsymbol{k}}\cdot\boldsymbol{z}-\frac{1}{2}|\hat{k}|^2\xi^2} + \frac{1}{N}\left[\sum_{j\in\text{deloc.}}\langle e^{i\boldsymbol{k}^0\cdot\boldsymbol{c}_j}\rangle_\chi \ldots \langle e^{i\boldsymbol{k}^n\cdot\boldsymbol{c}_j}\rangle_\chi\right] - \delta_{\hat{k},\hat{0}}, \tag{1.30}$$

[2] This can be understood as follows. If a particle at position $\boldsymbol{c}$ is delocalized, any non-zero value of $\boldsymbol{k}$, however small, will cause the "phase factor" $e^{i\boldsymbol{k}\cdot\boldsymbol{c}}$ to take on different values as $\boldsymbol{c}$ ranges over all space, and thus $\langle e^{i\boldsymbol{k}\cdot\boldsymbol{c}}\rangle_\chi = 0$; on the other hand, if a particle is localized, taking the limit $\boldsymbol{k}^\alpha \to \boldsymbol{0}$ will give unity to the phase factor. Thus in taking this limit, one is actually counting the fraction of localized particles.

where $\sum_{j\in\text{deloc.}}$ refers to a sum over the delocalized particles,

$$\tilde{\boldsymbol{k}} \equiv \sum_{\alpha=0}^{n} \boldsymbol{k}^{\alpha}, \tag{1.31}$$

$|\hat{k}|^2 \equiv \sum_{\alpha=0}^{n} |\boldsymbol{k}^{\alpha}|^2$, and $\delta_{\hat{k},\hat{0}} \equiv \prod_{\alpha=0}^{n} \delta_{\boldsymbol{k}^{\alpha},\boldsymbol{0}}$. Noting that the term

$$\frac{1}{N}\left[\sum_{j\in\text{deloc.}} \langle e^{i\boldsymbol{k}^0\cdot\boldsymbol{c}_j}\rangle_{\chi} \ldots \langle e^{i\boldsymbol{k}^n\cdot\boldsymbol{c}_j}\rangle_{\chi}\right] = \frac{1}{N}(N - GN)\delta_{\hat{k},\hat{0}}, \tag{1.32}$$

and using the fact that the system is statistically homogeneous, which implies that $P(\boldsymbol{z}) = 1/V$, one obtains

$$\langle \Omega_{\hat{k}} \rangle = G\delta_{\sum_{\alpha=0}^{n}\boldsymbol{k}^{\alpha},\boldsymbol{0}} \int_0^{\infty} d\tau P(\tau) \exp\left(-\sum_{\alpha=0}^{n} |\boldsymbol{k}^{\alpha}|^2/2\tau\right) - G\prod_{\alpha=0}^{n} \delta_{\hat{k},\hat{0}}, \tag{1.33}$$

where $\tau \equiv 1/\xi^2$ is the inverse square localization length, $P(\tau)$ is the distribution (reflecting the heterogeneity of the random solid) of the inverse localization lengths, and the number G is the gel fraction, i.e. the fraction of particles that are localized. We check that this Ansatz reflects the properties of a system that undergoes the vulcanization transition: in the liquid state the localization lengths are all infinite, and the first term of (1.33) vanishes unless $\boldsymbol{k}^{\alpha} = \boldsymbol{0}$. This implies that the value of $\langle \Omega_{\hat{k}} \rangle = 0$ in the liquid state. (One can also see this from another perspective: in the liquid state, the fraction G of localized particles is zero, so $\langle \Omega_{\hat{k}} \rangle = 0$.) On the other hand, as we have explained earlier, the gel fraction in the random solid state can be found by taking the limit $\boldsymbol{k}^{\alpha} \to \boldsymbol{0}$ in Eq. (1.26). When this limit is taken in (1.33), one obtains $\langle \Omega_{\hat{k}} \rangle = G$, which agrees with our requirement. The Kronecker delta in the first term of Eq. (1.33) reflects the fact that the random phase factors $\exp i\tilde{\boldsymbol{k}} \cdot \boldsymbol{z}$ in the first term of Eq. (1.30) adds up destructively when one sums over $\boldsymbol{z}$, unless the wave-vector sum is equal to zero. In real space, an elementary Fourier transform shows that the Ansatz

(1.33) becomes

$$\langle \Omega(\hat{r}) \rangle = G \int \frac{d\boldsymbol{z}}{V} \int d\tau P(\tau) \left(\frac{\tau}{2\pi} \right)^{(1+n)D/2} e^{-\frac{\tau}{2} \sum_{\alpha=0}^{n} |\boldsymbol{r}^{\alpha} - \boldsymbol{z}|^2} - \frac{G}{V^{1+n}}. \tag{1.34}$$

This form enables one to see that $\Omega^{\alpha}(\boldsymbol{r}^{\alpha}) \equiv \prod_{\alpha \neq \beta} \int d\boldsymbol{r}^{\beta} \Omega(\hat{r})$ vanishes. As we shall explain in Appendix B, this vanishing reflects the local incompressibility of the elastomer. Thus, in serving as an appropriate order parameter the argument of $\Omega_{\hat{k}}$ is restricted to having values drawn only from the "higher replica sector" (HRS), i.e., the set of replicated vectors $\{\boldsymbol{k}^0, \ldots, \boldsymbol{k}^n\}$ with more than one non-zero vector entry. In addition, we note the following points:

(i) As we explain in greater detail in Sec. 3.2, one can identify the zeroth replica in $\langle \Omega(\hat{r}) \rangle$ as describing the preparation ensemble, i.e., the thermodynamic ensemble of the system at the instant of cross-linking, where cross-links have formed between particles (ultimately resulting in the localization of some fraction G of particles).

(ii) The Ansatz assumes that the mean position of a given particle in the system long after the cross-linking was done coincides with its position at the instant of cross-linking, thus omitting the effects of random displacements (the randomness owing to the spatial heterogeneity present in a real elastomer) undergone by particles as the system relaxes to a mechanically equilibrated state after cross-linking.

Bearing in mind the scalar character of the vulcanization order parameter and the fact that its argument takes values from the HRS, one can now write down, based on symmetry and lengthscale considerations, a Landau free energy $H[\Omega]$ for the vulcanization transition. The Landau free energy should be invariant under independent translations and rotations of each replica. It is given by (cf. Ref. [7])

$$H = \overline{\sum_{\hat{k}}} \left(-\epsilon + \frac{1}{2} |\hat{k}|^2 \right) \Omega_{\hat{k}} \Omega_{-\hat{k}} - c \overline{\sum}_{\hat{k}_1, \hat{k}_2, \hat{k}_3} \Omega_{\hat{k}_1} \Omega_{\hat{k}_2} \Omega_{\hat{k}_3} \delta_{\hat{k}_1 + \hat{k}_2 + \hat{k}_3, \hat{0}}, \tag{1.35}$$

where $\overline{\sum}_{\hat{k}}$ denotes a sum over replicated wave-vectors belonging to the HRS, and the wave-vectors have been expressed in terms of some basic lengthscale (such as that of the radius of gyration of a single uncross-linked polymer). We see that there is at least a linear instability when $\epsilon < 0$, and this instability occurs in the HRS, implying that the associated phase transition is related to the change in correlations between the various replicas. The mean-field theory corresponds to the solution of the stationarity point equation,

$$\frac{\delta H}{\delta \Omega_{-\hat{k}}} = 0 \Rightarrow (-\epsilon + \frac{1}{2}|\hat{k}|^2)\Omega_{\hat{k}} - c\overline{\sum_{\hat{k}'}} \Omega_{\hat{k}'}\, \Omega_{\hat{k}-\hat{k}'} = 0. \tag{1.36}$$

For all ϵ, this equation has the solution $\Omega_{\hat{k}} = 0$, and this is globally stable for $\epsilon < 0$, and corresponds to the liquid state. For $\epsilon > 0$, a non-zero value of $\Omega_{\hat{k}}$ becomes stable, corresponding to the emergence of the random solid state. We substitute the physically motivated Ansatz for $\Omega_{\hat{k}}$ into this stationarity point equation, and thereby obtain stationarity conditions on G and $P(\tau)$. The stationary value of G is given, for $\epsilon > 0$, by

$$G = \frac{2\epsilon}{3}. \tag{1.37}$$

From the results of microscopic calculations (see, e.g., Refs. [6, 62]), one finds that $\epsilon \propto (\eta^2 - 1)$ (where η^2 is the number of cross-links per polymer). This implies the physically reasonable scenario in which the gel fraction increases with an increase in the strength of cross-linking.

From the stationarity condition one also obtains an integro-differential equation for the distribution of localization lengths:

$$\frac{\tau^2}{2}\frac{dP(\tau)}{d\tau} = \left(\frac{\epsilon}{2} - \tau\right) P(\tau) - \frac{\epsilon}{2}\int_0^\tau d\tau_1\, P(\tau_1)\, P(\tau - \tau_1). \tag{1.38}$$

One can simplify the equation by choosing the scaling variables

$$P(\tau) = (2/\epsilon)\pi(\theta); \qquad \tau = (\epsilon/2)\theta. \tag{1.39}$$

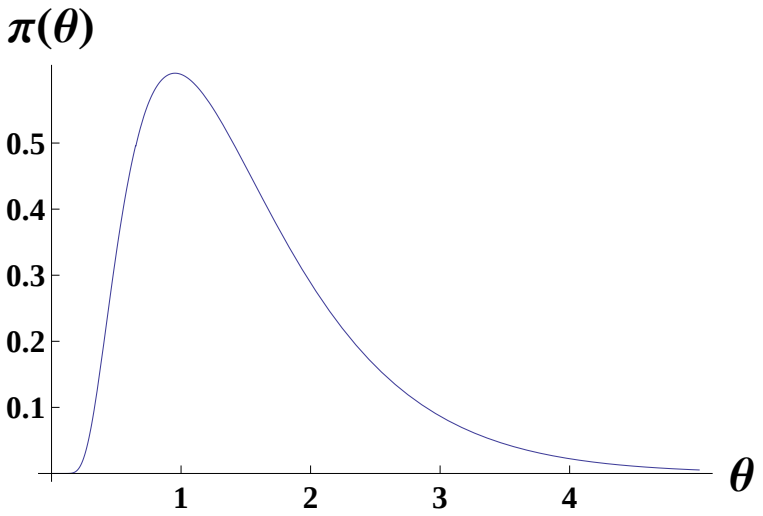

Figure 1.3: The function $\pi(\theta)$ governing the scaling of the probability distribution $P(\tau)$ of inverse square localization lengths.

The integro-differential equation then becomes

$$\frac{\theta^2}{2}\frac{d\pi}{d\theta} = (1-\theta)\pi(\theta) - \int_0^\theta d\theta'\,\pi(\theta')\,\pi(\theta-\theta'). \tag{1.40}$$

By solving this equation subject to the normalization constraint $\int_0^\infty d\theta\,\pi(\theta)$, one can derive the scaling function $\pi(\theta)$. One finds that this function decays rapidly as $\theta \to 0$ and $\theta \to \infty$, and in addition has a peak at $\theta \approx 1$ with a width of order unity (cf. Fig. 1.3), which implies [via Eq. (1.39)] that the typical localization length scales as $\epsilon^{-1/2}$ near the vulcanization transition.

1.3 Nematic elastomers

Having given an overview of the main ideas and approaches to the physics of nematic *liquid* crystals and of *elastomers*, we are now in a position to describe the physics of *nematic elastomers*. A nematic elastomer is a material formed by randomly and permanently cross-linking a large number of *liquid crystalline* polymers (LCP), until the system becomes a solid. A liquid crystalline polymer is a polymer containing rod-like units that are stiffer than the

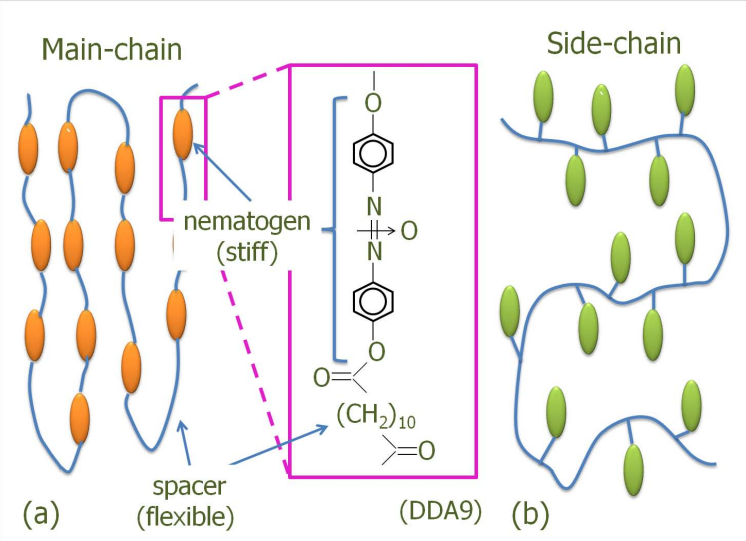

Figure 1.4: Two types of liquid-crystalline polymers (LCPs): (a) main-chain LCP; (b) side-chain LCP. An LCP consists of stiff, nematogenic units as well as more flexible chains, known as spacers. Here, solid ellipses represent the nematogenic units, and blue connecting lines represent spacers. Inset: an example of a segment of an LCP given by DDA9, consisting of a stiff, nematogenic unit and a flexible chain, the flexible chain consisting of repeated CH_2 units.

polymer backbone, and thus act as nematogens; such polymers can be categorized into two classes, depending on how the nematogens are attached to the more flexible polymer backbone. If the nematogens are connected together by means of more flexible elements known as spacers then one has the *main-chain* type of LCP. If, on the other hand, the nematogens are attached to a flexible polymer backbone as side groups then one has the *side-chain* type of LCP; see Fig. (1.4). Nematic elastomers thus possess both elasticity and some form of the orientational organization of liquid crystals (such as the ability to undergo a phase transition from an isotropic to a nematic state upon lowering the temperature).

Owing to the interplay between nematic and elastic degrees of freedom, nematic elastomers exhibit elastic and structural properties that are more exotic than one might anticipate. For example, the monodomain version of a nematic elastomer (i.e., one in which there is a direction along which nematogens are aligned on average) is characterized by a remarkable softness in its elasticity; see Refs. [16, 18, 19, 17, 20, 5]: the sample can undergo

a finite strain at no cost in elastic energy. This results from the strong coupling between the orientational order of liquid crystallinity and the elasticity of the polymer network. In particular, the alignment of the constituent mesogens influences—and is influenced by—the macroscopic shape of the nematic elastomer sample. Furthermore, the nematic alignment can be re-oriented along the stretching direction as a result of an externally imposed deformation. There can also be a spontaneous uniaxial deformation in response to external factors, such as temperature and light irradiation, that affect the orientational order parameter.

The example of soft elasticity, just discussed, gives us a foretaste of how the elastic and orientational properties of nematic elastomers can crucially depend on the way they are prepared. There are three principal preparation schemes. The first is the two-step cross-linking procedure of Küpfer and Finkelmann [15], in which the sample is lightly cross-linked in the isotropic state, then cooled to the nematic state, then stretched so that the system acquires uniform nematic alignment, and then cross-linked again to trap in this alignment. What results is a *monodomain nematic elastomer*, as it exhibits essentially uniform macroscopic nematic alignment. The second method involves the direct cross-linking of the system when it is in the nematic state. The resulting product is called a *nematic-genesis nematic elastomer* (NGNE). The third method is to directly cross-link the system in the isotropic state. The resulting product is called an *isotropic-genesis nematic elastomer* (IGNE). Macroscopically, the state is then isotropic, but locally there are domains of nematic alignment, typically of a micron or so in size, which are orientationally anti-correlated over distances of the order of 10 microns; see Refs. [28, 5, 51]. We shall employ the term *polydomain state* to refer to the kind of equilibrium state observed in IGNEs. Nematic elastomers also "memorize" both the positions of the chain segments and the orientations of the nematogen units at the instant of cross-linking. This memorization is, however, only partial, as a result of the thermal fluctuations that occur in the new, post-cross-linking equilibrium state; the strength of this memorization will depend on factors such as the temperature at which the system was cross-linked as well as the average number of cross-links per polymer [28].

What ingredients should a theory of nematic elastomers include? To appreciate the complexity and difficulty associated with the task of describing nematic elastomers theoretically, one should be mindful of the following features of nematic elastomers:

(i) The existence of *quenched* freedoms (i.e., random variables that are effectively fixed for a given sample but vary randomly from sample to sample), in addition to *thermal* (or *annealed*) freedoms (i.e., freedoms that relax on time-scales substantially shorter than experimental observations).

(ii) The existence of three levels of disorder, viz., (a) the quenched randomness just mentioned, associated with the permanent chemical structure originating in the random cross-linking process, (b) the *emergent* randomness in the mean positional and displacement statistics of the polymers that constitute the network medium, and (c) the familiar thermal randomness, associated with the Brownian positional and/or orientational motion of the constituents.

(iii) The presence of a large number (at least of the order of the Avogadro number) of nematogens and polymers, all of which undergo thermal fluctuations and interact with one another.

(iv) The dependence of the measured properties of a nematic elastomer on its statistical state at the instant of preparation.

These complexities enrich the study of nematic elastomers but also renders it more challenging. We now mention how certain ideas and methods have been adopted in this thesis in order to address the four challenging features of nematic elastomers noted above. Such ideas and methods will be developed and explained more fully in subsequent chapters. The presence of a large number of thermally fluctuating freedoms that interact with one another, indicated in (iii), implies that it would be impossible to determine the macroscopic properties of the system by computing the individual trajectories of constituent particles. In common with theoretical studies of other systems involving large numbers of particles, such as ferromagnets or liquids, a theoretical study of nematic elastomers should aim for a *statistical*

description, where one speaks of the probability of obtaining a certain physical configuration, rather than of the dynamics of particles at the microscopic level. Approximation schemes based on the use of perturbation theory can be utilized, once certain suitable, small physical parameters have been identified. In order to decouple these interacting freedoms, one may adopt a scheme that involves transforming the *discrete* problem of interacting *particles* into a *continuum* problem of interacting *fields*, and determining a saddle-point solution which corresponds physically to the case where there are no correlations between field fluctuations, and the effect of weak correlations is then computed via perturbations around the saddle-point solution. With regard to decoupling the large number of interacting particles, the approximation scheme employed by the present thesis is the Hubbard-Stratonovich decoupling scheme (which converts the discrete problem into a continuum field theory, which has the virtue of being amenable to the field theorist's toolkit). This necessitates the definition of collective fields. This is explained in Chapter 3. We shall see how the Ansatz of the saddle-point solution, proposed in Chapter 3, describes the second, emergent, level of randomness indicated in feature (ii–a). The other two levels of randomness are also taken into account by the theory described in the same chapter. In addition, to address the issue of quenched disorder, mentioned in (i), we have adopted a technique known as the replica method. Instead of an effective Hamiltonian, we shall be studying an effective replica Hamiltonian (see Secs. 2.4 and 4.2). As a result of using the replica method, one proceeds by studying the statistical mechanics of $1 + n$ thermodynamic ensembles or "replicas" of a system in which quenched disorder is absent. The application of replicas also takes care of the issue described in feature (iv); one of the replicas corresponds to the state of the system at the instant of preparation, whilst the other n replicas correspond to the state of the system when it is measured. The dependence of the measured properties on the state of the system at preparation corresponds, operationally, to the coupling in the effective replica Hamiltonian between freedoms belonging to the "preparation replica" and ones belonging to a "measurement replica".

1.4 Purpose of the present work

What issues does the present thesis aim to address? The first issue has to do with understanding the microscopic origin and stability of the macroscopically isotropic state (of which the polydomain state is a particular instance) observed in IGNEs. So far, work in this direction (see, e.g., Refs. [23, 22, 24, 25, 52]) have mostly adopted random-field models (reflecting the randomness originating in the spatially varying orientational anisotropy induced by cross-linking). The models implicitly assume that the network medium is not thermally fluctuating. However, for real elastomers, one should allow for the action of thermal fluctuations of the polymer network. We shall see that allowing this enables one to predict, for a suffiently strongly cross-linked IGNE, a novel type of nematic correlation behavior that is both oscillatory and decaying in real space, in addition to the more familiar type of simple exponential decay behavior that one encounters in nematic liquid crystals.

The second issue has to do with how to capture theoretically aspects of the memorization capability of an IGNE. For example, the IGNE's memory of the correlation pattern of thermal nematic fluctuations present at the instant of cross-linking can influence the subsequent correlation pattern of the nematic alignments that are "frozen" into the IGNE via the cross-linking process. Moreover, we shall also learn that the fidelity of this memorization of the initial fluctuation pattern depends on the strength of cross-linking as well as the temperature at which the system was cross-linked.

The third issue pertains to the elastic response of IGNEs, which is experimentally observed to be much softer than in ordinary elastomers (such as rubber). Rubber obeys Hooke's law for small strains, but IGNEs are known to have flat plateaus for their stress-strain curves [28]. We shall learn that long-wavelength thermal fluctuations of the nematogens make an IGNE more elastically compliant than an ordinary elastomer.

To see where the afore-mentioned issues are addressed in the chapters of this thesis, we now give an analytical outline of the thesis.

In Chapter 2, we describe a phenomenological model of the IGNE that takes into account the thermal fluctuations of the elastomeric network and is based on a microscopic model of the IGNE as a set of dimers that are randomly connected via springs. Via this model, we are able to make the following predictions: (i) the correlation length of the thermal nematic fluctuations in an IGNE having a weak random field is *shorter* than it is in a *liquid* nematic held at the same temperature; (ii) the thermal and glassy correlations of the liquid crystallinity in IGNEs having sufficiently strong random fields exhibit *oscillatory* spatial decay; and (iii) when the local nematic order present at the instant of cross-linking is spatially correlated over distances larger than the typical localization length of the network, the system strongly memorizes that local nematic order.

In Chapter 3, we describe a microscopic model of the IGNE in terms of dimers randomly that have been randomly connected by springs, and obtain a replica Landau-Wilson field theory of the IGNE via a Hubbard-Stratonovich procedure. We show that this microscopic model leads directly to the phenomenological theory described in Chapter 1.

In Chapter 4, we obtain the saddle-point approximation to the Landau-Wilson theory derived in Chapter 3.

In Chapter 5, we introduce the concept of non-affinity and describe how it can be captured via the use of a certain non-affinity correlator. We summarize the ideas and method behind two theories: (i) the theory of DiDonna and Lubensky [61], and (ii) the theory of Mao et al. [62] We shall then look at a certain class of replica Goldstone fluctuations associated with the broken relative translational symmetries of individual replicas in a replica field theory of elastomer, and interpret them as replicated combinations of non-affine deformations and thermal elastic fluctuations around the relaxed state. We show how the non-affinity correlator is related to the correlator of replica Goldstone fluctuations and, in the limit of vanishing strain deformation, what the correlator of replica Goldstone fluctuations tells one about the strength and range of disorder-averaged correlations of random displacements undergone by the volume elements of the elastomer due to its relaxation after cross-linking.

In Chapter 6, we investigate the effects of thermal and glassy nematic fluctuations on the elastic properties of IGNEs in the *high-temperature* regime. Using the replica field theory formulated in Chapter 3, we find: (i) that the elastic modulus of an IGNE is *softer* than that of ordinary rubber, the softening being induced by long-wavelength thermal nematic fluctuations, and (ii) that the disorder-averaged correlations of random displacements undergone by the volume elements of the elastomer during relaxation after cross-linking are *enhanced* in an IGNE (as compared with ordinary rubber) through the presence of glassy and thermal nematic fluctuations.

In Chapter 7, we investigate the effects of elastic fluctuations on the pattern of thermal and glassy nematic fluctuations in the *high-temperature* regime. We shall see that, owing to the long-range correlations of the elastic fluctuations, the effective correlation length of thermal nematic fluctuations of the IGNE is larger than that corresponding to a system without elastic fluctuations. We shall also see that elastic fluctuations enhance the glassy nematic fluctuations present in the IGNE.

In Chapter 8, we shall use the replica field theory to explore the stability of the macroscopically isotropic state of the IGNE in the *low-temperature* regime. To do this, we shall employ the replica Gaussian variational method [39, 40]. We shall discover that quenched disorder in the form of cross-linking constraints ensures that the macroscopically isotropic state is stable down to arbitrarily low temperatures.

In Chapter 9, we present the main conclusions arrived at in this thesis.

Chapter 2

Phenomenological model of the isotropic-genesis nematic elastomer

As described in the Introduction, the constituents of the IGNE medium undergo thermal position-fluctuations. The IGNE also possesses the ability to memorize the thermal nematic fluctuations at the instant of the cross-linking of the network constituents, and this memorization influences the subsequent liquid-crystalline behavior of the system. In this chapter, we focus on these aspects by constructing a phenomenological, Landau-type free energy [see Eq. (2.3)], which is valid for an IGNE at high temperatures and which involves two novel elements: (i) a lengthscale-dependent nematic-nematic interaction term, reflecting the short-lengthscale liquidity; and (ii) a random field that takes the memory effect into account. In addition, we introduce two types of thermodynamic ensembles: the *preparation* ensemble and the *measurement* ensemble. This phenomenological model leads to three predictions for the *high-temperature* regime of the IGNE:

(i) The correlation length of the thermal nematic fluctuations in an IGNE having a weak random field is *shorter* than it is in a *liquid* nematic held at the same temperature.

(ii) The thermal and glassy correlations of the liquid crystallinity in IGNEs having sufficiently strong random fields exhibit *oscillatory* spatial decay.

(iii) When the local nematic order present at the instant of cross-linking is spatially correlated over distances larger than the typical localization length of the network, the system strongly memorizes that local nematic order.

In Chapter 3, we justify the Landau-type free energy (2.3) employed in the present chapter, by deriving it from a microscopic model of the IGNE. The material presented in the present chapter is based on Ref. [29].

2.1 Landau-type description

To describe the structure and correlations of the system post cross-linking, we employ the local nematic order parameter field $Q_{dd'}(\mathbf{r})$, [1] introduced in the previous chapter, viz.,

$$Q_{dd'}(\mathbf{r}) = \frac{1}{N}\sum_{i=1}^{N}\left(N_d^i N_{d'}^i - D^{-1}\delta_{dd'}\right)\delta^{(D)}\big(\mathbf{r}-\mathbf{R}^i\big). \tag{2.1}$$

In addition, we characterize the random local environmental anisotropy, which tends to induce local nematic alignment $\mathbf{Q}$ in the post cross-linking system, in terms of the random tensor field $\mathbf{M}$:

$$\mathbf{M}(\mathbf{r}) = \mathbf{Y}(\mathbf{r}) + \frac{T}{T^0}\int d^D r'\, \mathrm{H}(\mathbf{r}-\mathbf{r}')\,\mathbf{Q}^0(\mathbf{r}'). \tag{2.2}$$

Here, T is the *measurement temperature* (i.e., the temperature at which the system is maintained, in equilibrium, long after the cross-linking process), and T^0 is the *preparation temperature* (i.e. the temperature of the equilibrium state into which cross-links are instantaneously created). The random environmental anisotropy described by $\mathbf{M}$ is caused by the thermally averaged part of random local spatial arrangement of the localized polymers at post-cross-linking equilibrium. It consists of two parts: (i) a part that is independent of the the pattern of local nematic alignment $\mathbf{Q}^0$ present at the instant of cross-linking, which we call the *memory-independent random field* and denote by $\mathbf{Y}$; and (ii) a part that is due to

[1] Two remarks are in order. First, there is in fact a slight difference from (1.7) in that the real-space nematic order parameter defined in this chapter has dimensions of inverse volume, whereas that in (1.7) is dimensionless. This is to make subsequent calculations in Fourier space more convenient, as the Fourier-space nematic order parameter $\mathbf{Q}_{\boldsymbol{p}}$ is then dimensionless. As for the real-space nematic correlators computed in subsequent chapters, contact can be re-established with experiment by multiplying the real-space nematic correlator by a factor of V^2, where V is the volume of the system. The second remark is less elementary and has to do with the question of whether $\langle\mathbf{Q}\rangle$ is an appropriate order parameter for an IGNE. The issue arises because in an IGNE, the head-tail symmetry of a nematogen, present in a nematic fluid, appears to be absent in an IGNE, because the nematogens are linked to polymer backbones. We shall consider disorder-averaged values of $\langle\mathbf{Q}\rangle$, which implies that for a given configuration in which a given nematogen is linked at one end to a given polymer, there is another configuration that the nematogen is linked at the other end to the same polymer. Thus, the appropriate order parameter for detecting the isotropic-to-nematic phase transition in an IGNE is not a polar vector but, rather, the disorder-averaged value of $\langle\mathbf{Q}\rangle$. The combined symmetry operation, viz., first inverting the nematogen about its center and then swapping the end(s) at which the nematogen is linked, is also implicit in the sum over realizations of quenched disorder, which we shall consider for the microscopic dimer/spring model in Chapter 3.

the pattern of $\mathbf{Q}^0$, which we call the *memory-dependent random field*. $\mathbf{Q}^0$ is partially imprinted in the network structure, and this imprint then partially elicits a response similar to $\mathbf{Q}^0$ in the post-cross-linking state. The relationship between $\mathbf{Q}$ and $\mathbf{Q}^0$ is characterized by a "smearing" kernel, which embodies the idea that $\mathbf{Q}$ (i.e., the post-cross-linking equilibrium-state memory of $\mathbf{Q}^0$) is partially erased, as a result of the thermal position fluctuations of the network. Because of such thermal fluctuations, the position of a given constituent of the network is not sharply localized; instead, this constituent is able to wander over distances of order a finite lengthscale, which we call the *localization length* [6]. We denote the *typical* value of the localization length of the network by the symbol ξ_L. A *large* value of ξ_L would indicate that the network constituents are *weakly* localized, whereas a *small* value would indicate *strong* localization.

Equivalently, viewed from wave-vector space the contribution from $\mathbf{Q}^0$ becomes $\mathrm{H}_{\boldsymbol{p}}\mathbf{Q}^0_{\boldsymbol{p}}$. Physically, we expect $\mathrm{H}(\boldsymbol{r})$ to be positive and bell-shaped, operative primarily over a region of order the typical localization length ξ_L, and to decay monotonically with increasing $|\boldsymbol{r}|$ over this lengthscale, ultimately tending to zero for $|\boldsymbol{r}| \gg \xi_L$. Correspondingly, in wave-vector space $\mathrm{H}_{\boldsymbol{p}}$ would decay monotonically to zero over a scale ξ_L^{-1}. Hence, we see that H serves as a "soft filter," de-amplifying—more strongly, the shorter the lengthscale—the contributions made by the Fourier components of $\mathbf{Q}^0$ to the random anisotropic environment on distance scales shorter than ξ_L. This is a natural consequence of the liquid-like character of the post-cross-linking system on lengthscales shorter than ξ_L. As for the overall *amplitude* of H, this we expect to *increase* with (i) the fraction G of polymers that are localized; (ii) the sharpness of localization $1/\xi_L$; (iii) the nematogen-nematogen aligning interaction J; and (iv) the length ℓ of the nematogens; and we expect this amplitude to *decrease* with the "measurement temperature" T (see below for more on this concept), because thermal fluctuations tend to moderate any aligning forces. A complementary microscopic calculation, which will be described in Chapter 3, bears out these expectations, yielding $\mathrm{H}_{\boldsymbol{p}} = \mathrm{H}_{\mathbf{0}} \exp(-p^2\xi_L^2/2)$, where the amplitude $\mathrm{H}_{\mathbf{0}} \propto G^2J^2(\ell/\xi_L)^4/T$.

In terms of these ingredients, we take as a model for the Landau-type free-energy cost F associated with the induction of local nematic order in the post-cross-linking system the form:

$$F = \frac{1}{2}\int_{\boldsymbol{p}} \Big(\big(\mathcal{A}t + \mathcal{L}p^2 + \mathrm{H}_{\boldsymbol{p}}\big)\big\{\mathbf{Q}_{\boldsymbol{p}}\mathbf{Q}_{-\boldsymbol{p}}\big\} - 2\big\{\big(\mathbf{Y}_{\boldsymbol{p}} + (T/T^0)\,\mathrm{H}_{\boldsymbol{p}}\,\mathbf{Q}^0_{\boldsymbol{p}}\big)\mathbf{Q}_{-\boldsymbol{p}}\big\}\Big). \tag{2.3}$$

Here, $\int_{\boldsymbol{p}}$ is shorthand for $\int d^D p/(2\pi)^D$, p^2 is the squared length of the vector $\boldsymbol{p}$, and the $R_{\boldsymbol{p}}$ is the Fourier transform $\int d^D r\, R(\mathbf{r})\, \exp(i\boldsymbol{p}\cdot\mathbf{r})$. Furthermore, $\mathcal{A}$ characterizes the aligning tendencies of nematic freedoms; and $\mathcal{L}$ is the generalized stiffness for nematic order, for which (for the sake of simplicity) we have adopted the Landau-de Gennes equivalent of the one-Frank-constant approximation.[2] The symbol t denotes the reduced measurement temperature;[3] the occurrence of two temperatures, T and T^0, stems from the fact that elastomers and related systems are characterized by not one but two statistical ensembles. One, which we call the *preparation ensemble*, provides a statistical description of the random (non-equilibrating, unmeasured) freedoms $\mathbf{Q}^0$ that characterize the local alignment immediately prior to cross-linking. The other ensemble describes the equilibrium state of the system long after cross-linking was done, via the statistics of the equilibrating variables $\mathbf{Q}$; we call it the *measurement ensemble*.

The free energy (2.3) consists of two terms. The first two elements of the first term constitute the familiar Landau-de Gennes free energy at quadratic order; higher-order terms have been neglected as we focus on the properties of IGNEs at $t > 0$. These elements describe the free-energy cost of inducing nematic alignment from the unaligned state. The second

[2]See, e.g., P.-G. de Gennes and J. Prost, *The Physics of Liquid Crystals*, 2nd edn (Clarendon Press, Oxford, 1993). As our primary aim is uncover the qualitative physics encoded in Eq. (2.3), we have neglected another possible gradient term, viz., $\mathcal{L}' \int_{\boldsymbol{p}} \sum_{d,d',d''=1}^{D} p_{d'}\, Q_{dd'}(\boldsymbol{p})\; p_{d''}\, Q_{dd''}(-\boldsymbol{p})$, where $\mathcal{L}'$ is the generalized stiffness corresponding to this term. Including this gradient term in Eq. (2.3) would result, e.g., in the five components of the nematic tensor $\mathbf{Q}$ not all having the same value of the oscillation wavelength $\xi_{G/T,o}$ at strong disorder. However, this inclusion would not change our results *qualitatively*, including our central result, viz., that spatially oscillatory decay arises for the glassy and thermal nematic correlators, provided the disorder is sufficiently strong.

[3]The reduced measurement temperature t is defined to be $(T - T^*)/T^*$, where T^* is the spinodal temperature for the spatially homogeneous isotropic-to-nematic transition in the nematic liquid.

term incorporates what we have described above, viz., the influences of (i) the configuration of the rod-like constituents at the instant of cross-linking, via $\mathbf{Q}^0$, together with (ii) the memory-independent random field $\mathbf{Y}$ caused by the localized polymers post cross-linking. From the (previously given) value of $\mathrm{H}_{\mathbf{0}}$ and Eq. (2.3), we see that the contribution to F/T involving $\mathbf{Q}^0$ carries a factor $(J/T^0)(G\ell^2/\xi_L^2)^2(J/T)$. In it, the two temperature factors show that the network is better able to store a given pattern $\mathbf{Q}^0$ the lower the preparation temperature T^0 and, similarly, better able to elicit $\mathbf{Q}^0$ from $\mathbf{Q}$ the lower the measurement temperature T. Taking the two terms together, F is minimized by the most probable nematic configuration $\widetilde{\mathbf{Q}}$, which is given by

$$\widetilde{\mathbf{Q}}_{\boldsymbol{p}} = \big(\mathbf{Y}_{\boldsymbol{p}} + (T/T^0)\,\mathrm{H}_{\boldsymbol{p}}\,\mathbf{Q}^0_{\boldsymbol{p}}\big)/\big(\mathcal{A}t + \mathcal{L}p^2 + \mathrm{H}_{\boldsymbol{p}}\big). \tag{2.4}$$

By completing the square with respect to the first and second terms in Eq. (2.3), we arrive at the following form for F (up to a non-thermally fluctuating term):

$$\frac{1}{2}\int_{\boldsymbol{p}} \big(\mathcal{A}t + \mathcal{L}p^2 + \mathrm{H}_{\boldsymbol{p}}\big)\big\{\big(\mathbf{Q}_{\boldsymbol{p}} - \widetilde{\mathbf{Q}}_{\boldsymbol{p}}\big)\big(\mathbf{Q}_{-\boldsymbol{p}} - \widetilde{\mathbf{Q}}_{-\boldsymbol{p}}\big)\big\}. \tag{2.5}$$

The third element in the first term of the free energy (2.3) is a new and central element. It encodes the essential physical difference between our model and previous models of IGNEs, viz., the elastomer's possession of a network that is localized randomly and fluctuating thermally, and is, furthermore, *liquid-like at sub-localization-length scales and solid-like at larger scales*. As can be seen from Eq. (2.5), this element gives rise to a nonlocal free-energy cost for creating a departure from the nematic pattern $\widetilde{\mathbf{Q}}_{\boldsymbol{p}}$. This cost arises because the network mediates additional nematic-nematic interactions. We emphasize that: (i) the mediated interactions addressed here are not of a type transmitted through coupling between the nematic order and elastic deformation, but of a novel type that is related to the short-lengthscale liquidity feature of the network; and (ii) the free-energy cost associated with

such mediated interactions arises from the competition between the tendency for nematic alignment and the localization forces (which are responsible for causing the short-range liquidity of the network). Thus, the nonlocal energy cost of creating a nematic departure from $\widetilde{\mathbf{Q}}$ that is essentially uniform over a lengthscale rather larger than ξ_L is relatively large, as at this lengthscale the solidness of the network becomes pronounced. Conversely, the nonlocal energy cost is relatively mild if the departure varies only over some lengthscale rather shorter than ξ_L, where the system has a more liquid-like character.

2.2 Diagnostics for structure and correlations

For a system with a given realization of quenched disorder, its statistical mechanics is, in essentially all cases, impossible to study theoretically, because of the huge number of parameters involved and the absence of symmetry. Moreover, the results would apply to a particular realization of disorder, and would not generally be helpful. Thus, for a useful theoretical treatment of systems with quenched disorder, the description should be in terms of disorder-averaged quantities. Similarly, for each given realization of quenched disorder, there are a large number of possible configurations of the thermally fluctuating variables, and these quantities should also be averaged, according to the standard precepts of Gibbs statistical mechanics.

What thermally and disorder-averaged physical quantities should one use to characterize the static local liquid crystalline structure of IGNEs in the high-temperature regime? These quantities should take into account the various levels of randomness present in IGNEs, and should be robust enough to describe their characteristic features as well as be able to describe the development of nematic order. Denoting disorder-averaged quantities by $[\cdots]$ (by which we mean, here, quantities averaged over suitably distributed $\mathbf{Y}$ and $\mathbf{Q}^0$), and thermally averaged quantities by $\langle\cdots\rangle$ (by which we mean quantities averaged over the measurement

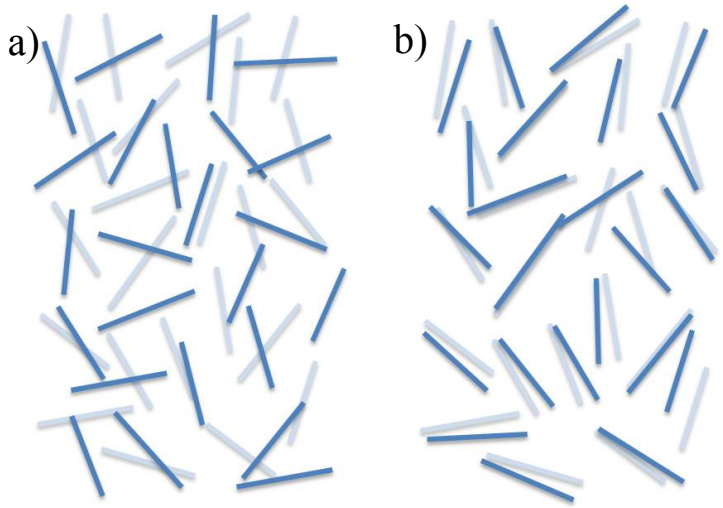

Figure 2.1: Schematic depictions of snapshots of nematogen locations and orientations at a particular instant (blue) and at a much earlier instant (shaded). (a) A conventional liquid crystal in the isotropic state. Such systems do not memorize the local pattern of nematogen alignment indefinitely. There is no correlation between the orientations of blue and shaded nematogens that are depicted near one another. Nor is there any preference for blue and shaded nematogens that are depicted near one another to be the same nematogen. (b) A liquid cystalline ealstomer in the macroscopically isotropic state. Such systems do memorize the local pattern of nematogen alignment indefinitely. The orientations of blue and shaded nematogens depicted near one another are likely to be correlated. For systems in which the nematogens are chemically bonded to an elastomer network, blue and shaded nematogens depicted near one another are likely to be the same nematogen. However, for systems in which the nematogens are not chemically bonded to a network there is no preference for blue and shaded nematogens depicted near one another to be the same nematogen.

ensemble), we shall focus on the following two quantities:[4] (i) the *glassy correlator*, defined via the formula

$$\mathcal{C}^G(\boldsymbol{r},\boldsymbol{r}') \equiv [\{\langle \mathbf{Q}(\boldsymbol{r})\rangle \, \langle \mathbf{Q}(\boldsymbol{r}')\}\rangle]; \tag{2.6a}$$

(ii) the *thermal fluctuation correlator*, defined via the formula

$$\mathcal{C}^T(\boldsymbol{r},\boldsymbol{r}') \equiv \big[\big\langle \big\{ \big(\mathbf{Q}(\boldsymbol{r}) - \langle \mathbf{Q}(\boldsymbol{r})\rangle\big) \, \big(\mathbf{Q}(\boldsymbol{r}') - \langle \mathbf{Q}(\boldsymbol{r}')\rangle\big) \big\} \big\rangle\big]. \tag{2.6b}$$

[4]Although we are focusing on the scalar aspects of the correlators, it is straightforward to reconstruct the full structure of the corresponding fourth-rank tensors, by appending suitable isotropic tensor factors constructed from Kronecker deltas.

The correlator $\mathcal{C}^T$ characterizes the strength of the thermal fluctuations of the nematic alignment away from the local mean value as well as the spatial range over which these fluctuations are correlated. Inter alia, through its range, $\mathcal{C}^T$ can be used to detect the occurrence of a continuous phase transition. The glassy correlator $\mathcal{C}^G$ is a diagnostic of particular value for nematic elastomers, as it detects the occurrence of randomly frozen (i.e., time-persistent) local nematic order. For the case where $\boldsymbol{r}$ and $\boldsymbol{r}'$ are co-located, it is the nematic analog of the Edwards-Anderson order parameter, introduced long ago for spin glasses [36], in the sense that it measures the magnitude of local nematic ordering, regardless of the orientation of that ordering. Moreover, how $\mathcal{C}^G$ varies with the separation of $\boldsymbol{r}$ and $\boldsymbol{r}'$ determines the spatial extent of regions that share a roughly common nematic alignment. Two mechanisms are responsible for the existence of these aligned regions. First, the formation of a random network causes a local breaking of rotational invariance, which has the effect of creating randomly anisotropic environments that tend to align the nematogens locally. Second, although the equilibrium state of the system at the instant prior to cross-linking is, on average, isotropic, a "snapshot" of its microscopic configuration at that instant would reveal local nematic order of the type that we normally call thermal fluctuations. As we shall see, the cross-linking process can trap these fluctuations in, either partially or fully, the extent depending on the strength of the cross-linking and the temperature at the moment of cross-linking.

In the high-temperature regime, the disorder-averaged quantity $[\langle \mathbf{Q}(\boldsymbol{r})\rangle]$ vanishes, owing to the macroscopic isotropy of the post-cross-linking state. On the other hand, the thermal average of the local order parameter for a specific realization of the quenched disorder $\langle \mathbf{Q}(\boldsymbol{r})\rangle$ is maintained at a nonzero, time-persistent, random value, which we shall compute shortly. This nonzero value is the result of the partial trapping, by the network, of the orientational randomness $\mathbf{Q}^0$ present at the instant of cross-linking, together with the memory-independent random field $\mathbf{Y}$ of the network, post cross-linking. The free energy (2.3) is quadratic in $\mathbf{Q}$, and therefore the computation of $\langle \mathbf{Q}\rangle$ and $\mathcal{C}^T$ using the statistical weight

$\exp(-F/T)$ is elementary, yielding

$$\langle \mathbf{Q}_{\boldsymbol{p}} \rangle = \widetilde{\mathbf{Q}}_{\boldsymbol{p}}; \tag{2.7a}$$

$$\left\langle \left\{ \left(\mathbf{Q}_{\boldsymbol{p}} - \langle \mathbf{Q}_{\boldsymbol{p}} \rangle \right) \left(\mathbf{Q}_{\boldsymbol{p}'} - \langle \mathbf{Q}_{\boldsymbol{p}'} \rangle \right) \right\} \right\rangle = \frac{T \mu_D \, \delta_{\boldsymbol{p}+\boldsymbol{p}',\mathbf{0}}}{\mathcal{A} t + \mathcal{L} p^2 + \mathrm{H}_{\boldsymbol{p}}}. \tag{2.7b}$$

Here, $\mu_D \equiv (D-1)(D+2)/2$ counts the number of degrees of freedom of $\mathbf{Q}$ and takes the value 5 for $D = 3$. Note that we have chosen units in which Boltzmann's constant has the value unity.

To perform the average over the quenched random variables $\mathbf{Y}$ and $\mathbf{Q}^0$, we must adopt a model for their statistics that is consistent with the physical origin each has. The choice we make is that $\mathbf{Y}$ and $\mathbf{Q}^0$ are independent, Gaussian-distributed random fields, with zero means and non-zero variances, the latter being given by

$$\left[\left\{ \mathbf{Q}^0_{\boldsymbol{p}} \, \mathbf{Q}^0_{\boldsymbol{p}'} \right\} \right] = T^0 \mu_D \, \frac{\delta_{\boldsymbol{p}+\boldsymbol{p}',\mathbf{0}}}{\mathcal{A}^0 t^0 + \mathcal{L}^0 p^2}, \tag{2.8a}$$

$$\left[\left\{ \mathbf{Y}_{\boldsymbol{p}} \, \mathbf{Y}_{\boldsymbol{p}'} \right\} \right] = T \, \mathrm{H}_{\boldsymbol{p}} \, \delta_{\boldsymbol{p}+\boldsymbol{p}',\mathbf{0}} \, . \tag{2.8b}$$

Here, $\mathcal{A}^0$ and $\mathcal{L}^0$ are, respectively, the preparation-ensemble counterparts to $\mathcal{A}$ and $\mathcal{L}$. The statistics of $\mathbf{Q}^0$ depend on the reduced temperature t^0 of the preparation ensemble;[5] it does not depend on H, because H encodes the physics of random but imperfect spatial localization, and this only comes into being post cross-linking. (The *impact* of $\mathbf{Q}^0$ *does* depend on H, as H controls the relaxation of $\mathbf{Q}$ from $\mathbf{Q}^0$ to its equilibrium value, post cross-linking.) By contrast, the statistics of $\mathbf{Y}$ *does* depend on H; this is because H characterizes the typical value of the memory-independent random field that results from the random (imperfect) spatial localization of the polymers constituting the network. In view of their distinct origins, it is natural that $\mathbf{Y}$ and $\mathbf{Q}^0$ be statistically uncorrelated.

However, it is not a coincidence (as we will indeed see from a microscopic calculation in

[5]The reduced *preparation* temperature is defined via $t^0 \equiv (T^0 - T^*)/T^*$, where T^* is the spinodal temperature of the liquid nematic just prior to the instant of cross-linking.

Chapter 3, but also natural, at least heuristically, that the H that characterizes the *orientational caging* induced by the network (via $\mathbf{Y}$) is the same H that determines the fidelity with which the network preserves the *orientational order* present immediately post cross-linking (i.e., $\mathbf{Q}^0$). It is, in fact, natural, because localization that is sharper and more widespread (i.e., involves a larger localized fraction) both *creates* more intense network-induced orientational caging and *enhances* the trapping-in of the local nematic order present immediately post cross-linking. Our physical expectation, borne out by a microscopic analysis, is that such strengthening of the localization would enhance memorization more strongly than it would orientational caging. This expectation is consistent with the phenomenological choice presented here, in which the corresponding contributions to the random anisotropy field, Eq. (2.2), scale as $\sqrt{\mathrm{H}}$ for the caging (i.e., $\mathbf{Y}$) part and H for the "memorization" (i.e., $\mathbf{Q}^0$) part. Such a "soft" random field is to be contrasted with the conventional, "hard" random field that is present at all length-scales, the latter being based on the assumption that the quenched disorder inhabits a thermally non-fluctuating background.[6]

Returning to the disorder-averaged diagnostics—the mean $[\langle\mathbf{Q}\rangle]$ and the correlators $\mathcal{C}^T$ and $\mathcal{C}^G$—we complete their computation using the statistics of the quenched disorder, Eqs. (2.8), to arrive at (with $[\langle\mathbf{Q}_{\boldsymbol{p}}\rangle] = 0$)

$$\mathcal{C}^T_{\boldsymbol{p}} = T\mu_D \, \frac{1}{\mathcal{A}t + \mathcal{L}p^2 + \mathrm{H}_{\boldsymbol{p}}}, \tag{2.9a}$$

$$\mathcal{C}^G_{\boldsymbol{p}} = T\mu_D \, \frac{\frac{T}{T^0}(\mathcal{A}^0 t^0 + \mathcal{L}^0 p^2)^{-1}|\mathrm{H}_{\boldsymbol{p}}|^2 + \mathrm{H}_{\boldsymbol{p}}}{\left(\mathcal{A}t + \mathcal{L}p^2 + \mathrm{H}_{\boldsymbol{p}}\right)^2}. \tag{2.9b}$$

[6]The random field Ising model is an example of such a system.

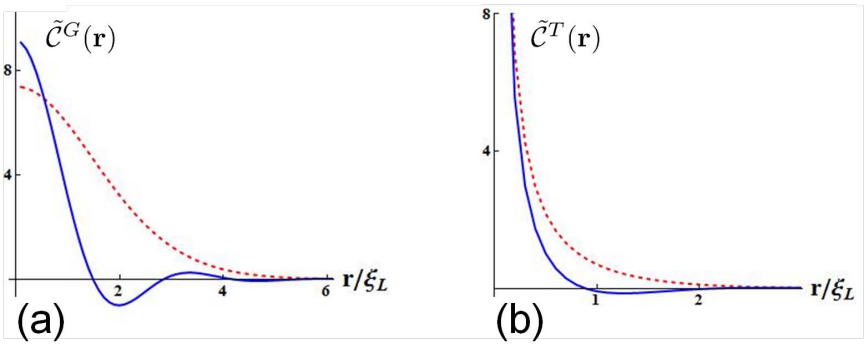

Figure 2.2: Real-space decay behavior of (a) the glassy correlator (rescaled) $\widetilde{\mathcal{C}}^G(r) \equiv (60\pi^2\mathcal{L}/T\mu_D)\,\mathcal{C}^G(r)$, for $t^0 \gg T\mathrm{H}_\mathbf{0}/T^0\mathcal{A}^0$; $t = 0.1\mathcal{L}/\mathcal{A}\xi_L^2$, at (i) $\mathrm{H}_\mathbf{0}/\mathrm{H}^{(c)} = 0.5$ (weak disorder; red, dashed) and (ii) $\mathrm{H}_\mathbf{0}/\mathrm{H}^{(c)} = 40$ (strong disorder; blue, solid). (b) the thermal correlator (rescaled) $\widetilde{\mathcal{C}}^T(r) \equiv (2\pi^2\mathcal{L}/T\mu_D)\,\mathcal{C}^T(r)$, for the same parameters. On going from weak to strong disorder, both correlators cross over from simple exponential decay to oscillatory decay of wavelength of order ξ_L.

2.3 High-measurement-temperature structure and correlations

Having computed the correlators $\mathcal{C}^T$ and $\mathcal{C}^G$, we now set about using them to study how the presence of a network modifies the organizational behavior of nematic freedoms. To do this, we first note that there are two emergent lengthscales present in IGNEs: (i) the typical localization length ξ_L, quantifying the sharpness of localization of polymers belonging to the network; and (ii) the *intrinsic nematic correlation length* ξ_N $[\equiv \sqrt{\mathcal{L}/\mathcal{A}t}]$, describing the range over which nematic freedoms would be correlated if there were no network present. On the other hand, we have the strength of the memory-independent random field $\mathbf{Y}$, which is characterized by $\sqrt{\mathrm{H}_\mathbf{0}}$. In what follows, we shall study the dependence of $\mathcal{C}^T$ and $\mathcal{C}^G$ on the parameters ξ_N, ξ_L and $\mathrm{H}_\mathbf{0}$, doing so for two specific systems: one prepared at $t^0 \gg T\mathrm{H}_\mathbf{0}/T^0\mathcal{A}^0$, and one at $t^0 < T\mathrm{H}_\mathbf{0}/T^0\mathcal{A}^0$. First consider the behaviors of $\mathcal{C}^T$ and $\mathcal{C}^G$ for $t^0 \gg T\mathrm{H}_\mathbf{0}/T^0\mathcal{A}^0$, so that any local nematic order present immediately post cross-linking (and thus available for trapping in) is spatially correlated only over distances far shorter than the typical localization length ξ_L; see Table 2.1. This separation of lengthscales implies that the local nematic order arising from $\mathbf{Q}^0$ would be heavily "washed out" by thermal fluctuations

Disorder strength	Weak ($\mathrm{H_0} < \mathrm{H}^{(c)}$)	Strong ($\mathrm{H_0} > \mathrm{H}^{(c)}$)
$\xi^2_{T,o}$	∞	$\frac{1}{2}\xi^2_L/\ln(\mathrm{H_0}/\mathrm{H}^{(c)})$
$\xi^2_{T,d}$	$\xi^2_N \frac{1-(\mathrm{H_0}/\mathrm{H}^{(c)})}{1+(\mathrm{H_0}/\mathcal{A}t)}$	$\sim \xi^2_L/\left(1+\frac{\xi^2_L}{2\xi^2_N}\right)$
$\xi^2_{G,o}$	∞	$\sim \xi^2_L/\ln(\mathrm{H_0}/\mathrm{H}^{(c)})$
$\xi^2_{G,d}$	$\frac{1}{2}\xi^2_L + 2\xi^2_N \frac{1-(\mathrm{H_0}/\mathrm{H}^{(c)})}{1+(\mathrm{H_0}/\mathcal{A}t)}$	$\sim \xi^2_L$

Table 2.1: Values of the correlation lengthscales ($\xi_{T,d}$ and $\xi_{G,d}$), and the oscillation wavelengths ($\xi_{T,o}$ and $\xi_{G,o}$) in the weak- and strong-disorder regimes for the case of IGNEs cross-linked at $t^0 \gg T\mathrm{H_0}/T^0\mathcal{A}^0$.

of the network. Thus, in this regime the dominant contribution to the trapped-in local nematic order originates in the memory-independent random field $\mathbf{Y}$.

Continuing with the case $t^0 \gg T\mathrm{H_0}/T^0\mathcal{A}^0$, we observe that $\mathcal{C}^T$ and $\mathcal{C}^G$ exhibit qualitatively distinct behaviors in two regimes, depending on the strength of the random field (see Fig. 2.2). For $\mathrm{H_0} < \mathrm{H}^{(c)}$ (where $\mathrm{H}^{(c)} \equiv 2\mathcal{L}/\xi^2_L$—the *weak-disorder regime*), $\mathcal{C}^T$ and $\mathcal{C}^G$ *decay simply* with increasing real-space separation. More specifically, by examining their small wave-vector behaviors we ascertain that the respective associated correlation lengths $\xi_{T,d}$ and $\xi_{G,d}$ have the values given in Table 2.1. We see, from the behavior of $\xi_{T,d}$, the physically reasonable result that the random network, with its thermal fluctuations, serves to shorten the nematic thermal fluctuation correlation length from the value it would have in the absence of the network, a phenomenon that conventional (i.e., non-thermally fluctuating) random-field approaches would not capture. As for $\xi^2_{G,d}$, it comprises two parts. One ($\propto \xi^2_{T,d}$) arises from the nematic thermal correlations; the other ($\propto \xi^2_L$) comes from the local aligning effect exerted by the cage. The fact that $\xi_{G,d}$ increases with ξ_L does not mean that a more weakly cross-linked network (for which ξ_L would be larger) aligns the nematogens more effectively. Whilst the *lengthscale* of aligned regions $\xi_{G,d}$ may increase, the *magnitude* of $\mathcal{C}^G$, which governs the intensity of the alignment locally, decreases.[7]

By contrast, for $\mathrm{H_0} > \mathrm{H}^{(c)}$ (i.e., the *strong-disorder regime*), the (weak-disorder) simple

[7]This can be seen by computing the value of $\mathcal{C}^G(\boldsymbol{r} = \mathbf{0})$, which is approximately given by $T\mu_D \mathrm{H_0}\xi_N/4\pi\mathcal{L}^2$ at weak disorder, and noting that $\mathrm{H_0}$ varies as ξ_L^{-4}.

decay of the correlators can give way to oscillatory decay, as we now discuss. Regardless of T, $\mathcal{C}^T$ oscillates, whereas $\mathcal{C}^G$ only does for sufficiently small T. The oscillation wavelengths $\xi_{T/G,o}$ are determined via the radii of the shells in wave-vector space on which the corresponding correlators are maximal. Thus, we arrive at an explicit (and, notably, T-independent) formula $\xi_{T,o} = \xi_L/\sqrt{2\ln(\mathrm{H}_{\mathbf{0}}/\mathrm{H}^{(c)})}$ and an implicit one for $\xi_{G,o}$, viz.,

$$1 + (\xi_N/\xi_{G,o})^2 + 4(\xi_N/\xi_L)^2 - (\mathrm{H}_{\mathbf{0}}/\mathcal{A}t)e^{-\xi_L^2/2\xi_{G,o}^2} = 0.$$

The cross-over boundary between the oscillatory and non-oscillatory regimes for $\mathcal{C}^T$ occurs at the threshold where the oscillation wavelength $\xi_{T,o}$ is about to shrink from infinity to a finite value. At this threshold, $\mathrm{H}_{\mathbf{0}} = \mathrm{H}^{(c)}$. Similarly, the cross-over boundary between the oscillatory and non-oscillatory regimes for $\mathcal{C}^G$ occurs at the threshold where the oscillation wavelength $\xi_{G,o}$ is about to shrink from infinity to a finite value. The phase boundary for glassy oscillations is given by

$$\mathrm{H}_{\mathbf{0}} = \mathcal{A}t + 2\mathrm{H}^{(c)}. \tag{2.10}$$

(See Fig. 2.3.)

The value of $\xi_{T/G,d}$ in this strong-disorder regime, given in Table 2.1, is estimated via the widths of the peaks of $\mathcal{C}^{T/G}$. Upon decreasing ξ_L at fixed ξ_N, the value of $\xi_{T,d}$ tends to ξ_L from above, indicating that the network is limiting the range over which the thermal nematic fluctuations are correlated. On the other hand, $\xi_{G,d}$ remains at the scale of ξ_L, indicating that the range of coherent nematic alignment is circumscribed by the network's typical localization length.

Oscillatory behavior can be regarded as the resolution of the interplay of two energetic costs of fluctuations. The cost of creating local nematic order via *rotations* of the nematogens is smaller for long-wavelength fluctuations. By contrast, the cost of creating nematic order via *local segregation* of nematogens according to their preferred orientation is smaller for short-wavelength fluctuations (which is a reflection of the short-lengthscale liquidity of

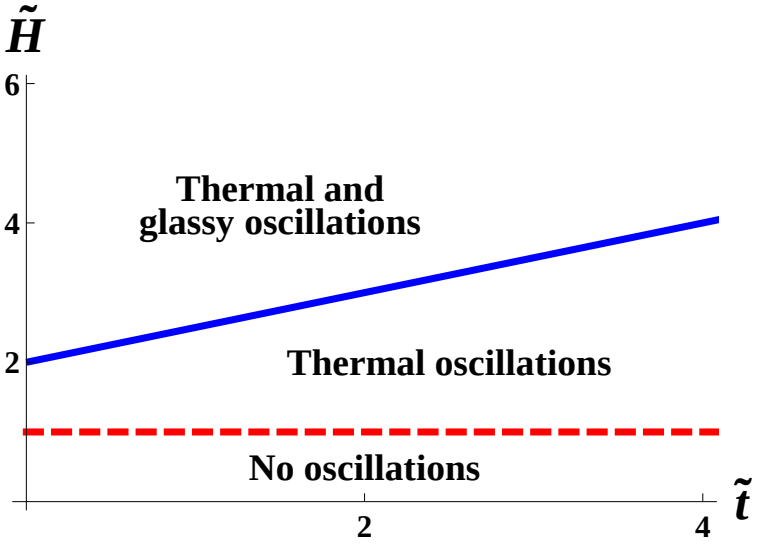

Figure 2.3: Crossover diagram for the glassy and thermal correlators, indicating the three qualitatively distinct regimes of behavior for a system that is cross-linked at a very high temperature. Here, $\tilde{H} \equiv \mathrm{H_0}/\mathrm{H}^{(c)}$ is a measure of the disorder strength, and $\tilde{t}$ is the rescaled reduced temperature, with the value $(\mathcal{A}\xi_L^2/\mathcal{L})t$. Above the blue solid line, both correlators oscillate and decay as a function of separation. Between the blue solid and red dashed lines, both correlators decay but only the thermal one also oscillates. Below the red dashed line, both correlators decay but neither oscillates.

the network). When the former mode dominates for all wavelengths, long-wavelength fluctuations are the most probable and, hence, correlations decay without oscillation. When the disorder is strong enough, however, the latter mode drives the most probable fluctuations to a finite wave-vector and, hence, correlations oscillate as they decay (cf. Figs. 2.4 and 2.5).[8]

Having considered the behaviors of $\mathcal{C}^T$ and $\mathcal{C}^G$ for systems prepared at high temperatures, we now consider the corresponding behavior for systems prepared at $t^0 < T\mathrm{H_0}/T^0\mathcal{A}^0$, so that the local nematic order present immediately post cross-linking is spatially correlated over distances larger than ξ_L. This regime can be reached in IGNEs by imposing a sufficiently large density of cross-links, such that the typical localization length of the network becomes comparable to or smaller than the nematic correlation length of the isotropic liquid of nematogens just prior to cross-linking. [9] As one can see from Eq. (2.9a), the behavior

[8]Such behavior is analogous to the micro-phase separation in cross-linked polymer blends; see Refs. [66, 67]

[9]We note that, in addition to IGNEs, the result that we have obtained for this regime also describes the strong memory effect present in nematic elastomers that have been prepared in the *nematic* state, at least

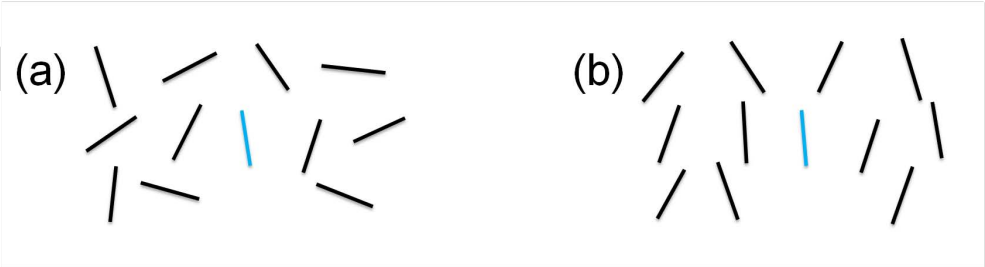

Figure 2.4: Nematogens in an IGNE can lower their energy by a mechanism via which each nematogen rotates such that the nematogens are locally aligned on average. To illustrate this mechanism, we have disregarded the ability of each rod to translate, and focused solely on their rotational capability. (a) Nematogens before rotation. (b) Nematogens having rotated to achieve local net alignment. The blue-colored rod remains in the same position, whilst undergoing rotation. This mechanism of energy reduction via local rotation is favored if the ends of the nematogens are not strongly localized by the network.

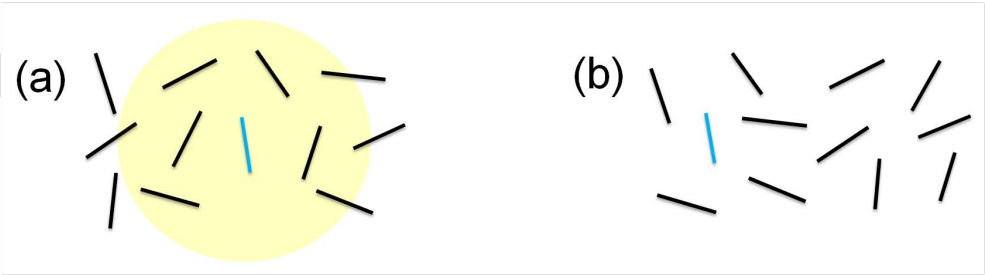

Figure 2.5: Nematogens in an IGNE can also lower their energy by *local segregations*, viz., rods undergo local translation such that rods of similar orientations become more proximate to each other. The extent of each nematogen's translation is restrained by its localization length. (The area over which the blue-colored rod has a higher probability of translating to is colored yellow.) To illustrate this mechanism, we have disregarded the capability of the rods to rotate, and focussed solely on their translational ability. (a) Nematogens before local segregation. (b) Nematogens after local segregation. The blue-colored rod has translated a certain distance whilst maintaining its orientation. Note that the resulting local nematic pattern is shows local *director* anti-correlation (the director being associated with the locally coarse-grained orientation density of the individual nematogens).

of $\mathcal{C}^T$ is unchanged, undergoing simple decay in real space at weak disorder but oscillatory decay at strong disorder. Conversely, $\mathcal{C}^G$ exhibits behavior qualitatively different from that of a system prepared at $t^0 \gg T\mathrm{H}_{\mathbf{0}}/T^0\mathcal{A}^0$, because it now receives its dominant contribution from the memorization of $\mathbf{Q}^0$. Specializing to $t \approx t^0$ and for wavelengths larger than ξ_L, we see from Eq. (2.9b) that $\mathcal{C}^G$ is approximately given by

$$\mathcal{C}^G_{\boldsymbol{p}} \approx \mu_D \left(\frac{T}{T^0}\right)^2 \frac{T^0}{\mathcal{A}^0 t^0 + \mathcal{L}^0 p^2}, \tag{2.11}$$

i.e., it is proportional to the correlator of the thermal nematic fluctuations immediately post cross-linking. This indicates that the pattern of these thermal fluctuations has been *faithfully memorized* by the network.

2.4 Effective replica Hamiltonian

To facilitate comparison with the microscopic dimer/spring model of an IGNE, which will be described in Chapter 3, in this section we consider deriving the disorder-averaged free energy for the phenomenological model of the IGNE via a technique known as the *replica method* [45]. In principle, one should be able to derive disorder-averaged quantities such as the glassy and thermal fluctuation correlators (2.9) from the disorder-averaged free energy (by appending suitable conjugate fields). However, in practice, directly disorder-averaging the free energy is difficult, if not impossible, owing to the presence of a logarithm function, and hence one has to resort to indirect methods such as the replica method.

Before we do that, however, we pause to explain why one should disorder-average the free energy rather than (say) the partition function. This is part of a more general notion that one should disorder-average *extensive* variables. We shall follow the explanation given by Brout [44]. Consider a very large system and divide it up into a large number of subsystems, such that each subsystem is macroscopic and clearly contains a statistically distinct set of

qualitatively [28].

quenched random variables. Assume that interactions in the system are short-ranged, so that one can ignore the coupling between the subsystems. Thus, the value of any extensive variable for the whole system is the sum of this quantity over the subsystems. Given the large number of subsystems, the average over the subsystems is equivalent to an average over all possible choices of the quenched disorder, according to a given, physically motivated, probability distribution for the quenched disorder. Just as in ordinary statistical mechanics, where we know that the relative fluctuations of the energy around its thermal equilibrium are $O(N^{-1/2})$, we expect that the relative fluctuations of the extensive variable also go to zero in the limit of large system. A quantity having this property is said to be *self-averaging*. For self-averaging quantities, not only can we expect the same results in experiments on different macroscopic samples, but we can also expect that a theoretical calculation of the disorder average of the quantity would give the same answer as experiments would.

Therefore, one appropriate quantity to be averaged is the free energy F but not the partition function Z. Moreover, an average of Z would be tantamount to treating quenched and annealed variables on the same footing, and thus would not reflect the equilibration of the annealed variables in the presence of a fixed background of quenched variables. We use the square brackets $[\cdots]$ to denote disorder averages, so that the disorder-averaged free energy $[F]$ is given by

$$[F] = -\sum_{\chi} P(\chi) F_{\chi} = -T \sum_{\chi} P(\chi) \ln Z_{\chi}, \tag{2.12}$$

where χ indexes the realizations of quenched disorder, and F_{χ} is the free energy for a given realization χ. The average over the realizations of disorder is weighted by some distribution of quenched disorder $P(\chi)$, for which a model form has to be determined.

We now use the replica method to perform the disorder average of the logarithm of the

partition function, $[\ln Z_\chi]$. This method is based on the following mathematical identity:

$$\begin{aligned} & x^n = e^{n \ln x} = 1 + n \ln x + O(n^2) \qquad \text{(for small } n\text{)} \\ \Rightarrow \quad & \ln x = \lim_{n \to 0} \frac{x^n - 1}{n}. \end{aligned} \tag{2.13}$$

This can be used to represent the logarithm in Eq. (2.12), so that one has

$$[F] = -T \sum_\chi P(\chi) \lim_{n \to 0} \frac{Z_\chi^n - 1}{n} = -T \lim_{n \to 0} \frac{[Z_\chi^n] - 1}{n}. \tag{2.14}$$

The problem now is to calculate the disorder average of Z_χ^n. Recall that each partition function $Z_\chi = \mathrm{Tr}_S\, e^{-\frac{H_\chi(S)}{T}}$ is a Boltzmann-weighted sum over all possible states S in the statistical ensemble for the system. (S might be the collection of conformations of the polymers or, in a magnetic system, the orientations of the spins.) Thus one can write

$$\begin{aligned} [Z_\chi^n] &= \left[\mathrm{Tr}_{S^1}\, e^{-\frac{H_\chi(S^1)}{T}}\, \mathrm{Tr}_{S^2}\, e^{-\frac{H_\chi(S^2)}{T}} \cdots \mathrm{Tr}_{S^n}\, e^{-\frac{H_\chi(S^n)}{T}} \right] \\ &= \mathrm{Tr}_{S^1} \mathrm{Tr}_{S^2} \cdots \mathrm{Tr}_{S^n} \left[e^{-\left(H_\chi(S^1) + H_\chi(S^2) + \cdots + H_\chi(S^n) \right)/T} \right] \\ &\equiv \prod_{\alpha=1}^{n} \mathrm{Tr}_{S^\alpha} e^{-H_{\mathrm{rep}}(S^1, \ldots, S^n)/T}, \end{aligned} \tag{2.15}$$

where $H_{\mathrm{rep}} \equiv -T \ln \left[\exp\left((H_\chi(S^1) + H_\chi(S^2) + \cdots + H_\chi(S^n))/T \right) \right]$. One thus arrives at a formulation in which there are n thermodynamical systems, or statistical ensembles (but each with the same realization of disorder χ). Each of these ensembles is known as a *replica*. They are *undecoupled* in Eq. (2.15). By exchanging the order of the disorder average $[\cdots]$ and the thermal average over each of the n replicas of the microscopic states (under the trace operations Tr_{S^α}), and performing the disorder average before the thermal average, one obtains an *effective replica Hamiltonian* $H_{\mathrm{rep}}(S^1, \ldots, S^n)$ which describes n replicas of a *pure* system, where the quenched disorder is absent. However, the price of obtaining such a replicated pure system is that the replicas are now, in general, *coupled* to one another.

For the phenomenological model described by Eq. (2.3), we can follow the procedure described above, taking $\mathbf{Q}^0$ and $\mathbf{Y}$ to be our quenched random variables and $[\cdots]$ to be an average over these quenched random variables. We find, after some computation, that the effective replica Hamiltonian is given by

$$\begin{aligned} H\left[\mathbf{Q}^1, \mathbf{Q}^2, \cdots, \mathbf{Q}^n\right] &= \frac{1}{2T}\sum_{\alpha=1}^{n}\sum_{\boldsymbol{p}}\left(\mathcal{A}t + \mathcal{L}p^2 + \mathrm{H}_{\boldsymbol{p}}\right)\{\mathbf{Q}^{\alpha}_{\boldsymbol{p}}\,\mathbf{Q}^{\alpha}_{-\boldsymbol{p}}\} \\ &\quad -\frac{1}{2T^2}\sum_{\alpha,\beta=1}^{n}\sum_{\boldsymbol{p}}[\{\mathbf{Y}_{\boldsymbol{p}}\,\mathbf{Y}_{-\boldsymbol{p}}\}]\{\mathbf{Q}^{\alpha}_{\boldsymbol{p}}\,\mathbf{Q}^{\beta}_{-\boldsymbol{p}}\} \\ &\quad -\frac{1}{2(T^0)^2}\sum_{\alpha,\beta=1}^{n}\sum_{\boldsymbol{p}}\mathrm{H}_{\boldsymbol{p}}\,\mathrm{H}_{-\boldsymbol{p}}\,[\{\mathbf{Q}^0\,\mathbf{Q}^0\}]\{\mathbf{Q}^{\alpha}_{\boldsymbol{p}}\,\mathbf{Q}^{\beta}_{-\boldsymbol{p}}\}. \end{aligned} \tag{2.16}$$

This effective replica Hamiltonian describes n replicas of a pure system, and the replicas are now coupled. This effective replica Hamiltonian enables one to determine $[F]$ via Eq. (2.14). In Chapter 3, the effective replica Hamiltonian will be compared with Eq. (4.7) to show that the microscopic model of the IGNE is equivalent, under coarse-graining, to the phenomenological model considered in the present chapter.

Chapter 3

Microscopic dimer/spring model of the IGNE

In this chapter, we justify the form of the Landau-type free energy (2.3) employed in the previous chapter, by deriving it from a microscopic model of IGNEs, a model that we describe in detail in Sec. 3.1. To deal with the problem of quenched disorder (which originates in the random cross-linking process), we implement the replica method in Sec. 3.2, paving the way for the Hubbard-Stratonovich decoupling scheme which is performed in Sec. 3.3. There, we develop a field theory for IGNEs, which involves an order parameter field $\mathbf{Q}$ that describes liquid crystalline ordering, and an order parameter field Γ that describes random solidification.

3.1 Ingredients of the model

We model an IGNE microscopically in terms of a system of dimers that are randomly and permanently linked via springs (see Fig. 3.1). The springs mimic the flexible constituents of liquid crystalline polymers, and also serve as cross-links; the dimers mimic the stiff constituents of liquid crystalline polymers. Each dimer (labeled by j, where $j = 1, \ldots, N$) consists of two particles at position vectors $\boldsymbol{c}_{j,1}$ and $\boldsymbol{c}_{j,2}$ that are separated by a fixed distance ℓ. The orientation of the j-th dimer is specified by the unit vector

$$\boldsymbol{n}_j = \frac{\boldsymbol{c}_{j,1} - \boldsymbol{c}_{j,2}}{|\boldsymbol{c}_{j,1} - \boldsymbol{c}_{j,2}|}. \tag{3.1}$$

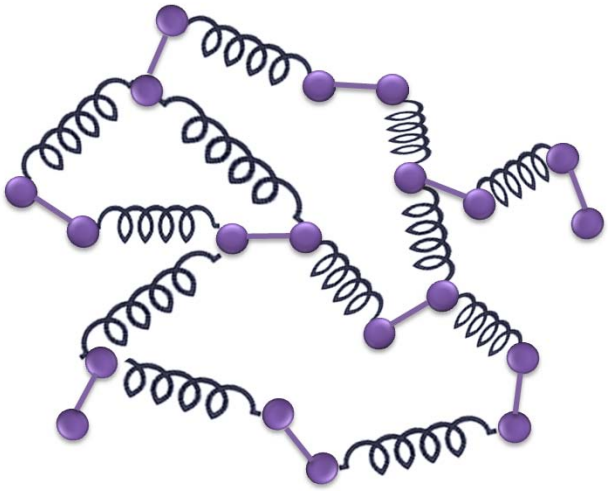

Figure 3.1: A model of dimers (purple) cross-linked via Hookean springs (black). Each dimer has a length ℓ and each spring has an r.m.s. length b. Each dimer has a center-of-mass position vector $\boldsymbol{c}_j$ (where $j = 1, \ldots, N$ labels the dimer) and an orientation specified by a unit vector $\boldsymbol{n}$.

The dimers interact via three types of forces. Firstly, there is an *orientational* interaction between dimers that promotes parallel or antiparallel alignment. We model such an interaction via a potential of the Maier-Saupe type, viz.,

$$H_{\rm nem} = -\frac{V}{2N} \sum_{i,j=1}^{N} J(\boldsymbol{c}_i - \boldsymbol{c}_j)(\boldsymbol{n}_i \cdot \boldsymbol{n}_j)^2, \tag{3.2}$$

where $\boldsymbol{c}_j \equiv (\boldsymbol{c}_{j,1} + \boldsymbol{c}_{j,2})/2$ is the position vector of the j-th dimer's center of mass. The factor of V/N is inserted for convenience. [1] We shall assume that the aligning interaction is short-range, and approximate the interaction kernel $J(\boldsymbol{c})$ by the value $\left(J_0/(2\pi a^2)^{d/2}\right) \exp(-c^2/2a^2)$. In Fourier space, the potential is given by $J_{\boldsymbol{p}} \approx J_0 \exp(-p^2 a^2/2)$. Here, a specifies the range of the interaction between dimers, and J_0 characterizes the strength of the interaction. In addition to the orientational interaction, the dimers experience a *positional* excluded-volume interaction between particles belonging to any pair of dimers. We model this positional

[1] The Hamiltonian $H_{\rm nem}$ remains extensive under this choice of prefactor, as the interaction is short-ranged. (On the other hand, if the interaction is infinite-ranged then one would need an extra factor $1/N$.)

excluded-volume interaction via an Edwards-type pseudo-potential [59],

$$H_{\text{ev}} = \frac{\lambda}{2} \sum_{i,j=1}^{N} \sum_{s,t=1,2} \delta(\boldsymbol{c}_{i,s} - \boldsymbol{c}_{j,t}), \tag{3.3}$$

where λ is the strength of the excluded-volume interaction. [2] Finally, any given pair of dimers that are connected by a spring interact additionally via the harmonic potential due to the spring. We specify such a potential by the following Hookean energy term:

$$H_{\text{xlink}} = \frac{T}{2b^2} \sum_{e=1}^{M} |\boldsymbol{c}_{i_e,s_e} - \boldsymbol{c}_{j_e,t_e}|^2. \tag{3.4}$$

Here, T denotes the temperature and b^2 denotes the mean squared separation of any two points connected by a spring. Note that the spring has zero rest-length. This accords with the behavior of Gaussian molecular chains, for which the ends of a given polymer segment of the network prefer to be near one another rather than apart, as the former situation gives rise to more conformations of the polymer segment, and thus is entropically favored. The network is prevented from collapsing into a globule only because of the presence of sufficiently large excluded-volume forces. The label e indexes the springs, and M denotes the number of springs. The indices $i_e, j_e \in \{1, \ldots, N\}$ refer to the pair of dimers that are connected by spring $e\,(= 1, \ldots, M)$. The indices $s_e, t_e \in \{1, 2\}$ label the particles that are connected by spring e.

For the microscopic model, the thermal and quenched random variables are themselves *microscopic*, in contrast to the *mesoscopic* (or coarse-grained) thermal and quenched random variables considered in Chapter 2. In the microscopic model, the thermal random variables are specified by variables $\boldsymbol{c}_{i,s}$, whilst the quenched random variables are given by: (i) the total number of springs M; and (ii) the set of possible ways of assigning these springs to

[2] In principle, one should allow the entire rod volume to be excluded. However, to do so would introduce more technical difficulties than would be appropriate to our essential aim of penalizing density fluctuations. Thus, we have employed the simplest possible formulation that enables one to achieve this aim, which is to make the ends of cross-linking springs subject to an excluded-volume interaction.

pairs of end-points of dimers. We can label a given realization of quenched disorder by $\chi = \{i_e, s_e; j_e, t_e\}_{e=1}^{M}$. The total Hamiltonian for the dimer model is then given by

$$H = H_{\rm nem} + H_{\rm xlink} + H_{\rm ev}, \tag{3.5}$$

and for a given realization χ of quenched disorder, the partition function is specified by

$$Z_\chi = \int \prod_{i,s} d\boldsymbol{c}_{i,s}\, e^{-H/T} \prod_{j=1}^{N} \delta(|\boldsymbol{c}_{j,1} - \boldsymbol{c}_{j,2}| - \ell). \tag{3.6}$$

As discussed in Sec. 2.4, it is appropriate to average the free energy of the system over all realizations of the quenched disorder. From this point onwards, we shall use the square brackets $[\cdots]$ to denote a quantity averaged over realizations χ of the quenched disorder, and angular brackets $\langle\cdots\rangle$ to denote a quantity averaged over the microscopic thermal configurations of the dimers. One is then in a position to write the disorder average of the free energy $[F]$ as

$$[F] = \sum_\chi P(\chi) F_\chi = -T \sum_\chi P(\chi) \ln Z_\chi\,, \tag{3.7}$$

where F_χ is the free energy for a given realization of quenched disorder χ.

3.2 Replicas and collective fields

What disorder statistics should we use to compute the disorder average of the free energy? In common with other elastomeric systems (such as rubber; see, e.g., Ref. [6]), we employ an elaboration of the Deam-Edwards distribution $P(\chi)$ [35]. This amounts to choosing

$$P(\chi) = \frac{1}{M!} \left(\frac{\tilde{V}\eta^2}{2N}\right)^M \frac{Z_\chi}{Z_1}\,, \tag{3.8}$$

where the dimensionless volume $\tilde{V}$ is defined to be $V/(2\pi b^2)^{d/2}$. The adoption of the Deam-Edwards distribution reflects a picture in which the system undergoes *instantaneous* cross-linking. In this process, one begins with a melt or solution at equilibrium and—so rapidly that hardly any relaxation has time to occur—one introduces permanent bonds between some random fraction of the pairs of dimers that happen, at the instant of cross-linking, to be nearby one another. The Poissonian factor in $P(\chi)$ reflects the fact that cross-links may or may not be formed between adjacent dimers during the cross-linking process, and the probability that cross-links form between any two adjacent dimers is controlled by η^2. (In Appendix A, we show that η^2 is related to the average number of cross-linking springs per dimer, via the formula $[M]/N = 2\eta^2$.) In addition, $P(\chi)$ is proportional to Z_χ, which describes the fact that the thermal configurations of the cross-linked system are more likely to be similar to the thermal configurations of the liquid system just prior to the instant of cross-linking. The factor Z_1 is present for normalization purposes. The disorder average of the logarithm of the partition function $[\ln Z_\chi]$ is carried out using the replica method, as described in Sec. 2.4. We write the logarithm in Eq. (3.7) as

$$[F] = -T \lim_{n\to 0} \sum_{\chi} P(\chi) \frac{Z_\chi^n - 1}{n}. \tag{3.9}$$

We then insert the Deam-Edwards distribution to obtain

$$[F] = -T \lim_{n\to 0} \sum_{\chi} \frac{\left(\frac{\tilde{V}\eta^2}{2N}\right)^M Z_\chi}{M! Z_1} \cdot \frac{Z_\chi^n - 1}{n}. \tag{3.10}$$

By exchanging the order of the disorder average $[\cdots]$ and the thermal average over the microscopic states of each replica, and performing the disorder average first (i.e., by summing over the realizations of the quenched disorder χ), we arrive at the statistical mechanics of $n+1$ (not n) thermal copies of the system absent of quenched disorder. The result thus

obtained is:

$$[F] = -T \lim_{n\to 0} \frac{1}{n} \left(\frac{Z_{1+n}}{Z_1} - 1 \right), \tag{3.11}$$

in which the "replica partition function" Z_{1+n} is given by

$$Z_{1+n} = \Big\langle \exp\Big(\frac{\tilde{V}\eta^2}{2N} \sum_{i\neq j} \sum_{s,t} e^{-\frac{1}{2b^2}|\hat{c}_{i,s} - \hat{c}_{j,t}|^2} \Big) \prod_{j=1}^{N} \delta(|\boldsymbol{c}_{j_1}^{\alpha} - \boldsymbol{c}_{j_2}^{\alpha}| - \ell) \Big\rangle_{N,n+1}. \tag{3.12}$$

(For details of the derivation of Eq. (3.12), see Appendix B.) Here, we have denoted by $\langle \cdots \rangle_{N,n+1}$ the thermal average over an $(n+1)$-fold replicated version of the Hamiltonian H. To simplify the notation, we have also introduced the symbol $\hat{c}$ to denote the $n+1$-fold replicated vector $(\boldsymbol{c}^0, \boldsymbol{c}^1, \ldots, \boldsymbol{c}^n)$, and $\alpha (= 0, 1, \ldots, n)$ labels the replicas.

To decouple the N interacting (replicated) dimers, we apply a sequence of Hubbard-Stratonovich transformations, so that we arrive at a system of N uncoupled copies of the *same* replicated one-dimer system. This decoupling is achieved at the price of introducing fluctuating auxiliary fields. The details of this decoupling scheme are presented in Appendix B. The advantage of the Hubbard-Stratonovich transformation is that it reduces the task of summing over the configurations of the system of N replicated dimers to that of summing over the configurations of *one single replicated dimer*, as well as the configurations of the collective fields, for which systematic procedures (such as saddle-point approximation and perturbative renormalization techniques) known from statistical field theory (see, e.g., Ref. [46]) can be applied. One can thus compute quantities that are otherwise difficult to compute using the microscopic theory. The Hubbard-Stratonovich procedure allows one to define collective fields $\gamma(\hat{r})$ and $\boldsymbol{q}(\boldsymbol{r})$, given by

$$\gamma(\hat{r}) \equiv \frac{1}{2N} \sum_{i=1}^{N} \sum_{s=-1,1} \prod_{\alpha=0}^{n} \delta\big(\boldsymbol{r}^{\alpha} - \boldsymbol{c}_{i,s}^{\alpha}\big) - \frac{1}{V^{1+n}} \tag{3.13}$$

and

$$q_{d_1 d_2}(\boldsymbol{r}) \equiv \frac{1}{N}\sum_{i=1}^{N}(n_{i\,d_1}n_{i\,d_2} - D^{-1}\delta_{d_1 d_2})\delta(\boldsymbol{r}-\boldsymbol{c}_i), \tag{3.14}$$

and to relate their disorder-averaged expectation values to the expectation values of auxiliary fields $\Gamma(\hat{r})$ and $\mathbf{Q}(\boldsymbol{r})$, via the equations (cf. Appendix B)

$$\lim_{n\to 0}\langle\Gamma(\hat{r})\rangle = \left[\left\langle\gamma(\hat{r})\right\rangle\right]; \tag{3.15a}$$

$$\lim_{n\to 0}\langle\mathbf{Q}^{\alpha}(\boldsymbol{r})\rangle = \left[\left\langle\boldsymbol{q}(\boldsymbol{r})\right\rangle\right], \tag{3.15b}$$

where on the LHS, the angular brackets $\langle\cdots\rangle$ refer to a thermal average over an effective replica Hamiltonian [cf. Eq. (3.19)], which involves Γ and $\mathbf{Q}^{\alpha}$, whereas on the RHS, $\langle\cdots\rangle$ refers to a thermal average over the microscopic positions $\boldsymbol{c}_i$ and orientations $\boldsymbol{n}_i$ of each dimer, subject to the constraints $|\boldsymbol{c}_{i,1}-\boldsymbol{c}_{i,2}|=\ell$; and $[\cdots]$ refers to disorder averaging over the realizations of cross-linking constraints.

How should one interpret the extra, or "zeroth," replica, as well as the remaining n replicas? Physically, the zeroth replica, which originates in the Deam-Edwards distribution, represents the *preparation ensemble* of the system (i.e., the ensemble of configurations of the system just prior to the instant of cross-linking), whereas the remaining n replicas represent the *measurement ensemble* (i.e., the ensemble of thermal configurations of the system measured at a time instant *long* after the instant of cross-linking). We have used the term *ensemble* because the choice of the instant of cross-linking the system is arbitrary, and corresponding to each different choice is a different thermal configuration of dimer positions and orientations at the instant of preparation (and also a different set of thermal configurations at the instants of measurement); all these different thermal configurations are subject though to the *same* cross-linking constraints. To appreciate these points better, one may re-write the disorder average of the product of $1+n$ thermal averages in the RHS of

Eq. (3.15a) as an autocorrelation function, viz.

$$\big[\langle g_{i,s}(\boldsymbol{r}^0)\rangle \ldots \langle g_{i,s}(\boldsymbol{r}^n)\rangle\big] \approx \big[\langle g_{i,s}(\boldsymbol{r}, t^0)\, g_{i,s}(\boldsymbol{r}, t^0+\tau^1) \ldots g_{i,s}(\boldsymbol{r}, t^0+\tau^n)\rangle\big] \tag{3.16}$$

in the limit where $|\tau^n - \tau^{n-1}|, \ldots, |\tau^2 - \tau^1|, \tau^1$ are each taken to be large compared with the longest relaxation time of the constituents of the system. Here, $g_{i,s}(\boldsymbol{r}, t) \equiv \delta\big((\boldsymbol{c}_{i,s}(t) - \boldsymbol{r}\big)$ refers to the distribution profile of the s-th end of the i-th dimer at a given time instant t. On the LHS of Eq. (3.16), the angular brackets refer to a thermal average over the microscopic positions and orientations of the dimer, whilst on the RHS of Eq. (3.16), the angular brackets refer to averaging over t^0. By considering the autocorrelation function on the RHS of Eq. (3.16), we can interpret t^0 [to which corresponds the zeroth replica $\langle g_{i,s}(\boldsymbol{r}^0)\rangle$] as the instant of cross-linking, whence the time instants $t^0 + \tau^1, \ldots, t^0 + \tau^n$ [to which correspond the replicas $\langle g_{i,s}(\boldsymbol{r}^1)\rangle \ldots \langle g_{i,s}(\boldsymbol{r}^n)\rangle$, respectively] are then times at which the system is measured long after cross-linking, each measurement instant being temporally far removed from other measurement instants. Because our replica framework maintains a conceptual distinction between the zeroth and the n remaining replicas, it is well adapted to investigations of nematic elastomers, whose measured properties are known to depend on their states of preparation; see, e.g., Ref. [28].

Based on the above discussion, we can interpret $\langle \Gamma(\hat{r})\rangle$ as the joint probability that a dimer-end is found at position $\boldsymbol{r}^0$ at the instant of cross-linking, and that the same dimer-end would be found at n subsequent, widely-separated, time instants at the positions $\boldsymbol{r}^1, \ldots, \boldsymbol{r}^n$. Similar to the order parameter $\Omega(\hat{r})$ described in Sec. 1.2.2, the value of $\langle \Gamma(\hat{r})\rangle$ vanishes if all the dimers are delocalized, and has a nonzero value if a fraction of dimers are localized. Thus, $\langle \Gamma(\hat{r})\rangle$ serves, for a system of dimers, as an order parameter to detect a phase transition from the liquid state to the random solid state. In Sec. 4.1, we shall discover (at the mean-field level) that the expectation value of Γ can be given an Ansatz of the same form as that for the expectation value of Ω (considered in Sec. 1.2.2). The expectation value $\langle \mathbf{Q}^0(\boldsymbol{r}^\alpha)\rangle$ can

be interpreted as the local nematic order parameter for the preparation ensemble, whilst the expectation value $\langle \mathbf{Q}^\alpha(\boldsymbol{r}^\alpha)\rangle$ (for $\alpha = 1, \ldots, N$) can be interpreted as the local nematic order parameter for the measurement ensemble.

3.3 Landau-Wilson free energy

By using the collective fields Γ and $\mathbf{Q}^\alpha$, we can express the effective replica theory as follows:

$$Z_{1+n} = \int \mathcal{D}\Gamma_{\hat{k}} \prod_{\alpha=0}^{n} \mathcal{D}Q^\alpha_{\boldsymbol{p}} \exp\big(-N f_{1+n}(\Gamma, \mathbf{Q}^\alpha)\big). \tag{3.17}$$

Here, the Landau-Wilson free energy per dimer f_{1+n} (scaled in units of T) is given by

$$\begin{aligned} f_{1+n}(\Gamma, \mathbf{Q}^\alpha) = {} & \frac{\tilde{\eta}^2}{2V^n} \overline{\sum_{\hat{k}}} \Delta_{\hat{k}} |\Gamma_{\hat{k}}|^2 + \frac{1}{2} \sum_{\alpha=0}^{n} \sum_{\boldsymbol{p}} \frac{J_{\boldsymbol{p}}}{T^\alpha} \{\mathbf{Q}^\alpha_{\boldsymbol{p}}\, \mathbf{Q}^\alpha_{-\boldsymbol{p}}\} \\ & - \ln \Bigg\langle \exp\Bigg(\frac{\tilde{\eta}^2}{2\tilde{V}^n} \overline{\sum_{\hat{k}}} \Delta_{\hat{k}} \Gamma_{\hat{k}} \sum_{s=1,-1} e^{-i\hat{k}\cdot(\hat{c}+\frac{1}{2}s\ell\hat{n})} \\ & + \sum_{\alpha=0}^{n} \sum_{\boldsymbol{p}} \frac{J_{\boldsymbol{p}}}{T^\alpha} Q^\alpha_{d_1 d_2}(\boldsymbol{p}) e^{-i\boldsymbol{p}\cdot\boldsymbol{c}^\alpha} (n^\alpha_{d_1} n^\alpha_{d_2} - D^{-1}\delta_{d_1 d_2}) \Bigg) \Bigg\rangle. \end{aligned} \tag{3.18}$$

Here, the symbol $\tilde{\eta}^2$ is defined by the value $4\eta^2$, Δ_k is defined by $\exp(-\frac{1}{2}b^2k^2)$, and $\hat{n}$ denotes the $1+n$-times replicated unit vector $(\boldsymbol{n}^0, \ldots, \boldsymbol{n}^n)$. [3] The symbol $\langle \ldots \rangle_{1,1+n}$ denotes Boltzmann weighting with respect to the $(n+1)$-fold replicated Hamiltonian of a single dimer. $\overline{\sum}_{\hat{k}}$ denotes the sum over replicated wave-vectors that are restricted to the *higher-replica sector* (denoted "HRS"), for which a replicated wave-vector $\hat{k}$ must have at least two non-zero vector entries: $\boldsymbol{k}^\alpha \neq 0$, $\boldsymbol{k}^\beta \neq 0$, and $\alpha \neq \beta$. For Γ, we have excluded the *one-replica sector* (denoted "1RS"), viz., the set of replicated wave-vectors that each have only one non-zero vector entry [i.e., $\hat{k} = (\mathbf{0}, \ldots, \boldsymbol{k}^\alpha, \ldots, \mathbf{0})$], as such fields would correspond

[3] We hope the reader will be unperturbed by our use of n both for the number of measurement replicas and for the dimer orientation.

to fluctuations in the macroscopic density of dimers (and show up, for example, as states with spatially modulated density). As we are assuming the IGNE to be incompressible, we shall neglect such fluctuations. Formally, the incompressibility is enforced by taking λ to have a very large value, such that fluctuations of Γ in the 1RS are heavily suppressed. We shall also define the *zero-replica sector* (denoted "0RS") to be the set whose only member is the replicated wave-vector that has zero for every entry. The *lower-replica sector* (denoted "LRS") refers to the union of the one-replica sector and the zero-replica sector.

To develop the expansion of the Landau-Wilson free energy, and hence the Landau theory, we expand the ln-trace term in Eq. (3.18) in powers of $\mathbf{Q}$ and Γ. As we are allowing for the possibility of a phase transition from the isotropic to the nematic state, controlled by the temperature T, we keep the $\mathbf{Q}$-only terms to quartic order. This collection of terms is the Landau-de Gennes free energy for nematics [1], replicated $1+n$ times. As we are also allowing for the phase transition from the liquid to the random solid state, controlled by the number of links per dimer η^2, we keep the Γ-only terms to cubic order. For terms coupling Γ and $\mathbf{Q}$, it is appropriate to keep only the ones proportional to $\mathbf{Q}\,\mathbf{Q}\,\Gamma$, $\mathbf{Q}\,\Gamma\,\Gamma$, and $\mathbf{Q}\,\mathbf{Q}\,\Gamma\,\Gamma$. We retain the last term because it is responsible for the pre-emption of macroscopic nematic alignment at low temperatures, as we shall discover. We obtain (see Appendix C for details)

$$f_{1+n}(\Gamma,\mathbf{Q}) = f_\Gamma(\Gamma) + f_Q(\mathbf{Q}) + f_{\text{coupling}}(\Gamma,\mathbf{Q}), \tag{3.19}$$

where f_Γ is the Landau-Wilson free energy per dimer (scaled in units of T) which describes a purely elastomeric network in the absence of nematic freedoms, f_Q describes a purely nematic liquid in the absence of an elastomeric network, and f_{coupling} describes the coupling between the nematic freedoms and the elastomeric network.

We first consider the free-energy contribution f_Γ. It is given by

$$f_\Gamma(\Gamma) = \frac{1}{2}\overline{\sum_{\hat{k}}}\big(r_1 + r_2|\hat{k}|^2\big)|\Gamma_{\hat{k}}|^2 - \frac{r_3}{3}\overline{\sum_{\hat{1},\hat{2},\hat{3}}}\Gamma_{\hat{k}_1}\Gamma_{\hat{k}_2}\Gamma_{\hat{k}_3}\,. \tag{3.20}$$

Here, the notation is that $\overline{\sum}_{\hat{1},\hat{2},\hat{3}} \equiv \overline{\sum}_{\hat{k}_1,\hat{k}_2,\hat{k}_3}\delta_{\hat{k}_1+\hat{k}_2+\hat{k}_3,\hat{0}}$, $r_1 \equiv \tilde{\eta}^2(1-\tilde{\eta}^2)$, $r_2 \equiv \tilde{\eta}^2\ell_r^2$ [where $\ell_r^2 \equiv 2(\tilde{\eta}^2-1/2)b^2+(1-\tilde{\eta}^2)\ell^2/6$], and $r_3 \equiv \tilde{\eta}^6$. The term f_Γ is the free energy that describes the vulcanization/random solidification transition for an ordinary elastomer [6, 7, 62]. It exhibits a linear instability at the critical value $\tilde{\eta}_c^2 = 1$,[4] which reflects the destabilization of the liquid state with respect to a gel/random solid state when the average number of cross-links per dimer is increased beyond a certain critical value.

Next, we consider the free-energy contribution f_Q. In the present chapter, we only consider its terms at quadratic order, and neglect higher-order terms, as we are focussing on the liquid-crystalline properties of IGNEs at high temperatures. (The effect of nematic terms at cubic and quartic order will be considered in Chapter 8, where we study the liquid-crystalline behavior of IGNEs at low temperatures.) From Appendix C we have that the relevant terms are given by

$$\frac{1}{2}\sum_{\alpha=0}^{n}\sum_{\boldsymbol{p}}(J_{\boldsymbol{p}}/T^\alpha)\{\mathbf{Q}^\alpha_{\boldsymbol{p}}\,\mathbf{Q}^\alpha_{-\boldsymbol{p}}\} - \frac{1}{2}\langle G_2(Q)^2\rangle. \tag{3.21}$$

These terms describe the free-energy cost of inducing nematic alignment from the unaligned state, and constitute the part of the familiar Landau-de Gennes free energy at quadratic order in $\mathbf{Q}$. We thus have

$$\begin{aligned} f_Q(\mathbf{Q}) \;=\; & \sum_{\alpha=0}^{n}\sum_{\boldsymbol{p}}\frac{1}{2T^\alpha}\mathcal{M}(T^\alpha,\boldsymbol{p})\{\mathbf{Q}^\alpha_{\boldsymbol{p}}\,\mathbf{Q}^\alpha_{-\boldsymbol{p}}\} \\ & -\sum_{\alpha=1}^{n}\left(\frac{v}{3T}\sum_{\boldsymbol{p}_1,\boldsymbol{p}_2}\{\mathbf{Q}^\alpha_{\boldsymbol{p}_1}\,\mathbf{Q}^\alpha_{\boldsymbol{p}_2}\,\mathbf{Q}^\alpha_{-\boldsymbol{p}_1-\boldsymbol{p}_2}\} + \frac{w}{4T}\sum_{\boldsymbol{p}_1,\boldsymbol{p}_2,\boldsymbol{p}_3}\{\mathbf{Q}^\alpha_{\boldsymbol{p}_1}\,\mathbf{Q}^\alpha_{\boldsymbol{p}_2}\}\{\mathbf{Q}^\alpha_{\boldsymbol{p}_3}\,\mathbf{Q}^\alpha_{-\boldsymbol{p}_1-\boldsymbol{p}_2-\boldsymbol{p}_3}\}\right), \end{aligned} \tag{3.22}$$

where T^0 corresponds to the preparation temperature, and T^α (for $\alpha = 1,\ldots,n$) corresponds

[4]This critical value $\tilde{\eta}^2$ implies that the critical average linking number $[M]/N$ is 1/2, which is consistent with that found for the randomly-linked particle model [62]. This is not surprising, as the connectivity of the network is a topological characteristic that should not vary with the shape of the connected constituents (e.g., if one were to replace point particles with extended rods).

to the measurement temperature. In the high-temperature regime, we can neglect terms of cubic and quartic order in $\mathbf{Q}$, as the nematic fluctuations are small. As we assume that the system is measured at one temperature (which we denote by T), we write T^α (for $\alpha = 1, \ldots, n$) as T. The parameters v and w scale as $v \sim O((J_0/T)^3)$ and $w \sim O((J_0/T)^4)$. The "mass function" $\mathcal{M}(T^\alpha, \boldsymbol{p})$ is defined via

$$\mathcal{M}(T^\alpha, \boldsymbol{p}) \equiv J_0 e^{-p^2a^2/2}\left(1 - \frac{2J_0}{15T^\alpha}e^{-p^2a^2/2}\right); \tag{3.23}$$

it can be expanded in powers of wave-vectors as

$$\mathcal{M}(T^\alpha, \boldsymbol{p}) \approx \mathcal{C}^\alpha t^\alpha + \mathcal{K}^\alpha p^2. \tag{3.24}$$

Here, t^0 corresponds to the reduced preparation temperature and has the value $(T^0 - T^*)/T^*$ (where T^* has the value $4J_0/15$); t^α (for $\alpha = 1, \ldots, n$) corresponds to the reduced measurement temperature, and has the value $(T - T^*)/T^*$. We write t^α [for $\alpha = (1, \ldots, n)$] as t. The parameter $\mathcal{C}^\alpha$ is a measure of the aligning strength of nematogens and has the value J_0T^*/T^α, whilst the parameter $\mathcal{K}^\alpha$ is a measure of the local nematic stiffness and has the value $(2T^* - T^\alpha)a^2\, J_0/2T^\alpha$. Hence, the nematic free energy f_Q can be expressed as

$$\begin{aligned} f_Q(\mathbf{Q}) \;\approx\; & \frac{1}{2T^0}\sum_{\boldsymbol{p}} \mathcal{M}(T^0, \boldsymbol{p})\{\mathbf{Q}^0_{\boldsymbol{p}}\, \mathbf{Q}^0_{-\boldsymbol{p}}\} + \sum_{\alpha=1}^{n}\sum_{\boldsymbol{p}} \frac{1}{2T}(\mathcal{C}t + \mathcal{K}p^2)\{\mathbf{Q}^\alpha_{\boldsymbol{p}}\, \mathbf{Q}^\alpha_{-\boldsymbol{p}}\} \\ & -\frac{v}{3T}\sum_{\alpha=1}^{n}\sum_{\boldsymbol{p}_1,\boldsymbol{p}_2}\{\mathbf{Q}^\alpha_{\boldsymbol{p}_1}\, \mathbf{Q}^\alpha_{\boldsymbol{p}_2}\, \mathbf{Q}^\alpha_{-\boldsymbol{p}_1-\boldsymbol{p}_2}\} + \frac{w}{4T}\sum_{\alpha=1}^{n}\sum_{\boldsymbol{p}_1,\boldsymbol{p}_2,\boldsymbol{p}_3}\{\mathbf{Q}^\alpha_{\boldsymbol{p}_1}\, \mathbf{Q}^\alpha_{\boldsymbol{p}_2}\}\,\{\mathbf{Q}^\alpha_{\boldsymbol{p}_3}\, \mathbf{Q}^\alpha_{-\boldsymbol{p}_1-\boldsymbol{p}_2-\boldsymbol{p}_3}\}, \end{aligned} \tag{3.25}$$

where $\mathcal{C}$ and $\mathcal{K}$ correspond, respectively, to the values of $\mathcal{C}^\alpha$ and $\mathcal{K}^\alpha$ for $\alpha = 1, \ldots, n$.

Lastly, we consider the free-energy contribution f_{coupling}. This consists of the following three pieces,

$$f_{\text{coupling}} = f_{Q\Gamma\Gamma} + f_{QQ\Gamma} + f_{QQ\Gamma\Gamma}. \tag{3.26}$$

The first, $f_{Q\Gamma\Gamma}$, accounts for the coupling of elastic fluctuations and nematic alignment fluctuations in an IGNE, as we shall see in Sec. 4.2; it is given by

$$f_{Q\Gamma\Gamma}(\Gamma,\mathbf{Q}) = -\sum_{\alpha=0}^{n}\sum_{\boldsymbol{p}}\overline{\sum_{\hat{k}}} m_1^{\alpha}\big(p_{d_1}\,p_{d_2} + (k^{\alpha}+(p/2))_{d_1}(k^{\alpha}+(p/2))_{d_2}\big)\Gamma_{\hat{k}}\,\Gamma_{-\hat{k}-\boldsymbol{p}\hat{\epsilon}^{\alpha}}\,Q^{\alpha}_{d_1d_2}(\boldsymbol{p}), \tag{3.27}$$

where, $m_1^{\alpha} \equiv J_0\tilde{\eta}^2\ell^2/10T^{\alpha}$. The next contribution to f_{coupling} in Eq. (3.26) is $f_{QQ\Gamma}$, which primarily describes the impact, on nematic fluctuation correlations, of quenched randomness arising from the cross-linking constraints. It is given by

$$f_{QQ\Gamma}(\Gamma,\mathbf{Q}) = -\sum_{\alpha\neq\beta}^{n}\sum_{\boldsymbol{p},\boldsymbol{q}} m_2^{\alpha}\,p_{d_1}\,p_{d_2}\,q_{d_3}\,q_{d_4}\,\Gamma_{-\boldsymbol{p}\hat{\epsilon}^{\alpha}-\boldsymbol{q}\hat{\epsilon}^{\beta}}\,Q^{\alpha}_{d_1d_2}(\boldsymbol{p})\,Q^{\beta}_{d_3d_4}(\boldsymbol{q}), \tag{3.28}$$

where $m_2^{\alpha} \equiv J_0^2\tilde{\eta}^4\ell^4/1600(T^{\alpha})^2$. At lengthscales much larger than the length ℓ of a dimer, this contribution is sub-dominant to another contribution, $f_{QQ\Gamma\Gamma}$, owing to the presence of a prefactor that is quartic in wave-vectors. The third contribution to f_{coupling} in Eq. (3.26) is $f_{QQ\Gamma\Gamma}$, which also describes the effects of quenched randomness on nematic fluctuation correlations. As we shall see later (cf. Sec. 4.2), this contribution leads to the non-local interaction term $\{\mathbf{Q}_{\boldsymbol{p}}\,\mathbf{Q}_{-\boldsymbol{p}}\}\mathrm{H}_{\boldsymbol{p}}$ of Eq. (2.3), which results in the real-space oscillatory decay behavior of nematic correlations in a certain regime (viz., the strong-disorder regime). The

term $f_{QQ\Gamma\Gamma}$ is given by

$$
\begin{aligned}
f_{QQ\Gamma\Gamma}(\Gamma,\mathbf{Q}) \;=\; & -\sum_{\alpha}^{n}\sum_{\boldsymbol{p},\boldsymbol{q}}\overline{\sum_{\hat{k}}} m_3^{\alpha}\,\Gamma_{\hat{k}}\,\Gamma_{-\hat{k}-(\boldsymbol{p}+\boldsymbol{q})\hat{\epsilon}^{\alpha}}\,Q^{\alpha}_{d_1d_2}(\boldsymbol{p})\,Q^{\alpha}_{d_3d_4}(\boldsymbol{q}) \\
& \quad\times\Big(\delta_{d_1d_3}\,\delta_{d_2d_4}-\frac{\ell^2}{7}(p+q)_{d_1}(p+q)_{d_3}\,\delta_{d_2d_4} \\
& -\frac{4\ell^2}{7}\big(k^{\alpha}+((p+q)/2)\big)_{d_1}\big(k^{\alpha}+((p+q)/2)\big)_{d_3}\delta_{d_2d_4}\Big) \\
& -\sum_{\alpha\neq\beta}^{n}\sum_{\boldsymbol{p},\boldsymbol{q}}\overline{\sum_{\hat{k}}} m_4^{\alpha}\,\Gamma_{\hat{k}}\,\Gamma_{-\hat{k}-\boldsymbol{p}\hat{\epsilon}^{\alpha}-\boldsymbol{q}\hat{\epsilon}^{\beta}}\,Q^{\alpha}_{d_1d_2}(\boldsymbol{p})\,Q^{\beta}_{d_3d_4}(\boldsymbol{q}) \\
& \quad\times\Big(k^{\alpha}_{d_1}\,k^{\alpha}_{d_2}\,k^{\beta}_{d_3}\,k^{\beta}_{d_4}+\frac{1}{4}(p_{d_1}\,k^{\alpha}_{d_2}+k^{\alpha}_{d_1}\,p_{d_2})(q_{d_3}\,k^{\beta}_{d_4}+k^{\beta}_{d_3}\,q_{d_4}) \\
& +\frac{1}{8}p_{d_1}\,p_{d_2}\,q_{d_3}\,q_{d_4}\Big) \\
& -\sum_{\alpha}\sum_{\hat{k}\in HRS}\sum_{\boldsymbol{p}} m_5^{\alpha}\,\Gamma_{-\hat{k}}\,\Gamma_{\hat{k}}\{\mathbf{Q}^{\alpha}_{\boldsymbol{p}}\,\mathbf{Q}^{\alpha}_{-\boldsymbol{p}}\}. \qquad (3.29)
\end{aligned}
$$

Here, $m_3^{\alpha}=2J_0^2\tilde{\eta}^4/15(T^{\alpha})^2$, $m_4^{\alpha}=J_0^2\tilde{\eta}^4\ell^4/450(T^{\alpha})^2$ and $m_5^{\alpha}=J_0^2\tilde{\eta}^4\ell^4/60(T^{\alpha})^2$. We note the overall minus sign in front of the coupling terms in Eqs. (3.27),(3.28) and (3.29). Physically, this means that the alignment of nematic freedoms with the random, locally anisotropic environments created by the cross-linking *lowers* the free energy of the system. The minus sign also ensures that the correlators or nematic susceptibilities that we shall compute in Sec. 4.2 are positive definite, and thus do not suggest any thermodynamic instabilities.

Chapter 4

Saddle-point approximation

To investigate whether the system is in an ordered state at some external condition (such as temperature or linking number), one can compute the equilibrium value of the corresponding order parameter. Computing the equilibrium values of the order parameters, $[\langle \boldsymbol{q} \rangle]$ [cf. (3.14)] and $[\langle \gamma \rangle]$ [cf. (3.13)], is difficult, but the task is facilitated by observing that $[\langle \boldsymbol{q} \rangle]$ and $[\langle \gamma \rangle]$ are equal to the equilibrium values of the auxiliary fields, $\lim_{n\to 0}\langle \mathbf{Q}^{\alpha} \rangle$ and $\lim_{n\to 0}\langle \Gamma \rangle$, respectively computed using the effective replica Hamiltonian (3.19). In turn, these field-theoretic equilibrium values are also hard to determine exactly, but there exists a procedure by which they can systematically be approximated. The first step is to make a mean-field approximation. Mathematically, this is equivalent to computing the saddle-point values of $\mathbf{Q}$ and Γ for given T and $\tilde{\eta}^2$, which are found by requiring that the free energy f_{1+n} [given by Eq. (3.19)] be stationary with respect to these fields. At high temperature and for a value of $\tilde{\eta}^2 > 1$ (i.e., the conditions in which the IGNE started out), the mean-field approximation yields a vanishing saddle-point value for $\bar{\mathbf{Q}}^{\alpha}$: $\bar{\mathbf{Q}} = 0$; and for Γ, its saddle-point value, $\bar{\Gamma}$, is given by Eq. (1.33), in which G is equal to $2(\tilde{\eta}^2 - 1)/3$ and $P(\xi)$ is a peaked distribution, centered about a typical value ξ_L whose value diverges as $\sqrt{\tilde{\eta}^2 - 1}$ near the vulcanization transition. In Sec. 4.2, we employ this mean-field picture to determine an effective replica Hamiltonian for local nematic order in the presence of the random network. This Hamiltonian enables one to derive expressions for the glassy and thermal fluctuation correlators. We also make a comparison of the effective replica Hamiltonian derived in this chapter with that presented in Sec. 2.4, and show that they are equivalent.

4.1 Stationarity equations

In this section, we solve—for a system in the macroscopically isotropic, random solid state—the saddle-point equations of the field theory, and approximate the expectation values $\langle\Gamma\rangle$ and $\langle\mathbf{Q}\rangle$ by their saddle-point values $\bar{\Gamma}$ and $\bar{\mathbf{Q}}$:

$$\left.\frac{\delta f_{1+n}}{\delta\Gamma}\right|_{\bar{\Gamma},\bar{Q}} = 0; \tag{4.1a}$$

$$\left.\frac{\delta f_{1+n}}{\delta Q_j^\alpha}\right|_{\bar{\Gamma},\bar{Q}} = 0; \tag{4.1b}$$

where the scalar freedoms Q_j are related to the matrix $\mathbf{Q}$ via the formula $\mathbf{Q} \equiv \sum_{j=0}^{4} \mathbf{I}_j\, Q_j$ (the matrices $\mathbf{I}_j$ are the five elements of a convenient basis for symmetric traceless 3×3 matrices, defined in Appendix D). As we are considering the system in the macroscopically isotropic state, we require the saddle-point value of $\mathbf{Q}$ to vanish: $\bar{\mathbf{Q}} = \mathbf{0}$. The saddle-point equation for $\bar{\Gamma}$ is obtained by applying (4.1a) to (3.20) (with $\mathbf{Q}^\alpha$ already set to its saddle-point value). This yields

$$\Big(1 - \tilde{\eta}^2 + \frac{1}{2}\ell_r^2\,|\hat{k}|^2\Big)\Gamma_{\hat{k}} - \tilde{\eta}^4 \overline{\sum_{\hat{k}'}}\, \Gamma_{\hat{k}'}\,\Gamma_{\hat{k}-\hat{k}'} = 0, \tag{4.2}$$

where we remind the reader that the basic lengthscale ℓ_r is given by $\ell_r^2 \equiv 2(\tilde{\eta}^2 - 1/2)b^2 + (1-\tilde{\eta}^2)\ell^2/6$. We observe that Eq. (4.2) is of the same form as Eq. (1.36), which implies that the value of $\langle\Gamma\rangle$ that has the form of the Ansatz for $\langle\Omega\rangle$ in Eq. (1.33) solves the saddle-point equation Eq. (4.2). The value of G that satisfies the stationarity condition Eq. (1.36) was determined in Ref. [7], and we can directly transplant his result into the present context by identifying $\tilde{\eta}^2 - 1$ with ϵ and $\tilde{\eta}^4$ with c. Observing that the wave-vectors in Eq. (1.35) are scaled in units of a basic lengthscale, which we can take to be given by ℓ_r, one finds that the

gel fraction in the IGNE has the value

$$G = 2(\tilde{\eta}^2 - 1)/3. \tag{4.3}$$

For simplicity, we set the distribution of localization lengths $P(\xi)$ to a sharp value $P(\xi) \to \delta(\xi - \xi_L)$, thus obtaining

$$\bar{\Gamma}_{\hat{k}} \approx G \int \frac{d\boldsymbol{z}}{V} e^{i \sum_\alpha \boldsymbol{k}^\alpha \cdot \boldsymbol{z} - \frac{1}{2}|\hat{k}|^2 \xi_L^2} - G\delta_{\hat{k},\hat{0}}, \tag{4.4}$$

i.e., an entity of order G. An elementary Fourier transformation shows that in real space, the order parameter is given by

$$\bar{\Gamma}(\hat{r}) = \frac{G}{(2\pi\xi_L^2)^{(1+n)D/2}} \int \frac{d\boldsymbol{z}}{V}\, e^{-|\hat{r}-\hat{z}|^2/2\xi_L^2} - \frac{G}{V^{1+n}}. \tag{4.5}$$

Here, $\hat{z}$ is a $(1+n)$-fold-replicated vector whose value is given by $(\boldsymbol{z}, \ldots, \boldsymbol{z})$. We can regard Eq. (4.5) as a variational Ansatz, which is to be substituted into the free energy Eq. (1.35) and made stationary with respect to ξ_L. This procedure is essentially the same as that described in Ref. [6], and yields the following value for the typical localization length: $\xi_L \approx (\tilde{\eta}^2 - 1)^{-1/2} \ell_r$. As with the case of vulcanized rubber, the typical localization lengthscale of the localized constituents in an IGNE diverges as the vulcanization transition is approached.

The values $\Gamma = \bar{\Gamma}$ and $\mathbf{Q} = \mathbf{0}$ also solve the second saddle-point equation (4.1b); this is shown in detail in Appendix E.

4.2 Effective theory of structure and correlations in IGNEs

In this section, we re-derive the results obtained for a high-temperature IGNE in Chapter 2. The re-derivation will occur in several stages. First, we derive an effective replica

Hamiltonian for the liquid crystalline behavior of an IGNE in the saddle-point approximation to Γ but with $\mathbf{Q}^\alpha$ allowed to undergo thermal fluctuations. We remind the reader that the saddle-point approximation for Γ corresponds to a situation in which the localized constituents of a network undergo uncorrelated thermal fluctuations, and the system does not undergo relaxation after cross-linking. Next, we show that this effective replica Hamiltonian is equivalent to the one considered in Chapter 2 [i.e., Eq. (2.16)], by matching the structure and parameters of the former to those of the latter. In addition, we compute the nematic glassy and thermal fluctuation correlators using the replica formalism. We shall find that the correlators computed in this way agree with those computed using the phenomenological approach.

In the saddle-point approximation, Γ is regarded as a *given* quantity, set to its saddle-point value $\bar{\Gamma}$, and one neglects the feedback of the nematic degrees of freedom on it. One also does not need to consider the free energy associated with the formation of the random solid itself, as it is a constant. Furthermore, at this level of approximation, the term proportional to $\bar{\Gamma}\bar{\Gamma}\mathbf{Q}^\alpha$ vanishes, as we show in Appendix F. Moreover, in the long-wavelength limit the term proportional to $\bar{\Gamma}\mathbf{Q}^\alpha\mathbf{Q}^\beta$ is subdominant to the term proportional to $\bar{\Gamma}\bar{\Gamma}\mathbf{Q}^\alpha\mathbf{Q}^\beta$. Thus, we only need to consider the replicated Landau-de Gennes theory plus the coupling term proportional to $\bar{\Gamma}\bar{\Gamma}\mathbf{Q}^\alpha\mathbf{Q}^\beta$ for the effective replica Hamiltonian of liquid crystallinity, which we denote by H_{1+n}. This H_{1+n} depends parametrically on $\bar{\Gamma}$ but statistical-mechanically on the [$(1+n)$-fold replicated] nematic order parameter $\mathbf{Q}^\alpha(\boldsymbol{r})$. Thus, we have that H_{1+n} is given by (cf. Appendix F)

$$\begin{aligned} H_{1+n}[\mathbf{Q}^\alpha] \;=\; & \sum_{\boldsymbol{p}} \frac{1}{2T^0}(\mathcal{C}^0 t^0 + \mathcal{K}^0 p^2)\{\mathbf{Q}^0_{\boldsymbol{p}}\,\mathbf{Q}^0_{-\boldsymbol{p}}\} + \sum_{\alpha=1}^{n}\sum_{\boldsymbol{p}} \frac{1}{2T}(\mathcal{C}t + \mathcal{K}p^2)\{\mathbf{Q}^\alpha_{\boldsymbol{p}}\,\mathbf{Q}^\alpha_{-\boldsymbol{p}}\} \\ & -\frac{1}{T^0}\sum_{\alpha=1}^{n}\sum_{\boldsymbol{p}} \mathrm{W}_{\boldsymbol{p}}\{\mathbf{Q}^0_{\boldsymbol{p}}\,\mathbf{Q}^\alpha_{-\boldsymbol{p}}\} - \frac{1}{2T}\sum_{\substack{\alpha,\beta=1\\(\alpha\neq\beta)}}^{n}\sum_{\boldsymbol{p}} \mathrm{W}_{\boldsymbol{p}}\{\mathbf{Q}^\alpha_{\boldsymbol{p}}\,\mathbf{Q}^\beta_{-\boldsymbol{p}}\}. \end{aligned} \tag{4.6}$$

Here, $\mathcal{C}$ and $\mathcal{K}$ correspond, respectively, to the values of $\mathcal{C}^\alpha$ and $\mathcal{K}^\alpha$ for $\alpha = 1, \ldots, n$. The

symbol $\mathrm{W}_{\boldsymbol{p}}$ is defined as $\mathrm{W}_{\mathbf{0}} e^{-\frac{1}{2}p^2\xi_L^2}$, and we refer to $\mathrm{W}_{\mathbf{0}}$ ($\equiv G^2 J_0^2 \tilde{\eta}^4 \ell^4/(900 T \xi_L^4)$ as the *disorder strength*, i.e., the strength of the disordering effects of the random network on the nematic order. The characteristic lengthscale beyond which $\mathrm{W}(\boldsymbol{r})$ is suppressed exponentially is ξ_L. The kernel $\mathrm{W}_{\boldsymbol{p}}$ is the manifestation of the physics of "melting" at short lengthscales, where thermal fluctuations of the polymer network cannot be neglected.

To find the effect that the preparation history has on the measurable liquid crystalline behavior, we integrate out the zeroth replica element, $\mathbf{Q}^0$, to obtain the effective free energy

$$\begin{aligned} H_{\text{eff}}\left[\{\mathbf{Q}^\alpha\}_{\alpha=1}^n\right] \;\equiv\; & \sum_{\alpha=1}^{n}\sum_{\boldsymbol{p}}\left(\frac{\mathcal{C}t+\mathcal{K}p^2}{2T}-\frac{|\mathrm{W}_{\boldsymbol{p}}|^2}{2T^0(\mathcal{C}^0t^0+\mathcal{K}^0p^2)}\right)\left\{\mathbf{Q}^\alpha_{\boldsymbol{p}}\mathbf{Q}^\alpha_{-\boldsymbol{p}}\right\} \\ & -\sum_{\substack{\alpha,\beta=1\\(\alpha\neq\beta)}}^{n}\sum_{\boldsymbol{p}}\left(\frac{\mathrm{W}_{\boldsymbol{p}}}{2T}+\frac{|\mathrm{W}_{\boldsymbol{p}}|^2}{2T^0(\mathcal{C}t^0+\mathcal{K}^0p^2)}\right)\left\{\mathbf{Q}^\alpha_{\boldsymbol{p}}\mathbf{Q}^\beta_{-\boldsymbol{p}}\right\}. \end{aligned} \tag{4.7}$$

We can now compare the replica free energy stemming from the microscopic model given in Eq. (4.7) with the replica free energy stemming from the phenomenological model in Eq. (2.16). We see that they agree, provided the following correspondences for $\mathcal{C}$, $\mathcal{C}^0$, $\mathrm{W}_{\boldsymbol{p}}$ and $[\{\mathbf{Y}_{\boldsymbol{p}}\,\mathbf{Y}_{-\boldsymbol{p}}\}]$ hold:

$$\mathcal{C} = \mathcal{A}\,(\equiv J_0\,T^*/T), \tag{4.8a}$$

$$\mathcal{C}^0 = \mathcal{A}^0\,(\equiv J_0\,T^*/T^0), \tag{4.8b}$$

$$\mathcal{K} = \mathcal{L}, \tag{4.8c}$$

$$\mathcal{K}^0 = \mathcal{L}^0, \tag{4.8d}$$

$$\mathrm{W}_{\boldsymbol{p}} = \mathrm{H}_{\boldsymbol{p}}\,(\equiv \mathrm{H}_{\mathbf{0}}\,e^{-p^2\xi_L^2/2}), \tag{4.8e}$$

$$\mathrm{W}_{\mathbf{0}} = \mathrm{H}_{\mathbf{0}}, \tag{4.8f}$$

$$[\{\mathbf{Y}_{\boldsymbol{p}}\,\mathbf{Y}_{-\boldsymbol{p}}\}] = T\,\mathrm{W}_{\boldsymbol{p}}\,. \tag{4.8g}$$

We learn from the microscopic field theory of the dimer model that H and $\mathbf{Y}$ have the same physical origins. As W is equal to H, W can be interpreted as arising from an unconventional,

"soft"type of random field which goes to zero at short lengthscales but assumes a non-vanishing value at long lengthscales. Such an unconventional, soft random field is to be contrasted with the conventional, "hard" random field that is present at all length-scales. The softness of the former reflects the fact that the elastomeric background that gives rise to quenched randomness is itself thermally fluctuating, as has been discussed in detail in Chapter 2 (see also [29]). The relation (4.8g) allows one to assert the statistics of the glassy nematic correlations in an IGNE: as Eq. (4.7) is Gaussian in the field variable $\mathbf{Q}^\alpha$, all odd moments vanish, the second moment is given by the glassy correlator, and higher even moments can be obtained using suitable products of glassy correlators. In the remainder of the thesis, we shall adhere to the notation established in Chapter 2, i.e., we shall use the notation $\mathcal{A}$, $\mathcal{L}$, H and $\mathrm{H}_{\mathbf{0}}$ instead of $\mathcal{C}$, $\mathcal{K}$, W and $\mathrm{W}_{\mathbf{0}}$.

Next, we turn to the computation of $\mathcal{C}^T$ and $\mathcal{C}^G$ via the effective replica Hamiltonian (4.7). We make use of the following identities (proved in Appendix G):

$$[\langle \mathbf{Q} \rangle] = \lim_{n\to 0} \langle\!\langle \mathbf{Q}^\alpha \rangle\!\rangle; \tag{4.9a}$$

$$[\{\langle \mathbf{Q} \rangle \langle \mathbf{Q} \rangle\}] = \lim_{n\to 0} \langle\!\langle \mathbf{Q}^\alpha \mathbf{Q}^\beta \rangle\!\rangle \qquad (\alpha \neq \beta); \tag{4.9b}$$

$$[\{\langle \mathbf{Q}\,\mathbf{Q} \rangle\}] = \lim_{n\to 0} \langle\!\langle \mathbf{Q}^\alpha \mathbf{Q}^\alpha \rangle\!\rangle. \tag{4.9c}$$

Here, $\langle\!\langle \cdots \rangle\!\rangle$ denotes an average performed with respect to the effective Hamiltonian H_{eff}. By using these identities, we can obtain $\mathcal{C}^T$ and $\mathcal{C}^G$ in wave-vector space from the diagonal and off-diagonal elements of the propagator matrix, thus arriving at the results

$$\mathcal{C}^T_{\boldsymbol{p}} = T\mu_D \, \frac{1}{\mathcal{A}t + \mathcal{L}p^2 + \mathrm{H}_{\boldsymbol{p}}}, \tag{4.10a}$$

$$\mathcal{C}^G_{\boldsymbol{p}} = T\mu_D \, \frac{\frac{T|\mathrm{H}_{\boldsymbol{p}}|^2}{T^0 \mathcal{M}(T^0,\boldsymbol{p})} + \mathrm{H}_{\boldsymbol{p}}}{\left(\mathcal{A}t + \mathcal{L}p^2 + \mathrm{H}_{\boldsymbol{p}}\right)^2}. \tag{4.10b}$$

Note that the correlators given in Eqs. (4.10) are the same as the correlators given in Eqs. (2.9). This again shows that the phenomenological model described in Chapter 1 can

be derived from the dimer/spring model described in the present chapter. The appearance of a scale-dependent function $\mathrm{H}_{\boldsymbol{p}}$ in the denominators is a significant feature of the present approach. $\mathrm{H}_{\boldsymbol{p}}$ follows directly from the absence of the replica-diagonal contributions to the term (4.7). Originating in the random network, $\mathrm{H}_{\boldsymbol{p}}$ leads to a scale-dependent, *downward* renormalization of the bare spinodal temperature T^*, as can be seen from the denominators of Eqs. (4.10).

Owing to the fact that the correlators in Eq. (4.10) have been derived from a theory that is at most quadratic in fluctuations of $\mathbf{Q}^\alpha$, we call these correlators "bare" correlators. They exhibit a singularity (which suggests an instability) at some (negative) value of the reduced temperature $t < 0$. For $\mathrm{H}_{\mathbf{0}}\xi_L^2/\mathcal{L} < 2$, i.e., in the weak-disorder regime, the denominator factor $\mathcal{A}t + \mathcal{L}p^2 + \mathrm{H}_{\boldsymbol{p}}$ has a minimum at $\boldsymbol{p} = \mathbf{0}$. Consequently, both of the bare correlators given in Eqs. (4.10) diverge, at $\boldsymbol{p} = \mathbf{0}$, at a critical (reduced, rescaled) temperature of $-\mathrm{H}_{\mathbf{0}}\xi_L^2/\mathcal{L}$. This suggests a continuous transition to a uniformly ordered (i.e., macroscopically anisotropic) nematic state. By contrast, for $\mathrm{H}_{\mathbf{0}}\xi_L^2/\mathcal{L} > 2$, i.e., in the strong-disorder regime, the denominator factors have a minimum at $p^2 = 2\ln(\mathrm{H}_{\mathbf{0}}\xi_L^2/2\mathcal{L})$; therefore, both bare correlators exhibit nonzero-wavelength divergences at a (reduced, rescaled) temperature $-2\ln(e\mathrm{H}_{\mathbf{0}}\xi_L^2/2\mathcal{L})$. This suggests a continuous phase transition to a state having periodic spatial modulations. As we shall see in Chapter 8, however, neither of these putative transitions actually occurs when terms cubic and quartic in $\mathbf{Q}^\alpha$ are taken into account, as the fluctuation corrections turn out to suppress the occurrence of the instabilities in 3 spatial dimensions.

Chapter 5

Replica Goldstone fluctuations and their physical meaning

With Chapters 5 and 6, we move to the topic of elasticity, studying it as a phenomenon that emerges from the underlying statistical mechanics of fluctuations of the constituents of the elastomer. In this chapter, we explain how non-affine correlations in random elastic media can be described via the replica formalism of vulcanization theory. This chapter sets the stage for the following ones, which describe how the elastic behavior of IGNEs is influenced by nematic fluctuations. The present chapter has three sections. First, we introduce the notion of non-affine displacement, which is an example of an elastic fluctuation, describing how it has been quantified in phenomenological approaches such as the one formulated by DiDonna and Lubensky [61]. In the following section, we examine a certain class of replica Goldstone fluctuations. We then explain how such "Goldstone-deformed" states in vulcanization theory can be interpreted in terms of a phenomenological theory of elastomers that takes non-affinity into account. In the final section, we show how the theory of "Goldstone-deformed" states can be employed to compute a certain correlator that reflects (i) the magnitude of the random displacements that volume elements of the elastomer undergo during the process of relaxation to mechanical equilibrium after cross-linking; and (ii) the departures from affinity that occur when the elastomer is stretched. This chapter is based on material from Refs. [61] and [62]. The main novelty that this chapter contains is an alternative derivation of the non-affinity correlator, made using the replica formalism, rather than via a calculation using an (unreplicated) phenomenological model, as was done in Ref. [62].

5.1 Non-affine correlations in random elastic media

According to the picture presented by the classical elasticity theory (see, e.g., Refs. [48, 63]), elastomers are spatially homogeneous media whose elastic moduli $K_{d_1 d_2 d_3 d_4}$ are spatially constant. When a uniform stress is applied to the boundary of such an elastomer, it undergoes an affine deformation [the concept of affinity was defined in Sec. 1.2.1; see Eq. (1.23)]. In reality, however, the deformation is expected to be non-affine, at least at lengthscales comparable to the typical localization length of the network, as the heterogeneities present at those lengthscales lead the individual constituents of the network to undergo inhomogeneous displacements in response to an applied stress. Such deviations from the volume element trajectories expected for affine deformation provide an example of what we term *elastic fluctuations*. Two other types of elastic fluctuations that we consider in this chapter and the following two are: (i) random displacements undergone by the volume elements of the network medium as it relaxes to mechanical equilibrium after cross-linking, which we call "relaxational displacements"; and (ii) thermally excited elastic excursions of volume elements from their mean positions. In the present section, we focus on a subset of elastic fluctuations, viz., the non-affine displacements, and describe a model proposed in Ref. [61] to capture the correlations between the non-affine displacements in random elastic media.

The procedure followed in Ref. [61] involves starting with a model of an elastic network in which particles occupy sites on a periodic or random lattice in their state of mechanical equilibrium, with each pair of particles being connected via permanent central-force springs described by a potential of the form,

$$V_b = \frac{k_b}{2}(R_b - R_{bR})^2 + \frac{g_b}{4}(R_b - R_{bR})^4. \tag{5.1}$$

Here, b labels the spring connecting two given particles, k_b and g_b are finite constants, and the distance between two particles occupying sites i and j in the *distorted* lattice (called the *target space*) is given by $R_b = |\boldsymbol{R}_i - \boldsymbol{R}_j|$. Here, $\boldsymbol{R}_i \equiv \boldsymbol{R}_{i0} + \boldsymbol{u}_i$ is the position of a

particle occupying site i when the lattice is distorted, $\boldsymbol{R}_{i0}$ is the position of the particle in the undistorted lattice (which we call the *reference space*), and $\boldsymbol{u}_i$ is the displacement undergone by the particle when the lattice is distorted. The total energy of the network is given by $U_T = \sum_b V_b(R_b)$.

It is useful to form a quantity called the discrete-lattice nonlinear strain v_b, defined relative to the reference state: $v_b \equiv (R_b^2 - R_{b0}^2) = \boldsymbol{R}_{b0} \cdot \Delta\boldsymbol{u}_b + \frac{1}{2}|\Delta\boldsymbol{u}_b|^2$. Here $\boldsymbol{R}_{b0} \equiv |\boldsymbol{R}_{i0} - \boldsymbol{R}_{j0}|$ is the separation between two particles occupying *neighboring* sites i and j in the *undistorted* lattice, and $\Delta\boldsymbol{u}_b \equiv \boldsymbol{u}_i - \boldsymbol{u}_j$. The lattice is then in a state of mechanical equilibrium when U_T is minimized with respect to v_b, and the elastic energy of distortion can be determined from the departures from the mechanically equilibrated state, in terms of $\Delta\boldsymbol{u}_b$. From the discrete model of the distorted lattice, DiDonna and Lubensky derived a continuum theory of elasticity, the elastic energy of which is given by

$$H = \int d^D\boldsymbol{r} \left(\frac{1}{2} K_{d_1 d_2 d_3 d_4}(\boldsymbol{r})\, u_{d_1 d_2}(\boldsymbol{r})\, u_{d_3 d_4}(\boldsymbol{r}) + \tilde{\sigma}_{d_1 d_2}(\boldsymbol{r})\, u_{d_1 d_2}(\boldsymbol{r}) \right), \tag{5.2}$$

where $u_{d_1 d_2}(\boldsymbol{r}) \equiv (\partial_{d_1} u_{d_2} + \partial_{d_2} u_{d_1} + \partial_{d_1}\boldsymbol{u} \cdot \partial_{d_2}\boldsymbol{u})$ is the *continuum*, Green–Saint Venant Lagrangian, strain tensor, related to v_b via $v_b \approx R_{b0,d_1} R_{b0,d_2} u_{d_1 d_2}(\boldsymbol{r})$. One can likewise define a continuum version $R_d(\boldsymbol{r})$ of the position vector of a particle in the target space, corresponding to the lattice position vector $\boldsymbol{R}_i$, and a continuum version $u_d(\boldsymbol{r})$ of the discrete displacement vector u_i (bearing in mind that d refers to Cartesian coordinates and i labels lattice sites). By defining a deformation gradient tensor $\underline{\underline{\Lambda}}$, corresponding to an external imposed deformation via

$$\Lambda_{d_1 d_2} \equiv \delta_{d_1 d_2} + \gamma_{d_1 d_2}, \tag{5.3}$$

one may write for the position vector of a particle residing in the *bulk* of the medium

$$R_d(\boldsymbol{r}) = \Lambda_{dd'} r_{d'} + u'_{d'}(\boldsymbol{r}); \tag{5.4a}$$

$$u_d(\boldsymbol{r}) = \gamma_{dd'} r_{d'} + u'_d(\boldsymbol{r}), \tag{5.4b}$$

where $\underline{\underline{\gamma}}\cdot\boldsymbol{r}$ and $\boldsymbol{u}'(\boldsymbol{r})$ refer, respectively, to the affine and non-affine parts of the displacement undergone by the particle when the external deformation is imposed. For a particle located at the boundary of the medium, the deformation is affine, and consequently $\boldsymbol{u}' = \boldsymbol{0}$.

The elastic moduli $K_{d_1d_2d_3d_4}$ and the internal stress $\tilde{\sigma}_{d_1d_2}(\boldsymbol{r})$ are related to the the parameters V_b, k_b and R_{b0} of the discrete model via

$$K_{d_1d_2d_3d_4}(\boldsymbol{r}) \equiv \frac{1}{2\mathrm{v}(\boldsymbol{r})}\sum_j k_b\, R_{b0}^{-2} R_{b0,d_1} R_{b0,d_2} R_{b0,d_3} R_{b0,d_4}|_{b=\langle i,j\rangle}; \tag{5.5a}$$

$$\tilde{\sigma}_{d_1d_2}(\boldsymbol{r}) \equiv \frac{1}{2\mathrm{v}(\boldsymbol{r})}\sum_j V_b'(R_{b0})(R_{b0,d_1}/R_{b0})R_{b0,d_2}|_{b=\langle i,j\rangle}, \tag{5.5b}$$

where $\langle i,j\rangle$ denotes a given pair of nearest particle neighbors occupying sites i and j, the sum over j is over all bonds having one end at i, and $\mathrm{v}(\boldsymbol{r})$ is the volume of a Voronoi cell centered at position $\boldsymbol{r} \equiv \boldsymbol{R}_{i0}$. For a lattice having random spring constants k_b, the elastic moduli $K_{d_1d_2d_3d_4}$ and internal stress $\tilde{\sigma}_{d_1d_2}$ of the corresponding continuum elastic theory will also be random, inherited from the randomness in k_b.

Via this approach, DiDonna and Lubensky showed that the non-affinity in the displacements of particles at microscopic (i.e., lattice-spacing) lengthscales can be captured by a continuum theory defined at much larger lengthscales, by studying the random statistics of the elastic moduli $K_{d_1d_2d_3d_4}(\boldsymbol{r})$ at position $\boldsymbol{r}$. It is useful to regard $K_{d_1d_2d_3d_4}(\boldsymbol{r})$ as comprising two components: (i) a spatially uniform average part $K_{d_1d_2d_3d_4}$, and (ii) a spatially fluctuating part $\delta K_{d_1d_2d_3d_4}(\boldsymbol{r})$. In particular, they showed that when the system is subject to a stress that leads to a macroscopic strain $\underline{\underline{\gamma}}$, the non-affine part of the resulting displacement (viz., $\boldsymbol{u}'$), is generated by the spatially fluctuating contribution $\delta K_{d_1d_2d_3d_4}(\boldsymbol{r})$. For $\delta K_{d_1d_2d_3d_4}(\boldsymbol{r})$ and $\gamma_{d_1d_2}$ both small, and writing $[\cdots]$ for the average over bond strengths k_b, DiDonna and Lubensky determined that the Fourier transform of the correlator of the non-affine displacement $G(\boldsymbol{r},\boldsymbol{0})$, defined by

$$G_{dd'}(\boldsymbol{r},\boldsymbol{0}) \equiv [u_d'(\boldsymbol{r})\, u_{d'}'(\boldsymbol{0})], \tag{5.6}$$

takes the functional form $\gamma^2 \Delta^K(\boldsymbol{p})/(p^2\, K^2)$, where $\Delta^K(\boldsymbol{p})$ is the Fourier transform of relevant components of the variance of the elastic modulus-tensor, K represents the disorder-averaged elastic modulus-tensor, and γ (*not* the same as the macroscopic strain $\underline{\underline{\gamma}}$) denotes appropriate components of $\underline{\underline{\Lambda}}$. In real space, and on lengthscales large compared with the correlation lengthscale of non-affinity, $G(\boldsymbol{r}, \boldsymbol{0})$ scales as $(\Delta^K/K^2)\gamma^2 |\boldsymbol{r}|^{-(D-2)}$ in D dimensions.

Having provided an overview non-affinity and its characterization via the phenomenological approach of DiDonna and Lubensky, we now consider an alternative approach, rooted in the replica field theory of vulcanization, which offers a picture in which non-affine displacements can be interpreted as a class of Goldstone fluctuations in the symmetry-broken state of vulcanized media. This alternative approach enables one to study (see Chapter 6), the impact of nematic fluctuation correlations on the elastic behavior of an IGNE and conversely, enables one to study the impact of elastic fluctuations on the liquid crystalline structure in an IGNE in the high-temperature regime (see Chapter 7). In the following two sections, we derive the replica-off-diagonal correlator of the Goldstone fluctuation field in a deformed rubber system, and show that it can be interpreted as the non-affinity correlator considered in Ref. [61].

5.2 Broken symmetries and Goldstone fluctuations: isotropic rubber and IGNEs

In this section, we employ the replica field theory approach to derive a theory of the elasticity of IGNEs in the high-temperature regime. To do this, we first consider the case of rubber, and describe the symmetries that are broken at the random solidification transition. Second, we identify the corresponding branch of "massless" (i.e., Goldstone) fluctuations of the order-parameter field Γ about the random-solid state. Third, we interpret the displacement field corresponding to such Goldstone fluctuations, for externally strained rubber, as replicated

copies of

$$\boldsymbol{v} + (\boldsymbol{v}_\Lambda - \boldsymbol{v}) + \boldsymbol{u}, \tag{5.7}$$

where $\boldsymbol{v}$ is the local displacement that the system undergoes as it relaxes after the instant of cross-linking, $\boldsymbol{v}_\Lambda - \boldsymbol{v}$ is the non-affine part of the deformation that the (relaxed, originally unstrained) system undergoes under the application of an external strain, and $\boldsymbol{u}$ refers to an instance of the thermally driven local displacements that the system undergoes about the relaxed, externally strained state. This interpretation is facilitated by comparing parameters in the disorder-averaged version of the phenomenological model (5.16) with parameters in the Goldstone fluctuation free energy (5.15).

In the replica approach, what symmetries are broken at the random solidification transition? In the liquid state, in which all particles are delocalized, the order parameter $\langle \Gamma \rangle = 0$ has the full symmetry of the Landau free energy of vulcanization [i.e., f_Γ of Eq. (3.20)], and this is the symmetry of independent translations and rotations of each replica. However, at the transition to the random solid state, the symmetry of *relative* translations between various replicas is broken, whilst the symmetry of *common* translations of all replicas is preserved. The preservation of the symmetry of *common* translations of all replicas is a reflection of the *macroscopic* or *statistical* homogeneity of the random solid, whilst the broken symmetry of relative translations of replicas is related to the positional localization of a macroscopic fraction of particles.

This point can be alternatively appreciated by regarding replicas as describing equilibrated copies of the system, probed at widely-separated time-instants, and localization implies that a particle will persist within some region of space for all time, whereas delocalization implies that the particle is able to explore the entire space, so that its positions at widely-separated times are essentially uncorrelated. The liquid state is thus invariant under independent translations of each replica. On the other hand, when the particles are localized, the positions of a particle in different replicas are correlated, and thus the symmetry

of relative translations between different replicas is broken. Such a reduction of symmetry is manifest in the value of $\langle\Gamma\rangle$ [cf. Eq. (4.5)].

In accordance with the conventional Landau paradigm, there would be a Goldstone fluctuation corresponding to each *independent* broken symmetry, the Goldstone fluctuation being defined as the fluctuation whose energy goes to zero as its wave-vector goes to zero. Let us consider the order parameter Γ in real space, as this reveals clearly what the broken and unbroken symmetry directions are in replica space. Considering the case of rubber, the order parameter $\langle\Omega(\hat{r})\rangle$ [cf. (1.34)] can be written in the form

$$\langle\Omega(\hat{r})\rangle = G\int\frac{d\boldsymbol{z}}{V}\left(\frac{1}{2\pi\xi_L^2}\right)^{(1+n)D/2}\exp\left(-\frac{|\hat{r}_\lambda-\hat{z}_\lambda|^2}{2\xi_L^2}-\frac{|\hat{r}_\tau|^2}{2\xi_L^2}\right)-\frac{G}{V^{n+1}}, \tag{5.8}$$

where, for the sake of simplicity, we have specialized to the case where all localized particles are localized with the same localization length ξ_L. Here, we have defined $\hat{z}_\lambda = (\boldsymbol{z},\ldots,\boldsymbol{z})/\sqrt{1+n}$, and decomposed the $(1+n)D$-dimensional position vector $\hat{r}$ into its longitudinal and transverse components, via

$$\hat{r}=\hat{r}_\lambda+\hat{r}_\tau,\quad \hat{r}_\lambda=(\hat{r}\cdot\hat{\epsilon}_\lambda),\quad \hat{r}_\tau=\hat{r}-\hat{r}_\lambda, \tag{5.9}$$

where we have defined the longitudinal basis vector $\hat{\epsilon}_\lambda$ in replica space (spanned by $\{\epsilon^\alpha|\alpha=0,\ldots,n\}$, a set of basis vectors in replica space) via the formula

$$\hat{\epsilon}_\lambda\equiv\sum_{\alpha=0}^{n}\frac{\epsilon^\alpha}{\sqrt{1+n}}. \tag{5.10}$$

From Eq. (5.8), we see that $\langle\Omega(\hat{r})\rangle$ does *not* depend on $\hat{r}_\lambda$, as changes in the latter can be accomodated by shifting the integration variable $\boldsymbol{z}$. This corresponds to the direction of common translations of all replicas. On the other hand, $\Omega(\hat{r})$ *does* depend on $\hat{r}_\tau$, so that the change in Ω (and correspondingly, the free energy of the state) evolves continuously from zero to a finite value as $\hat{r}_\tau$ is deformed continuously by a finite, position-dependent amount.

Thus, the displacement field associated with Goldstone fluctuations should be constructed as $\boldsymbol{z}$-dependent replicated translations $\hat{U}_\tau$ parallel to $\hat{r}_\tau$ in replica space.

There are nD components of $\hat{U}_\tau$ corresponding to the nD independent broken relative translation symmetries, consistent with the Goldstone counting argument, viz., that the number of Goldstone degrees of freedom is equal to the difference between the dimension of the symmetry-unbroken group of transformations (which for the present case is $\mathrm{T}^{(1+n)D}$, where T denotes the group of translations in one spatial dimension for one individual replica) and the symmetry-broken group (which for the present case is T^D, i.e., the group of common translation of all replicas in D spatial dimensions).

For our purpose it would be convenient to adopt a different representation of the Goldstone fluctuations. Consider the general case of a network subject to an imposed external deformation $\underline{\underline{\Lambda}}$ that maps a mass-point at position $\boldsymbol{z}$ at the instant of cross-linking to a position $\underline{\underline{\Lambda}} \cdot \boldsymbol{z}$ *instantaneously*, and subsequently relaxing, causing the same mass-point at position $\boldsymbol{z}$ at the instant of cross-linking to be mapped to a position $\underline{\underline{\Lambda}} \cdot \boldsymbol{z} + \boldsymbol{U}(\boldsymbol{z})$ at a time long after cross-linking. Recalling our earlier discussion pertaining to Eq. (3.16), where we observed that the zeroth replica can be interpreted as an equilibrated copy of the system at the instant of cross-linking and each of the remaining n replicas can be interpreted as equilibrated copies of the system at a time instant of measurement (each time instant of measurement being separated from other measurement time instants by a wide interval), we can express the new Goldstone parametrization via the replicated vector $\hat{U}(\boldsymbol{z})$, which is defined by $\hat{U}(\boldsymbol{z}) \equiv (\hat{R} - \hat{z}) = (\boldsymbol{0}, \boldsymbol{U}^1(\boldsymbol{z}), \ldots, \boldsymbol{U}^n(\boldsymbol{z}))$, where $\hat{R} = (\boldsymbol{R}^0, \ldots, \boldsymbol{R}^n)$ and $\boldsymbol{R}^0(\boldsymbol{z}) = \boldsymbol{z}$. In this parametrization, the "Goldstone-deformed" vulcanization order parameter configuration assumes the form

$$\langle \Omega(\hat{r}) \rangle = \frac{G}{(2\pi\xi_L^2)^{(1+n)D/2}} \int \frac{d\boldsymbol{z}}{V} \, e^{-\frac{1}{2\xi_L^2} \sum_{\alpha=0}^{n} |\boldsymbol{r}^\alpha - \boldsymbol{R}^\alpha(\boldsymbol{z})|^2} - \frac{G}{V^{1+n}}. \tag{5.11}$$

In Fourier space, this same order parameter configuration is given by

$$\Omega_{\hat{k}} = G \int \frac{d\boldsymbol{z}}{V} e^{\sum_{\alpha=0}^{n} i\boldsymbol{k}^{\alpha}\cdot\boldsymbol{R}^{\alpha}(\boldsymbol{z}) - \frac{1}{2}|\boldsymbol{k}^{\alpha}|^2\xi_L^2} - G\delta_{\hat{k},\hat{0}}. \tag{5.12}$$

The two representations of the Goldstone fluctuations—Eq. (5.8), parametrized by translations $\hat{U}_\tau(\boldsymbol{z})$ along the directions of broken translation symmetry of the replicas, and Eq. (5.11), parametrized by $\hat{U}(\boldsymbol{z})$ for which $\boldsymbol{U}^0(\boldsymbol{z}) = \boldsymbol{0}$—were shown to be equivalent in [62]. One can check that both forms certainly have the same number of degrees of freedom, i.e. nD. We adopt the second representation, as it is in line with our interpretation of the zeroth replica as the preparation ensemble, the absence of Goldstone fluctuations in the zeroth replica being consistent with the notion that the system has yet to relax at the instant of cross-linking.

The physical content of the Goldstone fluctuations $\boldsymbol{U}^\alpha(\boldsymbol{z})$ is suggested by a comparison of the free energy of Goldstone fluctuations in vulcanization theory with a phenomenological model of an elastomer that has spatially random elastic moduli and internal stresses (see, e.g., Ref. [62]). To determine, using the formalism of vulcanization theory, the free energy of Goldstone fluctuations for an externally unstrained, incompressible elastomer, one can follow the procedure of Ref. [62]: Starting with the Landau-Wilson free energy of the ordinary elastomer [which is given by (3.18) with J_0 and ℓ set to zero], the "Goldstone-deformed" value (5.12) is substituted for Ω. One integrates out the momenta $\hat{k}$ and the position vectors $\boldsymbol{c}^\alpha$ (in the log-trace part). The resulting expression for the Landau-Wilson free energy then involves quantities of the form $|\hat{R}(\boldsymbol{z}_1) - \hat{R}(\boldsymbol{z}_2)|^2$, which can be re-written in terms of the fluctuation $\Psi(\boldsymbol{z}_1, \boldsymbol{z}_2)$ as

$$|\hat{R}(\boldsymbol{z}_1) - \hat{R}(\boldsymbol{z}_2)|^2 \equiv (1+n)|\boldsymbol{z}_1 - \boldsymbol{z}_2|^2 + \Psi(\boldsymbol{z}_1, \boldsymbol{z}_2). \tag{5.13}$$

For small strains, the Landau-Wilson free energy is then expanded in powers of Ψ, and one

can write it as the sum of the free energy $H_{s.p.}$ of the saddle-point value of Ω and the free energy H_Ψ of Goldstone fluctuations, i.e.,

$$H_\Omega = H_{s.p.} + H_\Psi. \tag{5.14}$$

H_Ψ has been computed in Ref. [62]; it is given by

$$\begin{aligned} H_\Psi &= \frac{1}{2}\int d\boldsymbol{z}_1\, d\boldsymbol{z}_2\, K_1(\boldsymbol{z}_1,\boldsymbol{z}_2)\Psi(\boldsymbol{z}_1,\boldsymbol{z}_2) \\ &\quad -\frac{1}{8T}\int d\boldsymbol{z}_1\, d\boldsymbol{z}_2\, d\boldsymbol{z}_3\, d\boldsymbol{z}_4\, K_2(\boldsymbol{z}_1,\boldsymbol{z}_2,\boldsymbol{z}_3,\boldsymbol{z}_4)\Psi(\boldsymbol{z}_1,\boldsymbol{z}_2)\Psi(\boldsymbol{z}_3,\boldsymbol{z}_4), \end{aligned} \tag{5.15}$$

where $K_1(\boldsymbol{z}_1,\boldsymbol{z}_2)$ and $K_2(\boldsymbol{z}_1,\boldsymbol{z}_2,\boldsymbol{z}_3,\boldsymbol{z}_4)$ are bell-shaped functions of the separations of the positions $\{\boldsymbol{z}_1,\ldots,\boldsymbol{z}_4\}$, whose values are determined in Ref. [62]. For the case where all localized particles have the same localization length ξ_L, $K_1(\boldsymbol{z}_1,\boldsymbol{z}_2)$ and $K_2(\boldsymbol{z}_1,\boldsymbol{z}_2,\boldsymbol{z}_3,\boldsymbol{z}_4)$ are of the order of $(N/V)(1/\xi_L^3)T/\xi_L^2$ and $(N/V^3)(1/\xi_L^3)T/\xi_L^4$, respectively.

One then compares H_Ψ with the replica effective Hamiltonian derived from some microscopic, phenomenological model of elastomer with quenched disorder, in the hope that such a comparison (analogous to the one made between the phenomenological theory of an IGNE and the microscopic model in Sec. 4.2) will enable one to interpret the parameters of H_Ψ in terms of the more familiar phenomenological parameters. This comparison has also been done in Ref. [62], which models a continuous medium [with mass-points (i.e., coarse-grained volume elements) labeled by their position vectors $\boldsymbol{z}$ in the externally unstrained, reference state] by the following elastic free energy: [1]

$$H_G = \frac{1}{2}\int d^D\boldsymbol{z}_1\, d^D\boldsymbol{z}_2\, G(\boldsymbol{z}_1-\boldsymbol{z}_2)\left(|\boldsymbol{R}(\boldsymbol{z}_1)-\boldsymbol{R}(\boldsymbol{z}_2)|^2-|\boldsymbol{z}_1-\boldsymbol{z}_2|^2\right), \tag{5.16}$$

[1] We have simplified the model of Ref. [62] by assuming that the network does not suffer a contraction after cross-linking. In general, there should be a contraction by a factor that was determined in Ref. [62] to be approximately $(1-(\rho/D\lambda_0))$ in D spatial dimensions, where ρ is the mean shear modulus of the network and λ_0 is a parameter penalizing density fluctuations. As we are considering the case of an essentially incompressible IGNE, λ_0 will be very large, and we may therefore neglect this contraction.

where $G(\boldsymbol{z}_1-\boldsymbol{z}_2)$ is a *random*, nonlocal harmonic attraction between a mass-point located at $\boldsymbol{z}_1$ and another mass-point located at $\boldsymbol{z}_2$. This harmonic attraction stems from the entropy of polymer chains in the heterogeneous network. We characterize it by its disorder average $G^{(0)}(\boldsymbol{z}_1-\boldsymbol{z}_2) \equiv [G(\boldsymbol{z}_1,\boldsymbol{z}_2)]$ and disorder variance $[G(\boldsymbol{z}_1,\boldsymbol{z}_2)\,G(\boldsymbol{z}_3,\boldsymbol{z}_4)]-[G(\boldsymbol{z}_1,\boldsymbol{z}_2)][G(\boldsymbol{z}_3,\boldsymbol{z}_4)]$. The fluctuation part of $G(\boldsymbol{z}_1,\boldsymbol{z}_2)$ is given by

$$G^{(1)}(\boldsymbol{z}_1,\boldsymbol{z}_2) \equiv G(\boldsymbol{z}_1,\boldsymbol{z}_2) - G^{(0)}(\boldsymbol{z}_1-\boldsymbol{z}_2). \tag{5.17}$$

The disorder-average $G^{(0)}$ is translationally invariant, reflecting our physical requirement for a statistically homogeneous system; hence it is a function of the difference of the positions $\boldsymbol{z}_1$ and $\boldsymbol{z}_2$. It is shown in Ref. [62] that this microscopic phenomenological model leads to a Lagrangian theory of elasticity (i.e., one that involves strain tensors defined with respect to the mechanically equilibrated, externally unstrained state of the elastomer) that has spatially random elastic moduli and internal stresses, similar to the continuum theory of Lagrangian elasticity described by Eq. (5.2). The kernel $G(\boldsymbol{z}_1-\boldsymbol{z}_2)$ in Eq. (5.16) is a nonlocal generalization of the coefficient k_b in Eq. (5.1). Just as DiDonna and Lubensky [61] found that the randomness in the spring constant k_b generates spatially random elastic moduli and internal stresses, it was found in Ref. [62] that the randomness of $G(\boldsymbol{z}_1-\boldsymbol{z}_2)$ generates spatially random elastic moduli and internal stresses.

To make a comparison with the free energy of Goldstone fluctuations from the vulcanization theory, Ref. [62] uses the replica method to average H_G over the quenched disorder, G. The deformation field $\boldsymbol{R}(\boldsymbol{z})$ is regarded as a thermally fluctuating field in the presence of the disordered background supplied by $G(\boldsymbol{z}_1,\boldsymbol{z}_2)$. H_G is then regarded as the effective Hamiltonian for a given thermally fluctuating configuration specified by $\boldsymbol{R}(\boldsymbol{z})$, and the free energy for a given disordered realization, viz., $F_G = -T\ln Z_G$, can then be computed via

the partition function Z_G, given by

$$Z_G = \int \mathcal{D}R\, e^{-H_G(\boldsymbol{R}(\boldsymbol{z}))/T}. \tag{5.18}$$

The free energy F_G can then be disorder-averaged using the replica method:

$$[F_G] = -T \lim_{n\to 0} \frac{[Z_G^n] - 1}{n}, \tag{5.19}$$

where the square brackets $[\cdots]$ now refer to a disorder average over the statistics of G. Similar to the procedure employed in Chapter 3.2, one defines a "replica partition function" $Z_n \equiv [Z_G^n]$, given by

$$Z_n = \int \prod_{\alpha=1}^{n} \mathcal{D}R^\alpha e^{-H_n/T}, \tag{5.20}$$

where H_n is the effective Hamiltonian of a pure system governing the replicated deformation fields, given by

$$H_n \equiv -T \ln \left[e^{-\sum_{\alpha=1}^{n} H_G(\boldsymbol{R}^\alpha(\boldsymbol{z}))/T} \right]. \tag{5.21}$$

Via a cumulant expansion and the use of Eq. (5.16), one obtains for the effective Hamiltonian the following expression:

$$\begin{aligned} H_n &= -T \left(- \left[\sum_{\alpha=1}^{n} H_G(\boldsymbol{R}^\alpha(\boldsymbol{z}))/T \right]_c + \frac{1}{2} \left[\sum_{\alpha,\beta=1}^{n} H_G(\boldsymbol{R}^\alpha(\boldsymbol{z}))\, H_G(\boldsymbol{R}^\alpha(\boldsymbol{z}))/T \right]_c - \ldots \right) \\ &= \frac{1}{2} \int d\boldsymbol{z}_1\, d\boldsymbol{z}_2\, [G(\boldsymbol{z}_1, \boldsymbol{z}_2)]_c\, \Psi(\boldsymbol{z}_1, \boldsymbol{z}_2) \\ &\quad - \frac{1}{8T} \int d\boldsymbol{z}_1\, d\boldsymbol{z}_2\, d\boldsymbol{z}_3\, d\boldsymbol{z}_4\, [G(\boldsymbol{z}_1, \boldsymbol{z}_2)\, G(\boldsymbol{z}_3, \boldsymbol{z}_4)]_c\, \Psi(\boldsymbol{z}_1, \boldsymbol{z}_2)\, \Psi(\boldsymbol{z}_3, \boldsymbol{z}_4) - \ldots, \end{aligned} \tag{5.22}$$

where $[\cdots]_c$ refer to the connected cumulants. By comparing the form of H_n with the form of H_Ψ [cf. Eq. (5.15)], one arrives at the following determination of the quenched-disorder statistics of the microscopic phenomenological model (5.16) in terms of the parameters of

the free energy of Goldstone fluctuations (5.15) derived from vulcanization theory:

$$[G(\boldsymbol{z}_1, \boldsymbol{z}_2)]_c = K_1(\boldsymbol{z}_1, \boldsymbol{z}_2); \tag{5.23a}$$

$$[G(\boldsymbol{z}_1, \boldsymbol{z}_2)\, G(\boldsymbol{z}_3, \boldsymbol{z}_4)]_c = K_2(\boldsymbol{z}_1, \boldsymbol{z}_2, \boldsymbol{z}_3, \boldsymbol{z}_4). \tag{5.23b}$$

In particular, by determining the mechanically equilibrated (i.e., relaxed) state of the system described in (5.16) after cross-linking, for a given realization of quenched disorder, an expression is derived in Ref. [62] for the local, non-affine deformation $\boldsymbol{v}_\Lambda$, which is composed of two parts: (i) the random displacement that the system undergoes as it relaxes to mechanical equilibrium in the *externally unstrained* state after cross-linking, which we denote by $\boldsymbol{v}$; and (ii) the *non-affine* part of the deformation (which we denote by $\boldsymbol{v}_\Lambda - \boldsymbol{v}$) that the system undergoes as an external strain is imposed on it.

The state of mechanical equilibrium is found by minimizing H_G in (5.16) with respect to $\boldsymbol{R}(\boldsymbol{z})$. In Ref. [62], it was determined that $\boldsymbol{v}_\Lambda$ is given, in Fourier space, by

$$\boldsymbol{v}_\Lambda(\boldsymbol{p}) = \mathbf{P}_\Lambda^{\mathrm{T}} \cdot \boldsymbol{f}_\Lambda(\boldsymbol{p})/2(G_{\mathbf{0}}^{(0)} - G_{\boldsymbol{p}}^{(0)}), \tag{5.24}$$

where $\mathbf{P}_\Lambda^{\mathrm{T}}$ is the transverse projection tensor in Fourier space for the externally deformed state, i.e.,

$$\mathbf{P}_\Lambda^{\mathrm{T}} \equiv \mathrm{I} - \frac{(\underline{\underline{\Lambda}}^T)^{-1}\boldsymbol{p}\boldsymbol{p}\underline{\underline{\Lambda}}^{-1}}{\mathrm{Tr}\,(\boldsymbol{p}\boldsymbol{p}(\underline{\underline{\Lambda}}^T\underline{\underline{\Lambda}})^{-1})}, \tag{5.25}$$

and $\boldsymbol{f}_\Lambda(\boldsymbol{p})$ is the random, non-equilibrium force acting on the system at the instant of cross-linking, driving the system towards the state of mechanical equilibrium. The force $\boldsymbol{f}_\Lambda(\boldsymbol{p})$ is given by

$$\boldsymbol{f}_\Lambda(\boldsymbol{p}) \equiv -2i\left(\underline{\underline{\Lambda}} \cdot \frac{\partial}{\partial \boldsymbol{p}} G^{(0)}_{(\boldsymbol{p},\mathbf{0})} - \underline{\underline{\Lambda}} \cdot \left.\frac{\partial}{\partial \boldsymbol{q}}\right|_{\boldsymbol{q}=\mathbf{0}} G^{(0)}_{(\boldsymbol{p},\boldsymbol{q})}\right). \tag{5.26}$$

The disorder-averaged correlator of non-affine deformation can straightforwardly be com-

puted; its value is given by

$$[\boldsymbol{v}_\Lambda(\boldsymbol{p})\,\boldsymbol{v}_\Lambda(-\boldsymbol{p})] = \{\mathbf{P}_\Lambda^{\mathrm{T}}\,\mathbf{h}_\Lambda(\boldsymbol{p})\}/\big(G_{\mathbf{0}}^{(0)} - G_{\boldsymbol{p}}^{(0)}\big)^2, \tag{5.27}$$

where the parameter $\mathbf{h}_\Lambda(\boldsymbol{p})$ is defined via

$$\begin{aligned}\big(\mathbf{h}_\Lambda(\boldsymbol{p})\big)_{d_1 d_2} \;\equiv\; & \int d^D\boldsymbol{z}_1\, d^D\boldsymbol{z}_2\, d^D\boldsymbol{z}_3\, d^D\boldsymbol{z}_4\, [G(\boldsymbol{z}_1,\boldsymbol{z}_2)\, G(\boldsymbol{z}_3,\boldsymbol{z}_4)]_c \\ & \times\Lambda_{d_1 d_3}\Lambda_{d_2 d_4}(z_1 - z_2)_{d_3}(z_3 - z_4)_{d_4}(e^{-i\boldsymbol{p}\cdot\boldsymbol{z}_1} - e^{-i\boldsymbol{p}\cdot\boldsymbol{z}_2})(e^{i\boldsymbol{p}\cdot\boldsymbol{z}_3} - e^{i\boldsymbol{p}\cdot\boldsymbol{z}_4}) \\ = \; & \int d\boldsymbol{z}_1\, d\boldsymbol{z}_2\, d\boldsymbol{z}_3\, d\boldsymbol{z}_4 K(\boldsymbol{z}_1,\boldsymbol{z}_2,\boldsymbol{z}_3,\boldsymbol{z}_4) \\ & \times\Lambda_{d_1 d_3}\Lambda_{d_2 d_4}(z_1 - z_2)_{d_3}(z_3 - z_4)_{d_4}(e^{-i\boldsymbol{p}\cdot\boldsymbol{z}_1} - e^{-i\boldsymbol{p}\cdot\boldsymbol{z}_2})(e^{i\boldsymbol{p}\cdot\boldsymbol{z}_3} - e^{i\boldsymbol{p}\cdot\boldsymbol{z}_4}).\end{aligned} \tag{5.28}$$

Its functional dependence is the same as that of the non-affinity correlator computed in Ref. [61]. One sees that the function $\mathbf{h}_\Lambda(\boldsymbol{p})$ in the numerator of the non-affinity correlator (5.27) is proportional to the disorder variance $\gamma^2\,\Delta^K(\boldsymbol{p})$ of [61], and that $(G_{\mathbf{0}}^{(0)} - G_{\boldsymbol{p}}^{(0)})^2$ in the denominator is, in the limit of long wavelengths, proportional to p^2.

5.3 Deriving the non-affinity correlator using replicas

The same non-affinity correlator, which was derived in Ref. [62] via the phenomenological model (5.16), can be derived more efficiently using the Goldstone-deformed vulcanization

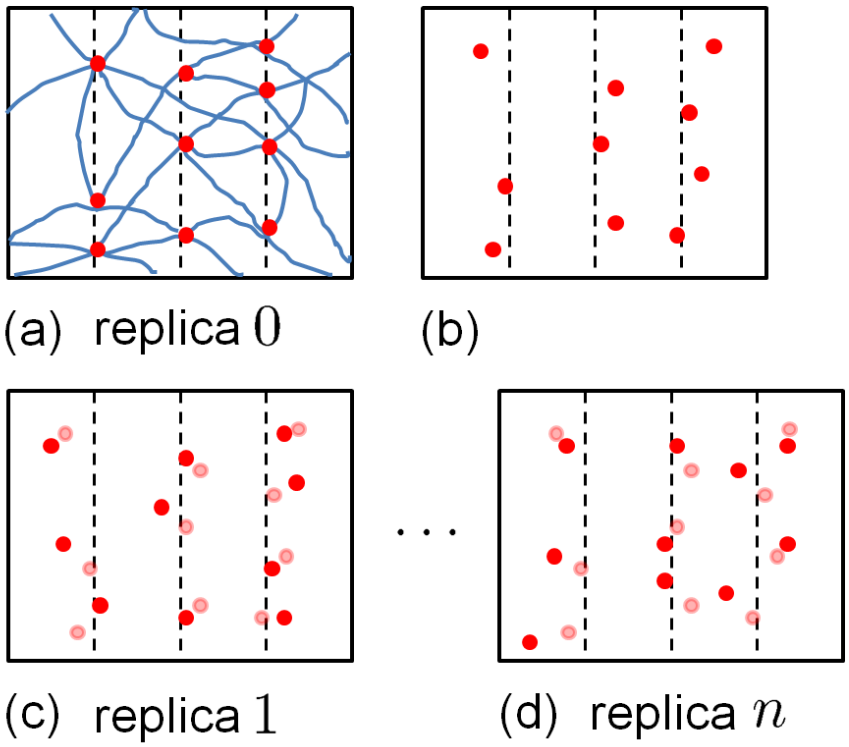

Figure 5.1: Schematic depiction of two types of elastic fluctuations present in an undeformed elastomer: (i) local, random, displacements $\boldsymbol{v}(\boldsymbol{z})$, that occur as the elastomer network relaxes after cross-linking; and (ii) thermally excited elastic fluctuations $\boldsymbol{u}(\boldsymbol{z})$ about the relaxed state, all for a given realization of quenched randomness, and of how such fluctuations are encoded via replicas: (a) Snapshot of an elastomer network at the instant of cross-linking, before it has time to relax. This is a configuration belonging to the preparation ensemble, which we also refer to as the zeroth replica. The blue lines represent polymers, each intersection of polymers represents a cross-link. For purposes of illustration we have introduced vertical dashed lines and displayed the cross-links that lie on the vertical dashed lines as red dots. (b) The same network after it has relaxed, but in the absence of thermal fluctuations. For simplicity, we ignore the "background" polymers and focus on the behavior of the red cross-links shown in (a). The positions of the red cross-links do not coincide with their corresponding positions on the vertical dashed lines in (a). This reflects the fact that as the network relaxes to mechanical equilibrium after cross-linking, the cross-links undergo local random displacements from their positions at the cross-linking instant. (c) Snapshot of replica 1, representing one thermal configuration from the measurement ensemble. The lighter red dots refer to the positions of the red cross-links in (b), whilst the bright red dots refer to the corresponding positions of the red cross-links when thermal fluctuations are present. (d) Snapshot of replica n, also representing a distinct thermal configuration from the measurement ensemble. The positions of the mass-points are different from those in snapshot (c), owing to thermal fluctuations. Note that if the elastomer is externally deformed, there would be an additional type of elastic fluctuation, viz., non-affine displacement.

theory (5.15), as we now show. From Eq. (5.13), it follows that

$$\begin{aligned}
\Psi(\boldsymbol{z}_1,\boldsymbol{z}_2) &\equiv \sum_{\alpha=1}^{n}(\boldsymbol{R}^{\alpha}(\boldsymbol{z}_1)-\boldsymbol{R}^{\alpha}(\boldsymbol{z}_2))^2 - n(\boldsymbol{z}_1-\boldsymbol{z}_2)^2 \\
&= \sum_{\alpha=1}^{n}\left(\Lambda\cdot(\boldsymbol{z}_1-\boldsymbol{z}_2)+(\boldsymbol{U}^{\alpha}_{\Lambda}(\boldsymbol{z}_1)-\boldsymbol{U}^{\alpha}_{\Lambda}(\boldsymbol{z}_2))\right)^2 - n(\boldsymbol{z}_1-\boldsymbol{z}_2)^2 \\
&= n(\Lambda-I)\cdot(\boldsymbol{z}_1-\boldsymbol{z}_2)+2\Lambda(\boldsymbol{z}_1-\boldsymbol{z}_2)\cdot\sum_{\alpha=1}^{n}(\boldsymbol{U}^{\alpha}_{\Lambda}(\boldsymbol{z}_1)-\boldsymbol{U}^{\alpha}_{\Lambda}(\boldsymbol{z}_2)) \\
&\qquad +\sum_{\alpha=1}^{n}\left(\boldsymbol{U}^{\alpha}_{\Lambda}(\boldsymbol{z}_1)-\boldsymbol{U}^{\alpha}_{\Lambda}(\boldsymbol{z}_2)\right)^2, \qquad (5.29)
\end{aligned}$$

the free energy cost of Goldstone fluctuations (5.15) around the externally deformed cross-linking state can be re-written, in Fourier space, as

$$\begin{aligned}
\frac{H'_{\Psi}}{T} &= \frac{1}{2T}\int d^D\boldsymbol{z}_1\, d^D\boldsymbol{z}_2\, K_1(\boldsymbol{z}_1,\boldsymbol{z}_2)\sum_{\alpha=1}^{n}|\boldsymbol{U}^{\alpha}_{\Lambda}(\boldsymbol{z}_1)-\boldsymbol{U}^{\alpha}_{\Lambda}(\boldsymbol{z}_2)|^2 \\
&\quad - \frac{1}{4T^2}\int d^D\boldsymbol{z}_1\, d^D\boldsymbol{z}_2\, d^D\boldsymbol{z}_3\, d^D\boldsymbol{z}_4\, K_1(\boldsymbol{z}_1,\boldsymbol{z}_2,\boldsymbol{z}_3,\boldsymbol{z}_4)\,\Lambda_{d_1d_3}(z_1-z_2)_{d_3}\,\Lambda_{d_2d_4}(z_1-z_2)_{d_4} \\
&\qquad \times\sum_{\alpha,\beta=1}^{n}\left(\boldsymbol{U}^{\alpha}_{\Lambda}(\boldsymbol{z}_1)-\boldsymbol{U}^{\alpha}_{\Lambda}(\boldsymbol{z}_2)\right)_{d_1}\left(\boldsymbol{U}^{\alpha}_{\Lambda}(\boldsymbol{z}_3)-\boldsymbol{U}^{\alpha}_{\Lambda}(\boldsymbol{z}_4)\right)_{d_2} \\
&= \sum_{\alpha=1}^{n}\sum_{\boldsymbol{p}}\frac{K_1(\boldsymbol{0})-K_1(\boldsymbol{p})}{TV}\left\{\mathbf{P}^{\mathrm{T}}_{\Lambda}\cdot\boldsymbol{U}^{\alpha}_{\Lambda}(\boldsymbol{p})\,\mathbf{P}^{\mathrm{T}}_{\Lambda}\cdot\boldsymbol{U}^{\alpha}_{\Lambda}(-\boldsymbol{p})\right\} \\
&\quad - \sum_{\alpha,\beta=1}^{n}\sum_{\boldsymbol{p}}\frac{(\mathbf{h}_{\Lambda}(\boldsymbol{p}))_{d_1d_2}}{4T^2V^2}(\mathbf{P}^{\mathrm{T}}_{\Lambda}\cdot\boldsymbol{U}^{\alpha}_{\Lambda}(\boldsymbol{p}))_{d_1}(\mathbf{P}^{\mathrm{T}}_{\Lambda}\cdot\boldsymbol{U}^{\beta}_{\Lambda}(\boldsymbol{p}))_{d_2}. \qquad (5.30)
\end{aligned}$$

where H'_{Ψ} is the same as H_{Ψ}, but with the constant terms excluded. Note that we have enforced transversality of elastic fluctuations (which reflects our linear-order approximation to the constraint that the rubber is incompressible, i.e., $\nabla\cdot\boldsymbol{U}=0$) by multiplying the terms with factors of $\mathbf{P}^{\mathrm{T}}_{\Lambda}$.

It can be deduced from Ref. [62] that the result given in Eq. (5.30) can be expressed, to

leading order in G^2 and at long wavelengths, by the formula

$$\begin{aligned}\frac{H'_\Psi}{T} &= \frac{N}{2V^2}\sum_{\alpha=1}^{n}\sum_{\boldsymbol{p}}\mu\, p^2\,\left\{\mathbf{P}_\Lambda^{\mathrm{T}}\cdot\boldsymbol{U}_\Lambda^\alpha(\boldsymbol{p})\,\mathbf{P}_\Lambda^{\mathrm{T}}\cdot\boldsymbol{U}_\Lambda^\alpha(-\boldsymbol{p})\right\} \\ &\quad -\frac{N}{2V^2}\sum_{\alpha,\beta=1}^{n}\sum_{\boldsymbol{p}}\mu'\Lambda_{d_1d_3}\,\Lambda_{d_2d_4}\big(p^2\delta_{d_3d_4}+2p_{d_3}p_{d_4}\big)(\mathbf{P}_\Lambda^{\mathrm{T}}\cdot\boldsymbol{U}_\Lambda^\alpha(\boldsymbol{p}))_{d_1}(\mathbf{P}_\Lambda^{\mathrm{T}}\cdot\boldsymbol{U}_\Lambda^\beta(\boldsymbol{p}))_{d_2},\end{aligned} \tag{5.31}$$

where the elastic constants μ, μ' are given by $(\mu, \mu') = (\eta^2 G^2/4)(2+\eta^2, \eta^2-1)$.

For an undeformed IGNE, the pattern of symmetry breaking at the vulcanization transition is analogous to that of undeformed rubber, as the symmetry breaking is associated with random localization. Correspondingly, the IGNE also possesses a branch of Goldstone fluctuations whose free energy has the same form as that given by Eq. (5.31) with $\underline{\underline{\Lambda}} \to \mathbf{I}$. It is straightforward to find the corresponding values of μ and μ' for an IGNE, as the saddle-point values of $\langle\Omega\rangle$ and $\langle\Gamma\rangle$ have the same form as one another [cf. Eqs. (1.34) and (4.5)]. We simply have to replace η^2 by $\tilde{\eta}^2$ and set the value of G to $2(\tilde{\eta}^2-1)/3$; cf. Eq (4.3).

From Eq. (5.30) one can straightforwardly compute the "glassy correlator" of Goldstone fluctuations, $\langle \boldsymbol{U}_\Lambda^\alpha(\boldsymbol{p})\boldsymbol{U}_\Lambda^\beta(-\boldsymbol{p})\rangle$ ($\alpha \neq \beta$), and see that it is equal, in the replica limit, to the value of the non-affinity correlator given by Eq. (5.27). This should not surprise us, if we consider the fact that the Goldstone fluctuations $\boldsymbol{U}_\Lambda^\alpha$ can be interpreted as arising from replicating the elastic fluctuation $\boldsymbol{U}_\Lambda$ for an elastomer system with a given realization of quenched disorder, where $\boldsymbol{U}_\Lambda \equiv \boldsymbol{v}_\Lambda + \boldsymbol{u}$ (and $\boldsymbol{u}$ are thermally-excited elastic fluctuations about the relaxed deformed state, $\underline{\underline{\Lambda}}\cdot\boldsymbol{z} + \boldsymbol{v}_\Lambda$; cf. Fig. 5.1). The thermal average of $\boldsymbol{U}_\Lambda$ for a given disordered realization is given by $\langle \boldsymbol{U}_\Lambda\rangle = \boldsymbol{v}_\Lambda$, which implies that the disorder-averaged correlator of non-affine deformations is given by $[\langle \boldsymbol{U}_\Lambda(\boldsymbol{p})\rangle\,\langle \boldsymbol{U}_\Lambda(-\boldsymbol{p})\rangle]$. In the formalism of replica field theory, such a correlator is precisely given by the replica-off-diagonal contribution to the inverse of the kernel of the term quadratic in $\boldsymbol{U}_\Lambda^\alpha(\boldsymbol{p})$, in a theory that is at most of quadratic order in $\boldsymbol{U}_\Lambda^\alpha(\boldsymbol{p})$.

Chapter 6

Effect of nematic fluctuations on IGNE elasticity in the high-temperature regime

In the Introduction, we saw how nematic elastomers are characterized by novel elastic properties such as softness. The discussions in the previous chapter have also revealed the physical meaning of the correlator of Goldstone fluctuations $\langle \boldsymbol{U}_\Lambda^\alpha \boldsymbol{U}_\Lambda^\beta \rangle$. In particular, in the limit $\underline{\underline{\Lambda}} \to \mathbf{I}$, this correlator describes the disorder-averaged square displacement undergone by the volume elements of the elastomer during relaxation. The purpose of this chapter is two-fold:

First, we explore one mechanism that leads to elastic softening in IGNEs. We focus on the small-strain regime (i.e., $\underline{\underline{\Lambda}} \to \mathbf{I}$) and show that the shear modulus of an IGNE is made smaller than the shear modulus of an ordinary rubber by the presence of long-wavelength thermal nematic fluctuations.

Second, the same replica formalism that enables one to derive the afore-mentioned result also enables us to determine the enhancement that frozen nematic fluctuations induce in the magnitude of random displacements undergone by volume elements of the elastomer when it relaxes after cross-linking. In principle, our approach should also enable one to determine the contribution that frozen nematic fluctuations make to the non-affinity correlator for an IGNE under *arbitrary* deformations. However, this would require us to solve the saddle-point equations (4.1) with $\bar{\mathbf{Q}} \neq \mathbf{0}$ in general (as $\mathbf{Q}$ should acquire a non-zero part due to finite strain). In this chapter, we focus on the simpler case of an IGNE in the limit that $\underline{\underline{\Lambda}} \to \mathbf{I}$, for which the saddle-point solution $\bar{\mathbf{Q}} = \mathbf{0}$ still holds.

The results obtained in this chapter are valid in the high-temperature regime of the IGNE, i.e., above the critical temperature.

To study the impact of nematic fluctuations on the elastic behavior of IGNEs, we shall augment the free energy of Goldstone fluctuations H'_Ψ (5.30) by the free energy of nematic fluctuations (4.7) as well as a term that linearly couples $\boldsymbol{U}^\alpha$ to $\mathbf{Q}^\alpha$, which is derived from the term $\langle G_1(\Gamma)^2\, G_2(Q)\rangle$ in the expansion of the log-trace term of (3.18). This coupling term is computed in Appendix I. This gives the following free energy of fluctuations:

$$\begin{aligned} H[\boldsymbol{U},\mathbf{Q}]/T \;=\; & \sum_{\alpha=1}^{n}\sum_{\boldsymbol{p}} \frac{K_1(\mathbf{0})-K_1(\boldsymbol{p})}{TV}\left\{\mathbf{P}^{\mathrm{T}}\cdot\boldsymbol{U}^\alpha(\boldsymbol{p})\,\mathbf{P}^{\mathrm{T}}\cdot\boldsymbol{U}^\alpha(-\boldsymbol{p})\right\} \\ & -\sum_{\alpha,\beta=1}^{n}\sum_{\boldsymbol{p}}(\mathbf{h}_{\Lambda\to\mathrm{I}}(\boldsymbol{p}))_{bc}\,(\mathbf{P}^{\mathrm{T}}\cdot\boldsymbol{U}^\alpha(\boldsymbol{p}))_b\,(\mathbf{P}^{\mathrm{T}}\cdot\boldsymbol{U}^\beta(\boldsymbol{p}))_c \\ & +i\sum_{\alpha=1}^{n}\sum_{\boldsymbol{p}} N\,\mathfrak{b}_{\boldsymbol{p}}\,\boldsymbol{U}^\alpha_{\boldsymbol{p}}\cdot\mathbf{Q}^\alpha_{\boldsymbol{p}}\cdot\boldsymbol{p} \\ & +\frac{N}{2T}\sum_{\alpha=1}^{n}\sum_{\boldsymbol{p}}\left(\mathcal{A}t+\mathcal{L}p^2-\frac{T|\mathrm{H}_{\boldsymbol{p}}|^2}{t^0(\mathcal{A}^0\,t^0+\mathcal{L}^0p^2)}\right)\{\mathbf{Q}^\alpha_{\boldsymbol{p}}\,\mathbf{Q}^\alpha_{-\boldsymbol{p}}\} \\ & -\frac{N}{2T}\sum_{\substack{\alpha,\beta=1\\(\alpha\neq\beta)}}^{n}\sum_{\boldsymbol{p}}\left(\mathrm{H}_{\boldsymbol{p}}+\frac{T|\mathrm{H}_{\boldsymbol{p}}|^2}{t^0(\mathcal{A}^0\,t^0+\mathcal{L}^0p^2)}\right)\{\mathbf{Q}^\alpha_{\boldsymbol{p}}\,\mathbf{Q}^\beta_{-\boldsymbol{p}}\}, \end{aligned} \tag{6.1}$$

where $P^{\mathrm{T}}_{d_1d_2}$ denotes the transverse projection tensor for the *undeformed* state, defined via $\delta_{d_1d_2}-\hat{p}_{d_1}\,\hat{p}_{d_2}$, where $\hat{p}_{d_1}\equiv p_{d_1}/|\boldsymbol{p}|$ is the unit vector aligned in the direction of $\boldsymbol{p}$. We have introduced the transverse projection tensor to eliminate the bulk deformation mode, as the IGNE is assumed to be incompressible. The function $\mathfrak{b}_{\boldsymbol{p}}$ describes the strength of nemato-elastic coupling in the deformed state, and takes the value $(G^2\tilde{\eta}^4J_0\ell^2/10T\xi_L^2V)\exp(-p^2\xi_L^2/2)$. We remind the reader that J_0 denotes the strength of nematic-nematic interaction, $\tilde{\eta}^2$ is proportional to the average number of cross-links per dimer, ℓ denotes the length of a nematic rod, G denotes the gel fraction, and ξ_L denotes the typical localization length of the elastomeric network; cf. Chapter 3. The function $\mathfrak{b}_{\boldsymbol{p}}$ is wavelength-dependent, being exponentially suppressed for large values of $\boldsymbol{p}$. This accords with the expectation that $\boldsymbol{U}^\alpha$ (which encode non-affinity and thermal elastic fluctuations) are physically meaningful only on lengthscales larger than ξ_L, and thus can have a well-defined coupling to local nematic

alignments only at those lengthscales. The parameter $\mathfrak{b_0}$ is a measure of the aligning capabilities of the IGNE, as longer nematogens and stronger nematogen-nematogen interactions give rise to larger values of $\mathfrak{b_0}$. To obtain the effective replica free energy $\mathcal{H}[\boldsymbol{U}]$ of the elastic deformations $\boldsymbol{U}^\alpha$, we integrate out $\mathbf{Q}^\alpha$, thus obtaining

$$\begin{aligned}\mathcal{H}[\boldsymbol{U}] &= \sum_{\alpha=1}^{n}\sum_{\boldsymbol{p}}\left(\frac{K_1(\mathbf{0})-K_1(\boldsymbol{p})}{TV}-\frac{N}{2}p^2|\mathfrak{b}_{\boldsymbol{p}}|^2\mathcal{C}^T(\boldsymbol{p})\right)\\ &\quad\times\left\{\mathbf{P}^{\mathrm{T}}\cdot\boldsymbol{U}^\alpha_{\boldsymbol{p}}\ \mathbf{P}^{\mathrm{T}}\cdot\boldsymbol{U}^\alpha_{-\boldsymbol{p}}\right\}\\ &\quad-\sum_{\alpha,\beta=1}^{n}\sum_{\boldsymbol{p}}\left((\mathbf{P}^{\mathrm{T}})_{a'a}\,(\mathbf{P}^{\mathrm{T}})_{b'b}\frac{(\mathbf{h}_{\Lambda\to\mathrm{I}}(\boldsymbol{p}))_{a'b'}}{4T^2V^2}+\frac{N}{2}p^2(\mathbf{P}^{\mathrm{T}})_{ab}\,|\mathfrak{b}_{\boldsymbol{p}}|^2\,\mathcal{C}^G(\boldsymbol{p})\right)\\ &\quad\times(\boldsymbol{U}^\alpha(\boldsymbol{p}))_a\,(\boldsymbol{U}^\beta(-\boldsymbol{p}))_b,\end{aligned}\tag{6.2}$$

where $\mathcal{C}^T_{\boldsymbol{p}}$ is the nematic thermal fluctuation correlator, which has a value given by

$$\mathcal{C}^T_{\boldsymbol{p}}=\frac{T}{\mathcal{A}\,t+\mathcal{L}p^2+\mathrm{H}_{\boldsymbol{p}}},\tag{6.3}$$

and $\mathcal{C}^G_{\boldsymbol{p}}$ is the nematic glassy correlator, which has a value given by

$$\mathcal{C}^G_{\boldsymbol{p}}=\frac{T\left(\mathrm{H}_{\boldsymbol{p}}+\frac{T|\mathrm{H}_{\boldsymbol{p}}|^2}{t^0(\mathcal{A}^0\,t^0+\mathcal{L}^0p^2)}\right)}{(\mathcal{A}\,t+\mathcal{L}p^2+\mathrm{H}_{\boldsymbol{p}})^2}.\tag{6.4}$$

The glassy correlator detects the presence of nematic alignments that are trapped in during the process of cross-linking (and are therefore time-persistent); see Chapter 2.

6.1 Correlations of random relaxational displacements in IGNEs

In the previous chapter, we have shown that the Fourier-space correlator of non-affine deformations, $[\boldsymbol{v}_\Lambda(\boldsymbol{p})\,\boldsymbol{v}_\Lambda(-\boldsymbol{p})]$ is given by $[\langle\boldsymbol{U}_\Lambda(\boldsymbol{p})\rangle\,\langle\boldsymbol{U}_\Lambda(-\boldsymbol{p})\rangle]$. The latter quantity is given by

the replica-off-diagonal part of the replica correlator $\langle \boldsymbol{U}_{\Lambda}^{\alpha}(\boldsymbol{p})\, \boldsymbol{U}_{\Lambda}^{\beta}(-\boldsymbol{p})\rangle$. For the case $\underline{\underline{\Lambda}} \to \mathbf{I}$, which gives the disorder-averaged correlator of random relaxational displacements in an IGNE, one can compute this correlator via the free energy (6.2). The result is

$$[\{\langle \boldsymbol{U}_{\boldsymbol{p}}\rangle\, \langle \boldsymbol{U}_{-\boldsymbol{p}}\rangle\}] = \frac{\frac{1}{2T^2V^2}\{\mathbf{h}_{\Lambda\to \mathrm{I}}(\boldsymbol{p})\mathbf{P}^{\mathrm{T}}\} + N\, p^2 |\mathfrak{b}_{\boldsymbol{p}}|^2 \mathcal{C}^G(\boldsymbol{p})}{\Big(\frac{2(K_1(\mathbf{0})-K_1(\boldsymbol{p}))}{TV} - N\, p^2 |\mathfrak{b}_{\boldsymbol{p}}|^2 \mathcal{C}^T(\boldsymbol{p})\Big)^2}. \tag{6.5}$$

Here, the notation $\mathbf{h}_{\Lambda\to \mathrm{I}}$ denotes the value of $\mathbf{h}_{\Lambda}$ evaluated in the limit that $\underline{\underline{\Lambda}}$ goes to the identity matrix I. For a system with no nematic freedoms present (i.e., ordinary rubber), $\mathfrak{b}_{\boldsymbol{p}} = 0$ and

$$[\{\langle \boldsymbol{U}_{\boldsymbol{p}}\rangle\, \langle \boldsymbol{U}_{-\boldsymbol{p}}\rangle\}] = \frac{\{\mathbf{h}_{\Lambda\to \mathrm{I}}(\boldsymbol{p})\mathbf{P}^{\mathrm{T}}\}}{8\big(K_1(\mathbf{0}) - K_1(\boldsymbol{p})\big)^2}. \tag{6.6}$$

By comparing Eqs. (6.5) and (6.6), one learns about the sources driving random relaxational displacements in IGNEs and in ordinary rubber. In ordinary rubber, random relaxational displacements are driven by the randomness of the elastic modulus (which is itself a manifestation of the quenched disorder introduced by cross-linking constraints). In IGNEs, on the other hand, the cross-linking constraints cause nematic alignments to be randomly frozen, and these randomly frozen alignments [represented by $\mathcal{C}^G$ in Eq. (6.5)], along with the randomness of the elastic modulus [represented by $\mathbf{h}_{\Lambda\to \mathrm{I}}(\boldsymbol{p})$ in Eq. (6.5)], act as sources driving random relaxational displacements.

6.2 Softening of elastic response in IGNEs

We now turn to the issue of determining the elastic modulus of an IGNE in the high-temperature regime, which we denote by the symbol K_{IGNE}. Consider the work done by the thermal environment in creating a strain fluctuation $\epsilon_{\boldsymbol{p}}$ of wavelength $(2\pi/p)$ for a given realization of quenched disorder. Such a strain fluctuation has an associated energy $E = K_{\boldsymbol{p}}\, |\epsilon_{\boldsymbol{p}}|^2/2$ (with $K_{\boldsymbol{p}}$ having dimensions of T/V^2). By the Equipartition Theorem, the thermally averaged strain energy $\langle E\rangle = T/2$. The strain fluctuation is measured relative to

the relaxed state, and thus the corresponding thermally averaged strain energy is given by $(K_{\boldsymbol{p}}/2)\langle|\epsilon_{\boldsymbol{p}}|^2\rangle = K_{\boldsymbol{p}}\langle\{(\boldsymbol{U}_{\boldsymbol{p}} - \langle\boldsymbol{U}_{\boldsymbol{p}}\rangle)(\boldsymbol{U}_{-\boldsymbol{p}} - \langle\boldsymbol{U}_{-\boldsymbol{p}}\rangle)\}\rangle\, p^2/2$. The elastic modulus $K_{\boldsymbol{p}}$ is the response of the thermally averaged mean-square strain fluctuation to the thermal energy, and for a given realization of quenched disorder, one obtains the following fluctuation-response relation,

$$K_{\boldsymbol{p}} = \frac{T}{\langle\{(\boldsymbol{U}_{\boldsymbol{p}} - \langle\boldsymbol{U}_{\boldsymbol{p}}\rangle)(\boldsymbol{U}_{-\boldsymbol{p}} - \langle\boldsymbol{U}_{-\boldsymbol{p}}\rangle)\}\rangle\, p^2}. \tag{6.7}$$

The experimentally measurable $K_{\rm IGNE}$ is equal to the long-wavelength limit of the disorder average of $K_{\boldsymbol{p}}$. In the replica approach, $[\langle\{(\boldsymbol{U}_{\boldsymbol{p}} - \langle\boldsymbol{U}_{-\boldsymbol{p}}\rangle)(\boldsymbol{U}_{-\boldsymbol{p}} - \langle\boldsymbol{U}_{-\boldsymbol{p}}\rangle)\}\rangle]$ is given by any of the replica-diagonal elements of the correlator matrix $\langle\boldsymbol{U}_{\boldsymbol{p}}^{\alpha}\,\boldsymbol{U}_{-\boldsymbol{p}}^{\beta}\rangle$, viz.,

$$\langle\boldsymbol{U}_{\boldsymbol{p}}^{\alpha}\,\boldsymbol{U}_{-\boldsymbol{p}}^{\beta}\rangle = T/(2(K_1(\boldsymbol{0}) - K_1(\boldsymbol{p}))) - 1/(N\,p^2|\mathfrak{b}_{\boldsymbol{p}}|^2\mathcal{C}^T(\boldsymbol{p})). \tag{6.8}$$

This allows one to find $K_{\rm IGNE}$ for small strain:

$$K_{\rm IGNE} = \big(2(K_1(\boldsymbol{0}) - K_1(\boldsymbol{p}))/p^2 - N\,|\mathfrak{b}_{\boldsymbol{p}}|^2\mathcal{C}^T(\boldsymbol{p})\big)|_{\boldsymbol{p}\to\boldsymbol{0}}. \tag{6.9}$$

For ordinary rubber, $\mathfrak{b}_{\boldsymbol{p}} = 0$, and $K = 2(K_1(\boldsymbol{0}) - K_1(\boldsymbol{p}))/p^2|_{\boldsymbol{p}\to\boldsymbol{0}}$, which agrees with the value of the shear modulus of rubber found in Ref. [62]. Equation (6.9) shows that the elastic modulus of an IGNE in the high-temperature regime is smaller than the elastic modulus of ordinary rubber by an amount proportional to the thermal nematic fluctuation correlator in the limit $|\boldsymbol{p}| \to 0$. We thus see that long-wavelength thermal nematic fluctuations induce a softening of the elastic response.

Chapter 7

Effect of elastic fluctuations on IGNE structure in the high-temperature regime

In the previous chapter, we looked at the ways in which thermal and glassy nematic fluctuations modify the elastic properties of an IGNE. In the present chapter, we study the impact of elastic fluctuations of the mass-points of the elastomer network on the liquid crystalline behavior of an *undeformed* IGNE. In Chapters 2 and 3, where we worked at the saddle-point level for Γ but allowed for nematic fluctuations, we made certain predictions pertaining to the thermal and glassy correlators of nematic fluctuations; in particular, we showed that the thermal and glassy correlators can undergo an oscillatory type of decay in real space, provided the disorder strength $\mathrm{H}_{\mathbf{0}}$ is sufficiently large.

The question therefore arises as to whether such oscillatory-decaying behavior survives when elastic fluctuations of the localized network constituents are taken into account. In this chapter, we show that, at least in the *high-temperature* regime, such fluctuations do not result in any *qualitative* change to the oscillatory-decaying behavior of $\mathcal{C}^T$ and $\mathcal{C}^G$ at sufficiently large values of $\mathrm{H}_{\mathbf{0}}$; instead, the boundaries of the correlator behavior, separating non-oscillatory and oscillatory decay in the disorder-strength vs. temperature phase diagram are only *quantitatively* modified. In addition, we derive the corrections that elastic fluctuations make to the glassy and thermal correlation lengths in the *weak-disorder*, *high-temperature* regime for a system prepared at high temperatures, as well as a correction to the glassy correlator of a system prepared at $t^0 < T\mathrm{H}_{\mathbf{0}}/T^0\mathcal{A}^0$.

7.1 Elastic-fluctuation-corrected effective theory of liquid crystallinity

To obtain an effective theory of local nematic order in the macroscopically isotropic state, which also takes into account the effects of elastic fluctuations of the localized network constituents, we consider a fluctuation free energy that consists of three contributions: (i) a contribution of quadratic order in $\boldsymbol{U}^{\alpha}$, solely arising from Goldstone fluctuations and given by Eq. (5.31); (ii) a contribution describing nematic fluctuations, given by Eq. (4.6); and (iii) a contribution arising from the coupling of elastic fluctuations to nematic fluctuations; we also consider the linear coupling term proportional to $\boldsymbol{U}^{\alpha}\,\mathbf{Q}^{\alpha}$, derived from a term proportional to $\Gamma\,\Gamma\mathbf{Q}^{\alpha}$ in the Landau-Wilson free energy (cf. Appendix I). We have already encountered this coupling term in the previous chapter [cf. Eq. (6.1)]. The free energy of elastic fluctuations per dimer, H_{el}, is given by the sum of the contributions (i) and (iii):

$$\frac{H_{\mathrm{el}}}{T} = \frac{1}{2V^2}\sum_{\boldsymbol{p}}\sum_{\alpha,\beta} P^{\mathrm{T}}_{d_1 d_2}\,\mathcal{G}^{\alpha\beta}_{\boldsymbol{p}}\,U^{\alpha}_{d_1}(\boldsymbol{p})\,U^{\beta}_{d_2}(-\boldsymbol{p}) + i\sum_{\alpha}\sum_{\boldsymbol{p}}\mathfrak{b}_{\boldsymbol{p}}\;\boldsymbol{p}\cdot\mathbf{Q}^{\alpha}_{\boldsymbol{p}}\cdot\boldsymbol{U}^{\alpha}_{-\boldsymbol{p}}, \tag{7.1}$$

where the kernel $\mathcal{G}^{\alpha\beta}_{\boldsymbol{p}}$ has the value $(\mu\delta^{\alpha\beta} - \mu'\mathbf{1}^{\alpha\beta})p^2$, in which $\mathbf{1}^{\alpha\beta}$ is an $n\times n$ matrix whose entries are all equal to unity. Equation (7.1) is essentially Eq. (6.1) for the case of an undeformed IGNE (i.e., $\underline{\underline{\Lambda}} = \mathrm{I}$) with the contribution of purely nematic fluctuations omitted. The inverse of $\mathcal{G}^{\alpha\beta}_{\boldsymbol{p}}$, viz., $(\mathcal{G}^{-1}_{\boldsymbol{p}})^{\alpha\beta}$, which is proportional to the Fourier-space replica elastic fluctuation correlator $\langle\!\langle \boldsymbol{U}^{\alpha}_{\boldsymbol{p}}\,\boldsymbol{U}^{\beta}_{-\boldsymbol{p}}\rangle\!\rangle$, is given by the formula $(\mathcal{G}^{-1}_{\boldsymbol{p}})^{\alpha\beta} = \mathcal{D}^{T}_{\boldsymbol{p}}\delta^{\alpha\beta} + \mathcal{D}^{G}_{\boldsymbol{p}}\mathbf{1}^{\alpha\beta}$, where we call $\mathcal{D}^{T}_{\boldsymbol{p}} \equiv 1/(\mu\,p^2)$ the elastic thermal fluctuation correlator and $\mathcal{D}^{G}_{\boldsymbol{p}} \equiv \mu'/(\mu^2\,p^2)$ the elastic glassy fluctuation correlator. As $\mathcal{D}^{T}_{\boldsymbol{p}}$ is given by the replica-diagonal element of $\langle\!\langle \boldsymbol{U}^{\alpha}_{\boldsymbol{p}}\,\boldsymbol{U}^{\beta}_{-\boldsymbol{p}}\rangle\!\rangle$, it is a measure of the elastic "softness" of the system, as explained in Sec. 6.2; analogously, as $\mathcal{D}^{G}_{\boldsymbol{p}}$ is given by the replica-off-diagonal element of $\langle\!\langle \boldsymbol{U}^{\alpha}_{\boldsymbol{p}}\,\boldsymbol{U}^{\beta}_{-\boldsymbol{p}}\rangle\!\rangle$, it quantifies the magnitude of random displacements undergone by the volume elements of the elastomer during relaxation.

Mode	Expression in terms of $\mathbf{Q}$
Longitudinal, $\phi_{\boldsymbol{p}}$	$\hat{p}_a\,\hat{p}_b\,Q_{ab}(\boldsymbol{p})$
Transverse, $W_{d_1d_2}(\boldsymbol{p})$	$P^{\mathrm{T}}_{d_1d_3}\,P^{\mathrm{T}}_{d_2d_4}\,Q_{d_3d_4}$
	$-\frac{1}{2}\big(P^{\mathrm{T}}_{d_5d_3}\,P^{\mathrm{T}}_{d_5d_4}\,Q_{d_3d_4}+\phi\big)P^{\mathrm{T}}_{d_1d_2}$
Mixed, $X_{d_1}(\boldsymbol{p})$	$P^{\mathrm{T}}_{d_1d_2}\,\hat{p}_{d_3}\,Q_{d_2d_3}(\boldsymbol{p})$

Table 7.1: The five independent modes of $\mathbf{Q}_{\boldsymbol{p}}$, utilized in Eq. (7.6). Here, $\hat{p}_d \equiv p_d/|\boldsymbol{p}|$ is the unit vector aligned in the direction of $\boldsymbol{p}$, and $P^{\mathrm{T}}_{d_1d_2} \equiv \delta_{d_1d_2} - \hat{p}_{d_1}\hat{p}_{d_2}$ is an operator that projects a D-dimensional vector onto the plane transverse to the direction of $\boldsymbol{p}$.

To obtain the elastic fluctuation-induced correction to the liquid crystalline behavior of an IGNE, we integrate out the elastic fluctuation fields $\boldsymbol{U}^\alpha$ from the Landau-Wilson free energy, thus obtaining

$$\begin{aligned}\frac{H_{\text{correction}}}{T} &= -\frac{V^2}{2}\sum_{\boldsymbol{p}}\sum_{\alpha\beta}(\mathfrak{b}_{\boldsymbol{p}})^2\,(\mathcal{G}^{-1}_{\boldsymbol{p}})^{\alpha\beta}P^{\mathrm{T}}_{d_1d_2}\,Q^{\alpha}_{d_1d_3}(\boldsymbol{p})\,Q^{\beta}_{d_2d_4}(-\boldsymbol{p})\,p_{d_3}\,p_{d_4}\\ &= -\frac{1}{2}\sum_{\alpha\beta}\sum_{\boldsymbol{p}}\left(\mathcal{D}^T_{\boldsymbol{p}}\delta^{\alpha\beta}+\mathcal{D}^G_{\boldsymbol{p}}\mathbf{1}^{\alpha\beta}\right)p^2\,\mathrm{B}_{\boldsymbol{p}}\,\{\boldsymbol{X}^\alpha_{\boldsymbol{p}}\,\boldsymbol{X}^\beta_{-\boldsymbol{p}}\},\end{aligned} \tag{7.2}$$

where $\mathrm{B}_{\boldsymbol{p}}$ and $\boldsymbol{X}_{\boldsymbol{p}}$ are defined via

$$\mathrm{B}_{\boldsymbol{p}} \equiv \frac{G^4\tilde{\eta}^8 J_0^2\,\ell^4}{100\,T^2\,\xi_L^4}e^{-p^2\xi_L^2}; \tag{7.3}$$

$$X_{d_1}(\boldsymbol{p}) \equiv P^{\mathrm{T}}_{d_1d_2}\,\hat{p}_{d_3}\,Q_{d_2d_3}(\boldsymbol{p}). \tag{7.4}$$

$\mathrm{B}_{\mathbf{0}}$ describes the strength of nemato-elastic coupling. It is larger for longer nematogens and stronger nematogen-nematogen interactions.

We are now in a position to write down the Landau free energy for an effective theory of local nematic order in an IGNE, by combining the free energy contributions that involve nematic fluctuations but do not originate from elastic fluctuations [i.e., Eq. (4.6)], with the elastic fluctuation-induced correction term (7.2). We thus obtain the following effective

Hamiltonian:

$$\begin{aligned}\frac{H_{1+n}[\{\mathbf{Q}^\alpha\}_{\alpha=0}^n]}{T} &= \sum_{\boldsymbol{p}} \frac{1}{2T^0}\mathcal{M}(T^0,\boldsymbol{p})\{\mathbf{Q}^0_{\boldsymbol{p}}\,\mathbf{Q}^0_{-\boldsymbol{p}}\} + \sum_{\alpha=1}^{n}\sum_{\boldsymbol{p}} \frac{1}{2T}(\mathcal{A}t+\mathcal{L}p^2)\{\mathbf{Q}^\alpha_{\boldsymbol{p}}\,\mathbf{Q}^\alpha_{-\boldsymbol{p}}\} \\ &\quad -\frac{1}{T^0}\sum_{\alpha=1}^{n}\sum_{\boldsymbol{p}} \mathrm{H}_{\boldsymbol{p}}\{\mathbf{Q}^0_{\boldsymbol{p}}\,\mathbf{Q}^\alpha_{-\boldsymbol{p}}\} - \frac{1}{2T}\sum_{\substack{\alpha,\beta=1\\(\alpha\neq\beta)}}^{n}\sum_{\boldsymbol{p}} \mathrm{H}_{\boldsymbol{p}}\{\mathbf{Q}^\alpha_{\boldsymbol{p}}\,\mathbf{Q}^\beta_{-\boldsymbol{p}}\} \\ &\quad -\frac{1}{2}\sum_{\alpha=1}^{n}\sum_{\boldsymbol{p}} p^2\,\mathrm{B}_{\boldsymbol{p}}\,\mathcal{D}^T_{\boldsymbol{p}}\{\boldsymbol{X}^\alpha_{\boldsymbol{p}}\,\boldsymbol{X}^\alpha_{-\boldsymbol{p}}\} - \frac{1}{2}\sum_{\alpha,\beta=1}^{n}\sum_{\boldsymbol{p}} p^2\,\mathrm{B}_{\boldsymbol{p}}\,\mathcal{D}^G_{\boldsymbol{p}}\{\boldsymbol{X}^\alpha_{\boldsymbol{p}}\,\boldsymbol{X}^\beta_{-\boldsymbol{p}}\}.\end{aligned} \tag{7.5}$$

Next, following the procedure described in Sec. 4.2, we integrate out the zeroth replica element $\mathbf{Q}^0$ in order to determine the effect that the preparation history has on the measured liquid crystalline behavior. This yields

$$\begin{aligned}\frac{H_{\text{eff}}\,[\{\mathbf{Q}^\alpha\}_{\alpha=0}^n]}{T} &= \sum_{\alpha=1}^{n}\sum_{j=0}^{2}\sum_{\boldsymbol{p}}\left(\frac{\mathcal{A}t+\mathcal{L}p^2}{2T} - \frac{|\mathrm{H}_{\boldsymbol{p}}|^2}{2T^0\mathcal{M}(T^0,\boldsymbol{p})}\right)\left(\{\boldsymbol{W}^\alpha_{\boldsymbol{p}}\,\boldsymbol{W}^\alpha_{-\boldsymbol{p}}\} + \phi^\alpha_{\boldsymbol{p}}\,\phi^\alpha_{-\boldsymbol{p}}\right) \\ &\quad -\sum_{\substack{\alpha,\beta=1\\(\alpha\neq\beta)}}^{n}\sum_{\boldsymbol{p}}\left(\frac{\mathrm{H}_{\boldsymbol{p}}}{2T} + \frac{|\mathrm{H}_{\boldsymbol{p}}|^2}{2T^0\mathcal{M}(T^0,\boldsymbol{p})}\right)\left(\{\boldsymbol{W}^\alpha_{\boldsymbol{p}}\,\boldsymbol{W}^\beta_{-\boldsymbol{p}}\} + \phi^\alpha_{\boldsymbol{p}}\,\phi^\beta_{-\boldsymbol{p}}\right) \\ &\quad +\sum_{\alpha=1}^{n}\sum_{\boldsymbol{p}}\left(\frac{\mathcal{A}t+\mathcal{L}p^2}{2T} - \frac{|\mathrm{H}_{\boldsymbol{p}}|^2}{2T^0\mathcal{M}(T^0,\boldsymbol{p})} - \frac{1}{2}(\mathcal{D}^T_{\boldsymbol{p}}+\mathcal{D}^G_{\boldsymbol{p}})\,p^2\,\mathrm{B}_{\boldsymbol{p}}\right)\{\boldsymbol{X}^\alpha_{\boldsymbol{p}}\,\boldsymbol{X}^\alpha_{-\boldsymbol{p}}\} \\ &\quad -\sum_{\substack{\alpha,\beta=1\\(\alpha\neq\beta)}}^{n}\sum_{\boldsymbol{p}}\left(\frac{\mathrm{H}_{\boldsymbol{p}}}{2T} + \frac{|\mathrm{H}_{\boldsymbol{p}}|^2}{2T^0\mathcal{M}(T^0,\boldsymbol{p})} + \frac{1}{2}p^2\,\mathrm{B}_{\boldsymbol{p}}\,\mathcal{D}^G_{\boldsymbol{p}}\right)\{\boldsymbol{X}^\alpha_{\boldsymbol{p}}\,\boldsymbol{X}^\beta_{-\boldsymbol{p}}\}.\end{aligned} \tag{7.6}$$

Here, we have made the following Fourier-space decomposition of the symmetric, traceless field $\mathbf{Q}_{\boldsymbol{p}}$ into the independent components $\phi_{\boldsymbol{p}}$, $\boldsymbol{X}_{\boldsymbol{p}}$ and $\boldsymbol{W}_{\boldsymbol{p}}$:

$$Q_{d_1d_2}(\boldsymbol{p}) = \phi_{\boldsymbol{p}}\,\hat{p}_{d_1}\,\hat{p}_{d_2} + P^{\mathrm{T}}_{d_1d_3}\,\hat{p}_{d_2}\,X_{d_3}(\boldsymbol{p}) + P^{\mathrm{T}}_{d_2d_3}\,\hat{p}_{d_1}\,X_{d_3}(\boldsymbol{p}) + W_{d_1d_2}(\boldsymbol{p}).$$

Here, $W_{d_1d_2}$ is a matrix that has three independent components (including ϕ), defined by

$$W_{d_1d_2}(\boldsymbol{p}) \equiv P^{\mathrm{T}}_{d_1d_3}P^{\mathrm{T}}_{d_2d_4}Q_{d_3d_4} - \frac{1}{2}\big(P^{\mathrm{T}}_{d_5d_3}P^{\mathrm{T}}_{d_5d_4}Q_{d_3d_4} + \phi\big)P^{\mathrm{T}}_{d_1d_2}. \tag{7.7}$$

We call $\phi_{\boldsymbol{p}}$ the longitudinal mode as it is the nematic mode that is projected onto the direction parallel to the wave-vector, $\boldsymbol{p}$. We call $\boldsymbol{X}_{\boldsymbol{p}}$ the mixed mode, as it receives contributions from both longitudinal and transverse channels of $\mathbf{Q}$, and we call $\boldsymbol{W}_{\boldsymbol{p}}$ the transverse mode, as it is defined to be transverse to $\boldsymbol{p}$. These modes are summarized in Tabe 7.1.

By applying the identities (4.9) to each of the fluctuation modes, we can obtain, from the diagonal and off-diagonal elements of the propagator matrix in wave-vector space, the thermal and glassy correlators for the longitudinal mode ϕ, mixed modes $\boldsymbol{X}$ and transverse modes $\boldsymbol{W}$:

$$\langle\!\langle \phi^{\alpha}_{\boldsymbol{p}}\phi^{\beta}_{-\boldsymbol{p}} \rangle\!\rangle = T\frac{\frac{T|\mathrm{H}_{\boldsymbol{p}}|^2}{T^0\mathcal{M}(T^0,\boldsymbol{p})} + \mathrm{H}_{\boldsymbol{p}}}{\big(\mathcal{A}t+\mathcal{L}p^2+\mathrm{H}_{\boldsymbol{p}}\big)^2}\mathrm{I}^{\alpha\beta} + \frac{T}{\mathcal{A}t+\mathcal{L}p^2+\mathrm{H}_{\boldsymbol{p}}}\delta^{\alpha\beta}; \tag{7.8a}$$

$$\langle\!\langle \{\boldsymbol{W}^{\alpha}_{\boldsymbol{p}}\boldsymbol{W}^{\beta}_{-\boldsymbol{p}}\} \rangle\!\rangle = 2T\frac{\frac{T|\mathrm{H}_{\boldsymbol{p}}|^2}{T^0\mathcal{M}(T^0,\boldsymbol{p})} + \mathrm{H}_{\boldsymbol{p}}}{\big(\mathcal{A}t+\mathcal{L}p^2+\mathrm{H}_{\boldsymbol{p}}\big)^2}\mathrm{I}^{\alpha\beta} + \frac{2T}{\mathcal{A}t+\mathcal{L}p^2+\mathrm{H}_{\boldsymbol{p}}}\delta^{\alpha\beta}; \tag{7.8b}$$

$$\langle\!\langle \{\boldsymbol{X}^{\alpha}_{\boldsymbol{p}}\boldsymbol{X}^{\beta}_{-\boldsymbol{p}}\} \rangle\!\rangle = 2T\frac{\frac{T|\mathrm{H}_{\boldsymbol{p}}|^2}{T^0\mathcal{M}(T^0,\boldsymbol{p})} + \mathrm{H}_{\boldsymbol{p}} + Tp^2\,\mathrm{B}_{\boldsymbol{p}}\,\mathcal{D}^{G}_{\boldsymbol{p}}}{\big(\mathcal{A}t+\mathcal{L}p^2+\mathrm{H}_{\boldsymbol{p}} - T\,p^2\,\mathrm{B}_{\boldsymbol{p}}\,\mathcal{D}^{T}_{\boldsymbol{p}}\big)^2}\mathrm{I}^{\alpha\beta} + \frac{2T}{\mathcal{A}t+\mathcal{L}p^2+\mathrm{H}_{\boldsymbol{p}} - T\,p^2\,\mathrm{B}_{\boldsymbol{p}}\,\mathcal{D}^{T}_{\boldsymbol{p}}}\delta^{\alpha\beta}. \tag{7.8c}$$

The behavior of the correlators of $\boldsymbol{X}$ differs from the behavior of the correlators of $\boldsymbol{W}$ as well as the behavior of the correlator of ϕ, owing to the fact that the elastic fluctuation field $\boldsymbol{U}^{\alpha}$ is transverse and couples only to $\boldsymbol{X}$. The nematic correlator $\langle\!\langle Q^{\alpha}_{d_1d_2}(\boldsymbol{p})Q^{\beta}_{d_3d_4}(-\boldsymbol{p})\rangle\!\rangle$ is then found by adding the correlators in Eqs. (7.8) and appending a suitable tensorial factor

as follows:

$$\begin{aligned}\langle\langle Q^{\alpha}_{d_1d_2}(\boldsymbol{p})Q^{\beta}_{d_3d_4}(-\boldsymbol{p})\rangle\rangle &= \frac{1}{D(D+1)}\left(\delta_{d_1d_3}\delta_{d_2d_4}+\delta_{d_1d_4}\delta_{d_2d_3}\right)\\ &\quad\times\Big(\langle\langle\phi^{\alpha}(\boldsymbol{p})\phi^{\beta}(-\boldsymbol{p})\rangle\rangle+\langle\langle\{(\boldsymbol{X}^{\alpha}(\boldsymbol{p})\boldsymbol{X}^{\beta}(-\boldsymbol{p})\}\rangle\rangle\\ &\quad+\langle\langle\{\boldsymbol{W}^{\alpha}(\boldsymbol{p})\boldsymbol{W}^{\beta}(-\boldsymbol{p})\}\rangle\rangle\Big)\\ &\equiv \frac{1}{D(D+1)}\left(\delta_{d_1d_3}\delta_{d_2d_4}+\delta_{d_1d_4}\delta_{d_2d_3}\right)\left(\mathcal{C}^{T}_{\boldsymbol{p}}\delta^{\alpha\beta}+\mathcal{C}^{G}_{\boldsymbol{p}}\mathrm{I}^{\alpha\beta}\right). \quad (7.9)\end{aligned}$$

From this above equation, we see that the nematic thermal fluctuation correlator $\mathcal{C}^{T}_{\boldsymbol{p}}$ and the nematic glassy correlator $\mathcal{C}^{G}_{\boldsymbol{p}}$ are given by

$$\mathcal{C}^{T}_{\boldsymbol{p}} = \frac{3T}{\mathcal{A}t+\mathcal{L}p^2+\mathrm{H}_{\boldsymbol{p}}}+\frac{2T}{\mathcal{A}t+\mathcal{L}p^2+\mathrm{H}_{\boldsymbol{p}}-T\,p^2\,\mathrm{B}_{\boldsymbol{p}}\,\mathcal{D}^{T}_{\boldsymbol{p}}}; \quad (7.10a)$$

$$\mathcal{C}^{G}_{\boldsymbol{p}} = 3T\frac{\frac{T|\mathrm{H}_{\boldsymbol{p}}|^2}{T^0\mathcal{M}(T^0,\boldsymbol{p})}+\mathrm{H}_{\boldsymbol{p}}}{\left(\mathcal{A}t+\mathcal{L}p^2+\mathrm{H}_{\boldsymbol{p}}\right)^2}+2T\frac{\frac{T|\mathrm{H}_{\boldsymbol{p}}|^2}{T^0\mathcal{M}(T^0,\boldsymbol{p})}+\mathrm{H}_{\boldsymbol{p}}+Tp^2\,\mathrm{B}_{\boldsymbol{p}}\,\mathcal{D}^{G}_{\boldsymbol{p}}}{\left(\mathcal{A}t+\mathcal{L}p^2+\mathrm{H}_{\boldsymbol{p}}-T\,p^2\,\mathrm{B}_{\boldsymbol{p}}\,\mathcal{D}^{T}_{\boldsymbol{p}}\right)^2}. \quad (7.10b)$$

Having computed the correlators $\mathcal{C}^{T}$ and $\mathcal{C}^{G}$, we are now in a position to study how elastic fluctuations modify our results obtained in Sec. 2.3.

7.2 Nematic fluctuation correlations in the weak-disorder regime

How do elastic fluctuations modify the behavior of the glassy and thermal fluctuation correlators in an IGNE in the weak-disorder, high-temperature regime? For simplicity, we focus on systems prepared at high temperatures, so we that do not have to consider the influence of local nematic order arising from $\mathbf{Q}^0$. The qualitative understanding of the physical modification introduced by elastic fluctuations is aided by approximating $\mathcal{C}^{T}_{\boldsymbol{p}}$ in Eq. (7.10) via a Taylor expansion of the functions $\mathrm{H}_{\boldsymbol{p}}$ and $\mathrm{B}_{\boldsymbol{p}}$ in their denominators to quadratic order in $\boldsymbol{p}$,

for small values of $\mathrm{H_0}/\mathrm{H}^{(c)}$. This yields

$$\mathcal{C}_{\boldsymbol{p}}^{T} \approx \frac{3T}{(\mathcal{A}t+\mathrm{H_0})\left(1+\xi_{T,d}^{2}p^{2}\right)}+\frac{2T}{(\mathcal{A}t+\zeta(\tilde{\eta}^{2},T)\mathrm{H_0})\left(1+\tilde{\xi}_{T,d}^{2}p^{2}\right)}. \tag{7.11}$$

Here, the function $\zeta(\tilde{\eta}^2, T)$ is given by $(\mathrm{H}_0 - (T/\mu)\mathrm{B}_0)/\mathrm{H}_0 \approx 1 - 0.0045G^2\tilde{\eta}^4/\mu$. The first term in this function encodes the effect of the quenched randomness of the cross-linking constraints on the nematic correlations, whilst the second term encodes the effect of elastic fluctuations on the nematic correlations. The lengthscale $\xi_{T,d}^2 \approx \left(\mathcal{L} - \frac{1}{2}\mathrm{H_0}\xi_L^2\right)/\left(\mathcal{A}t + \mathrm{H_0}\right)$ is the squared thermal correlation length for the longitudinal mode ϕ and transverse mode $\boldsymbol{W}$, and the lengthscale $\tilde{\xi}_{T,d}^2 \approx \left(\mathcal{L} - \frac{1}{2}\mathrm{H_0}\xi_L^2 + \frac{3T\mathrm{B_0}\xi_L^2}{4\mu}\right)/\left(\mathcal{A}t + \zeta(\tilde{\eta}^2, T)\mathrm{H_0}\right)$ is the squared thermal correlation length for the mixed mode $\boldsymbol{X}$. We can make the following three observations about Eq. (7.11):

(i) In contrast to the effect of the quenched randomness of the cross-linking constraints, which is to *decrease* the effective critical temperature, the effect of the elastic fluctuations is to *increase* the effective critical temperature of the system (i.e., to make the system more prone to macroscopic ordering). The mixed fluctuation mode $\boldsymbol{X}$ is most prone to destabilization; its critical temperature T_c is given by $T_c = (1 - \mathrm{H_0}/\mathcal{A})T^*/(1 - T^*\mathrm{B_0}/(\mu\,\mathcal{A}))$, which is larger than the value $(1 - \mathrm{H_0}/\mathcal{A})T^*$ corresponding to the critical temperature of an IGNE without elastic fluctuations.

(ii) The upward renormalization of the critical temperature by elastic fluctuations is associated with the enhancement of the thermal correlation length of the mixed mode, i.e., $\tilde{\xi}_{T,d}$. This enhancement is expected because elastic fluctuations have long-range correlations in real space, owing to their "masslessness."

(iii) Elastic fluctuations have a more pronounced effect on nematic correlations for larger values of $\tilde{\eta}^2$ and J_0/T. This is to be expected, as a larger density of cross-links results in greater elastic rigidity (and hence a stronger influence from elastic fluctuations), and a larger value of J_0/T also results in stronger nemato-elastic coupling, which then enables

elastic fluctuations to have a greater impact on local nematic ordering.

Turning now to the form of $\mathcal{C}^T$ in real space, one finds, after performing an inverse Fourier transformation on Eq. (7.11), that it is given by the familiar Yukawa-type potential encountered in studies of nematic liquid crystals (see, e.g., Ref. [1]), with the magnitude and correlation length renormalized by elastic fluctuations, viz.,

$$\mathcal{C}^T(\boldsymbol{x}-\boldsymbol{y}) \approx \frac{T\exp\big(-|\boldsymbol{x}-\boldsymbol{y}|/\tilde{\xi}_{T,d}\big)}{2\pi\left(\mathcal{A}t+\zeta(\tilde{\eta}^2,T)\mathrm{H}_{\mathbf{0}}\right)\tilde{\xi}_{T,d}^2|\boldsymbol{x}-\boldsymbol{y}|}+\frac{3T\exp\big(-|\boldsymbol{x}-\boldsymbol{y}|/\xi_{T,d}\big)}{4\pi\left(\mathcal{A}t+\mathrm{H}_{\mathbf{0}}\right)\xi_{T,d}^2|\boldsymbol{x}-\boldsymbol{y}|}. \quad (7.12)$$

This result allows one to see that the real-space decay of the nematic thermal fluctuation correlator is simple exponential, qualitatively the same as the real-space thermal fluctuation correlator decay of a system in the absence of elastic fluctuations. On the other hand, the presence of elastic fluctuations has resulted in an enhancement of the *effective* nematic thermal correlation length.

Next, we study the effect that elastic fluctuations have on the glassy nematic order in the weak-disorder regime. In order to see the qualitative effects of introducing elastic fluctuations more readily, we consider making an approximation to the nematic glassy correlator in this regime by Taylor-expanding the functions $\mathrm{H}_{\mathbf{p}}$ and $\mathrm{B}_{\mathbf{p}}$ in the denominator of $\mathcal{C}_{\boldsymbol{p}}^G$ in Eq. (7.10) to quadratic order in $\boldsymbol{p}$, and then approximating the denominator by an exponential function, viz.,

$$\mathcal{C}_{\boldsymbol{p}}^G \approx \frac{3T\mathrm{H}_{\mathbf{0}}\,e^{-\xi_{G,d}^2p^2}}{\left(\mathcal{A}t+\mathrm{H}_{\mathbf{0}}\right)^2}+\frac{2T\mathrm{H}_{\mathbf{0}}\,e^{-\left(\frac{1}{2}\xi_L^2+2\tilde{\xi}_{T,d}^2\right)p^2}}{\left(\mathcal{A}t+\zeta(\tilde{\eta}^2,T)\mathrm{H}_{\mathbf{0}}\right)^2}-\frac{2T^2\mathrm{B}_{\mathbf{0}}\,p^2\,\mathcal{D}_{\boldsymbol{p}}^G\,e^{-\left(\frac{3}{4}\xi_L^2+2\tilde{\xi}_{T,d}^2\right)p^2}}{\left(\mathcal{A}t+\zeta(\tilde{\eta}^2,T)\mathrm{H}_{\mathbf{0}}\right)^2}. \quad (7.13)$$

By performing an inverse Fourier transformation, one can compute the value of the real-space

nematic glassy correlator; it is given by

$$\begin{aligned}\mathcal{C}^{G}(\boldsymbol{x}-\boldsymbol{y}) \;\approx\; & \frac{3T\mathrm{H}_{\mathbf{0}}\exp\left(-|\boldsymbol{x}-\boldsymbol{y}|^{2}/4\xi_{G,d}^{2}\right)}{(4\pi)^{3/2}\left(\mathcal{A}t+\mathrm{H}_{\mathbf{0}}\right)^{2}\xi_{G,d}^{3}} \\ & +\frac{2T\mathrm{H}_{\mathbf{0}}\exp\left(-|\boldsymbol{x}-\boldsymbol{y}|^{2}/4\left(\frac{1}{2}\xi_{L}^{2}+2\tilde{\xi}_{T,d}^{2}\right)\right)}{(4\pi)^{3/2}\left(\mathcal{A}t+\zeta(\tilde{\eta}^{2},T)\mathrm{H}_{\mathbf{0}}\right)^{2}\left(\frac{1}{2}\xi_{L}^{2}+2\tilde{\xi}_{T,d}^{2}\right)^{3/2}} \\ & +\frac{(2T\,\mu'\,\mathrm{B}_{\mathbf{0}}/\mu^{2})\exp\left(-|\boldsymbol{x}-\boldsymbol{y}|^{2}/4\left(\frac{3}{4}\xi_{L}^{2}+2\tilde{\xi}_{T,d}^{2}\right)\right)}{(4\pi)^{3/2}\left(\mathcal{A}t+\zeta(\tilde{\eta}^{2},T)\mathrm{H}_{\mathbf{0}}\right)^{2}\left(\frac{3}{4}\xi_{L}^{2}+2\tilde{\xi}_{T,d}^{2}\right)^{3/2}}. \end{aligned} \tag{7.14}$$

The decay of the nematic glassy correlator is also simple exponential, qualitatively the same as the real-space glassy correlator decay of a system in the absence of elastic fluctuations. Just as the effective nematic thermal correlation length is enhanced by elastic fluctuations, these elastic fluctuations also lead to enhancement of the effective nematic glassy correlation length.

Equation (7.14) allows one to determine the local nematic intensity, i.e., $\mathcal{C}^{G}(\boldsymbol{r}=\mathbf{0})$:

$$\mathcal{C}^{G}(\boldsymbol{r}=\mathbf{0})\approx\frac{T}{(4\pi)^{3/2}\left(\mathcal{A}t\right)^{2}}\left(\frac{3\mathrm{H}_{\mathbf{0}}}{\xi_{G,d}^{3}}+\frac{2\mathrm{H}_{\mathbf{0}}}{\left(\frac{1}{2}\xi_{L}^{2}+2\tilde{\xi}_{T,d}^{2}\right)^{3/2}}+\frac{2\mu'\,\mathrm{B}_{\mathbf{0}}/\mu^{2}}{\left(\frac{3}{4}\xi_{L}^{2}+2\tilde{\xi}_{T,d}^{2}\right)^{3/2}}\right). \tag{7.15}$$

This result implies that random displacements undergone by the volume elements of the elastomer during relaxation (reflected by the presence of the coefficient μ'/μ^{2}) would enhance the intensity of frozen nematic alignments. This is natural on physical grounds, as the random, relaxational, displacements made by the volume elements of the elastomer introduce local strain fields, which induce local orientational anisotropy, thereby causing an increase in the intensity of glassy nematic order.

7.3 Real-space oscillatory-decaying behavior of the correlators $\mathcal{C}^T$ and $\mathcal{C}^G$

Having studied the effect of elastic fluctuations on the liquid crystalline correlation behavior of IGNEs in the weak-disorder, high-temperature regime, we now consider the effect of elastic fluctuations in the strong-disorder, high-temperature regime. We continue to focus on systems that have been prepared at high temperatures. Specifically, we are interested in studying whether the real-space oscillatory-decay behavior of the glassy and thermal fluctuation correlators for sufficiently large values of $\mathrm{H}_{\mathbf{0}}$ survives when elastic fluctuations are taken into consideration. We proceed by determining how elastic fluctuations modify the cross-over boundaries in the disorder-strength vs. temperature phase diagram between the oscillatory- and non-oscillatory-decay regimes of the glassy and thermal fluctuation correlators. Following the procedure described in Sec. 2.3, we first determine the values of the wave-vectors at which $\mathcal{C}^T_{\boldsymbol{p}}$ and $\mathcal{C}^G_{\boldsymbol{p}}$ are maximal, in the strong-disorder regime. We then set these values to zero, as we are interested in the threshold at which the simple decay of correlators first changes to oscillatory decay; this allows us to obtain equations for $\mathrm{H}_{\mathbf{0}}$ that depends on t, describing the boundary separating oscillatory and non-oscillatory decay for the glassy and thermal fluctuation correlators. For the thermal fluctuation correlator, one finds that the boundary is described by the condition

$$\mathrm{H}_{\mathbf{0}} = \mathrm{H}^{(c)} + \frac{4T\mathrm{B}_{\mathbf{0}}/(5\mu)}{1 - 3T\mathrm{B}_{\mathbf{0}}/(5\mu(\mathcal{A}t + \mathrm{H}_{\mathbf{0}}))}. \tag{7.16}$$

This can be further simplified to the following condition [by omitting the contribution of $T\mathrm{B}_{\mathbf{0}}/(\mu(\mathcal{A}t + \mathrm{H}_{\mathbf{0}}))$ which is much smaller than unity in the high-temperature regime], so that the condition becomes

$$\mathrm{H}_{\mathbf{0}} \approx (1 + 0.0035G^2\tilde{\eta}^4/\mu)\mathrm{H}^{(c)}. \tag{7.17}$$

Equation (7.17) implies that elastic fluctuations serve to *increase* the minimum value of the disorder strength $\mathrm{H}_{\mathbf{0}}$ required for the real-space oscillatory decay of $\mathcal{C}^T$ to occur. Intuitively, one can understand this result in the following way. As the local strain field induced by thermal elastic fluctuations tends to promote the local alignment of nematogens, one requires a larger disorder strength to inhibit such local alignment, in order that the translational aggregation mechanism (which leads to local *anti*-alignment, i.e., the real-space oscillatory-decaying behavior of $\mathcal{C}^T$) can occur.

Following the same procedure used in deriving Eq. (7.17), one finds that the cross-over boundary between the oscillatory and non-oscillatory regimes for the glassy correlator is described by the following equation,

$$\mathrm{H}_{\mathbf{0}} \approx \big(1 - 0.0036G^2\tilde{\eta}^4(1 + (\mu'/\mu))/\mu\big)\mathcal{A}t + \big(2 - 0.0072G^2\tilde{\eta}^4/\mu\big)\mathrm{H}^{(c)}. \tag{7.18}$$

Remarkably, this equation shows that the effect of elastic fluctuations is to *decrease*, at any given t (in the high-temperature regime), the minimum value of $\mathrm{H}_{\mathbf{0}}$ required for the appearance of real-space oscillatory decay of $\mathcal{C}^G$. The physical reason is that the time-persistent random strain fields created by the random, relaxational, displacements of the volume elements of the elastomer after the instant of cross-linking enhance the effective disorder strength, thereby making it easier for the translational aggregation mechanism to occur (and also make it harder for nematogens to align via local rotations).

7.4 Memorization capability of IGNEs

What effect do elastic fluctuations have on the memorization capability of an IGNE? Let us focus on the behavior of the glassy correlator for a system prepared at a temperature $t^0 < T\mathrm{H}_{\mathbf{0}}/T^0\mathcal{A}^0$, and study the effect of elastic fluctuations on the glassy correlator's fidelity in reflecting the thermal nematic fluctuation pattern present at the instant of cross-linking.

As in Sec. 2.3, we specialize to $t \approx t^0$ (i.e., to the temperature at cross-linking) and consider wavelengths larger than ξ_L. We thus find that $\mathcal{C}^G$ is approximately given by

$$\mathcal{C}^G_{\boldsymbol{p}} = \left(3 + \frac{2|\mathrm{H}_{\boldsymbol{p}}|^2}{\left(\mathrm{H}_{\boldsymbol{p}} + \frac{T}{\mu}\mathrm{B}_{\boldsymbol{p}}\right)^2}\right) \frac{T^2/T^0}{\mathcal{M}(T^0, \boldsymbol{p})}. \tag{7.19}$$

This indicates that the pattern of thermal nematic fluctuations present at the instant of cross-linking is *less* faithfully memorized by the network when elastic fluctuations are present. This reduction in fidelity of memorization is due to the smearing out of the memorized fluctuation pattern by elastic fluctuations; this smearing is reflected in the presence of the functions $\mathrm{H}_{\boldsymbol{p}}$ and $\mathrm{B}_{\boldsymbol{p}}$ in Eq. (7.19).

Chapter 8

Order and stability in the low-temperature regime

Having explored liquid crystalline and elastic aspects of an IGNE in the high-temperature regime, we now turn to the exploration of an aspect of IGNE physics in the low-temperature regime. For simplicity, we consider the issue of ordering and stability of the externally undeformed, macroscopically isotropic state of the IGNE in the absence of elastic fluctuations, and show that this state possesses the striking property of being, at least locally, stable at low temperatures. The material presented in this chapter is based on Ref. [32].

8.1 Gaussian variational method

To probe the issue of ordering and stability of the macroscopically isotropic state in the low-temperature regime, we need to include terms of cubic and quartic order in $\mathbf{Q}^{\alpha}$ in the effective Hamiltonian of Eq. (4.7), as the interactions between nematic fluctuations about the disordered state have the possibility of being strong. Thus, we focus on the following

effective Hamiltonian:

$$\begin{aligned}\frac{H_{\text{eff}}\left[\{\mathbf{Q}^{\alpha}\}_{\alpha=1}^{n}\right]}{T} &= \sum_{\alpha=1}^{n}\sum_{\boldsymbol{p}}\left(\frac{\mathcal{A}t+\mathcal{L}p^{2}}{2T}-\frac{|\mathrm{H}_{\boldsymbol{p}}|^{2}}{2T^{0}\mathcal{M}(T^{0},\boldsymbol{p})}\right)\left\{\mathbf{Q}^{\alpha}_{\boldsymbol{p}}\mathbf{Q}^{\alpha}_{-\boldsymbol{p}}\right\} \\ &\quad -\sum_{\substack{\alpha,\beta=1\\(\alpha\neq\beta)}}^{n}\sum_{\boldsymbol{p}}\left(\frac{\mathrm{H}_{\boldsymbol{p}}}{2T}+\frac{|\mathrm{H}_{\boldsymbol{p}}|^{2}}{2T^{0}\mathcal{M}(T^{0},\boldsymbol{p})}\right)\left\{\mathbf{Q}^{\alpha}_{\boldsymbol{p}}\mathbf{Q}^{\beta}_{-\boldsymbol{p}}\right\} \\ &\quad -\frac{v}{3T}\sum_{\alpha=1}^{n}\sum_{\boldsymbol{p}_1,\boldsymbol{p}_2}\{\mathbf{Q}^{\alpha}_{\boldsymbol{p}_1}\,\mathbf{Q}^{\alpha}_{\boldsymbol{p}_2}\,\mathbf{Q}^{\alpha}_{-\boldsymbol{p}_1-\boldsymbol{p}_2}\} \\ &\quad +\frac{w}{4T}\sum_{\alpha=1}^{n}\sum_{\boldsymbol{p}_1,\boldsymbol{p}_2,\boldsymbol{p}_3}\{\mathbf{Q}^{\alpha}_{\boldsymbol{p}_1}\,\mathbf{Q}^{\alpha}_{\boldsymbol{p}_2}\}\,\{\mathbf{Q}^{\alpha}_{\boldsymbol{p}_3}\,\mathbf{Q}^{\alpha}_{-\boldsymbol{p}_1-\boldsymbol{p}_2-\boldsymbol{p}_3}\}.\end{aligned} \tag{8.1}$$

To compute the thermal and glassy correlators, we should employ an approximation scheme that takes into account the nonlinear terms in the effective Hamiltonian. One method that enables this is the *Gaussian variational method* (which we shall denote as GVM; see, e.g., Ref. [37]; for the method applied to systems having quenched randomness, see Refs. [39, 40, 38, 41]). The GVM is described as follows. We approximate $\langle Q^{\alpha}Q^{\beta}\rangle_{H_{\text{eff}}}$ by $\langle Q^{\alpha}Q^{\beta}\rangle_{H_0}$, where H_{eff} is the original nonlinear effective Hamiltonian given by Eq. (8.1), and H_0 a quadratic trial Hamiltonian. By so doing, we are "absorbing" the nonlinearities present in H_{eff} into the unknown coefficients of the linear- and quadratic-order terms of H_0, whose values can then be estimated via a variational approximation. For our setting, we choose H_0 to have the form

$$\frac{H_0}{T} = \frac{1}{2}\sum_{\alpha,\beta=1}^{n}\sum_{\boldsymbol{p}_1,\boldsymbol{p}_2}\Gamma^{\alpha\beta}(\boldsymbol{p}_1,\boldsymbol{p}_2)\,\mathrm{Tr}\left\{\left(\mathbf{Q}^{\alpha}(\boldsymbol{p}_1)-\bar{\mathbf{Q}}(\boldsymbol{p}_1)\right)\left(\mathbf{Q}^{\beta}(\boldsymbol{p}_2)-\bar{\mathbf{Q}}(\boldsymbol{p}_2)\right)\right\} \tag{8.2a}$$

$$= \frac{1}{2}\sum_{\alpha,\beta=1}^{n}\sum_{j=0}^{4}\sum_{\boldsymbol{p}_1,\boldsymbol{p}_2}(G^{-1})^{\alpha\beta}(\boldsymbol{p}_1,\boldsymbol{p}_2)Q^{\alpha}_{j}(\boldsymbol{p}_1)Q^{\beta}_{j}(\boldsymbol{p}_2). \tag{8.2b}$$

The trial Hamiltonian H_0 generically features a nonvanishing mean value $\bar{\mathbf{Q}}$ together with a kernel $\Gamma^{\alpha\beta}$. This is seen in Eq. (8.2a). Strictly speaking, the structure of the kernel

$\Gamma^{\alpha\beta}$ should allow for anisotropy for the case of $\bar{\mathbf{Q}} \neq \mathbf{0}$. Our main analysis, however, only concerns the macroscopically isotropic state, for which $\bar{\mathbf{Q}} = \mathbf{0}$. Thus, in Eq. (8.2b) we have also set $\bar{\mathbf{Q}} = \mathbf{0}$. Equation (8.2a) expresses the trial Hamiltonian in Cartesian tensor form, whilst Eq. (8.2b) expresses it in terms of the five scalar degrees of freedom of $\mathbf{Q}^\alpha$. The corresponding kernel is a transformation of $\Gamma^{\alpha\beta}$, and we have denoted it by $(G^{-1})^{\alpha\beta}$. We can check that $\langle Q_i^\alpha Q_j^\beta \rangle_{H_0} = G^{\alpha\beta}$. The variational parameters in $(G^{-1})^{\alpha\beta}$ computed via the GVM are *renormalized* quantities, in which the effect of nonlinear nematic fluctuations have been nonperturbatively taken into account, at least approximately.

Assuming that replica permutation symmetry remains unbroken, [1] we may parametrize the replica-space inverse of $(G^{-1})^{\alpha\beta}$ as

$$G^{\alpha\beta}(\boldsymbol{p}_1, \boldsymbol{p}_2) = \delta_{\boldsymbol{p}_1+\boldsymbol{p}_2,\mathbf{0}} \left(\mathcal{C}_{\mathrm{r}}^T(\boldsymbol{p}_1)\delta^{\alpha\beta} + \mathcal{C}_{\mathrm{r}}^G(\boldsymbol{p}_1) \right), \tag{8.3}$$

where $\mathcal{C}_{\mathrm{r}}^T(\boldsymbol{p})$ and $\mathcal{C}_{\mathrm{r}}^G(\boldsymbol{p})$ are the *renormalized* thermal and glassy correlators, in which fluctuations are then approximately accounted for. Together with the mean nematic order parameter $\bar{\mathbf{Q}}$, they are to be determined self-consistently, by minimizing the resulting variational free energy

$$F_{\mathrm{var}} = \left\langle H_{\mathrm{eff}} - H_0 \right\rangle_{H_0} - T \ln \int \prod_{\alpha=1}^{n} \mathcal{D}\mathbf{Q}^\alpha \, \mathrm{e}^{-H_0/T}, \tag{8.4}$$

where $\langle \cdots \rangle_{H_0}$ denotes averaging with respect to the Boltzmann weight $e^{-H_0/T}$. This calcu-

[1] We have assumed that the spontaneous breaking of replica symmetry does not occur for an IGNE. Such an assumption is motivated by the fact that glassy phenomena such as hysteresis in the stress-strain behavior of IGNEs have not been observed in experiments to date.

lation is done in Appendix H and yields

$$\begin{aligned}\frac{2}{5n\,T}F_{\rm var} &= \frac{1}{T}\sum_{\boldsymbol{p}}\left(\mathcal{A}t+\mathcal{L}p^2-\frac{|\mathrm{H}_{\boldsymbol{p}}|^2}{\mathcal{M}(T^0,\boldsymbol{p})}\right)\left(\mathcal{C}_{\rm r}^T(\boldsymbol{p})+\mathcal{C}_{\rm r}^G(\boldsymbol{p})\right)\\ &\quad+\frac{1}{T}\sum_{\boldsymbol{p}}\left(\mathrm{H}_{\boldsymbol{p}}+\frac{|\mathrm{H}_{\boldsymbol{p}}|^2}{\mathcal{M}(T^0,\boldsymbol{p})}\right)\mathcal{C}_{\rm r}^G(\boldsymbol{p})\\ &\quad+\frac{7w}{2T}\left(\sum_{\boldsymbol{p}}\left(\mathcal{C}_{\rm r}^T(\boldsymbol{p})+\mathcal{C}_{\rm r}^G(\boldsymbol{p})\right)\right)^2-\sum_{\boldsymbol{p}}\left(\ln\mathcal{C}_{\rm r}^T(\boldsymbol{p})+\frac{\mathcal{C}_{\rm r}^G(\boldsymbol{p})}{\mathcal{C}_{\rm r}^T(\boldsymbol{p})}\right).\end{aligned}\tag{8.5}$$

By minimizing $F_{\rm var}$ with respect to $\mathcal{C}_{\rm r}^T$ and $\mathcal{C}_{\rm r}^G$ we obtain the self-consistency equations

$$\begin{aligned}\mathcal{A}t+\mathcal{L}p^2-\frac{|\mathrm{H}_{\boldsymbol{p}}|^2}{\mathcal{M}(T^0,\boldsymbol{p})}+7w\sum_{\boldsymbol{p}}\left(\mathcal{C}_{\rm r}^T(\boldsymbol{p})+\mathcal{C}_{\rm r}^G(\boldsymbol{p})\right)&\\ -T\big(\mathcal{C}_{\rm r}^T(\boldsymbol{p})\big)^{-1}+\frac{T\,\mathcal{C}_{\rm r}^G(\boldsymbol{p})}{\big(\mathcal{C}_{\rm r}^T(\boldsymbol{p})\big)^2} &= 0,\end{aligned}\tag{8.6a}$$

$$\mathcal{A}t+\mathcal{L}p^2+\mathrm{H}_{\boldsymbol{p}}+7w\sum_{\boldsymbol{p}}\left(\mathcal{C}_{\rm r}^T(\boldsymbol{p})+\mathcal{C}_{\rm r}^G(\boldsymbol{p})\right)-T\big(\mathcal{C}_{\rm r}^T(\boldsymbol{p})\big)^{-1} = 0.\tag{8.6b}$$

At the mean-field level (i.e., in the high-temperature regime, where we omitted the effects of cubic and quartic terms in $\mathbf{Q}^\alpha$), we saw that $T\big(\mathcal{C}_{\boldsymbol{p}}^T\big)^{-1}=\mathcal{A}t+\mathcal{L}p^2+\mathrm{H}_{\boldsymbol{p}}$. By inspecting Eq. (8.6b), we see that we can define a renormalized reduced temperature t_R via the formula

$$t_R=t+7\frac{w}{\mathcal{A}}\sum_{\boldsymbol{p}}\left(\mathcal{C}_{\rm r}^T(\boldsymbol{p})+\mathcal{C}_{\rm r}^G(\boldsymbol{p})\right).\tag{8.7}$$

We can further re-scale t, t^0 and t_R as $\tilde{t}$, $\tilde{t}_p$ and $\tilde{t}_R$, via

$$\tilde{t}\equiv(\mathcal{A}\xi_L^2/\mathcal{L})t;\tag{8.8a}$$

$$\tilde{t}_p\equiv(\mathcal{A}\xi_L^2/\mathcal{L})t^0;\tag{8.8b}$$

$$\tilde{t}_R\equiv(\mathcal{A}\xi_L^2/\mathcal{L})t_R.\tag{8.8c}$$

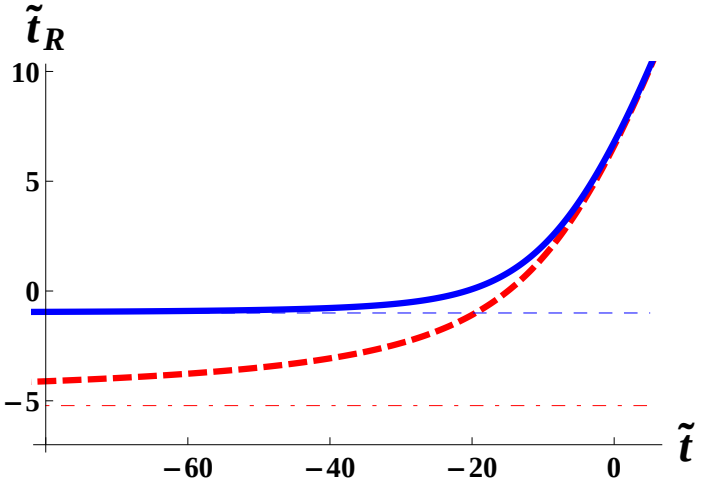

Figure 8.1: Renormalized reduced temperature $\tilde{t}_R$ vs. reduced temperature $\tilde{t}$ for $wTV/(\xi_L^3(\mathrm{H}^{(c)})^2) = \pi/80$. Disorder strength $\mathrm{H}_{\mathbf{0}}/\mathrm{H}^{(c)} = 1/4$, i.e., weak disorder (blue bold-solid); $\mathrm{H}_{\mathbf{0}}/\mathrm{H}^{(c)} = 5/4$, i.e., strong disorder (red bold-dashed). As $\tilde{t} \to \infty$, the saturation values of $\tilde{t}_R$ are $-2\mathrm{H}_{\mathbf{0}}/\mathrm{H}^{(c)}$ (for weak disorder, i.e., $\mathrm{H}_{\mathbf{0}}/\mathrm{H}^{(c)} < 1$) and $-2\ln(e\mathrm{H}_{\mathbf{0}}/\mathrm{H}^{(c)})$ (for strong disorder, i.e., $\mathrm{H}_{\mathbf{0}}/\mathrm{H}^{(c)} > 1$).

One thus obtains the *renormalized* thermal and glassy correlators

$$\mathcal{C}_{\mathrm{r}}^{T}(\boldsymbol{p}) = \frac{T}{\mathcal{A}t_R + \mathcal{L}p^2 + \mathrm{H}_{\boldsymbol{p}}}, \tag{8.9a}$$

$$\mathcal{C}_{\mathrm{r}}^{G}(\boldsymbol{p}) = \frac{T\mathrm{H}_{\boldsymbol{p}}\left(1 + \frac{\mathrm{H}_{\boldsymbol{p}}}{\mathcal{M}(T^0,\boldsymbol{p})}\right)}{\left(\mathcal{A}t_R + \mathcal{L}p^2 + \mathrm{H}_{\boldsymbol{p}}\right)^2}. \tag{8.9b}$$

Note that the renormalized correlators in Eqs. (8.9) are structurally identical to their "bare" counterparts, given in Eqs. (7.8), the only difference being the replacement of the "bare" reduced temperature t by its renormalized counterpart t_R. The relation (8.7) between t_R and t determines the existence, or lack thereof, of a transition out of the macroscopically isotropic state. By power counting, one can see that the one-loop correction involving the wave-vector sum over $\mathcal{C}^T$ implies the breakdown of long-range order below two spatial dimensions. This correction result confirms the Mermin-Wagner theorem [42], according to which models having rotationally symmetric order parameters do not have long-range order in two or fewer spatial dimensions. If no quenched disorder were present, the lower critical dimension of the IGNE would indeed be two, and the frustration of long-range order would be due to

thermal nematic fluctuations alone. On the other hand, in the present context, the one-loop correction involving the wave-vector sum over $\mathcal{C}^G$ implies the breakdown of long-range order below *four* spatial dimensions. This correction arises from the presence of quenched disorder (as the numerator is proportional to $\mathrm{H}_{\mathbf{0}}$, which is introduced via the saddle-point value of the order parameter $\langle\Gamma\rangle$ for random localization). The quenched disorder has caused an increase of the lower critical dimension from two to four.

The relation (8.7) is depicted graphically in Fig. 8.1, which also shows us that $\tilde{t}_R$ saturates at a finite value as $\tilde{t} \to -\infty$. To see that the renormalized correlators are consistent with the bare correlators in the high-temperature regime, we observe that the second term on the RHS of Eq. (8.7), proportional to w, can be neglected in this regime. Thus, t_R is essentially the bare reduced temperature t, and the renormalized correlators (8.9) reduce to the bare correlators (7.8), as they should.

What happens at lower temperatures? As $\tilde{t}$ is reduced, the intensities of $\mathcal{C}^T_{\mathrm{r}}$ and $\mathcal{C}^G_{\mathrm{r}}$ become larger, and the corrections due to fluctuations, present in Eq. (8.7), increase. The essential question is then: Do the denominators in Eqs. (8.9) *vanish* at some wave-vector $\boldsymbol{p}$ for low enough temperature? If this were indeed to happen, it would signify a continuous phase transition to some macroscopically ordered state. Now, the low-temperature physics of our model depends sensitively on the value of $\mathrm{H}_{\mathbf{0}}\xi_L^2/\mathcal{L}$. For $(\mathrm{H}_{\mathbf{0}}\xi_L^2/\mathcal{L}) < 2$, the denominator factor in Eqs. (8.9), viz., $\mathcal{A}t_R + \mathcal{L}p^2 + \mathrm{H}_{\boldsymbol{p}}$, has a minimum at $\boldsymbol{p} = \mathbf{0}$. Assuming that a continuous phase transition occurs at a finite (and negative) value t_c of t, this denominator would have to vanish for $\boldsymbol{p} = \mathbf{0}$. In three dimensions, however, the wave-vector integral in Eq. (8.7) diverges, and thus $t_R(t_c) = +\infty$, implying that the denominator actually diverges to $+\infty$, which contradicts our original assumption. We therefore conclude that in three dimensions and for $\mathrm{H}_{\mathbf{0}}\xi_L^2/\mathcal{L} < 2$ there can be no continuous transition to any state having long-range nematic order.

For $\mathrm{H}_{\mathbf{0}}\xi_L^2/\mathcal{L} > 2$, the factor $\mathcal{A}t + \mathcal{L}p^2 + \mathrm{H}_{\boldsymbol{p}}$ has a minimum at $p^2 = 2\ln(\mathrm{H}_{\mathbf{0}}\xi_L^2/2\mathcal{L})$. In this case, to have a continuous phase transition (towards a macroscopically periodically

modulated phase) would require the vanishing of the denominator at $p^2 = 2\ln(\mathrm{H}_{\mathbf{0}}\xi_L^2/2\mathcal{L})$. However, again, the integral in Eq. (8.7) would diverge; thus, the present level of approximation indicates that no continuous phase transition occurs. Owing to quenched fluctuations, *the isotropic phase is always stable, for any positive* $\mathrm{H}_{\mathbf{0}}$.

8.2 Low-measurement-temperature structure for a system prepared at T^0 far above T^*

In this section, we unpack the physics encoded in the correlators computed via the GVM. As with the results we found in Chapter 2, we shall see, e.g., that the glassy and thermal nematic fluctuation correlations in an IGNE are capable of undergoing oscillatory decay for sufficiently high cross-linking temperature T^0 and high disorder strength $\mathrm{H}_{\mathbf{0}}$. By revisiting the case of a system that was cross-linked at a very high temperature, we shall also see how the structural behavior of the IGNE in the low measurement-temperature regime is *modified*, via the presence of fluctuation-induced corrections, from its behavior in the high measurement-temperature regime. For such systems, we shall contrast the effects of disorder in the weak- (i.e., $\mathrm{H}_{\mathbf{0}}\,\xi_L^2/\mathcal{L} < 2$) and strong- (i.e., $\mathrm{H}_{\mathbf{0}}\,\xi_L^2/\mathcal{L} > 2$) disorder regimes.

8.2.1 Weak disorder

In this regime, the thermal and glassy correlators each have a finite peak at zero wave-vector, indicating spatial decay without oscillation, in contrast with the strong-disorder regime (see below, Sec. 8.2.2). To estimate the lengthscales $\xi_{T,d}^{(\mathrm{r})}$ and $\xi_{G,d}^{(\mathrm{r})}$ over which $\mathcal{C}_{\mathrm{r}}^T$ and $\mathcal{C}_{\mathrm{r}}^G$ respectively decay, we examine their small wave-vector behavior, thus obtaining the lengths

$$\xi_{T,d}^2 \approx \frac{2 - (\mathrm{H}_{\mathbf{0}}\,\xi_L^2/\mathcal{L})}{2(\tilde{t}_R + (\mathrm{H}_{\mathbf{0}}\,\xi_L^2/\mathcal{L}))}\xi_L^2, \qquad \xi_{G,d}^2 \approx 2\xi_{T,d}^2 + \tfrac{1}{2}\xi_L^2. \tag{8.10}$$

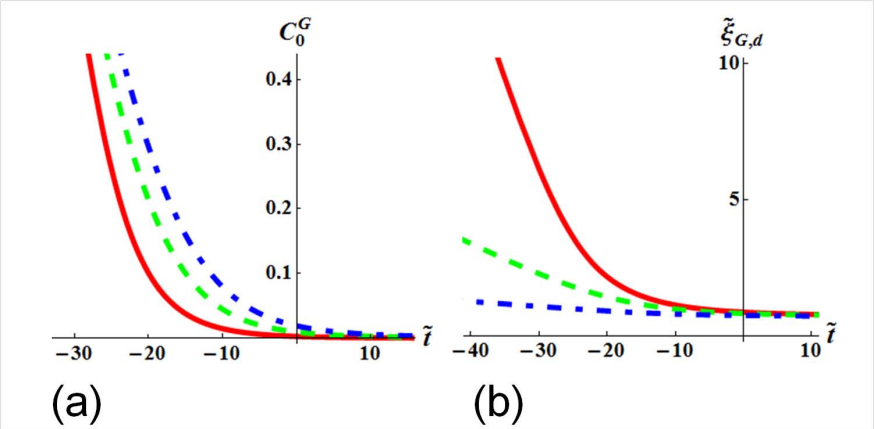

Figure 8.2: (a) Glassy order parameter $\mathcal{C}_{\mathbf{0}}^{G} \equiv (4\pi^3 \mathrm{H}^{(c)} \xi_L^3/T)\mathcal{C}^{G}(\boldsymbol{r})|_{\boldsymbol{r}=\mathbf{0}}$ and (b) glassy correlation length $\tilde{\xi}_{G,d} \equiv \xi_{G,d}/\xi_L$ as a function of $\tilde{t}$ for three cases of weak disorder: $\mathrm{H}_{\mathbf{0}}/\mathrm{H}^{(c)} = 0.1$ (red solid), $\mathrm{H}_{\mathbf{0}}/\mathrm{H}^{(c)} = 0.35$ (green dashed) and $\mathrm{H}_{\mathbf{0}}/\mathrm{H}^{(c)} = 0.75$ (blue dot-dashed), where we have set $wTV/(\xi_L^3(\mathrm{H}^{(c)})^2) = \pi/80$.

In the high measurement-temperature regime, t_R is approximately t, and the behaviors that are observed for $\xi_{T,d}$ and $\xi_{G,d}$ also apply to $\xi_{T,d}^{(\mathrm{r})}$ and $\xi_{G,d}^{(\mathrm{r})}$. On the other hand, for decreased measurement temperature, the nematogens tend to align with one another, driven by their direct interactions, and this tendency is reflected in the accompanying rapid growth of the strength of the glassy order parameter $\mathcal{C}_{\mathrm{r}}^{G}(\boldsymbol{r})|_{\boldsymbol{r}=\mathbf{0}}$ and a similar rapid growth in $\xi_{G,d}^{(\mathrm{r})}$ (see Fig. 8.2), and $\xi_{G,d}^{(\mathrm{r})}$ sets the lengthscale of the domain size in the *weak*-disorder regime. This is to be contrasted with another lengthscale that sets the domain size in the *strong*-disorder regime, as we shall learn in the following sub-section. This "inflation" of the domain size in the presence of *weak* disorder is to be contrasted with the manner in which the domain size shrinks and ultimately saturates with decreasing temperature in the presence of *strong* disorder, which we shall explore in the following subsection.

8.2.2 Strong disorder

In the strong-disorder regime (i.e., $\mathrm{H}_{\mathbf{0}}\,\xi_L^2/\mathcal{L} > 2$), the correlators $\mathcal{C}_{\mathrm{r}}^{T}$ and $\mathcal{C}_{\mathrm{r}}^{G}$ each have a peak at a nonzero wave-vector. The peak of $\mathcal{C}_{\mathrm{r}}^{T}(\boldsymbol{p})$ coincides with that of $\mathcal{C}_{\boldsymbol{p}}^{T}$, residing at $|\boldsymbol{p}| = \sqrt{2\ln(\mathrm{H}_{\mathbf{0}}\,\xi_L^2/2\mathcal{L})}/\xi_L$. However, the peak of $\mathcal{C}_{\mathrm{r}}^{G}(\boldsymbol{p})$ is located at a momentum value

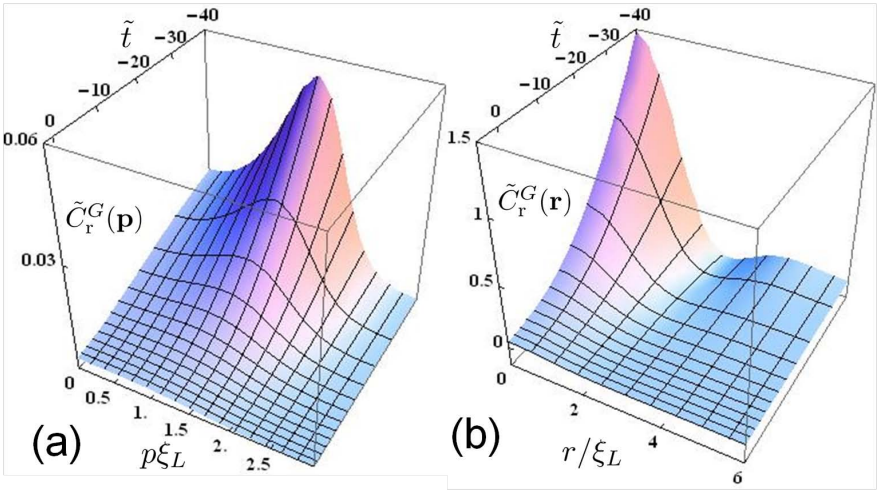

Figure 8.3: (a) Rescaled glassy correlator $\tilde{\mathcal{C}}^G_{\rm r}(\boldsymbol{p}) \equiv (\mathcal{L}^2/(T\mathrm{H}_{\mathbf{0}}\xi_L^4))\mathcal{C}^G_{\rm r}(\boldsymbol{p})$ at $\mathrm{H}_{\mathbf{0}}/\mathrm{H}^{(c)} = 5$ as a function of rescaled reduced temperature $\tilde{t} \equiv (\mathcal{A}\xi_L^2/\mathcal{L})t$ and reduced wave-vector $p\xi_L$; (b) Glassy correlator $\tilde{\mathcal{C}}^G_{\rm r}(\boldsymbol{r}) \equiv (2\pi^2\mathcal{L}^2/T\mathrm{H}_{\mathbf{0}}\xi_L)\mathcal{C}^G_{\rm r}(\boldsymbol{r})$ at $\mathrm{H}_{\mathbf{0}}/\mathrm{H}^{(c)} = 5$ as a function of rescaled reduced temperature $\tilde{t}$ and rescaled separation distance r/ξ_L. Note the progression in (a) of the peak location from zero wave-vector to nonzero wave-vector with decreasing $\tilde{t}$. The peak at nonzero wave-vector is associated with the spatial oscillations observed in (b) for the glassy correlator in real-space. For both panels, we have set $wTV/(\xi_L^3(\mathrm{H}^{(c)})^2) = \pi/80$. Note also in (b) that the intensity $\tilde{\mathcal{C}}^G_{\rm r}(\boldsymbol{r})|_{\boldsymbol{r}=0}$ rapidly increases as the temperature is reduced.

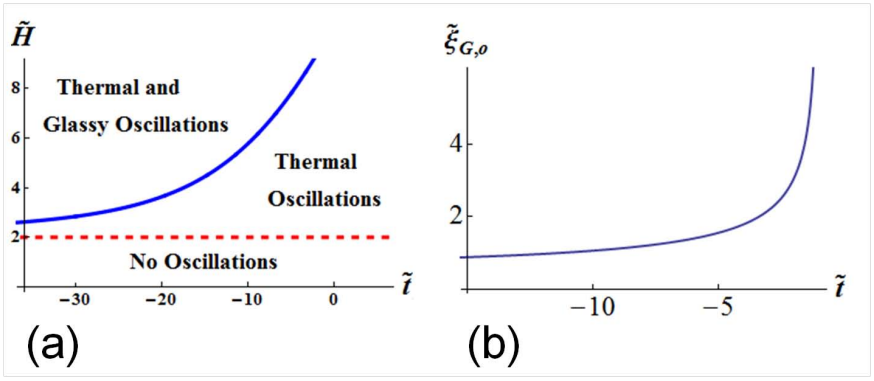

Figure 8.4: (a) Behavior diagram for the glassy and thermal correlators, indicating the three qualitatively distinct regimes. Here, $\tilde{H} \equiv \mathrm{H}_{\mathbf{0}}/\mathrm{H}^{(c)}$ is a measure of the disorder strength and $\tilde{t}$ is the rescaled reduced temperature, having the value $(\mathcal{A}\xi_L^2/\mathcal{L})t$. Above the blue solid line, both correlators oscillate and decay as a function of separation. Between the blue solid and red dashed lines, both correlators decay but only the thermal one also oscillates. Below the red dashed line, both correlators decay but neither oscillates. (b) Rescaled oscillation wavelength $\tilde{\xi}_{G,o}$ ($\equiv \xi_{G,o}/\xi_L$) as a function of $\tilde{t}$ for $\mathrm{H}_{\mathbf{0}}/\mathrm{H}^{(c)} = 5$. As $\tilde{t}$ is decreased, $\tilde{\xi}_{G,o}$ eventually saturates at a nonzero value of order unity (which implies that $\xi_{G,o}$ saturates at the order of ξ_L). For both panels, we have set $wTV/(\xi_L^3(\mathrm{H}^{(c)})^2) = \pi/80$.

different from that of $\mathcal{C}^G_{\boldsymbol{p}}$, viz., it occurs at the momentum value $|\boldsymbol{p}| = (\xi^{(\mathrm{r})}_{G,o})^{-1}$, with $\xi^{(\mathrm{r})}_{G,o}$ obeying

$$\mathcal{A}\, t_R + 4(\mathcal{L}/\xi_L^2) + \mathcal{L}(\xi^{(\mathrm{r})}_{G,o})^{-2} - \mathrm{H}_{\mathbf{0}} \exp\big(-\xi_L^2/(2(\xi^{(\mathrm{r})}_{G,o})^2)\big) = 0. \tag{8.11}$$

As with the case of the finite-wave-vector peaks in $\mathcal{C}^T_{\boldsymbol{p}}$ and $\mathcal{C}^G_{\boldsymbol{p}}$, the peaks in $\mathcal{C}^T_{\mathrm{r}}(\boldsymbol{p})$ and $\mathcal{C}^G_{\mathrm{r}}(\boldsymbol{p})$ are associated with the oscillatory decay of the correlators in real space. The crossover in their behavior, from non-oscillatory to oscillatory, as the disorder strength $\mathrm{H}_{\mathbf{0}}$ is increased, is shown in Fig. 8.4. The evolution of the location of the peak of $\mathcal{C}^G_{\mathrm{r}}(\boldsymbol{p})$, from the origin to a nonzero wave-vector, as the measurement temperature is decreased at disorder strength $\mathrm{H}_{\mathbf{0}}\, \xi_L^2/\mathcal{L} = 10$ is shown in Fig. 8.3. Provided the system is in the "under-damped" regime, in which the renormalized glassy correlation length $\xi^{(\mathrm{r})}_{G,d}$ exceeds the wavelength $\xi^{(\mathrm{r})}_{G,o}$ of the oscillations of the renormalized glassy correlator, the lengthscale $\xi^{(\mathrm{r})}_{G,o}$ would reflect the size of domains of local nematic alignment. Also, note from Eq. (8.11) that as the measurement temperature is decreased, $\xi^{(\mathrm{r})}_{G,o}$ decreases, and ultimately saturates at the order of the typical localization length (see Fig. 8.4). This reflects qualitatively the experimental observation (see, e.g., Ref. [5], Fig. 8.18 of Sec. 8.4.2, and Ref. [51]) that the domain size of the IGNE shrinks as temperature decreases, and saturates at a finite value. Comparison with the corresponding experimental measurements of the domain size in the low-temperature regime [28, 51] indicates that ξ_L is of the order of micrometers.

Chapter 9

Conclusions

The objective of this thesis has been to develop a theoretical approach to the elastic and liquid crystalline properties of isotropic-genesis nematic elastomers (IGNEs), in which local nematic order—both in the preparation and the measurement ensembles—and random localization are naturally incorporated. We have proposed a novel Landau-type theory of an IGNE, which features a nonlocal nematic-nematic interaction term as well as a random-field term that reflects the memorization of nematic fluctuations present at the instant of cross-linking. Subsequently, we have justified this Landau-type theory via a microscopic model of an IGNE consisting of dimers randomly, permanently and instantaneously cross-linked via springs.

Via the microscopic model of the IGNE, we have acquired the following main results:

(1) By taking the thermal fluctuations of the elastomer medium into account, we have been able to predict, for a sufficiently strongly cross-linked IGNE, a novel type of correlation behavior of nematic alignments trapped into the network via cross-linking, which is oscillatory-decaying in real space. Such oscillatory-decay behavior is qualitatively consistent with the anti-correlation pattern observed by Urayama et al. [28].

(2) By means of a Gaussian variational analysis, we have found that the macroscopically isotropic state of an IGNE (and thus also the polydomain state) is locally stable in the low-temperature regime. This result is consistent with the lack of any experimental observation, to date, of the formation of long-range nematic order in IGNEs in the low-temperature regime. Through the glassy and thermal fluctuation correlators computed via the Gaussian variational method, we have been able to study the nematic structure and correlations in a macroscopically isotropic IGNE at low temperatures.

(3) We have shown that the IGNE's memory of the correlation pattern of thermal nematic fluctuations that are present at the instant of cross-linking directly influences the subsequent correlation pattern of the nematic alignments that are "frozen" into the IGNE by the cross-linking process. Moreover, we have also shown that the fidelity of the memorization of the initial fluctuation correlation pattern depends on the strength of cross-linking and the temperature at which the system was cross-linked, becoming better as the density of cross-links is increased and the preparation temperature is decreased.

(4) We have shown, at least for the case of small strain, that the thermal fluctuations of the nematic freedoms in an IGNE result in the softening of the elastic response of the IGNE in the high-temperature regime.

(5) We have derived the functional form of the disorder-averaged correlator of random relaxational displacements present in an IGNE, in particular explicating the dependence of this correlator on the glassy and thermal fluctuation correlators of the nematic freedoms.

Apart from its relevance to the specific subject of liquid crystalline elastomers, the present work brings to light a more general issue, viz., that the concept of a quenched random field employed to describe an IGNE should be broadened to incorporate not only the conventional, "frozen" type, which does not fluctuate thermally, but also the type necessary for understanding media such as liquid crystalline elastomers, in which the frozen nature of the random field is present only at longer lengthscales, fading out as the lengthscale progresses down through a characteristic localization length, owing to the thermal position fluctuations of the network's constituents.

The approach described in this thesis opens up a path for studying more challenging problems, such as the following few:

(i) The soft elasticity of a monodomain nematic elastomer (in which nematogens are uniaxially aligned on average) has been studied by previous workers (see, e.g., Refs. [5, 18, 19, 20]). These works have uniformly been based on the assumption that the constituents of the elastomer medium deform *affinely* when a homogeneous external stress is applied to

its boundary. One of the major insights arising from these works is the role played by the broken symmetry of the underlying liquid crystal system on the vanishing of certain elastic constants; such vanishing leads to "ideal softness," for which the gradient of the stress-strain curve is *zero* at small strains. However, as discussed in the thesis, the bulk constituents of the medium actually undergo *non-affine* displacements when subjected to a homogeneous stress at the boundary. It is also experimentally well known (see, e.g., Ref. [5]) that instead of being ideally soft, the monodomain nematic elastomer is "semi-soft," which means that the gradient of the stress-strain curve is small but *finite* at small strains. It has been shown in Ref. [31] that the soft elasticity described in the theories of Refs. [5, 18, 19, 20] can be derived from a replica field theory that couples Γ to $\mathbf{Q}^{\alpha}$, with the value of Γ set to its saddle-point value (which has an *anisotropic* exponent for the case of a monodomain nematic elastomer, rather than an *isotropic* exponent as we have seen for the case of an IGNE). One can study the branch of Goldstone fluctuations around this anisotropic saddle-point value of Γ, integrating out the non-affinity and examining the resulting shear modulus. Such non-affinity would presumably generate semi-soft corrections to the elasticity of a monodomain nematic elastomer.

(ii) We have also explored the shear behavior of a slightly deformed IGNE in the high-temperature regime, for which thermally driven elastic fluctuations are small. It is worthwhile to probe the medium's shear modulus in the low-temperature regime as well; to do this, one would have to consider nonlinear strain fluctuations, as elastic fluctuations can be large in the low-temperature regime. This is because the inverse shear modulus depends on the thermal nematic fluctuation correlator, and we have seen in Chapter 8 that this correlator has a large value in the low-temperature regime.

(iii) One could also generalize the approach presented in Chapters 6 and 7 to the case of IGNEs subject to a non-infinitesimal externally imposed strain deformation. In principle, our approach takes the non-affinity present in deformed IGNEs into account. Thus, one could determine the non-affinity correlator of IGNEs and derive the contribution that frozen

nematic alignment makes to non-affinity in IGNEs.

The framework elucidated in the present work can also be extended, with suitable modifications, to explore the statistical physics of other randomly cross-linked systems, such as smectic elastomers and actin filament networks.

Appendix A

Calculation of the average linking number per dimer

In the Appendices, we show components of the calculations that are necessary for deriving the results presented in the main body of the thesis. In this Appendix, we show that the average number of springs connected to a dimer, $[M]/N$, is equal to $2\eta^2$. By definition,

$$
\begin{aligned}
[M] &= \frac{1}{Z_1}\sum_{M=0}^{\infty}\sum_{\substack{i_1,j_1=1\\(i_1\neq j_1)}}^{N}\sum_{s_1,t_1=-1,1}\cdots\sum_{\substack{i_M,j_M=1\\(i_M\neq j_M)}}^{N}\sum_{s_M,t_M=-1,1}\frac{M}{M!}\Big(\frac{\eta^2 V}{2N(2\pi b^2)^{D/2}}\Big)^M \\
&\quad\times Z_L\left\langle\prod_{e=1}^{M}\Delta(|\boldsymbol{c}_{i_e,s_e}-\boldsymbol{c}_{j_e,t_e}|)\right\rangle_{H_0} \\
&= \frac{\eta^2 V}{2N(2\pi b^2)^{D/2}}\frac{1}{Z_1}\Big\langle\Big(\sum_{i\neq j}\sum_{s,t}\Delta(|\boldsymbol{c}_{i,s}-\boldsymbol{c}_{j,t}|)\Big)\sum_{M=1}^{\infty}\frac{1}{(M-1)!}\Big(\frac{\eta^2 V}{2N(2\pi b^2)^{D/2}}\Big)^{M-1} \\
&\quad\times Z_L\Big(\sum_{i\neq j}\sum_{s,t}\Delta(|\boldsymbol{c}_{i,s}-\boldsymbol{c}_{j,t}|)\Big)^{M-1}\Big\rangle_{H_0} \\
&= \frac{\eta^2 V}{2N(2\pi b^2)^{D/2}}\frac{1}{Z_1}\Big\langle Z_L\Big(\sum_{i\neq j}\sum_{s,t}\Delta(|\boldsymbol{c}_{i,s}-\boldsymbol{c}_{j,t}|) \\
&\quad\times\exp\Big(\frac{\eta^2 V}{2N(2\pi b^2)^{D/2}}\sum_{i\neq j}\sum_{s,t}\Delta(|\boldsymbol{c}_{i,s}-\boldsymbol{c}_{j,t}|)\Big)\Big\rangle_{H_0} \\
&= \eta^2\frac{d\ln Z_1}{d\eta^2}
\end{aligned}
\tag{A.1}
$$

Here, Z_L is the partition function of an un-cross-linked liquid of dimers, given by

$$
\prod_{i=1}^{N}\int d\boldsymbol{c}_{i,1}d\boldsymbol{c}_{i,2}\exp(-H_{\rm nem}-H_{\rm ev})\delta(|\boldsymbol{c}_{i,1}-\boldsymbol{c}_{i,2}|-\ell). \tag{A.2}
$$

H_0 denotes the Hamiltonian of the un-cross-linked liquid, and has the value $H_{\rm nem} + H_{\rm ev}$. $\langle \ldots \rangle_{H_0}$ denotes a Boltzmann average over this Hamiltonian. $\Delta(|\boldsymbol{c}|)$ has the value $e^{-c^2/2b^2}$, where D is the number of spatial dimensions and b is the r.m.s. spring-length. On going from the second to the third line, we have summed over M to obtain an exponential series. In the fourth line, we have made use of the definition of the normalization factor Z_1; it is given by

$$\begin{aligned}
Z_1 \;=\; & \sum_{M=0}^{\infty} \sum_{\substack{i_1,j_1=1 \\ (i_1 \neq j_1)}}^{N} \sum_{s_1,t_1=-1,1} \cdots \sum_{\substack{i_M,j_M=1 \\ (i_M \neq j_M)}}^{N} \sum_{s_M,t_M=-1,1} \frac{1}{M!} \Big(\frac{\eta^2 V}{2N(2\pi b^2)^{D/2}} \Big)^M \\
& \times Z_L(V) \left\langle \prod_{e=1}^{M} \Delta(|\boldsymbol{c}_{i_e,s_e} - \boldsymbol{c}_{j_e,t_e}|) \right\rangle_{H_0} \\
= & \sum_{M=0}^{\infty} \sum_{\substack{i_1,j_1=1 \\ (i_1 \neq j_1)}}^{N} \sum_{s_1,t_1=-1,1} \cdots \sum_{\substack{i_M,j_M=1 \\ (i_M \neq j_M)}}^{N} \sum_{s_M,t_M=-1,1} \frac{1}{M!} \Big(\frac{\eta^2 V}{2N(2\pi b^2)^{D/2}} \Big)^M Z_L(V) \\
& \times \int \prod_{i=1}^{N} \int d\boldsymbol{c}_i d\boldsymbol{n}_i e^{-\frac{\lambda^2}{2T} \sum_{i,j=1}^{N} \sum_{s,t} \delta\left((\boldsymbol{c}_i + \frac{s\ell}{2}\boldsymbol{n}_i) - (\boldsymbol{c}_j + \frac{t\ell}{2}\boldsymbol{n}_j) \right) + \frac{V}{2N} \sum_{i,j=1}^{N} J(\boldsymbol{c}_i - \boldsymbol{c}_j)(\boldsymbol{n}_i \cdot \boldsymbol{n}_j)^2} \\
& \times \exp\Big(\frac{\eta^2 V}{2N(2\pi b^2)^{D/2}} \sum_{i \neq j} \sum_{s,t} e^{-\frac{|(\boldsymbol{c}_i + \frac{s\ell}{2}\boldsymbol{n}_i) - (\boldsymbol{c}_j + \frac{t\ell}{2}\boldsymbol{n}_j)|^2}{2b^2}} \Big). \qquad \text{(A.3)}
\end{aligned}$$

To compute Z_1 we approximate the system as a dilute gas of particles, for instance, in approximating the delta function by $1/V$ and $\exp(-|\boldsymbol{c}_i - \boldsymbol{c}_j|^2/(2b^2))$ by $(2\pi b^2)^{D/2}/V$. This allows one to approximate Z_1 by

$$Z_1 \propto V^N e^{-\frac{\lambda^2 N^2}{2TV} + 2N\eta^2}, \qquad \text{(A.4)}$$

where the proportionality constant is independent of η^2. By substituting this value of Z_1 into Eq. (A.1), one finds that $[M]/N = 2\eta^2$.

Appendix B

Hubbard-Stratonovich decoupling procedure

In this Appendix, we present the details of the Hubbard-Stratonovich decoupling scheme that leads to Eq. (3.18). We first compute the replica partition function Z_{1+n} which appears in Eq. (3.11) and is defined by

$$Z_{1+n} \equiv \sum_{\chi} \frac{1}{M!} \left(\frac{V\eta^2}{2N(2\pi b^2)^{D/2}} \right)^M Z_\chi(V) Z_\chi(V)^n. \tag{B.1}$$

This gives

$$\begin{aligned}
Z_{1+n} &= \sum_{M=0}^{\infty} \sum_{i_1 \neq j_1}^{N} \cdots \sum_{i_M \neq j_M}^{N} \sum_{s_1,t_1} \cdots \sum_{s_M,t_M} \frac{1}{M!} \left(\frac{V\eta^2}{2N(2\pi b^2)^{D/2}} \right)^M \\
&\quad \times \prod_{\alpha=0}^{n} \int \prod_i \frac{d\boldsymbol{c}_{i,1}^\alpha \, d\boldsymbol{c}_{i,2}^\alpha}{4\pi\ell^2 V} e^{\frac{1}{2}\sum_{\alpha=0}^{n}\sum_{i,j} \frac{J_{ij}}{T^\alpha}\left((\boldsymbol{n}_i^\alpha \cdot \boldsymbol{n}_j^\alpha)^2 - \frac{1}{d}\right) - \frac{1}{2b^2}\sum_{\alpha=0}^{n}\sum_{e=1}^{M} |\boldsymbol{c}_{i_e,s_e}^\alpha - \boldsymbol{c}_{j_e,t_e}^\alpha|^2} \\
&\quad \times e^{-\frac{1}{2}\sum_{\alpha=0}^{n}\sum_{i,j}\sum_{s,t} \frac{\lambda}{T^\alpha}\delta(\boldsymbol{c}_{i,s}{}^\alpha - \boldsymbol{c}_{j,t}{}^\alpha)} \prod_{j=1}^{N} \delta(|\boldsymbol{c}_{j_1}^\alpha - \boldsymbol{c}_{j_2}^\alpha| - l) \\
&= \prod_{\alpha=0}^{n} \int \prod_i \frac{d\boldsymbol{c}_{i,1}^\alpha \, d\boldsymbol{c}_{i,2}^\alpha}{4\pi\ell^2 V} e^{\frac{1}{2}\sum_{\alpha=0}^{n}\sum_{i,j} J_{ij} T^\alpha \left((\boldsymbol{n}_i^\alpha \cdot \boldsymbol{n}_j^\alpha)^2 - \frac{1}{d}\right) - \frac{1}{2}\sum_{\alpha=0}^{n}\sum_{i,j}\sum_{s,t} \frac{\lambda}{T^\alpha}\delta(\boldsymbol{c}_{i,s}^\alpha - \boldsymbol{c}_{j,t}^\alpha)} \\
&\quad \times \exp\left(\frac{V\eta^2}{2N(2\pi b^2)^{D/2}} \sum_{i\neq j}\sum_{s,t} e^{-\frac{1}{2b^2}\sum_{\alpha=0}^{n} |\boldsymbol{c}_{i,s}^\alpha - \boldsymbol{c}_{j,t}^\alpha|^2} \right) \prod_{j=1}^{N} \delta(|\boldsymbol{c}_{j_1}^\alpha - \boldsymbol{c}_{j_2}^\alpha| - l).
\end{aligned} \tag{B.2}$$

In the last step we have summed over all realizations of quenched disorder. This results in an exponentiation of the Hookean energy term. The expression for Z_{1+n} involves a constraint that fixes the dimer rod length at ℓ. We can eliminate the constraint by directly working with the centre-of-mass coordinate $\boldsymbol{c} \equiv (\boldsymbol{c}_1 + \boldsymbol{c}_2)/2$ and dimer orientation $\boldsymbol{n} \equiv (\boldsymbol{c}_2 - \boldsymbol{c}_1)/\ell$.

In terms of these new coordinates, Eq. (B.2) becomes

$$
\begin{aligned}
Z_{1+n} &= \prod_{\alpha=0}^{n}\int\prod_{i}\frac{d\boldsymbol{c}_i^{\alpha}d\boldsymbol{n}_i^{\alpha}}{4\pi V}e^{\frac{V}{2N}\sum_{\alpha=0}^{n}\sum_{i,j}\frac{J(\boldsymbol{c}_i^{\alpha}-\boldsymbol{c}_j^{\alpha})}{T^{\alpha}}\left(n_{ia}^{\alpha}n_{ib}^{\alpha}-\frac{1}{d}\delta_{ab}\right)\left(n_{ja}^{\alpha}n_{jb}^{\alpha}-\frac{1}{d}\delta_{ab}\right)} \\
&\quad\times e^{-\sum_{\alpha=0}^{n}\frac{\lambda}{2T^{\alpha}}\int d\boldsymbol{r}^{\alpha}\sum_{i,s}\delta\left((\boldsymbol{c}_i{}^{\alpha}+\frac{s\ell}{2}\boldsymbol{n}_i^{\alpha})-\boldsymbol{r}^{\alpha}\right)\sum_{j,t}\delta\left((\boldsymbol{c}_j{}^{\alpha}+\frac{t\ell}{2}\boldsymbol{n}_j^{\alpha})-\boldsymbol{r}^{\alpha}\right)} \\
&\quad\times\exp\Big(\frac{2NV\eta^2}{(2\pi b^2)^{D/2}}\int d\hat{x}\,d\hat{y}e^{-\frac{|\hat{x}-\hat{y}|^2}{2b^2}}\frac{1}{2N}\sum_{i,s}\delta\big(\hat{x}-(\hat{c}_i+\frac{s\ell}{2}\hat{n}_i)\big) \\
&\quad\times\frac{1}{2N}\sum_{j,t}\delta\big(\hat{y}-(\hat{c}_j+\frac{t\ell}{2}\hat{n}_j)\big)\Big).
\end{aligned}
\tag{B.3}
$$

Here, we have made a continuum approximation to $J_{i,j}$, viz. $J_{i,j}\approx(V/N)J(\boldsymbol{c}_i^{\alpha}-\boldsymbol{c}_j^{\alpha})$, and $J(\boldsymbol{c})$ is defined by $\big(J_0/(2\pi a^2)^{d/2}\big)\exp(-c^2/2a^2)$. Next, we define the following collective fields:

$$
q_{ab}^{\alpha}(\boldsymbol{r}^{\alpha}) = \frac{1}{N}\sum_{i=1}^{N}(n_{ia}^{\alpha}n_{ib}^{\alpha}-d^{-1}\delta_{ab})\delta(\boldsymbol{r}^{\alpha}-\boldsymbol{c}_i^{\alpha}), \tag{B.4}
$$

$$
\gamma^{\alpha}(\boldsymbol{r}^{\alpha}) = \frac{1}{2N}\sum_{i=1}^{N}\sum_{s=-1,1}\delta\big((\boldsymbol{c}_i{}^{\alpha}+\frac{s\ell}{2}\boldsymbol{n}_i^{\alpha})-\boldsymbol{r}^{\alpha}\big), \tag{B.5}
$$

$$
\gamma(\hat{r}) = \frac{1}{2N}\sum_{i=1}^{N}\sum_{s=-1,1}\delta\big(\hat{r}-(\hat{c}_j+\frac{s\ell}{2}\hat{n}_j)\big). \tag{B.6}
$$

In Fourier space, these take the form

$$
q_{ab}^{\alpha}(\boldsymbol{p}) = \frac{1}{N}\sum_{i=1}^{N}e^{i\boldsymbol{p}\cdot\boldsymbol{c}_i^{\alpha}}(n_{ia}^{\alpha}n_{ib}^{\alpha}-d^{-1}\delta_{ab}), \tag{B.7}
$$

$$
\gamma_{\boldsymbol{p}}^{\alpha} = \frac{1}{2N}\sum_{i=1}^{N}\sum_{s=-1,1}e^{-i\boldsymbol{p}\cdot(\boldsymbol{c}_i^{\alpha}+\frac{s\ell}{2}\boldsymbol{n}_i^{\alpha})}, \tag{B.8}
$$

$$
\gamma_{\hat{k}} = \frac{1}{2N}\sum_{i=1}^{N}\sum_{s=-1,1}e^{-i\hat{k}\cdot(\hat{c}_i+\frac{s\ell}{2}\hat{n}_i)}. \tag{B.9}
$$

Here, the argument of $\gamma_{\hat{k}}$ can take any value in replica Fourier space. Note that $\gamma_{\boldsymbol{p}\hat{\epsilon}^\alpha} = \gamma^\alpha_{\boldsymbol{p}}$. Boltzmann averages are denoted by the following symbols

$$\begin{aligned}\langle \cdots \rangle_{N,1+n} &\equiv \prod_{\alpha=0}^{n} \int \prod_{j=1}^{N} \frac{d\boldsymbol{c}_j^\alpha d\boldsymbol{n}_j^\alpha}{4\pi V}; \\ \langle \cdots \rangle_{1,1+n} &\equiv \prod_{\alpha=0}^{n} \int \frac{d\boldsymbol{c}^\alpha d\boldsymbol{n}^\alpha}{4\pi V}.\end{aligned} \tag{B.10}$$

We substitute the collective fields into Eq. (B.3), taking care to separate out the 0RS, 1RS and HRS parts of the terms involving $\gamma_{\hat{k}}$. The replica partition function now becomes

$$\begin{aligned}Z_{1+n} = \Bigg\langle & \exp\left(\frac{N}{2}\sum_{\alpha=0}^{n}\sum_{\boldsymbol{p}}\frac{J_{\boldsymbol{p}}}{T^\alpha}|q^\alpha_{ab}(\boldsymbol{p})|^2 - \frac{2N^2}{V}\sum_{\alpha=0}^{n}\frac{\lambda}{T^\alpha}|\gamma^\alpha_{\boldsymbol{0}}|^2 - \frac{2N^2}{V}\sum_{\alpha=0}^{n}{\sum_{\boldsymbol{p}}}'\lambda^\alpha|\gamma^\alpha_{\boldsymbol{p}}|^2\right) \\ & \times \exp\Big(\frac{2N\eta^2}{V^n}|\gamma_{\hat{0}}|^2 + \frac{2N\eta^2}{(2\pi b^2)^{D/2}V^n}\sum_{\alpha=0}^{n}{\sum_{\boldsymbol{p}}}'\Delta_{\boldsymbol{p}\epsilon^\alpha}|\gamma_{\boldsymbol{p}\epsilon^\alpha}|^2 \\ & + \frac{2N\eta^2}{(2\pi b^2)^{D/2}V^n}\sum_{\alpha=0}^{n}{\sum_{\hat{k}}}'\Delta_{\hat{k}}|\gamma_{\hat{k}}|^2\Big)\Bigg\rangle_{N,1+n} \\ \propto \Bigg\langle & \exp\Big(\frac{N}{2}\sum_{\alpha=0}^{n}\sum_{\boldsymbol{p}}\frac{J_{\boldsymbol{p}}}{T^\alpha}|q^\alpha_{ab}(\boldsymbol{p})|^2 - \frac{N}{2}\sum_{\alpha=0}^{n}{\sum_{\boldsymbol{p}}}'\frac{\tilde{\lambda}_{\boldsymbol{p}}}{T^\alpha}|\gamma^\alpha_{\boldsymbol{p}}|^2 \\ & + \frac{N\tilde{\eta}^2}{2(2\pi b^2)^{D/2}V^n}\sum_{\alpha=0}^{n}\sum_{\hat{k}\in HRS}\Delta_{\hat{k}}|\gamma_{\hat{k}}|^2\Big)\Bigg\rangle_{N,1+n},\end{aligned} \tag{B.11}$$

where ${\sum_{\boldsymbol{p}}}'$ denotes a sum over all wave-vectors $\boldsymbol{p}$ excluding $\boldsymbol{p} = \boldsymbol{0}$. The symbols $\Delta_k \equiv (2\pi b^2)^{D/2}\exp(-\frac{1}{2}b^2k^2)$, $\tilde{\eta}^2 \equiv 4\eta^2$, and $\tilde{\lambda}/T^\alpha \equiv (4N/\tilde{V})\lambda^\alpha/T^\alpha - (4\eta^2/\tilde{V}^n)\Delta_{\boldsymbol{p}\epsilon^\alpha}$. $\tilde{\lambda}^\alpha$ has the physical meaning of an excluded volume interaction between dimers that has been renormalized by the attractive interactions between cross-links. In Eq. (B.11), the set of all wave-vectors has been decomposed into different replica sectors. The replica sectors are defined as follows: if a replicated momentum vector $\hat{p} \equiv (\boldsymbol{p}^0, \boldsymbol{p}^1, \ldots, \boldsymbol{p}^n)$ has no non-zero component, then $\hat{p}$ belongs to the zero-replica sector (denoted by "0RS"). If there is only one component $\boldsymbol{p}^\alpha$ which is nonzero, while all other components $\boldsymbol{p}^\beta = 0$, then $\hat{p}$ belongs to

the one-replica sector (denoted by "1RS"). If two or more components of $\hat{p}$ are non-zero, then $\hat{p}$ belongs to the higher-replica sector (denoted by "HRS"). We also define the lower replica sector (denoted by "LRS") as the union of the zero-replica and one-replica sectors. The virtue of this decomposition is that in the context of elastomeric systems, it allows one to distinguish two types of phase transitions according to the sector it occurs in. If a phase transition occurs in the HRS, it is the random solidication transition, i.e., a transition from the liquid state to the random solid state. If a phase transition occurs in the 1RS, it is *not* the random solidication transition, but rather a transition from a liquid state to a state with periodic modulation in density, associated with the condensation of density fluctuations.

We now implement the Hubbard-Stratonovich transformation which is based on the following set of equalities for complex variables q and ω:

$$e^{-J|q|^2} = \frac{J}{\pi}\int d(\mathrm{Re}\omega)d(\mathrm{Im}\omega)e^{-J|\omega|^2+2iJ\mathrm{Re}q\omega^*}; \tag{B.12a}$$

$$e^{+J|q|^2} = \frac{J}{\pi}\int d(\mathrm{Re}\omega)d(\mathrm{Im}\omega)e^{-J|\omega|^2+2J\mathrm{Re}q\omega^*}. \tag{B.12b}$$

Here q may be thought of as a complex-variable analogue of a collective field and ω is the complex-variable analogue of its conjugate auxiliary field. We shall now establish the relation in Eq. (3.15) by considering a one-dimensional system having the following partition function:

$$\begin{aligned} Z &= \langle e^{Jq^2+hq}\rangle_{H_0(q)} \times \int dq e^{-H_0(q)} \\ &= \int dq\, e^{-H_0(q)} e^{Jq^2+hq}. \end{aligned} \tag{B.13}$$

Here, the notation $\langle\ldots\rangle_{H_0(q)} \equiv \int dq\,(\ldots)e^{-H_0(q)}/\int dq\, e^{-H_0(q)}$ denotes thermal averaging with respect to the "microscopic" Hamiltonian $H_0(q)$ governing the microscopic variable q. This partition function can be re-written in the following form by introducing an auxiliary variable

ω introduced previously:

$$\begin{aligned} Z &= \sqrt{J/\pi}\int d\omega \exp\left(-J\omega^2 + \ln\langle e^{2J\omega q+hq}\rangle_{H_0(q)}\right) \times \int dq e^{-H_0(q)} \\ &\equiv \sqrt{J/\pi}\int d\omega \exp\left(-H(\omega)\right) \times \int dq e^{-H_0(q)}, \end{aligned} \tag{B.14}$$

where $H(\omega)$ is the "field-theoretic" Hamiltonian governing the auxiliary variable ω. Then one can see that

$$\begin{aligned} \langle\omega\rangle_{H(\omega)} &= \frac{\int d\omega\omega \exp\left(-J\omega^2 + hq + \ln\langle e^{2J\omega q+hq}\rangle_{H_0(q)}\right)}{\int d\omega \exp\left(-J\omega^2 + hq + \ln\langle e^{2J\omega q+hq}\rangle_{H_0(q)}\right)} \\ &= \frac{\int d\omega \int dq\omega \exp\left(-J\omega^2 + hq + 2J\omega q - H_0(q)\right)}{\int d\omega \int dq \exp\left(-J\omega^2 + hq + 2J\omega q - H_0(q)\right)} \\ &= \frac{\int d\omega \int dq\omega \exp\left(-J(\omega-q)^2 + Jq^2 + hq + 2J\omega q - H_0(q)\right)}{\int d\omega \int dq \exp\left(-J(\omega-q)^2 + Jq^2 + hq + 2J\omega q - H_0(q)\right)} \\ &= \frac{\int dqq \exp\left(Jq^2 + hq + 2J\omega q - H_0(q)\right)}{\int dq \exp\left(Jq^2 + hq + 2J\omega q - H_0(q)\right)} \\ &= \langle q\rangle_{H(q)}, \end{aligned} \tag{B.15}$$

where $H(q) \equiv H_0(q) - Jq^2 - hq$. Generalizing q and ω to collective field $\boldsymbol{q}$ (γ) and auxiliary field $\mathbf{Q}$ (Γ), we obtain Eq. (3.15).

The Hubbard-Stratonovich procedure allows us to write the replica partition function Z_{1+n} as a functional integral expression in terms of the auxiliary fields Γ [whose argument we restrict to the HRS via the constraint $\Gamma_{\boldsymbol{p}\epsilon^\alpha}$, in accordance with the replica-sector division laid out in Eq. (B.11)], Γ^α (which is formally Γ but with its argument taking values in the 1RS), and $\mathbf{Q}^\alpha$ [conjugate to (resp.) γ, γ^α, and $\boldsymbol{q}^\alpha$]. In terms of these auxiliary fields, the replica partition function Z_{1+n} is given by

$$Z_{1+n} = \int \mathcal{D}\Gamma \prod_{\alpha=0}^{n} \mathcal{D}\Gamma^\alpha \mathcal{D}\mathbf{Q}^\alpha \exp\{-N f_{1+n}[\Gamma, \Gamma^\alpha, \mathbf{Q}^\alpha]\}. \tag{B.16}$$

Here the Landau-Wilson free energy per dimer f_{1+n} (scaled in units of T) is given by

$$\begin{aligned} f_{1+n}(\Gamma,\Gamma^\alpha,\mathbf{Q}^\alpha) &= \frac{\tilde{\eta}^2}{2(2\pi b^2)^{D/2}V^n}\overline{\sum_{\hat{k}}}\Delta_{\hat{k}}|\Gamma_{\hat{k}}|^2+\frac{1}{2}\sum_{\alpha=0}^{n}{\sum_{\boldsymbol{p}}}'\frac{\tilde{\lambda}_{\boldsymbol{p}}}{T^\alpha}|\Gamma^\alpha_{\boldsymbol{p}}|^2+\frac{1}{2}\sum_{\alpha=0}^{n}\sum_{\boldsymbol{p}}\frac{J_{\boldsymbol{p}}}{T^\alpha}|Q^\alpha_{ab}(\boldsymbol{p})|^2 \\ &\quad -\ln\Bigg\langle \exp\Bigg(\frac{\tilde{\eta}^2}{2(2\pi b^2)^{D/2}V^n}\overline{\sum_{\hat{k}}}\Delta_{\hat{k}}\Gamma_{\hat{k}}\sum_{s=1,-1}e^{-i\hat{k}\cdot(\hat{c}+\frac{s\ell}{2}\hat{n})} \\ &\quad +\frac{i}{2}\sum_{\alpha=0}^{n}{\sum_{\boldsymbol{p}}}'\frac{\tilde{\lambda}_{\boldsymbol{p}}}{T^\alpha}\Gamma^\alpha_{\boldsymbol{p}}\sum_{s=1,-1}e^{-i\boldsymbol{p}\cdot(\boldsymbol{c}^\alpha+\frac{s\ell}{2}\boldsymbol{n}^\alpha)} \\ &\quad +\sum_{\alpha=0}^{n}\sum_{\boldsymbol{p}}\frac{J_{\boldsymbol{p}}}{T^\alpha}Q^\alpha_{ab}(\boldsymbol{p})e^{-i\boldsymbol{p}\cdot\boldsymbol{c}^\alpha}(n^\alpha_a n^\alpha_b-d^{-1}\delta_{ab})\Bigg)\Bigg\rangle_{1,1+n}. \end{aligned} \tag{B.17}$$

By expanding the Landau-Wilson free energy per dimer f_{1+n} for small values of the auxiliary fields, one obtains a Landau theory with Γ, Γ^α and $\mathbf{Q}^\alpha$, which are, respectively, the order-parameter fields for the random solidification transition, the crystallization transition, and the isotropic-nematic transition. As we assume that IGNEs are incompressible, there will be no fluctuations in the density of dimers (which can be enforced by making $\tilde{\lambda}$ extremely large), and thus there will be no corresponding instability in the 1RS. We shall therefore disregard the contribution from Γ^α. The free energy, Eq. (3.18), then becomes

$$\begin{aligned} f_{1+n}(\Gamma,\mathbf{Q}) &= \frac{\tilde{\eta}^2}{2(2\pi b^2)^{D/2}V^n}\overline{\sum_{\hat{k}}}\Delta_{\hat{k}}|\Gamma_{\hat{k}}|^2+\frac{1}{2}\sum_{\alpha=0}^{n}\sum_{\boldsymbol{p}}\frac{J_{\boldsymbol{p}}}{T^\alpha}|Q^\alpha_{ab}(\boldsymbol{p})|^2 \\ &\quad -\ln\langle\exp[G_1(\Gamma)+G_2(Q)]\rangle_{1,1+n}. \end{aligned} \tag{B.18}$$

We have introduced the abbreviations

$$G_1(\Gamma) \equiv \frac{\tilde{\eta}^2}{2(2\pi b^2)^{D/2}V^n}\sum_{\hat{k}\in HRS}\Delta_{\hat{k}}\Gamma_{\hat{k}}\sum_{s=1,-1}e^{-i\hat{k}\cdot(\hat{c}+\frac{s\ell}{2}\hat{n})}, \tag{B.19}$$

$$G_2(Q) \equiv \sum_{\alpha=0}^{n}\sum_{\boldsymbol{p}}\frac{J_{\boldsymbol{p}}}{T^\alpha}Q^\alpha_{ab}(\boldsymbol{p})e^{-i\boldsymbol{p}\cdot\boldsymbol{c}^\alpha}\left(n^\alpha_a n^\alpha_b-\frac{1}{3}\delta_{ab}\right), \tag{B.20}$$

and specialized to three spatial dimensions (i.e., $d=3$).

Appendix C

Terms in the Landau expansion

In this section we expand the log trace term in Eq. (B.18) for small Γ and $\mathbf{Q}^\alpha$. This gives us

$$\begin{aligned} f_{1+n}(\Gamma,\mathbf{Q}) &= \frac{\tilde{\eta}^2}{2(2\pi b^2)^{D/2}V^n}\overline{\sum_{\hat{k}}}\Delta_{\hat{k}}|\Gamma_{\hat{k}}|^2 - \frac{1}{2}\langle G_1(\Gamma)^2\rangle_{1,1+n} - \frac{1}{6}\langle G_1(\Gamma)^3\rangle_{1,1+n} \\ &\quad + \frac{1}{2}\sum_{\alpha=0}^{n}\sum_{\boldsymbol{p}}\frac{J_{\boldsymbol{p}}}{T^\alpha}|Q^\alpha_{ab}(\boldsymbol{p})|^2 - \frac{1}{2}\langle G_2(Q)^2\rangle_{1,1+n} \\ &\quad - \frac{1}{6}\langle G_2(Q)^3\rangle_{1,1+n} - \frac{1}{24}\langle G_2(Q)^4\rangle_{1,1+n} \\ &\quad - \frac{1}{2}\langle G_1(\Gamma)^2 G_2(Q)\rangle_{1,1+n} - \frac{1}{2}\langle G_1(\Gamma) G_2(Q)^2\rangle_{1,1+n} \\ &\quad - \frac{1}{4}\big(\langle G_1(\Gamma)^2 G_2(Q)^2\rangle_{1,1+n} - \langle G_1(\Gamma)^2\rangle_{1,1+n}\langle G_2(Q)^2\rangle_{1,1+n}\big) \end{aligned} \tag{C.1}$$

C.1 Terms proportional to $\Gamma\Gamma$

First, we compute the quadratic term for the vulcanization part of the Landau theory:

$$\begin{aligned} \langle G_1(\Gamma)^2\rangle_{1,1+n} &= \frac{\tilde{\eta}^4}{4(2\pi b^2)^D}\overline{\sum}_{\hat{k}_1,\hat{k_2}}\Delta_{\hat{k}_1}\Delta_{\hat{k}_2}\Gamma_{\hat{k}_1}\Gamma_{\hat{k}_2}\sum_{s,t}\Big\langle e^{-i\left(\hat{k}_1\cdot(\hat{c}+\frac{s\ell}{2}\hat{n})+\hat{k}_2\cdot(\hat{c}+\frac{t\ell}{2}\hat{n})\right)}\Big\rangle_{1,1+n} \\ &= \frac{\tilde{\eta}^4}{2(2\pi b^2)^D}\overline{\sum_{\hat{k}}}\Delta^2_{\hat{k}}\Gamma_{\hat{k}}\Gamma_{-\hat{k}}\left\{1+\prod_{\alpha=0}^{n}\frac{\sin(k^\alpha\ell)}{k^\alpha\ell}\right\} \end{aligned} \tag{C.2}$$

C.2 Terms proportional to $\Gamma\Gamma\Gamma$

We compute the cubic term for the vulcanization part of the Landau theory:

$$\begin{aligned}\langle G_1(\Gamma)^3\rangle_{1,1+n} &= \frac{\tilde{\eta}^6}{8(2\pi b^2)^{3D/2}}\overline{\sum}_{\hat{k}_1,\hat{k}_2,\hat{k}_3}\Delta_{\hat{k}_1}\Delta_{\hat{k}_2}\Delta_{\hat{k}_3}\Gamma_{\hat{k}_1}\Gamma_{\hat{k}_2}\Gamma_{\hat{k}_3}\\ &\quad\times\sum_{s_1,s_2,s_3}\Big\langle e^{-i\left(\hat{k}_1\cdot(\hat{c}+\frac{s_1\ell}{2}\hat{n})+\hat{k}_2\cdot(\hat{c}+\frac{s_2\ell}{2}\hat{n})+\hat{k}_3\cdot(\hat{c}+\frac{s_3\ell}{2}\hat{n})\right)}\Big\rangle_{1,1+n}\\ &= \frac{\tilde{\eta}^6}{4(2\pi b^2)^{3D/2}}\overline{\sum}_{\hat{k}_1,\hat{k}_2}\Delta_{\hat{k}_1}\Delta_{\hat{k}_2}\Delta_{-\hat{k}_1-\hat{k}_2}\Gamma_{\hat{k}_1}\Gamma_{\hat{k}_2}\Gamma_{-\hat{k}_1-\hat{k}_2}\\ &\quad\times\left(1+\prod_{\alpha=0}^{n}\frac{\sin(k_1^\alpha l)}{k_1^\alpha l}+\prod_{\alpha=0}^{n}\frac{\sin(k_2^\alpha \ell)}{k_2^\alpha \ell}+\prod_{\alpha=0}^{n}\frac{\sin(|\boldsymbol{k}_1^\alpha+\boldsymbol{k}_2^\alpha|\ell)}{|\boldsymbol{k}_1^\alpha+\boldsymbol{k}_2^\alpha|\ell}\right)\end{aligned} \tag{C.3}$$

C.3 Terms proportional to $\mathbf{Q}^\alpha\mathbf{Q}^\alpha$

Next, we compute the quadratic terms from the nematic part of the Landau theory:

$$\begin{aligned}\langle G_2(Q)^2\rangle_{1,1+n} &= \sum_{\alpha,\beta}\sum_{\boldsymbol{p},\boldsymbol{q}}\sum_{s,t=1,-1}\frac{J_{\boldsymbol{p}}J_{\boldsymbol{q}}}{(T^\alpha)^2}Q_{ab}^\alpha(\boldsymbol{p})Q_{cd}^\beta(\boldsymbol{q})\\ &\quad\times\Big\langle e^{-i(\boldsymbol{p}\cdot\boldsymbol{c}^\alpha+\boldsymbol{q}\cdot\boldsymbol{c}^\beta)}\big(n_a^\alpha n_b^\alpha-\frac{1}{3}\delta_{ab}\big)\big(n_c^\beta n_d^\beta-\frac{1}{3}\delta_{cd}\big)\Big\rangle_{1,1+n}.\end{aligned} \tag{C.4}$$

Note that this term vanishes for $\alpha\neq\beta$. For $\alpha=\beta$, one computes that

$$\begin{aligned}\langle G_2(Q)^2\rangle_{1,1+n} &= \frac{1}{4\pi}\sum_{\alpha}\sum_{\boldsymbol{p}}\frac{|J_{\boldsymbol{p}}|^2}{(T^\alpha)^2}Q_{ab}^\alpha(\boldsymbol{p})Q_{cd}^\alpha(-\boldsymbol{p})\\ &\quad\times\int d\boldsymbol{n}^\alpha\big(n_a^\alpha n_b^\alpha n_c^\alpha n_d^\alpha-\frac{1}{3}n_a^\alpha n_b^\alpha\delta_{cd}-\frac{1}{3}n_c^\alpha n_d^\alpha\delta_{ab}+\frac{1}{9}\delta_{ab}\delta_{cd}\big)\\ &= \frac{1}{15}\sum_{\alpha}\sum_{\boldsymbol{p}}\frac{|J^\alpha(\boldsymbol{p})|^2}{(T^\alpha)^2}Q_{ab}^\alpha(\boldsymbol{p})Q_{cd}^\alpha(-\boldsymbol{p})\big(\delta_{ac}\delta_{bd}+\delta_{ad}\delta_{bc}-\frac{2}{3}\delta_{ab}\delta_{cd}\big),\end{aligned} \tag{C.5}$$

where we have used the equalities $\int d\boldsymbol{n} n_a n_b = \frac{1}{3}\delta_{ab}$ and $\int d\boldsymbol{n} n_a n_b n_c n_d = \frac{1}{15}(\delta_{ab}\delta_{cd} + \delta_{ac}\delta_{bd} + \delta_{ad}\delta_{bc})$.

C.4 Terms proportional to $\Gamma\mathbf{Q}^\alpha\mathbf{Q}^\beta$ and $\Gamma\Gamma\mathbf{Q}^\alpha$

The terms that couple the nematic order parameter to the vulcanization order parameter give rise to the physics of nematic elastomers. At cubic order in Γ and $\mathbf{Q}$ (i.e., $\Gamma\mathbf{Q}^\alpha\mathbf{Q}^\beta$ or $\Gamma\Gamma\mathbf{Q}^\alpha$), there are two such terms. They have been computed in [31], and are given by the following equations:

$$\begin{aligned}\langle G_1(\Gamma)G_2(Q)^2\rangle_{1,1+n} &= \frac{\tilde{\eta}^2}{800(2\pi b^2)^{D/2}}\sum_{\alpha\neq\beta}^{n}\sum_{\boldsymbol{p},\boldsymbol{q}}\Delta_{-\boldsymbol{p}\hat{\boldsymbol{e}}^\alpha-\boldsymbol{q}\hat{\boldsymbol{e}}^\beta}\frac{J_{\boldsymbol{p}}\,J_{\boldsymbol{q}}}{T^\alpha\,T^\beta}\Gamma_{-\boldsymbol{p}\hat{\boldsymbol{e}}^\alpha-\boldsymbol{q}\hat{\boldsymbol{e}}^\beta} \\ &\quad\times Q^\alpha_{ab}(\boldsymbol{p})Q^\beta_{cd}(\boldsymbol{q})p_a p_b q_c q_d, \end{aligned} \tag{C.6a}$$

$$\begin{aligned}\langle G_1(\Gamma)^2G_2(Q)\rangle_{1,1+n} &= \frac{\tilde{\eta}^4\ell^2}{5(2\pi b^2)^{D}}\sum_{\alpha=0}^{n}\sum_{\boldsymbol{p}}\sum_{\hat{k}\in HRS}\Delta_{\hat{k}}\Delta_{-\hat{k}-\boldsymbol{p}\hat{\boldsymbol{e}}^\alpha}\frac{J_{\boldsymbol{p}}}{T^\alpha}\Gamma_{\hat{k}}\Gamma_{-\hat{k}-\boldsymbol{p}\hat{\boldsymbol{e}}^\alpha}Q^\alpha_{ab}(\boldsymbol{p}) \\ &\quad\times\big(p_a p_b + (k^\alpha + p/2)_a(k^\alpha + p/2)_b\big). \end{aligned} \tag{C.6b}$$

C.5 Terms proportional to $\Gamma\Gamma\mathbf{Q}^\alpha\mathbf{Q}^\beta$

For reasons to be discussed in Appendix F, the foregoing coupling terms do not give the leading-order contribution to the novel liquid crystalline behavior that our theory predicts for IGNEs. This is why we further consider the higher-order terms that are proportional to $\Gamma\Gamma\mathbf{Q}^\alpha\mathbf{Q}^\beta$. We note that such terms are of two types: connected and disconnected. We first consider the disconnected type, which is proportional to the product $\langle G_1(\Gamma)^2\rangle\langle G_2(Q)^2\rangle$. By using the expressions obtained for $\langle G_1(\Gamma)^2\rangle_{1,1+n}$ in Eq. (C.2) and $\langle G_2(Q)^2\rangle_{1,1+n}$ in Eq. (C.5),

we obtain

$$\langle G_1(\Gamma)^2\rangle_{1,1+n}\langle G_2(Q)^2\rangle_{1,1+n} = \frac{8\tilde{\eta}^4}{15(2\pi b^2)^D}\sum_{\alpha=0}^{n}\overline{\sum_{\hat{k}}}\sum_{\boldsymbol{p}}\Delta_{\hat{k}}^2\left(\frac{J_{\boldsymbol{p}}}{T^\alpha}\right)^2\Gamma_{\hat{k}}\Gamma_{-\hat{k}}Q^\alpha_{ab}(\boldsymbol{p})Q^\alpha_{ab}(-\boldsymbol{p}). \tag{C.7}$$

Next, we consider $\langle G_1(\Gamma)^2 G_2(Q)^2\rangle_{1,1+n}$:

$$\begin{aligned}
\langle G_1(\Gamma)^2 G_2(Q)^2\rangle_{1,1+n} &= \frac{\tilde{\eta}^4}{(2\pi b^2)^D}\sum_{\alpha,\beta=0}^{n}\overline{\sum_{\hat{k}_1,\hat{k}_2}}\sum_{\boldsymbol{p},\boldsymbol{q}}\sum_{s,t=1,-1}\Delta_{\hat{k}_1}\Delta_{\hat{k}_2}\Gamma_{\hat{k}_1}\Gamma_{\hat{k}_2}\frac{J_{\boldsymbol{p}}J_{\boldsymbol{q}}}{T^\alpha T^\beta}Q^\alpha_{ab}(\boldsymbol{p})Q^\beta_{cd}(\boldsymbol{q}) \\
&\quad\times\Big\langle e^{-i\sum_{\gamma=0}^{n}\left(\boldsymbol{k}_1^\gamma\cdot(\boldsymbol{c}^\gamma+\frac{s\ell}{2}\boldsymbol{n}^\gamma)+\boldsymbol{k}_2^\gamma\cdot(\boldsymbol{c}^\gamma+\frac{t\ell}{2}\boldsymbol{n}^\gamma)\right)-i\boldsymbol{p}\cdot\boldsymbol{c}^\alpha-i\boldsymbol{q}\cdot\boldsymbol{c}^\beta} \\
&\quad\times\big(n_a^\alpha n_b^\alpha-\frac{1}{3}\delta_{ab}\big)\big(n_c^\beta n_d^\beta-\frac{1}{3}\delta_{cd}\big)\Big\rangle_{1,1+n} \\
&\approx \frac{8\tilde{\eta}^4}{15(2\pi b^2)^D}\sum_{\alpha=0}^{n}\sum_{\boldsymbol{p},\boldsymbol{q}}\sum_{\hat{k}\in HRS}\frac{J_{\boldsymbol{p}}\,J_{\boldsymbol{q}}}{(T^\alpha)^2} \\
&\quad\times\Delta_{\hat{k}}\Delta_{-\hat{k}-(\boldsymbol{p}+\boldsymbol{q})\hat{\epsilon}^\alpha}\Gamma_{\hat{k}}\Gamma_{-\hat{k}-(\boldsymbol{p}+\boldsymbol{q})\hat{\epsilon}^\alpha}Q^\alpha_{ab}(\boldsymbol{p})Q^\alpha_{cd}(\boldsymbol{q}) \\
&\quad\times\Big(\delta_{ac}\delta_{bd}-\frac{\ell^2}{7}(p+q)_a(p+q)_c\delta_{bd} \\
&\quad-\frac{4\ell^2}{7}\big(k^\alpha+(p+q)/2\big)_a\big(k^\alpha+(p+q)/2\big)_c\delta_{bd}\Big) \\
&\quad+\frac{2\tilde{\eta}^4\ell^4}{225(2\pi b^2)^D}\sum_{\substack{\alpha,\beta=0\\(\alpha\neq\beta)}}^{n}\sum_{\boldsymbol{p},\boldsymbol{q}}\sum_{\hat{k}\in HRS}\frac{J_{\boldsymbol{p}}\,J_{\boldsymbol{q}}}{T^\alpha T^\beta} \\
&\quad\times\Delta_{\hat{k}}\Delta_{-\hat{k}-\boldsymbol{p}\hat{\epsilon}^\alpha-\boldsymbol{q}\hat{\epsilon}^\beta}\Gamma_{\hat{k}}\Gamma_{-\hat{k}-\boldsymbol{p}\hat{\epsilon}^\alpha-\boldsymbol{q}\hat{\epsilon}^\beta}Q^\alpha_{ab}(\boldsymbol{p})Q^\beta_{cd}(\boldsymbol{q}) \\
&\quad\times\Big(k_a^\alpha k_b^\alpha k_c^\beta k_d^\beta+\frac{1}{4}(p_a k_b^\alpha+k_a^\alpha p_b)(q_c k_d^\beta+k_c^\beta q_d)+\frac{1}{8}p_a p_b q_c q_d\Big),
\end{aligned} \tag{C.8}$$

in which the $\mathbf{Q}^\alpha$ matrices are now constrained to be symmetric and traceless. This term receives a contribution from two distinct replica channels.

Appendix D

Basis matrices for symmetric traceless matrices

A complete set of orthonormal traceless, symmetric tensors $\mathbf{I}_j$ that satisfy the constraint $\mathrm{Tr}\,\mathbf{I}_i\mathbf{I}_j = \delta_{ij}$ can be introduced, viz.

$$\mathbf{I}_0 = \sqrt{\frac{2}{3}}\begin{pmatrix} -\frac{1}{2} & 0 & 0 \\ 0 & -\frac{1}{2} & 0 \\ 0 & 0 & 1 \end{pmatrix}, \qquad \mathbf{I}_1 = \frac{1}{\sqrt{2}}\begin{pmatrix} 1 & 0 & 0 \\ 0 & -1 & 0 \\ 0 & 0 & 0 \end{pmatrix},$$

$$\mathbf{I}_2 = \frac{1}{\sqrt{2}}\begin{pmatrix} 0 & 1 & 0 \\ 1 & 0 & 0 \\ 0 & 0 & 0 \end{pmatrix}, \qquad \mathbf{I}_3 = \frac{1}{\sqrt{2}}\begin{pmatrix} 0 & 0 & 1 \\ 0 & 0 & 0 \\ 1 & 0 & 0 \end{pmatrix},$$

$$\mathbf{I}_4 = \frac{1}{\sqrt{2}}\begin{pmatrix} 0 & 0 & 0 \\ 0 & 0 & 1 \\ 0 & 1 & 0 \end{pmatrix}. \tag{D.1}$$

The z-direction can be defined as the direction of the momentum transfer, $\boldsymbol{p}/|\boldsymbol{p}|$.

Appendix E

Saddle-point equation for Q

Here, we shall show that the values $\Gamma = \bar{\Gamma}$ and $\mathbf{Q} = \mathbf{0}$ solve the saddle-point equation (4.1b), owing to the rotational symmetry of $\Gamma = \bar{\Gamma}$. Without loss of generality, we need to prove that the following two equations hold:

$$\begin{aligned}
&\overline{\sum_{\hat{k}}} \bar{\Gamma}_{\hat{k}} \bar{\Gamma}_{-\hat{k}-\boldsymbol{p}\epsilon^{\alpha}} \big(|k_x^{\alpha}|^2 - |k_y^{\alpha}|^2\big) = 0; \\
&\overline{\sum_{\hat{k}}} \bar{\Gamma}_{\hat{k}} \bar{\Gamma}_{-\hat{k}-\boldsymbol{p}\epsilon^{\alpha}} k_x^{\alpha}\, k_y^{\alpha} = 0.
\end{aligned} \tag{E.1}$$

Here, the subscripts x and y refer to the Cartesian components of the vector $\boldsymbol{k}^{\alpha}$. The dependence on $\boldsymbol{p}$ vanishes as $\bar{\Gamma}_{\hat{k}} \bar{\Gamma}_{-\hat{k}-\boldsymbol{p}\epsilon^{\alpha}}$ is proportional to $\delta_{\sum_{\gamma} \boldsymbol{k}^{\gamma}, \boldsymbol{0}} \delta_{-\sum_{\gamma} \boldsymbol{k}^{\gamma} - \boldsymbol{p}, \boldsymbol{0}}$, forcing $\boldsymbol{p} = 0$. The left hand side of the first line of Eq. (E.1) then gives

$$\begin{aligned}
&\overline{\sum_{\hat{k}}} \bar{\Gamma}_{\hat{k}} \bar{\Gamma}_{-\hat{k}} \big(|k_x^{\alpha}|^2 - |k_y^{\alpha}|^2\big) \\
= \;& G^2 \overline{\sum_{\hat{k}}} \int \frac{d\boldsymbol{z}_1\, d\boldsymbol{z}_2}{V^2} e^{i \sum_{\gamma} \boldsymbol{k}^{\gamma} \cdot (\boldsymbol{z}_1 - \boldsymbol{z}_2) - \xi_L^2 |\hat{k}|^2} \big(|k_x^{\alpha}|^2 - |k_y^{\alpha}|^2\big) \\
= \;& G^2 \overline{\sum_{\hat{k}}} \int \frac{d\boldsymbol{c}\, d\boldsymbol{r}}{V^2} e^{-\xi_L^2 \sum_{\gamma} \left(\boldsymbol{k}^{\gamma} - i \frac{\boldsymbol{r}}{2\xi_L^2}\right)^2 - (n+1) \frac{r^2}{4\xi_L^2}} \big(|k_x^{\alpha}|^2 - |k_y^{\alpha}|^2\big) \\
= \;& G^2 \overline{\sum_{\hat{k}}} \int \frac{d\boldsymbol{c}\, d\boldsymbol{r}}{V^2} e^{-(n+1) \frac{r^2}{4\xi_L^2} - \xi_L^2 \sum_{\gamma} |\boldsymbol{k}^{\gamma}|^2} \\
& \times \big(|k_x^{\alpha}|^2 + \frac{i \boldsymbol{r}_x \cdot \boldsymbol{k}_x^{\alpha}}{\xi_L^2} - \frac{r_x^2}{4\xi_L^2} - |k_y^{\alpha}|^2 - \frac{i \boldsymbol{r}_y \cdot \boldsymbol{k}_y^{\alpha}}{\xi_L^2} + \frac{r_y^2}{4\xi_L^2}\big) = 0.
\end{aligned} \tag{E.2}$$

In the last line, the pair consisting of the first and fourth terms and the pair consisting of the third and sixth terms cancel by rotational symmetry, while the second and fifth terms vanish under odd parity upon integration over $\boldsymbol{r}$. A similar and straightforward computation can be done to prove the second line of Eq. (E.1), whose vanishing arises owing to rotational symmetry.

Appendix F

Evaluating the coupling terms at the saddle-point value $\bar{\Gamma}$

F.1 Terms proportional to $\bar{\Gamma}\bar{\Gamma}\mathbf{Q}^\alpha$

The terms $\int d\hat{r}\,\Gamma(\hat{r})\Gamma(\hat{r})\nabla^\alpha_{d_1}\nabla^\alpha_{d_2}Q^\alpha_{d_1d_2}(\boldsymbol{r}^\alpha)$ and $\int d\hat{r}\,\nabla^\alpha_{d_1}\Gamma(\hat{r})\nabla^\alpha_{d_2}\Gamma(\hat{r})Q^\alpha_{d_1d_2}(\boldsymbol{r}^\alpha)$ for an elastomer with uniaxial symmetry give rise to the Neoclassical Theory of nematic elastomers [5, 31]. However, for an IGNE, the terms give no contribution when Γ is set to its saddle-point value $\bar{\Gamma}$. $\int d\hat{r}\,\nabla^\alpha_{d_1}\Gamma(\hat{r})\nabla^\alpha_{d_2}\Gamma(\hat{r})Q^\alpha_{d_1d_2}(\boldsymbol{r}^\alpha)$ vanishes because the random solid state is macroscopically isotropic, and thus $\nabla^\alpha_{d_1}\Gamma(\hat{r})\nabla^\alpha_{d_2}\Gamma(\hat{r})$ can only be proportional to $\delta_{d_1d_2}$ in the absence of external strain. Contracting this with $\mathbf{Q}^\alpha$ will cause the term to vanish, as $\mathbf{Q}^\alpha$ is traceless. On the other hand, by explicitly computing the value of $\int d\hat{r}\,\Gamma(\hat{r})\Gamma(\hat{r})\nabla^\alpha_{d_1}\nabla^\alpha_{d_2}Q^\alpha_{d_1d_2}(\boldsymbol{r}^\alpha)$ using the value of $\bar{\Gamma}(\hat{r})$ given by (4.5), one sees that the result is proportional to

$$\int d\boldsymbol{r}^\alpha\,\nabla^\alpha_{d_1}\nabla^\alpha_{d_2}Q^\alpha_{d_1d_2}(\boldsymbol{r}^\alpha), \tag{F.1}$$

which vanishes as the boundary is at infinity.

F.2 Terms proportional to $\bar{\Gamma}\mathbf{Q}^\alpha\mathbf{Q}^\beta$

To lowest order, the term is given by $\sum_{\alpha\neq\beta}\sum_{\boldsymbol{p},\boldsymbol{q}}p_{d_1}p_{d_2}q_{d_3}q_{d_4}\bar{\Gamma}_{-\boldsymbol{p}\epsilon^\alpha-\boldsymbol{q}\epsilon^\beta}Q^\alpha_{d_1d_2}(\boldsymbol{p})Q^\beta_{d_3d_4}(\boldsymbol{q})$. However, at long length-scales, this term is small compared to the terms proportional to $\bar{\Gamma}\bar{\Gamma}\mathbf{Q}^\alpha\mathbf{Q}^\beta$. This is because the momentum factors $\boldsymbol{k}^\alpha$ in the term $\bar{\Gamma}\bar{\Gamma}\mathbf{Q}^\alpha\mathbf{Q}^\beta$ can be of the order of the inverse localization length ξ_L^{-1}, whereas the term $\bar{\Gamma}\mathbf{Q}^\alpha\mathbf{Q}^\beta$ receives contributions

from those modes $\boldsymbol{p}$ and $\boldsymbol{q}$ that have magnitudes smaller than ξ_L^{-1}—as the momentum modes with magnitudes larger than ξ_L^{-1} are exponentially suppressed by Γ (this exponential suppression reflecting the liquid-like character of the network at short length-scales). Thus, we can neglect the contribution from the term proportional to $\bar{\Gamma}\mathbf{Q}^\alpha\mathbf{Q}^\beta$.

F.3 Terms proportional to $\bar{\Gamma}\bar{\Gamma}\mathbf{Q}^\alpha\mathbf{Q}^\beta$

We shall prove, at the saddle point value of Γ, that the disconnected part of the coupling term $\langle G_1(\Gamma)^2\rangle_{1,1+n}\langle G_2(Q)^2\rangle_{1,1+n}$ vanishes. It is sufficient for our purpose to consider the value of $\overline{\sum_{\hat{k}}}\,\bar{\Gamma}_{\hat{k}}\,\bar{\Gamma}_{-\hat{k}}$. Using the identity $\overline{\sum_{\hat{k}}}\delta_{\hat{k},\hat{0}}\delta_{-\hat{k},\hat{0}} = \delta_{\hat{0},\hat{0}} = 1$ and Eq. (4.4), one obtains

$$\begin{aligned}
\overline{\sum_{\hat{k}}}\bar{\Gamma}_{\hat{k}}\bar{\Gamma}_{-\hat{k}} &= \left(1 - 2\int\frac{d\boldsymbol{z}}{V} + \overline{\sum_{\hat{k}}}\int\frac{d\boldsymbol{z}_1 d\boldsymbol{z}_2}{V^2}e^{-\xi_L^2|\hat{k}|^2 - i\sum_{\gamma=0}^{n}\boldsymbol{k}^\gamma\cdot(\boldsymbol{z}_1-\boldsymbol{z}_2)}\right)G^2 \\
&= \left(-1 + \overline{\sum_{\hat{k}}}\int\frac{d\boldsymbol{c}\,d\boldsymbol{r}}{V^2}e^{-\sum_{\gamma=0}^{n}\left(\xi_L^2|\boldsymbol{k}^\gamma + \frac{i\boldsymbol{r}}{2\xi_L^2}|^2\right) - \frac{(1+n)r^2}{4\xi_L^2}}\right)G^2 \\
&= \left(-1 + \frac{V^{1+n}\cdot V}{V^2}\frac{1}{(2\pi)^{(1+n)d}}\left(\frac{4\pi\xi_L^2}{1+n}\right)^{d/2}\left(\frac{\pi}{\xi_L^2}\right)^{(1+n)d/2}\right)G^2 \\
&= n\ln\left(\frac{V}{(2\pi)^d\xi_L^d}\right)G^2 + O(n^2).
\end{aligned} \tag{F.2}$$

In the replica limit ($n \to 0$), the above result is zero. Here, we have used the definition $\overline{\sum}_{\hat{k}} \equiv \frac{V^{1+n}}{(2\pi)^{(1+n)d}}\int d\hat{k}$ when performing the integral over $\hat{k}$. In the last step, we have integrated over $\hat{k}$, $\boldsymbol{r}$, and $\boldsymbol{c}$.

We shall now consider the connected part of the term proportional to $\bar{\Gamma}\bar{\Gamma}\mathbf{Q}^\alpha\mathbf{Q}^\beta$, i.e., $\langle G_1(\Gamma)^2 G_2(Q)^2\rangle$. This term, which is important for our purpose of studying the polydomain state of IGNEs, is given by $\nabla_{d_1}^\alpha\nabla_{d_2}^\alpha\bar{\Gamma}(\hat{r})\nabla_{d_3}^\beta\nabla_{d_4}^\beta\bar{\Gamma}(\hat{r})Q_{d_1d_2}^\alpha(\boldsymbol{r}^\alpha)Q_{d_3d_4}^\beta(\boldsymbol{r}^\beta)$ in real space. Despite being of higher order in Γ, the term has long wavelength properties that are sufficiently hard. The physical significance of this coupling term is that it encodes into the theory the fact that the nematic degrees of freedom inhabit an environment that is at the microscopic

level anisotropic, inhomogeneous and thermally fluctuating, but that no remnants of this anisotropy, inhomogeneity, or fluctuations survive to the macroscopic level.

At the saddle-point level, the coupling term, $\langle G_1(\Gamma)^2 G_2(Q)^2\rangle$, is invariant under the common translation of all replicas. In real space, this means that

$$\nabla^\alpha_{d_1}\nabla^\alpha_{d_2}\bar{\Gamma}(\hat{r})\nabla^\beta_{d_3}\nabla^\beta_{d_4}\bar{\Gamma}(\hat{r})Q^\alpha_{d_1d_2}(\boldsymbol{r}^\alpha)Q^\beta_{d_3d_4}(\boldsymbol{r}^\beta) \tag{F.3}$$

can be expressed in the form $U_{d_1d_2d_3d_4}(\boldsymbol{r}^\alpha-\boldsymbol{r}^\beta)Q^\alpha_{d_1d_2}(\boldsymbol{r}^\alpha)\,Q^\alpha_{d_3d_4}(\boldsymbol{r}^\beta)$, where the kernel $U_{d_1d_2d_3d_4}(\boldsymbol{r}^\alpha-\boldsymbol{r}^\beta)$ depends only on the separation $\boldsymbol{r}^\alpha-\boldsymbol{r}^\beta$. Now, if the term is replica-diagonal, U would be a constant, which means that the term can only give at most a local contribution. However, it turns out that with the form of the saddle point value of Γ, the kernel vanishes. This can be seen by considering the replica-diagonal part of Eq. (C.8). Noting that $\bar{\Gamma}_{\hat{k}}\bar{\Gamma}_{-\hat{k}-(\boldsymbol{p}+\boldsymbol{q})\epsilon^\alpha}\propto\delta_{\sum_\gamma \boldsymbol{k}^\gamma,\boldsymbol{0}}\delta_{-\sum_\gamma \boldsymbol{k}^\gamma-\boldsymbol{p}-\boldsymbol{q},\boldsymbol{0}}$, this implies that $\boldsymbol{p}+\boldsymbol{q}=\boldsymbol{0}$. Thus the replica-diagonal contribution to $\langle G_1(\Gamma)^2G_2(Q)^2\rangle$ (with Γ set to $\bar{\Gamma}$) becomes proportional to the quantity,

$$\sum_\alpha\sum_{\boldsymbol{p}}\overline{\sum_{\hat{k}}}\bar{\Gamma}_{\hat{k}}\bar{\Gamma}_{-\hat{k}}Q^\alpha_{d_1d_2}(\boldsymbol{p})Q^\alpha_{d_3d_4}(-\boldsymbol{p})\left(\delta_{d_1d_3}\delta_{d_2d_4}-\frac{4\ell^2}{7}k^\alpha_{d_1}k^\alpha_{d_3}\delta_{d_2d_4}\right). \tag{F.4}$$

The first term vanishes, as we showed in Eq. (F.2). On the other hand, the second term also vanishes, as we can see by doing a direct computation,

$$\begin{aligned}
&\overline{\sum_{\hat{k}}}k^\alpha_{d_1}k^\alpha_{d_3}\bar{\Gamma}_{\hat{k}}\bar{\Gamma}_{-\hat{k}}\\
&\propto\int\frac{d\boldsymbol{z}_1\,d\boldsymbol{z}_2}{V^2}k^\alpha_{d_1}\,k^\alpha_{d_3}\,e^{-\xi_L^2|\hat{k}|^2-i\sum_{\gamma=0}^n\boldsymbol{k}^\gamma\cdot(\boldsymbol{z}_1-\boldsymbol{z}_2)}\\
&=\int\frac{d\boldsymbol{c}\,d\boldsymbol{r}}{V^2}k^\alpha_{d_1}\,k^\alpha_{d_3}\,e^{-\xi_L^2\sum_\gamma|\boldsymbol{k}^\gamma+i\frac{\boldsymbol{r}}{2\xi_L^2}|^2-\frac{(n+1)r^2}{4\xi_L^2}}\\
&\propto\delta_{d_1d_3}\frac{1}{2\xi_L^2}\left(\frac{\pi}{\xi_L^2}\right)^{(n+1)d/2}\left(\frac{4\pi\xi_L^2}{n+1}\right)^{d/2}\left(1-\frac{1}{n+1}\right)\\
&=0,
\end{aligned} \tag{F.5}$$

on taking the replica limit. On going to the second step, we have changed to center-of-mass coordinate $\boldsymbol{c}$ and relative coordinate $\boldsymbol{r}$, and on going to the third step we have shifted the momentum $\boldsymbol{k}^\gamma \to \boldsymbol{k}^\gamma - i\boldsymbol{r}/(2\xi_L^2)$ and integrated over $\boldsymbol{k}^\gamma$ ($\gamma = 0, 1, \ldots, n$) and $\boldsymbol{r}$.

Next, we compute the replica off-diagonal contribution to $\langle G_1(\Gamma)^2 G_2(Q)^2 \rangle$ with Γ set to $\bar{\Gamma}$. As we are considering lengthscales larger than the typical localization length ξ_L, the terms with coefficients in $\boldsymbol{p}$ and/or $\boldsymbol{q}$ are smaller than those with coefficients in $\boldsymbol{k}^\alpha$, and we can neglect the former. It is thus sufficient to consider the following contribution:

$$
\begin{aligned}
&\sum_{\alpha\neq\beta}^{n} \sum_{\boldsymbol{p},\boldsymbol{q}} \sum_{\hat{k}\in HRS} \bar{\Gamma}_{\hat{k}} \bar{\Gamma}_{-\hat{k}-\boldsymbol{p}\hat{\epsilon}^\alpha-\boldsymbol{q}\hat{\epsilon}^\beta} Q^\alpha_{d_1 d_2}(\boldsymbol{p}) Q^\beta_{d_3 d_4}(\boldsymbol{q})\, k^\alpha_{d_1} k^\alpha_{d_2} k^\beta_{d_3} k^\beta_{d_4} \\
= \;& G^2 V^{n+3} \int \prod_{\gamma=0}^{n} \frac{d^3k^\gamma}{(2\pi)^3} \frac{d^3p}{(2\pi)^3} \frac{d^3q}{(2\pi)^3} \int \frac{d\boldsymbol{z}_1}{V} \frac{d\boldsymbol{z}_2}{V} \sum_{\substack{\alpha,\beta=0 \\ (\alpha\neq\beta)}}^{n} Q^\alpha_{d_1 d_2}(\boldsymbol{p}) Q^\beta_{d_3 d_4}(\boldsymbol{q})\, k^\alpha_{d_1} k^\alpha_{d_2} k^\beta_{d_3} k^\beta_{d_4} \\
&\times \exp\Big(- \sum_{\gamma\neq\alpha,\beta} \xi_L^2 \left| \boldsymbol{k}^\gamma + i\frac{\boldsymbol{z}_1-\boldsymbol{z}_2}{2\xi_L^2} \right|^2 - \frac{(n-1)|\boldsymbol{z}_1-\boldsymbol{z}_2|^2}{4\xi_L^2} - \frac{1}{2}\xi_L^2(p^2+q^2) - i(\boldsymbol{p}+\boldsymbol{q})\cdot\boldsymbol{z}_1 \\
&\quad -\xi_L^2 \left| \boldsymbol{k}^\alpha + i\frac{\boldsymbol{z}_1-\boldsymbol{z}_2}{2\xi_L^2} + \frac{1}{2}\boldsymbol{p} \right|^2 + \xi_L^2 \left| i\frac{\boldsymbol{z}_1-\boldsymbol{z}_2}{2\xi_L^2} + \frac{1}{2}\boldsymbol{p} \right|^2 - \xi_L^2 \left| \boldsymbol{k}^\beta + i\frac{\boldsymbol{z}_1-\boldsymbol{z}_2}{2\xi_L^2} + \frac{1}{2}\boldsymbol{q} \right|^2 \\
&\quad +\xi_L^2 \left| i\frac{\boldsymbol{z}_1-\boldsymbol{z}_2}{2\xi_L^2} + \frac{1}{2}\boldsymbol{q} \right|^2 \Big).
\end{aligned}
\tag{F.6}
$$

We replace the coordinates $\boldsymbol{z}_1$ and $\boldsymbol{z}_2$ by the "relative coordinate" R and "centre-of-mass coordinate" C, defined respectively by $\mathrm{R} = \boldsymbol{z}_1 - \boldsymbol{z}_2$ and $\mathrm{C} = (\boldsymbol{z}_1 + \boldsymbol{z}_2)/2$, and integrate over C, which results in a factor of $(2\pi)^d V \delta(\boldsymbol{p}+\boldsymbol{q}, \boldsymbol{0})$. Next, we integrate over $\boldsymbol{q}$ to enforce the equality $\boldsymbol{q} = -\boldsymbol{p}$. We then integrate out the $\boldsymbol{k}^\gamma$ for $\gamma \neq \alpha, \beta$. After having done all this, the RHS of Eq. (F.6) becomes

$$
\begin{aligned}
&\frac{G^2 V^{n+2}}{(2\pi)^{(n-1)d}} \left(\frac{\pi}{\xi_L^2}\right)^{(n-1)d/2} \sum_{\substack{\alpha,\beta=0 \\ (\alpha\neq\beta)}}^{n} \int \frac{d\boldsymbol{k}^\alpha}{(2\pi)^d} \frac{d\boldsymbol{k}^\beta}{(2\pi)^d} \frac{d\boldsymbol{p}}{(2\pi)^d} \int \frac{d\mathrm{R}}{V} Q^\alpha_{d_1 d_2}(\boldsymbol{p}) Q^\beta_{d_3 d_4}(\boldsymbol{q}) \\
&\times \big(k^\alpha - \frac{i\mathrm{R}}{2\xi_L^2} - \frac{p}{2}\big)_{d_1} \big(k^\alpha - \frac{i\mathrm{R}}{2\xi_L^2} - \frac{p}{2}\big)_{d_2} \big(k^\beta - \frac{i\mathrm{R}}{2\xi_L^2} + \frac{p}{2}\big)_{d_3} \big(k^\beta - \frac{i\mathrm{R}}{2\xi_L^2} + \frac{p}{2}\big)_{d_4} \\
&\times \exp\Big(- \frac{1}{2}p^2\xi_L^2 - \frac{(n+1)r^2}{4\xi_L^2} - \big(|\boldsymbol{k}^\alpha|^2 + |\boldsymbol{k}^\alpha|^2\big)\xi_L^2 \Big).
\end{aligned}
\tag{F.7}
$$

As we focus on the properties at length-scales larger than ξ_L (below ξ_L, the system is liquid-like), we can neglect the terms with prefactors of $\boldsymbol{p}$ and/or $\boldsymbol{q}$, as they will be smaller than the terms with prefactors of $\boldsymbol{k}$ and/or $i\mathrm{R}/(2\xi_L^2)$ ($\boldsymbol{k}$ and $i\mathrm{R}/(2\xi_L^2)$ being of order $1/\xi_L$). Integrating over R, $\boldsymbol{k}^\alpha$ and $\boldsymbol{k}^\beta$, the RHS of Eq. (F.6) becomes

$$\frac{G^2}{2\xi_L^4}\sum_{\alpha\neq\beta}\sum_{\boldsymbol{p}} e^{-\frac{1}{2}p^2\xi_L^2}\{\mathbf{Q}^\alpha_{\boldsymbol{p}}\,\mathbf{Q}^\beta_{-\boldsymbol{p}}\}. \tag{F.8}$$

From this, one can deduce that the coupling term $-\frac{1}{4}\langle G_1(\Gamma)^2\,G_2(\mathbf{Q})^2\rangle$ is given by

$$-\frac{1}{4}\langle G_1(\Gamma)^2\,G_2(\mathbf{Q})^2\rangle = -\frac{\tilde{\eta}^2\ell^4 J_0^2 G^2}{900\xi_L^4\,T^\alpha\,T^\beta}\sum_{\boldsymbol{p}}\exp(-p^2\xi_L^2/2)\{\mathbf{Q}^\alpha_{\boldsymbol{p}}\,\mathbf{Q}^\beta_{-\boldsymbol{p}}\}. \tag{F.9}$$

Appendix G

Expressing microscopic observables in terms of field-theoretic quantities

Here, we derive expressions for the physical quantities $[\langle \boldsymbol{q}_{\boldsymbol{p}} \rangle]$ and $[\langle \boldsymbol{q}_{\boldsymbol{p}_1} \rangle \langle \boldsymbol{q}_{\boldsymbol{p}_2} \rangle]$ in terms of the conjugate fields $\mathbf{Q}_{\boldsymbol{p}}$ and the effective replica free energy H_{eff} [Eq. (4.7)]. We do this for the general case of $[\langle \boldsymbol{q}_{\boldsymbol{p}_1} \rangle \dots \langle \boldsymbol{q}_{\boldsymbol{p}_P} \rangle]$ ($P \in \{1, 2, 3, \dots\}$).

$$
\begin{aligned}
[\langle \boldsymbol{q}_{\boldsymbol{p}_1} \rangle \dots \langle \boldsymbol{q}_{\boldsymbol{p}_P} \rangle] \;=\; & \Bigg[\frac{1}{Z_\chi} \int \prod_i \frac{d\boldsymbol{c}_{i,1}^{\alpha_1}\, d\boldsymbol{c}_{i,2}^{\alpha_1}}{4\pi\ell^2 V} \boldsymbol{q}_{\boldsymbol{p}_1}^{\alpha_1} e^{-\frac{H_{\text{nem}}[\boldsymbol{n}^{\alpha_1}]}{T^{\alpha_1}} - \frac{H_{\text{ev}}[\boldsymbol{c}^{\alpha_1}, \boldsymbol{n}^{\alpha_1}]}{T^{\alpha_1}} - \frac{H_{\text{xlink},\chi}[\boldsymbol{c}^{\alpha_1}, \boldsymbol{n}^{\alpha_1}]}{T^{\alpha_1}}} \\
& \times \prod_{i=1}^{N} \delta(|\boldsymbol{c}_{i_1}^{\alpha_1} - \boldsymbol{c}_{i_2}^{\alpha_1}| - \ell) \\
& \times \cdots \\
& \times \frac{1}{Z_\chi} \int \prod_i \frac{d\boldsymbol{c}_{i,1}^{\alpha_1}\, d\boldsymbol{c}_{i,2}^{\alpha_1}}{4\pi\ell^2 V} \boldsymbol{q}_{\boldsymbol{p}_P}^{\alpha_P} e^{-\frac{H_{\text{nem}}[\boldsymbol{n}^{\alpha_P}]}{T^{\alpha_P}} - \frac{H_{\text{ev}}[\boldsymbol{c}^{\alpha_P}, \boldsymbol{n}^{\alpha_P}]}{T^{\alpha_P}} - \frac{H_{\text{xlink},\chi}[\boldsymbol{c}^{\alpha_P}, \boldsymbol{n}^{\alpha_P}]}{T^{\alpha_P}}} \\
& \times \prod_{j=1}^{N} \delta(|\boldsymbol{c}_{j_1}^{\alpha_P} - \boldsymbol{c}_{j_2}^{\alpha_P}| - \ell) \Bigg] \\
=\; & \lim_{n \to 0} \sum_\chi P(\chi) \frac{1}{Z_\chi^n} \int \prod_i \frac{d\boldsymbol{c}_{i,1}^{\alpha_1}\, d\boldsymbol{c}_{i,2}^{\alpha_1}}{4\pi\ell^2 V} \boldsymbol{q}_{\boldsymbol{p}_1}^{\alpha_1} \cdots \boldsymbol{q}_{\boldsymbol{p}_P}^{\alpha_P} \\
& \times e^{-\sum_{\gamma=1}^{n} \left(\frac{H_{\text{nem}}[\boldsymbol{n}^\gamma]}{T^\gamma} + \frac{H_{\text{ev}}[\boldsymbol{c}^\gamma, \boldsymbol{n}^\gamma]}{T^\gamma} + \frac{H_{\text{xlink},\chi}[\boldsymbol{c}^\gamma, \boldsymbol{n}^\gamma]}{T^\gamma} \right)} \prod_{\gamma=0}^{n} \prod_{j=1}^{N} \delta(|\boldsymbol{c}_{j_1}^\gamma - \boldsymbol{c}_{j_2}^\gamma| - \ell),
\end{aligned}
\tag{G.1}
$$

where in the second step, we have multiplied numerator and denominator by $n - P$ copies of

$$
Z_\chi = \int \prod_i \frac{d\boldsymbol{c}_{i,1}^{\alpha_1}\, d\boldsymbol{c}_{i,2}^{\alpha_1}}{4\pi\ell^2 V} e^{-\frac{H_{\text{nem}}[\boldsymbol{n}]}{T^\gamma} - \frac{H_{\text{ev}}[\boldsymbol{c}, \boldsymbol{n}]}{T^\gamma} - \frac{H_{\text{xlink},\chi}[\boldsymbol{c}, \boldsymbol{n}]}{T^\gamma}} \prod_{i=1}^{N} \delta(|\boldsymbol{c}_{i_1} - \boldsymbol{c}_{i_2}| - \ell). \tag{G.2}
$$

This produces a factor of Z_χ^n in the denominator which goes to unity once the replica limit is taken. We now perform the average over realizations of quenched disorder:

$$
\begin{aligned}
[\langle \boldsymbol{q}_{\boldsymbol{p}_1}\rangle \dots \langle \boldsymbol{q}_{\boldsymbol{p}_P}\rangle] &= \lim_{n\to 0}\sum_{\chi}\frac{1}{M!Z_1}\left(\frac{V\eta^2}{2(2\pi b^2)^{D/2}N}\right)^M \prod_{\gamma=0}^{n}\prod_{i=1}^{N}\delta(|\boldsymbol{c}_{i_1}^\gamma-\boldsymbol{c}_{i_2}^\gamma|-\ell) \\
&\quad \times\prod_i \frac{d\boldsymbol{c}_{i,1}^{\alpha_1}\,d\boldsymbol{c}_{i,2}^{\alpha_1}}{4\pi\ell^2 V}\boldsymbol{q}_{\boldsymbol{p}_1}^{\alpha_1}\dots\boldsymbol{q}_{\boldsymbol{p}_P}^{\alpha_P} e^{-\sum_{\gamma=0}^n\left(\frac{H_{\rm nem}[\boldsymbol{n}^\gamma]}{T^\gamma}+\frac{H_{\rm ev}[\boldsymbol{c}^\gamma,\boldsymbol{n}^\gamma]}{T^\gamma}+\frac{H_{{\rm xlink},\chi}[\boldsymbol{c}^\gamma,\boldsymbol{n}^\gamma]}{T^\gamma}\right)} \\
&= \lim_{n\to 0}\frac{1}{Z_1}\prod_{\gamma=0}^{n}\prod_i\frac{d\boldsymbol{c}_{i,1}^{\alpha_1}\,d\boldsymbol{c}_{i,2}^{\alpha_1}}{4\pi\ell^2 V}\boldsymbol{q}_{\boldsymbol{p}_1}^{\alpha_1}\dots\boldsymbol{q}_{\boldsymbol{p}_P}^{\alpha_P} \\
&\quad \times e^{\sum_{\gamma=0}^n\sum_{i,j}\frac{J_{ij}}{2T^\gamma}\left((\boldsymbol{n}_i^\gamma\cdot\boldsymbol{n}_j^\gamma)^2-\frac{1}{D}\right)-\sum_{\gamma=0}^n\sum_{i,j}\sum_{s,t}\frac{\lambda}{2T^\gamma}\delta(\boldsymbol{c}_{i,s}^\gamma-\boldsymbol{c}_{j,t}^\gamma)} \\
&\quad \times\exp\left(\frac{V\eta^2}{2(2\pi b^2)^{D/2}N}\sum_{i\neq j}\sum_{s,t}e^{-\frac{1}{2b^2}|\boldsymbol{c}_{i,s}^\gamma-\boldsymbol{c}_{j,t}^\gamma|^2}\right)\prod_{i=1}^{N}\delta(|\boldsymbol{c}_{i_1}^\gamma-\boldsymbol{c}_{i_2}^\gamma|-\ell) \\
&= \lim_{n\to 0}\frac{B_n}{Z_1}\Big\langle \boldsymbol{q}_{\boldsymbol{p}_1}^{\alpha_1}\dots\boldsymbol{q}_{\boldsymbol{p}_P}^{\alpha_P} e^{\frac{N}{2}\sum_{\alpha=0}^n\sum_{\boldsymbol{p}}\frac{J_{\boldsymbol{p}}}{T^\alpha}\{\boldsymbol{q}_{\boldsymbol{p}}^\alpha\,\boldsymbol{q}_{-\boldsymbol{p}}^\alpha\}} \\
&\quad \times e^{-\frac{N}{2}\sum_{\alpha=0}^n{\sum_{\boldsymbol{p}}}'\frac{\tilde\lambda_{\boldsymbol{p}}}{T^\alpha}|\widetilde\Gamma_{\boldsymbol{p}}^\alpha|^2+\frac{N}{2}\tilde\eta^2\sum_{\alpha=0}^n\sum_{\hat k}\overline{\Sigma}\Delta_{\hat k}|\widetilde\Gamma_{\hat k}|^2}\Big\rangle_{N,1+n},
\end{aligned}
\tag{G.3}
$$

where B_n is a constant. Here, $\{\alpha_1,\dots,\alpha_P\}\subseteq\{1,\dots,n\}$, as we are interested in nematic correlators in the measurement ensemble. In the second step, we summed over M to obtain an exponential function. To proceed further, we note that the factors of $\boldsymbol{q}_{\boldsymbol{p}}^\alpha$ can be generated by introducing, in the replica partition function Z_{1+n}, a source field $\mathfrak{H}_{\boldsymbol{p}}^\alpha$ that is linearly coupled to $\boldsymbol{q}_{\boldsymbol{p}}^\alpha$; we denote the resulting replica partition function by the symbol $Z_{1+n}[\mathfrak{H}]$. By functionally differentiating $Z_{1+n}[\mathfrak{H}]$ with respect to $\mathfrak{H}_{\boldsymbol{p}}^\alpha$, one can recover the correlators of $\boldsymbol{q}_{\boldsymbol{p}}^\alpha$. At the end of the computation, one has to take the replica limit, $\mathfrak{H}\to 0$. Following this

procedure, one obtains the following,

$$
\begin{aligned}
[\langle \boldsymbol{q}_{\boldsymbol{p}_1}\rangle \ldots \langle \boldsymbol{q}_{\boldsymbol{p}_P}\rangle] &= (-)^P \lim_{n\to 0}\lim_{\tilde{\mathfrak{H}}\to 0} \frac{B_n}{Z_1}\Bigg\langle \frac{\delta}{\delta \mathfrak{H}^{\alpha_1}_{\boldsymbol{p}_1}} \ldots \frac{\delta}{\delta \mathfrak{H}^{\alpha_P}_{\boldsymbol{p}_P}} e^{\frac{N}{2}\sum_{\alpha=0}^{n}\sum_{\boldsymbol{p}}\frac{J_{\boldsymbol{p}}}{T^\alpha}\{\boldsymbol{q}^\alpha_{\boldsymbol{p}}\,\boldsymbol{q}^\alpha_{-\boldsymbol{p}}\}-\sum_{\alpha=1}^{n}\sum_{\boldsymbol{p}}\mathfrak{H}^\alpha_{\boldsymbol{p}}\boldsymbol{q}^\alpha_{-\boldsymbol{p}}} \\
&\quad \times e^{-\frac{N}{2}\sum_{\alpha=0}^{n}\sum_{\boldsymbol{p}}{}'\frac{\tilde{\lambda}_{\boldsymbol{p}}}{T^\alpha}|\widetilde{\Gamma}^\alpha_{\boldsymbol{p}}|^2+\frac{N}{2}\tilde{\eta}^2\sum_{\alpha=0}^{n}\overline{\sum_{\hat{k}}}\Delta_{\hat{k}}|\widetilde{\Gamma}_{\hat{k}}|^2}\Bigg\rangle_{N,1+n} \\
&= (-)^P \lim_{n\to 0}\lim_{\tilde{\mathfrak{H}}\to 0} \frac{B_n}{Z_1}\Bigg\langle \frac{\delta}{\delta \mathfrak{H}^{\alpha_1}_{\boldsymbol{p}_1}} \ldots \frac{\delta}{\delta \mathfrak{H}^{\alpha_P}_{\boldsymbol{p}_P}} e^{\frac{N}{2}\sum_{\boldsymbol{p}}\frac{J_{\boldsymbol{p}}}{T^0}\{\boldsymbol{q}^\alpha_{\boldsymbol{p}}\,\boldsymbol{q}^\alpha_{-\boldsymbol{p}}\}} \\
&\quad \times e^{\frac{N}{2}\sum_{\alpha=1}^{n}\sum_{\boldsymbol{p}}\frac{J_{\boldsymbol{p}}}{T^\alpha}\left\{\left(\boldsymbol{q}^\alpha_{\boldsymbol{p}}-\frac{T^\alpha}{NJ_{\boldsymbol{p}}}\mathfrak{H}^\alpha_{\boldsymbol{p}}\right)\left(\boldsymbol{q}^\alpha_{-\boldsymbol{p}}-\frac{T^\alpha}{NJ_{-\boldsymbol{p}}}\mathfrak{H}^\alpha_{-\boldsymbol{p}}\right)\right\}} \\
&\quad \times e^{-\sum_{\alpha=1}^{n}\sum_{\boldsymbol{p}}\frac{(T^\alpha)^2}{2NJ_{\boldsymbol{p}}J_{-\boldsymbol{p}}}\{\mathfrak{H}^\alpha_{\boldsymbol{p}}\mathfrak{H}^\alpha_{-\boldsymbol{p}}\}} \\
&\quad \times e^{-N\sum_{\alpha=0}^{n}\sum_{\boldsymbol{p}}{}'\frac{\tilde{\lambda}_{\boldsymbol{p}}}{2T^\alpha}|\widetilde{\Gamma}^\alpha_{\boldsymbol{p}}|^2+\frac{N}{2}\tilde{\eta}^2\sum_{\alpha=0}^{n}\overline{\sum_{\hat{k}}}\Delta_{\hat{k}}|\widetilde{\Gamma}_{\hat{k}}|^2}\Bigg\rangle_{N,1+n}. \qquad \text{(G.4)}
\end{aligned}
$$

In the calculation above, we have completed the square in $\boldsymbol{q}^\alpha_{\boldsymbol{p}}$, generating extra quadratic terms $\frac{(T^\alpha)^2}{2NJ^\alpha_{\boldsymbol{p}}J^\alpha_{-\boldsymbol{p}}}\{\mathfrak{H}^\alpha_{\boldsymbol{p}}\,\mathfrak{H}^\alpha_{-\boldsymbol{p}}\}$. The Hubbard-Stratonovich transformation can now be performed, with $\boldsymbol{q}^\alpha_{\boldsymbol{p}}-\frac{T^\alpha}{NJ_{\boldsymbol{p}}}\mathfrak{H}^\alpha_{\boldsymbol{p}}$, $\widetilde{\Gamma}^\alpha_{\boldsymbol{p}}$, and $\widetilde{\Gamma}_{\hat{k}}$ serving as the analogues of the field ω in Eqs. (B.12). Making use of the following relation

$$
\begin{aligned}
&B_n\Bigg\langle e^{N\sum_{\boldsymbol{p}}\frac{J_{\boldsymbol{p}}}{2T^0}\{\boldsymbol{q}^\alpha_{\boldsymbol{p}}\,\boldsymbol{q}^\alpha_{-\boldsymbol{p}}\}+N\sum_{\alpha=1}^{n}\sum_{\boldsymbol{p}}\frac{J_{\boldsymbol{p}}}{2T^\alpha}\{\boldsymbol{q}^\alpha_{\boldsymbol{p}}-\frac{T^\alpha}{NJ_{\boldsymbol{p}}}\mathfrak{H}^\alpha_{\boldsymbol{p}}\,\boldsymbol{q}^\alpha_{-\boldsymbol{p}}-\frac{T^\alpha}{NJ_{-\boldsymbol{p}}}\mathfrak{H}^\alpha_{-\boldsymbol{p}}\}} \\
&\quad \times e^{-N\sum_{\alpha=0}^{n}\sum_{\boldsymbol{p}}{}'\frac{\tilde{\lambda}_{\boldsymbol{p}}}{2T^\alpha}|\widetilde{\Gamma}^\alpha_{\boldsymbol{p}}|^2+\frac{N}{2}\tilde{\eta}^2\sum_{\alpha=0}^{n}\overline{\sum_{\hat{k}}}\Delta_{\hat{k}}|\widetilde{\Gamma}_{\hat{k}}|^2}\Bigg\rangle_{N,1+n} \\
&\quad = \int \mathcal{D}\Gamma\prod_{\alpha=0}^{n}\mathcal{D}\Gamma^\alpha\mathcal{D}\mathbf{Q}^\alpha e^{-Nf_{1+n}(\Gamma_{\hat{k}},\Gamma^\alpha,\mathbf{Q}^\alpha)-\sum_{\alpha=1}^{n}\sum_{\boldsymbol{p}}\mathfrak{H}^\alpha_{\boldsymbol{p}}\mathbf{Q}^\alpha_{-\boldsymbol{p}}}, \qquad \text{(G.5)}
\end{aligned}
$$

we can compute

$$
\begin{aligned}
[\langle \boldsymbol{q}_{\boldsymbol{p}_1}\rangle \ldots \langle \boldsymbol{q}_{\boldsymbol{p}_P}\rangle] &= (-)^P \lim_{n\to 0}\lim_{\mathfrak{H}\to 0} \frac{1}{Z_1}\frac{\delta}{\delta \mathfrak{H}^{\alpha_1}_{\boldsymbol{p}_1}} \ldots \frac{\delta}{\delta \mathfrak{H}^{\alpha_P}_{\boldsymbol{p}_P}} \\
&\quad \times \int \mathcal{D}\Gamma \prod_{\alpha=0}^{n} \mathcal{D}\Gamma^\alpha \mathcal{D}\mathbf{Q}^\alpha \exp\Big(- N f_{1+n}(\Gamma, \Gamma^\alpha, \mathbf{Q}^\alpha) \\
&\quad - \sum_{\alpha=1}^{n}\sum_{\boldsymbol{p}} \mathfrak{H}^\alpha_{\boldsymbol{p}} \mathbf{Q}^\alpha_{-\boldsymbol{p}} - \sum_{\alpha=1}^{n}\sum_{\boldsymbol{p}} \frac{(T^\alpha)^2}{2N J_{\boldsymbol{p}}\, J_{-\boldsymbol{p}}} \{\mathfrak{H}^\alpha_{\boldsymbol{p}}\, \mathfrak{H}^\alpha_{-\boldsymbol{p}}\}\Big) \\
&= \lim_{n\to 0} \frac{Z_{1+n}}{Z_1} \frac{\int \mathcal{D}\Gamma \prod_{\alpha=0}^{n} \mathcal{D}\Gamma^\alpha \mathcal{D}\mathbf{Q}^\alpha \left(\mathbf{Q}^{\alpha_1}_{\boldsymbol{p}_1} \ldots \mathbf{Q}^{\alpha_P}_{\boldsymbol{p}_P}\right) e^{-N f_{1+n}(\Gamma, \Gamma^\alpha, \mathbf{Q}^\alpha)}}{\int \mathcal{D}\Gamma \prod_{\alpha=0}^{n} \mathcal{D}\Gamma^\alpha \mathcal{D}\mathbf{Q}^\alpha e^{-N f_{1+n}(\Gamma, \Gamma^\alpha, \mathbf{Q}^\alpha)}} \\
&\approx \lim_{n\to 0} \frac{\int \prod_{\alpha=1}^{n} \mathcal{D}\mathbf{Q}^\alpha \left(\mathbf{Q}^{\alpha_1}_{\boldsymbol{p}_1} \ldots \mathbf{Q}^{\alpha_P}_{\boldsymbol{p}_P}\right) e^{-N H_{\rm eff}(\mathbf{Q}^\alpha)}}{\int \prod_{\alpha=1}^{n} \mathcal{D}\mathbf{Q}^\alpha e^{-N H_{\rm eff}(\mathbf{Q}^\alpha)}} \\
&\equiv \langle\!\langle \mathbf{Q}^{\alpha_1}_{\boldsymbol{p}_1} \ldots \mathbf{Q}^{\alpha_P}_{\boldsymbol{p}_P} \rangle\!\rangle
\end{aligned}
\tag{G.6}
$$

On going from Eq. (G.4) to Eq. (G.6), we have performed the Hubbard-Stratonovich transformation with an extra linear coupling term $\mathfrak{H}^\alpha \mathbf{Q}^\alpha$. This originates in the extra part $\frac{T^\alpha}{N J_{\boldsymbol{p}}} \mathfrak{H}^\alpha_{\boldsymbol{p}}$ in $\boldsymbol{q}^\alpha_{\boldsymbol{p}}(\boldsymbol{p}) - \frac{T^\alpha}{N J_{\boldsymbol{p}}} \mathfrak{H}^\alpha_{\boldsymbol{p}}$ which we took to be our collective field. This linear coupling term was originally in the log trace but can be taken out of the log trace straight-forwardly as it does not involve the microscopic statistical variables $\boldsymbol{n}$ and $\boldsymbol{c}$. The Hubbard-Stratonovich transformation is implemented after we have taken out the functional derivatives with respect to the source field from the microscopic trace $\langle \ldots \rangle_{N,1+n}$. After the Hubbard-Stratonovich transformation has been done, we are left with a quantity that the source-field functional derivatives operate on, generating $\mathbf{Q}^{\alpha_1}_{\boldsymbol{p}_1} \ldots \mathbf{Q}^{\alpha_P}_{\boldsymbol{p}_P}$ within the field-theoretic trace. After this has been done, we take the limit $\mathfrak{H} \to 0$ which gets rid of the quadratic and linear terms in $\mathfrak{H}$. We have also multiplied numerator and denominator by Z_{1+n}. The factor $Z_{1+n}/Z_1 = 1 + O(n)$ and is equal to unity in the replica limit.

Appendix H

Variational free energy for liquid crystalline systems in the macroscopically isotropic state

Here, we shall derive the variational free energy [Eq. (8.5)] from the effective Hamiltonian for liquid crystalline order [Eq. (4.7)]. Recall that the variational free energy is given by

$$\frac{F_{\rm var}}{T} = \frac{1}{T}\big\langle H_{\rm eff} - H_0 \big\rangle_{H_0} - \ln \int \prod_{\alpha=1}^{n} \mathcal{D}\mathbf{Q}^{\alpha} \, \exp(-H_0/T), \tag{H.1}$$

where $\langle \cdots \rangle_{H_0}$ denotes averaging with respect to the Boltzmann weight $\exp(-H_0/T)$. The trial Hamiltonian is given by

$$\frac{H_0}{T} = \frac{1}{2} \sum_{\alpha,\beta=1}^{n} \sum_{j=0}^{4} \sum_{\boldsymbol{p}_1,\boldsymbol{p}_2} (G^{-1})^{\alpha\beta}(\boldsymbol{p}_1,\boldsymbol{p}_2) Q_j^{\alpha}(\boldsymbol{p}_1) Q_j^{\beta}(\boldsymbol{p}_2), \tag{H.2}$$

with the kernel given by

$$G^{\alpha\beta}(\boldsymbol{p}_1,\boldsymbol{p}_2) \equiv \delta_{\boldsymbol{p}_1,\boldsymbol{p}_2}\big(\mathcal{C}^T(\boldsymbol{p}_1)\delta^{\alpha\beta} + \mathcal{C}^G(\boldsymbol{p}_1)\big), \tag{H.3}$$

For reasons explained in Chapter 8, we have neglected possible non-zero parameters $\bar{Q}_j$ and assumed that the kernel is isotropic. First, we consider $\langle H_0 \rangle_{H_0}$. By the equipartition theorem, this is equal to $5n/2$ (measured in units of $k_B T$), a constant which we can disregard. Next, we consider $\langle H_{\rm eff} \rangle_{H_0}$. To evaluate this, we first express $H_{\rm eff}$ in terms of the five independent degrees of freedom of Q, viz., Q_J $(J = 0, 1, \ldots, 4)$, which are related to Q_{ij} via the equality $Q_{ij} \equiv \sum_{J=0}^{4} I_{ij}^J Q_J$. Here, $\underline{\underline{I}}^J$ are the basis matrices for symmetric traceless 3×3

matrices, introduced in Appendix D. We obtain

$$
\begin{aligned}
H_{\text{eff}}\left[\mathbf{Q}^{\alpha}\right] \;=\; & \frac{1}{2}\sum_{\alpha=1}^{n}\sum_{j=0}^{4}\sum_{\boldsymbol{p}}\left(t+Kp^{2}-\frac{(h\omega(\boldsymbol{p}))^{2}}{t^{0}+Kp^{2}}\right)|Q_{j}^{\alpha}(\boldsymbol{p})|^{2}\\
& -\frac{v}{3}\sum_{\alpha=1}^{n}\sum_{\boldsymbol{p}_1,\boldsymbol{p}_2,\boldsymbol{p}_3}\delta_{\boldsymbol{p}_1+\boldsymbol{p}_2+\boldsymbol{p}_3,\mathbf{0}}\Big(\frac{1}{2}\sqrt{\frac{2}{3}}Q_{0}^{\alpha}(\boldsymbol{p}_1)Q_{0}^{\alpha}(\boldsymbol{p}_2)Q_{0}^{\alpha}(\boldsymbol{p}_3)\\
& \quad -\sqrt{\frac{3}{2}}Q_{0}^{\alpha}(\boldsymbol{p}_1)\big(Q_{1}^{\alpha}(\boldsymbol{p}_2)Q_{1}^{\alpha}(\boldsymbol{p}_3)+Q_{2}^{\alpha}(\boldsymbol{p}_2)Q_{2}^{\alpha}(\boldsymbol{p}_3)\big)\\
& \quad +\frac{1}{2}\sqrt{\frac{3}{2}}Q_{0}^{\alpha}(\boldsymbol{p}_1)\big(Q_{3}^{\alpha}(\boldsymbol{p}_2)Q_{3}^{\alpha}(\boldsymbol{p}_3)+Q_{4}^{\alpha}(\boldsymbol{p}_2)Q_{4}^{\alpha}(\boldsymbol{p}_3)\big)\Big)\\
& -\frac{v}{6\sqrt{2}}\sum_{\alpha=1}^{n}\sum_{\boldsymbol{p}_1,\boldsymbol{p}_2,\boldsymbol{p}_3}\delta_{\boldsymbol{p}_1+\boldsymbol{p}_2+\boldsymbol{p}_3,\mathbf{0}}\Big(3Q_{1}^{\alpha}(\boldsymbol{p}_1)\big(Q_{2}^{\alpha}(\boldsymbol{p}_2)Q_{2}^{\alpha}(\boldsymbol{p}_3)-Q_{3}^{\alpha}(\boldsymbol{p}_2)Q_{3}^{\alpha}(\boldsymbol{p}_3)\big)\\
& \quad +6Q_{2}^{\alpha}(\boldsymbol{p}_1)Q_{3}^{\alpha}(\boldsymbol{p}_2)Q_{4}^{\alpha}(\boldsymbol{p}_3)\Big)\\
& +\frac{w}{4}\sum_{\alpha=1}^{n}\sum_{\boldsymbol{p}_1,\boldsymbol{p}_2,\boldsymbol{p}_3,\boldsymbol{p}_4}\delta_{\boldsymbol{p}_1+\boldsymbol{p}_2+\boldsymbol{p}_3+\boldsymbol{p}_4,\mathbf{0}}\Big(\sum_{j=0}^{4}Q_{j}^{\alpha}(\boldsymbol{p}_1)Q_{j}^{\alpha}(\boldsymbol{p}_2)Q_{j}^{\alpha}(\boldsymbol{p}_3)Q_{j}^{\alpha}(\boldsymbol{p}_4)\\
& \quad +\sum_{\substack{i,j=0\\(i\neq j)}}^{4}Q_{i}^{\alpha}(\boldsymbol{p}_1)Q_{i}^{\alpha}(\boldsymbol{p}_2)Q_{j}^{\alpha}(\boldsymbol{p}_3)Q_{j}^{\alpha}(\boldsymbol{p}_4)\Big)\\
& -\frac{1}{2}\sum_{\substack{\alpha,\beta=1\\(\alpha\neq\beta)}}^{n}\sum_{j=0}^{4}\sum_{\boldsymbol{p}}\left(h\omega(\boldsymbol{p})+\frac{(h\omega(\boldsymbol{p}))^{2}}{t^{0}+Kp^{2}}\right)Q_{j}^{\alpha}(\boldsymbol{p})Q_{j}^{\beta}(-\boldsymbol{p}).
\end{aligned}
\tag{H.4}
$$

Averaging H_{eff} over H_0 yields the following result:

$$
\begin{aligned}
\frac{2}{5n}\langle H\rangle_{H_0} \;=\; & \sum_{\boldsymbol{p}}\left(t+Kp^{2}-\frac{\big(h\omega(\boldsymbol{p})\big)^{2}}{t^{0}+Kp^{2}}\right)\big(\mathcal{C}^{T}(\boldsymbol{p})+\mathcal{C}^{G}(\boldsymbol{p})\big)\\
& +\sum_{\boldsymbol{p}}\left(h\omega(\boldsymbol{p})+\frac{\big(h\omega(\boldsymbol{p})\big)^{2}}{t^{0}+Kp^{2}}\right)\mathcal{C}^{G}(\boldsymbol{p})\\
& +\frac{7w}{2}\sum_{\boldsymbol{p}_1,\boldsymbol{p}_2,\boldsymbol{p}_3,\boldsymbol{p}_4}\delta_{\boldsymbol{p}_1+\boldsymbol{p}_2+\boldsymbol{p}_3+\boldsymbol{p}_4,\mathbf{0}}\Big(\delta_{\boldsymbol{p}_1+\boldsymbol{p}_2,\mathbf{0}}\delta_{\boldsymbol{p}_3+\boldsymbol{p}_4,\mathbf{0}}\\
& \quad \times\big(\mathcal{C}^{T}(\boldsymbol{p}_1)+\mathcal{C}^{G}(\boldsymbol{p}_1)\big)\big(\mathcal{C}^{T}(\boldsymbol{p}_3)+\mathcal{C}^{G}(\boldsymbol{p}_3)\big)\Big).
\end{aligned}
\tag{H.5}
$$

Finally, we look at the log-trace term,

$$\begin{aligned}\ln \int \prod_{\gamma=1}^{n} \mathcal{D}\mathbf{Q}^{\gamma} e^{-H_0/T} &= \ln \int \prod_{\gamma=1}^{n} \mathcal{D}\mathbf{Q}^{\gamma} \exp\left(\frac{1}{2}\sum_{\alpha,\beta=1}^{n}\sum_{j=0}^{4}\sum_{\boldsymbol{p}_1,\boldsymbol{p}_2}(G^{-1})^{\alpha\beta}(\boldsymbol{p}_1,\boldsymbol{p}_2)Q_j^{\alpha}(\boldsymbol{p}_1)Q_j^{\beta}(\boldsymbol{p}_2)\right) \\ &= \frac{5}{2}\sum_{\boldsymbol{p}} \ln\left(\mathrm{Det}(\underline{\underline{G}})\right), \end{aligned} \tag{H.6}$$

where $\underline{\underline{G}}$ is the $n \times n$ replica matrix defined by $G^{\alpha\beta} \equiv \left(\mathcal{C}^T(\boldsymbol{p})\delta^{\alpha\beta} + \mathcal{C}^G(\boldsymbol{p})\mathbf{1}^{\alpha\beta}\right)$. (The symbol $\mathbf{1}^{\alpha\beta}$ denotes an $n \times n$ matrix with every entry set to one.) The determinant of $\underline{\underline{G}}$ is equal to the product of eigenvalues of $\underline{\underline{G}}$, so we have to determine what its eigenvalues are. First, note that $\mathbf{1}^{\alpha\beta}$ has one eigenvector $(1, 1, \ldots, 1)$ corresponding to the eigenvalue n, and $n-1$ other eigenvectors

$$\begin{gathered}(n-1, \quad -1, \quad -1, \quad \ldots, \quad -1, \quad -1), \\ (-1, \quad n-1, \quad -1, \quad \ldots, \quad -1, \quad -1), \\ \vdots \\ (-1, \quad -1, \quad -1, \quad \ldots, \quad -1, \quad n-1),\end{gathered}$$

corresponding to the eigenvalue 0. Thus $\underline{\underline{G}}$ has one eigenvalue $\mathcal{C}^T(\boldsymbol{p}) + n\mathcal{C}^G(\boldsymbol{p})$ and $n-1$ other eigenvalues $\mathcal{C}^T(\boldsymbol{p})$. The log-trace term then becomes

$$\begin{aligned} -\frac{2}{5n}\ln \int \prod_{\gamma=1}^{n} \mathcal{D}\mathbf{Q}^{\gamma} e^{-H_0/T} &= -\frac{1}{n}\sum_{\boldsymbol{p}} \ln\left(\left(\mathcal{C}^T(\boldsymbol{p}) + n\mathcal{C}^G(\boldsymbol{p})\right)\left(\mathcal{C}^T(\boldsymbol{p})\right)^{n-1}\right) \\ &= -\frac{1}{n}\sum_{\boldsymbol{p}} \left(n\ln \mathcal{C}^T(\boldsymbol{p}) + \ln\left(1 + \frac{n\mathcal{C}^G(\boldsymbol{p})}{\mathcal{C}^T(\boldsymbol{p})}\right)\right) \\ &\approx -\sum_{\boldsymbol{p}} \left(\ln \mathcal{C}^T(\boldsymbol{p}) + \frac{\mathcal{C}^G(\boldsymbol{p})}{\mathcal{C}^T(\boldsymbol{p})}\right). \end{aligned} \tag{H.7}$$

Combining the results of Eqs. (H.5) and (H.7) and re-expressing the five scalar degrees of freedom of $\mathbf{Q}^{\alpha}$ in terms of tensor components then gives us the variational free energy in

Eq. (8.5).

Appendix I

Computation of the term coupling the elastic fluctuation and local nematic order

In this Appendix, we shall derive the leading order contribution (in G and at large wavelengths) to the term proportional to $\boldsymbol{U}^\alpha \mathbf{Q}^\alpha$ from the term proportional to $\Gamma\Gamma\mathbf{Q}^\alpha$ in the Landau-Wilson free energy, by considering the $O(\boldsymbol{U}^\alpha)$ contribution to $-\frac{1}{2}\langle G_1(\Gamma)^2 G_2(Q)\rangle$. Let us consider the general case of the Goldstone-deformed vulcanization order parameter in the *deformed* cross-linking state, for which the position of a given particle at the instant of cross-linking is given by $\Lambda \cdot \boldsymbol{z}$ (Λ being the deformation gradient). At the end of the calculation, we will set Λ to identity, and obtain the linear nematic-elastic fluctuation coupling term for the un-deformed cross-linking state.

The Goldstone-deformed order parameter Γ is given in Fourier space by

$$\Gamma_{\hat{k}} = \int \frac{d\boldsymbol{z}}{V} e^{-i\boldsymbol{k}^0\cdot\boldsymbol{z} - i\sum_{\alpha=1}^n \boldsymbol{k}^\alpha\cdot(\Lambda\boldsymbol{z}+\boldsymbol{U}^\alpha(\boldsymbol{z})) - \frac{1}{2}|\hat{k}|^2\xi_L^2}. \tag{I.1}$$

Plugging this into Eq. (C.6b), and Taylor-expanding the exponential to leading order in $\boldsymbol{U}^\alpha$,

one obtains

$$\sum_{\alpha=1}^{n}\sum_{\boldsymbol{p}}\overline{\sum_{\hat{k}}}\Gamma_{\hat{k}-(\boldsymbol{p}/2)\epsilon^{\alpha}}\Gamma_{-\hat{k}-(\boldsymbol{p}/2)\epsilon^{\alpha}}Q^{\alpha}_{d_1\,d_2}(\boldsymbol{p})(p_{d_1}p_{d_2}+(k^{\alpha}+(p/2))_{d_1}(k^{\alpha}+(p/2))_{d_2})$$
$$=-\frac{iG^2}{V}\sum_{\alpha=1}^{n}\sum_{\boldsymbol{p},\boldsymbol{q}}\overline{\sum_{\hat{k}}}\int\frac{d\boldsymbol{c}\,d\boldsymbol{r}}{V^2}Q^{\alpha}_{d_1\,d_2}(\boldsymbol{p})(p_{d_1}p_{d_2}+(k^{\alpha}+(p/2))_{d_1}(k^{\alpha}+(p/2))_{d_2})$$
$$\times\Bigg(\big((\boldsymbol{k}^{\alpha}-(\boldsymbol{p}/2))\cdot\boldsymbol{U}^{\alpha}_{\boldsymbol{q}}+\sum_{\substack{\gamma=1\\(\gamma\neq\alpha)}}^{n}\boldsymbol{k}^{\gamma}\cdot\boldsymbol{U}^{\gamma}_{\boldsymbol{q}}\big)e^{i(\boldsymbol{q}/2)\cdot\boldsymbol{r}}$$
$$-\big((\boldsymbol{k}^{\alpha}+(\boldsymbol{p}/2))\cdot\boldsymbol{U}^{\alpha}_{\boldsymbol{q}}+\sum_{\substack{\gamma=1\\(\gamma\neq\alpha)}}^{n}\boldsymbol{k}^{\gamma}\cdot\boldsymbol{U}^{\gamma}_{\boldsymbol{q}}\big)e^{-i(\boldsymbol{q}/2)\cdot\boldsymbol{r}}\Bigg)$$
$$\times e^{-i\boldsymbol{k}^0\cdot\boldsymbol{r}-i\sum_{\alpha=1}^{n}\boldsymbol{k}^{\alpha}\cdot\Lambda\boldsymbol{r}+i\boldsymbol{p}\cdot\Lambda\boldsymbol{c}-|\hat{k}|^2\xi_L^2-\frac{1}{4}p^2\xi_L^2+i\boldsymbol{q}\cdot\boldsymbol{c}}. \tag{I.2}$$

We integrate over $\boldsymbol{c}$ and $\boldsymbol{q}$, which has the effect of changing $\boldsymbol{q}$ into $-\Lambda^T\cdot\boldsymbol{p}$. Shifting $\boldsymbol{k}^{\gamma}\to\boldsymbol{k}^{\gamma}-\frac{i\Lambda\cdot\boldsymbol{r}}{2\xi_L^2}$ (to eliminate cross-terms involving $\boldsymbol{k}^{\gamma}$ in the exponential) and neglecting a contribution proportional to $p_{d_1}\,p_{d_2}$ (which will lead to terms of cubic order in momentum), one obtains, for the terms proportional to $\big((\boldsymbol{k}^{\alpha}-(\boldsymbol{p}/2))\cdot\boldsymbol{U}^{\alpha}_{\boldsymbol{q}}+\sum_{\substack{\gamma=1\\(\gamma\neq\alpha)}}^{n}\boldsymbol{k}^{\gamma}\cdot\boldsymbol{U}^{\gamma}_{\boldsymbol{q}}\big)e^{i(\boldsymbol{q}/2)\cdot\boldsymbol{r}}$ in Eq. (I.2), the following,

$$-\frac{iG^2}{V}\sum_{\alpha=1}^{n}\sum_{\boldsymbol{p}}\overline{\sum_{\hat{k}}}\int\frac{d\boldsymbol{r}}{V}Q^{\alpha}_{d_1\,d_2}(\boldsymbol{p})(k^{\alpha}-\frac{i(\Lambda\cdot r)}{2\xi_L^2}+(p/2))_{d_1}(k^{\alpha}-\frac{i(\Lambda\cdot r)}{2\xi_L^2}+(p/2))_{d_2}$$
$$\times\Bigg(\big(\boldsymbol{k}^{\alpha}-\frac{i\Lambda\cdot\boldsymbol{r}}{2\xi_L^2}-(\boldsymbol{p}/2)\big)\cdot\boldsymbol{U}^{\alpha}(-\Lambda^T\cdot\boldsymbol{p})+\sum_{\substack{\gamma=1\\(\gamma\neq\alpha)}}^{n}\big(\boldsymbol{k}^{\gamma}-\frac{i\Lambda\cdot\boldsymbol{r}}{2\xi_L^2}\big)\cdot\boldsymbol{U}^{\gamma}(-\Lambda^T\cdot\boldsymbol{p})\Bigg)$$
$$\times e^{-\frac{r^2}{4\xi_L^2}-|\hat{k}|^2\xi_L^2-\frac{i}{2}\boldsymbol{p}\cdot\Lambda\boldsymbol{r}-\frac{1}{4}p^2\xi_L^2}. \tag{I.3}$$

Next, we shift $\boldsymbol{r}\to\boldsymbol{r}-i\xi_L^2\Lambda^T\cdot\boldsymbol{p}$ (to eliminate cross-terms involving $\boldsymbol{r}$ in the exponential).

This allows one to obtain

$$
\begin{aligned}
&-\frac{iG^2}{V}\sum_{\alpha=1}^{n}\sum_{\boldsymbol{p}}\overline{\sum_{\hat{k}}}\int\frac{d\boldsymbol{r}}{V}Q^{\alpha}_{d_1\,d_2}(\boldsymbol{p})\big(k^{\alpha}-\frac{i(\Lambda\cdot r)}{2\xi_L^2}+((\Lambda\Lambda^T-I)\cdot p/2)\big)_{d_1}\\
&\times\big(k^{\alpha}-\frac{i(\Lambda\cdot r)}{2\xi_L^2}+((\Lambda\Lambda^T-I)\cdot p/2)\big)_{d_2}\\
&\times\Bigg((\boldsymbol{k}^{\alpha}-\frac{i\Lambda\cdot\boldsymbol{r}}{2\xi_L^2}-((\Lambda\Lambda^T-I)\cdot\boldsymbol{p}/2))\cdot\boldsymbol{U}^{\alpha}(-\Lambda^T\cdot\boldsymbol{p})\\
&\quad+\sum_{\substack{\gamma=1\\(\gamma\neq\alpha)}}^{n}(\boldsymbol{k}^{\gamma}-\frac{i\Lambda\cdot\boldsymbol{r}}{2\xi_L^2}-(\Lambda\Lambda^T\cdot\boldsymbol{p}/2))\cdot\boldsymbol{U}^{\gamma}(-\Lambda^T\cdot\boldsymbol{p})\Bigg)\\
&\quad\times e^{-\frac{r^2}{4\xi_L^2}-|\hat{k}|^2\xi_L^2-\frac{1}{4}((\Lambda^T\cdot p)^2+p^2)\xi_L^2}.
\end{aligned}
\tag{I.4}
$$

We perform a similar procedure for the terms proportional to $\big((\boldsymbol{k}^{\alpha}+(\boldsymbol{p}/2))\cdot\boldsymbol{U}^{\alpha}_{\boldsymbol{q}}+\sum^{n}_{\substack{\gamma=1\\(\gamma\neq\alpha)}}\boldsymbol{k}^{\gamma}\cdot\boldsymbol{U}^{\gamma}_{\boldsymbol{q}}\big)e^{-i(\boldsymbol{q}/2)\cdot\boldsymbol{r}}$ in Eq. (I.2), shifting $\boldsymbol{k}^{\gamma}\rightarrow\boldsymbol{k}^{\gamma}-\frac{i\Lambda\cdot\boldsymbol{r}}{2\xi_L^2}$ (to eliminate cross-terms involving $\boldsymbol{k}^{\gamma}$ in the exponential) and neglecting a contribution proportional to $p_{d_1}\,p_{d_2}$, and next shifting $\boldsymbol{r}\rightarrow\boldsymbol{r}+i\xi_L^2\Lambda^T\cdot\boldsymbol{p}$ (to eliminate cross-terms involving $\boldsymbol{r}$ in the exponential). This allows one to obtain

$$
\begin{aligned}
&-\frac{iG^2}{V}\sum_{\alpha=1}^{n}\sum_{\boldsymbol{p}}\overline{\sum_{\hat{k}}}\int\frac{d\boldsymbol{r}}{V}Q^{\alpha}_{d_1\,d_2}(\boldsymbol{p})(k^{\alpha}-\frac{i(\Lambda\cdot r)}{2\xi_L^2}+((\Lambda\Lambda^T+I)\cdot p/2))_{d_1}\\
&\times(k^{\alpha}-\frac{i(\Lambda\cdot r)}{2\xi_L^2}+((\Lambda\Lambda^T+I)\cdot p/2))_{d_2}\\
&\times\Bigg(\big(\boldsymbol{k}^{\alpha}-\frac{i\Lambda\cdot\boldsymbol{r}}{2\xi_L^2}+((\Lambda\Lambda^T+I)\cdot\boldsymbol{p}/2)\big)\cdot\boldsymbol{U}^{\alpha}(-\Lambda^T\cdot\boldsymbol{p})\\
&\quad+\sum_{\substack{\gamma=1\\(\gamma\neq\alpha)}}^{n}\big(\boldsymbol{k}^{\gamma}-\frac{i\Lambda\cdot\boldsymbol{r}}{2\xi_L^2}+(\Lambda\Lambda^T\cdot\boldsymbol{p}/2)\big)\cdot\boldsymbol{U}^{\gamma}(-\Lambda^T\cdot\boldsymbol{p})\Bigg)\\
&\quad\times e^{-\frac{r^2}{4\xi_L^2}-|\hat{k}|^2\xi_L^2-\frac{1}{4}((\Lambda^T\cdot p)^2+p^2)\xi_L^2}.
\end{aligned}
\tag{I.5}
$$

By adding (I.4) and (I.5), summing over the discrete wave-vectors $\hat{k}$, and integrating over $\boldsymbol{r}$,

one obtains the following,

$$\sum_{\alpha=1}^{n}\sum_{\boldsymbol{p}}\overline{\sum_{\hat{k}}}\Gamma_{\hat{k}-(\boldsymbol{p}/2)\epsilon^{\alpha}}\Gamma_{-\hat{k}-(\boldsymbol{p}/2)\epsilon^{\alpha}}Q^{\alpha}_{d_1\,d_2}(\boldsymbol{p})(p_{d_1}p_{d_2}+(k^{\alpha}+(p/2))_{d_1}(k^{\alpha}+(p/2))_{d_2})$$
$$=\frac{iG^2}{V\xi_L^2}\sum_{\alpha=1}^{n}\sum_{\boldsymbol{p}}e^{-\frac{1}{4}((\Lambda^T\cdot p)^2+p^2)\xi_L^2}\boldsymbol{U}^{\alpha}(-\Lambda^T\cdot\boldsymbol{p})\cdot\mathbf{Q}^{\alpha}_{\boldsymbol{p}}\cdot\Lambda\Lambda^T\cdot\boldsymbol{p}. \tag{I.6}$$

For the un-deformed cross-linking state, $\Lambda = I$. The term $-\frac{1}{2}\langle G_1(\Gamma)^2G_2(Q)\rangle$ from the Landau-Wilson free energy (C.1) is then equal to

$$-\frac{1}{2}\langle G_1(\Gamma)^2G_2(Q)\rangle=-\frac{iG^2\tilde{\eta}^4J_0\ell^2}{10TV\xi_L^2}\sum_{\alpha=1}^{n}\sum_{\boldsymbol{p}}e^{-\frac{1}{2}p^2\xi_L^2}\boldsymbol{U}^{\alpha}(-\boldsymbol{p})\cdot\mathbf{Q}^{\alpha}_{\boldsymbol{p}}\cdot\boldsymbol{p}. \tag{I.7}$$

This is the elastic fluctuation–nematic linear coupling term at lowest order in momentum.

References

[1] De Gennes, P.–G. & Prost, J. *The Physics of Liquid Crystals*. Oxford University Press (1993).

[2] M. Kleman and O. Lavrentovich, *Soft Matter Physics: An Introduction*. Springer (2002).

[3] L. R. G. Treloar, *The Physics of Rubber Elasticity*. Clarendon Press, Oxford (1975).

[4] M. Rubinstein and R. Colby, *Polymer Physics*. Oxford (2003).

[5] Warner, M. & Terentjev, E. M. *Liquid Crystal Elastomers*. Oxford University Press (2003).

[6] Goldbart, P. M., Castillo, H. E. & Zippelius, A. Randomly cross-linked macromolecular systems: vulcanization transition to and properties of the amorphous solid state. *Adv. Phys.* **45**, 393–468 (1996).

[7] Peng, W., Castillo, H. E., Goldbart, P. M. & Zippelius, A. Universality and its origins at the amorphous solidification transition. *Phys. Rev. B* **57**, 839–847 (1998).

[8] L. Onsager, Ann. N. Y. Acad. Sci. **51**, 627 (1949).

[9] W. Maier and A. Saupe, Z. Naturforsch. A 13: 564 (1958).theorie des nematischen kristallinflussigen zustandes"

[10] W. Maier and A. Saupe, Z. Naturforsch. A 14: 882 (1959).

[11] W. Maier and A. Saupe, Z. Naturforsch. A 15: 287 (1960).

[12] P.–G. de Gennes, Mol. Cryst. liquid Cryst. **12**, 193.

[13] P.–G. de Gennes, J. Phys. (Paris) **36**, 1049 (1976); ibid., **37**, L1 (1976).

[14] D. Stauffer, J. Chem. Soc. Faraday Trans. II **72**, 1354 (1976).

[15] J. Küpfer and H. Finkelmann, Makromol. Chem. Rap. Commun. 12, 717 (1991).

[16] Warner, M., Bladon, P. & Terentjev, E. M. "Soft elasticity" – deformation without resistance in liquid crystal elastomers. *J. Phys. II (France)* **4**, 93–102 (1994).

[17] Verwey, G. & Warner, M. Soft rubber elasticity. *Macromol.* **28**, 4303–4306 (1995).

[18] Olmsted, P. D. Rotational invariance and Goldstone modes in nematic elastomers and gels. *J. Phys. II (France)* **4**, 2215–2230 (1994).

[19] Golubovic, L. & Lubensky, T. C., Nonlinear elasticity of amorphous solids *Phys. Rev. Lett.* **63**, 1082-1085 (1989).

[20] Lubensky, T. C., Mukhopadhyay, R., Radzihovsky, L. & Xing, X. Symmetries and Elasticity of Nematic Gels. *Phys. Rev. E* **66**, 011702 (2002).

[21] de Gennes, P.-G. *C. R. Acad. Sci. Ser. B* **281**, 101 (1975)

[22] Uchida, N. Elastic Effects in Disordered Nematic Networks *Phys. Rev. E* **60**, R13-R16 (1999).

[23] Uchida, N. Soft and nonsoft structural transitions in disordered nematic networks. *Phys. Rev. E* **62**, 5119–5136 (2000).

[24] Fridrikh, S. V. & Terentjev, E. M. Polydomain-monodomain transition in nematic elastomers. *Phys. Rev. E* **60**, 1847–1857 (1999).

[25] Petridis, L. & Terentjev, E. Nematic-isotropic transition with quenched disorder. *Phys. Rev. E* **74**, 051707 (2006).

[26] Petridis, L. & Terentjev, E. Quenched disorder and spin-glass correlations in XY nematics. *J. Phys. A: Math. Gen.* **39**, 9693–9708 (2006).

[27] Urayama, K. Selected issues in liquid crystal elastomers and gels. *Macromol.* **40**, 2277–2288 (2007).

[28] Urayama, K., Kohmon, E., Kojima, M. & Takigawa, T. Polydomain-monodomain transition of randomly disordered nematic elastomers with different cross-linking histories. *Macromol.* **42**, 4084–4089 (2009).

[29] B.–S. Lu, F. Ye, X. Xing, P. M. Goldbart, *Phys. Rev. Lett.* **108**, 257803 (2012).

[30] W. Peng and P. M. Goldbart, *Phys. Rev. E* **61**, 3339 (2000).

[31] Xing, X., Pfahl, S., Mukhopadhyay, S., Goldbart, P. M. & Zippelius, A. Nematic elastomers: from a microscopic model to macroscopic elasticity theory. *Phys. Rev. E* **77**, 051802 (2008).

[32] Lu, B.-S., Ye, F., Xing, X. & Goldbart, P. M. Polydomain structure and its origins in isotropic-genesis nematic elastomers. *arXiv:1101.1323*, 2011.

[33] B.–S. Lu, F. Ye, X. Xing, P. M. Goldbart, manuscript in preparation (2012). The microscopic model examined in this paper involves a system of dimers that are randomly and permanently connected by harmonic springs, and interact with one another via Maier-Saupe and excluded-volume forces.

[34] S. F. Edwards, P. W. Anderson, J. Phys. F: Metal Phys. **5**, 965 (1975).

[35] Deam, R. T. & Edwards, S. F. The theory of rubber elasticity. *Phil. Trans. R. Soc. A* **280**, 317–353 (1976).

[36] Edwards, S. F. & Anderson, P. W. Theory of spin glasses. *J. Phys. F: Metal Phys.* **5**, 965 (1975).

[37] Feynman, R. P. *Statistical Mechanics: A Set of Lectures.* Westview Press, 2nd Edn. (1998).

[38] Shakhnovich, E. I. & Gutin, A. M. Formation of microdomains in a quenched disordered heteropolymer. *J. Phys. (France)* **50**, 1843–1850 (1989).

[39] Mézard, M. & Parisi, G. Interfaces in a random medium and replica symmetry breaking. *J. Phys. A: Math. Gen.* **23**, L1229–L1234 (1990).

[40] Mézard, M. & Parisi, G. Replica field theory for random manifolds. *J. Phys. I (France)* **1**, 809–836 (1991).

[41] Stepanow, S., Dobrynin, A. V., Vilgis, T. A., & Binder, K. Copolymer melts in disordered media. *J. Phys. I (France)* **6**, 837–857 (1996).

[42] Mermin, N. D. & Wagner, H. Absence of ferromagnetism or antiferromagnetism in one- or two-dimensional isotropic Heisenberg models. *Phys. Rev. Lett.* **17**, 1133-1136 (1966).

[43] The Kupfer-Finkelmann procedure is as follows. The nematic polymer melt is weakly cross-linked to form a weak gel, afterwhich it is uniaxially stretched in the nematic state until it becomes a macroscopic nematically-ordered state. Keeping the sample stretched, a second cross-linking reaction is initiate, which fixes the enforced uniaxial alignment.

[44] R. Brout, Phys. Rev. 115, 824 (1959)

[45] M. Mezard, G. Parisi and M. Virasoro, *Spin Glass Theory and Beyond*, World Scientific Publishing Company, Singapore (1986).

[46] G. Parisi, *Statistical Field Theory* Westview Press (1998).

[47] N. Goldenfeld, *Lectures on Phase Transitions and the Renormalization Group*, Westview Press (1992).

[48] P. M. Chaikin and T. C. Lubensky, *Principles of Condensed Matter Physics*, Cambridge University Press (1995).

[49] M. Kardar, *Statistical Physics of Fields*, Cambridge University Press (2007).

[50] Ye, F., Mukhopadhyay, R., Stenull, O. & Lubensky, T. C. Semisoft nematic elastomers and nematics in crossed electric and magnetic fields *Phys. Rev. Lett.* **98**, 147801 (2007).

[51] Clarke, S. M., Terentjev, E. M., Kundler, I. & Finkelmann, H. Texture evolution during the polydomain-monodomain transition in nematic elastomers. *Macromol.* **31**, 4862–4872 (1998).

[52] Petridis, L. & Terentjev, E. Quenched disorder and spin-glass correlations in XY nematics. *J. Phys. A: Math. Gen.* **39**, 9693–9708 (2006).

[53] Selinger, J. V. & Ratna, B. R. Isotropic-nematic transition in liquid-crystalline elastomers: lattice model with quenched disorder. *Phys. Rev. E* **70**, 041707 (2004).

[54] Biggins, J. S., Bhattacharya, K. & Warner, M. Elasticity of polydomain liquid crystal elastomers. *arXiv:0911.3513v1*, 2009.

[55] Biggins, J. S., Warner, M. & Bhattacharya, K. Supersoft elasticity in polydomain nematic elastomers. *Phys. Rev. Lett.* **103**, 037802 (2009).

[56] Imry, Y. & Ma, S.-K. Random-field instability of the ordered state of continuous symmetry. *Phys. Rev. Lett.* **35**, 1399–1401 (1975).

[57] Radzihovsky, L. & Toner, J. Smectic liquid crystals in random environments. *Phys. Rev. B* **60**, 206-257 (1999).

[58] Feldman, D. E. Quasi-long-range order in nematics confined in random porous media. *Phys. Rev. Lett.* **84**, 4886–4889 (2000).

[59] S. F. Edwards, Proc. Phys. Soc. **85**, 87 (1965); S. F. Edwards, Proc. Phys. Soc. **88**, 109 (1966).

[60] M. Doi and S. F. Edwards, *The Theory of Polymer Dynamics*. Oxford University Press, New York (1986).

[61] B.A. DiDonna, T.C. Lubensky, Phys. Rev. E **72**, 066619 (2005).

[62] Mao, X., Goldbart, P., Xing, X. & Zippelius, A. Soft random solids and their heterogeneous elasticity. *Phys. Rev. E* **80**, 031140 (2009).

[63] See e.g., L. D. Landau and E. M. Lifshitz, *Theory of Elasticity*, Butterworth-Heinemann (1986).

[64] Shakhnovich, K. A. & Goldbart, P. M. Statistical mechanics of permanent random atomic and molecular networks: Structure and heterogeneity of the amorphous solid state. *Phys. Rev. B* **60**, 3862-3884 (1999).

[65] De Gennes, P. G. *Scaling Concepts in Polymer Physics*. Cornell University Press, Ithaca (1979).

[66] P. G. de Gennes, J. Phys. (France) Lett. **40**, L-69 (1979).

[67] C. Wald, P. M. Goldbart, A. Zippelius, J. Chem. Phys. **124**, 214905 (2006); C. Wald, A. Zippelius, P. M. Goldbart, Europhys. Lett. **70**, 843 (2005).